



# **University of Udine**

Ph.D. course in Biomedical Science and Biotechnology

Cycle 32°

**Role of HDAC4 in the process of oncogenesis in human cells**

**Ph.D. Student**

Harikrishnareddy Paluvai

**Supervisor**

Prof. Claudio Brancolini

**Co-supervisor**

Dott. Eros Di Giorgio, *PhD*

**Academic year 2019/2020**

## Abstract

The resetting of epigenetics is a common feature of cancer cells. In contrast, how epigenetic regulators trigger oncogenic transformation is a mystery. Previous studies reported that the hyper-activation of an epigenetic regulator HDAC4 transforms murine cells. However, the transformation process of human cells is much more complex and are relatively resistant to oncogenesis. In the present thesis we addressed the oncogenic potential of HDAC4 in human primary fibroblasts (BJ). The over-expression of an hyper-active mutant of HDAC4 in human fibroblasts triggers a permanent cell cycle arrest typical a feature of oncogene induced senescence. The contemporary inactivation of p53 and pRb/p16 pathways achieved by the transduction of the cells with SV40 LT allows the transformation of HDAC4-TM cells.

Transcriptomic analysis of HDAC4-TM and RAS transformed cells evidenced that both the oncogenes require the repression of the interferon-response to transform the human cells. Further we have compared our signature with other two oncogenes like RAS and c-MYC which favour *in vitro* transformation in BJ-hTERT SV40 LT/ST. The tumorigenic properties driven by the three oncogenes rely on the activation of some common molecular pathways, but not on the activation and repression of the same genes. Importantly, commonly dysregulated genes, both up-regulated and down-regulated during *in vitro* transformation contribute to a worst survival rate in some cancer types. To gain insight on the cellular pathways supervised by HDAC4 and responsible for the transformation of human cells we investigated the genomic instability of leiomyosarcoma cells knocked out of HDAC4. In this cancer cell removal of HDAC4 results in the induction of cellular senescence through the augmentation of the DNA damage and the activation of the interferon response.

### **Aim of study**

This PhD project aims to investigate the contribution of class IIa HDACs to senescence and escape of senescence in human cells. A genetic depletion of HDAC4 in tumor cells and expression of hyperactive mutant of HDAC4 in human fibroblasts triggered senescence and induced DNA damage. Our goal is to understand, relationship between DNA damage response triggered by absence of HDAC4.

## **Acknowledgements**

First and foremost, I want to thank my supervisor Prof. Claudio Brancolini for giving me an opportunity to work in his lab and without your support I couldn't get my PhD. It was my dream to do PhD since I was kid and finally it came true because of you and Eros.

I would like to say thanks to my co-supervisor and my promoter, Eros Di Giorgio PhD who has taught me, both consciously and unconsciously, how to do a good research in science. He loves the joy and enthusiasm for research. During my entire PhD program, you motivated me alot, more than a father and a brother. I still remember how ignorant I was in science when I came to Udine and now what I am is because of you. Thanks for your effort and trust in me. I am also thankful to my Professor and Eros for being an excellent example of successful researchers.

Some people, they come in our life and teach something, and Magda was for me. During my entire PhD program, she extremely supported me mentally. I always remember your countless sacrifices to help me get to this point. Just by words I can't express how grateful I am to her. Thanks for being a part of it.

I would like to say thanks to my all family members, especially my mother and father, who have been steadfast and supportive. My brothers who continued their support and encouragement in achieving this.

Finally, the other part of my life is my friends, thanks to Valentina, Gerard, Yamanappa, Ashraf who are always with me in Udine and helped me when I needed them. Next I would like to say thanks to my colleagues Elisa, Valentina, Sonia, Martina and Luca for their company of friendly atmosphere in the lab.

## **Abbreviations**

HDAC: Histone deacetylases

HAT: Histone acetyltransferases

PcG: Polycomb Protein G

PRC: Polycomb repressive complexes

TF: Transcription factor

MEF2: Myocyte Enhancer factor 2

OIS: Oncogene Induced senescence

RS: Replicative senescence

SIPS: Stress Induced Premature senescence

DDR: DNA damage response

DDSB: DNA double strand break

53BP1: p53 binding protein 1

SV40: Simian Virus 40

LT: Large T antigen

ST: Small T antigen

SASP: Senescence associated secretory protein

SAHF: Senescence associated heterochromatinization factor

SA- $\beta$ -gal: Senescence associated  $\beta$  galactosidase

NF- $\kappa$ B: Nuclear factor kappa-light-chain-enhancer of activated B cells

**Abstract**

**Aim of thesis**

**Acknowledgments**

**Abbreviations**

**Introduction**

**1. Senescence.....1**

**1.1 Types of senescence.....3**

        1.1.1 Replicative senescence

        1.1.2 Oncogene induced senescence

        1.1.3 Oxidative stress induced senescence

        1.1.4 Drug induced senescence

        1.1.5 Epigenetically induced senescence

        1.1.6 Paracrine senescence

**1.2 Hallmarks of senescence.....6**

        1.2.1 Morphological changes during senescence

        1.2.2 DNA damage response

        1.2.3 Senescence associated heterochromatinization (SAHF)

        1.2.4 Changes in Nuclear architecture

        1.2.5 Senescence associated secretory proteins (SASP)

        1.2.6 Senescence associated- $\beta$ -galactosidase (SA- $\beta$ -gal)

**1.3 Role of senescence *in vivo*.....13**

        1.3.1 Replicative senescence

        1.3.2 OIS *in vivo*

        1.3.3 Senescence during Embryogenesis

**1.4 Epigenetic changes during cellular senescence and aging.....15**

**2. Oncogene Induced Senescence (OIS).....16**

    2.1 Factors influencing OIS

    2.2 OIS as a barrier for cancer progression

**3. Transformation.....22**

    3.1 Immortalization

    3.2 Malignant transformation

<b>4. Histone deacetylases (HDACs)</b> .....	24
<b>5. Material and Methods</b> .....	35
<b>6. Results</b> .....	41
6.1 Senescence Induced by Nuclear mutant of HDAC4 in BJ-hTERT fibroblasts	
6.2 Transformation of BJ-hTERT fibroblasts by HDAC4-TM	
6.3 Senescence Induced by HDAC4 knock out in cellular models	
<b>7. Discussion</b> .....	65
<b>8. Bibliography</b> .....	68
<b>9 Publications</b> .....	79

## Introduction

### 1. Senescence

The replicative senescence was discovered by Hayflick and Moorhead in 1961, who observed that normal human fibroblasts could divide a limited number of times *in vitro* and enter in a stage of irreversible growth arrest. This phenotype was different from quiescence for being irreversible and contributing a powerful anti-tumorigenic mechanism (Braig et al., 2005; Collado et al., 2005; Hayflick & Moorhead et al., 1961). Apoptosis and senescence are the two main barriers that prevent the emergence of transformed cells. There are two major events which can promote the permanent replicative arrest: the first involves the existence of a molecular clock (telomere shortening) which keeps track of cell divisions and eventually stop them (Hayflick & Moorhead et al., 1961); the second is often mentioned as premature cellular senescence and can be achieved also in the absence of telomere dysfunction (Hanahan & Weinberg, et al., 2011).

In addition to a permanent cell cycle arrest, senescent cells are characterised by the presence of low DNA replication capacity, high senescence-associated  $\beta$ -galactosidase (Sa $\beta$ -gal) activity, increased cell size and flattened morphology, chromatin and nuclear rearrangements and increased expression of hallmark regulatory proteins, such as p53, p21 and p16 (Burton & Krizhanovsky, 2014; Campisi & d'Adda di Fagagna, 2007; Ivanov et al., 2013). Furthermore, senescent cells acquire other markers which intrinsically influence cell behaviour by producing some cytokines, chemokines and matrix remodelling proteins together called as senescence-associated secretory phenotype (SASP) (Acosta et al., 2014; Campisi & d'Adda di Fagagna, 2007; Kuilman & Peeper, 2009; Nelson et al., 2012). A detailed list of cellular senescence markers are reported in below table 1.

In mammals, cellular senescence acts as a double edge sword, where it triggers cells to undergo permanent growth arrest condition and prevent cancer arising, while on other hand it causes age related diseases like atherosclerosis, diabetes and aging (Mattson & Arumugam, 2018).

These two processes are characterized by excessive and aberrant accumulation of cellular damage and cell dysfunctions that negatively impact on cell proliferation. During aging process most of the tissues loose regenerative capacity (Chang, 2016; Sousa-Victor et al., 2014)

Senescence is also involved in some biological processes like embryogenesis, tissue repair and in wound healing (Muñoz-Espín et al., 2013; Storer et al., 2013). Developmental senescence is transient, and its involves immune-mediated clearance (Muñoz-Espín et al., 2013; Storer et al., 2013). The induction of senescence during embryogenesis is p21 dependent and genetic

ablations of p21 results in escape of senescence by developing abnormalities (Muñoz-Espín et al., 2013; Storer et al., 2013).

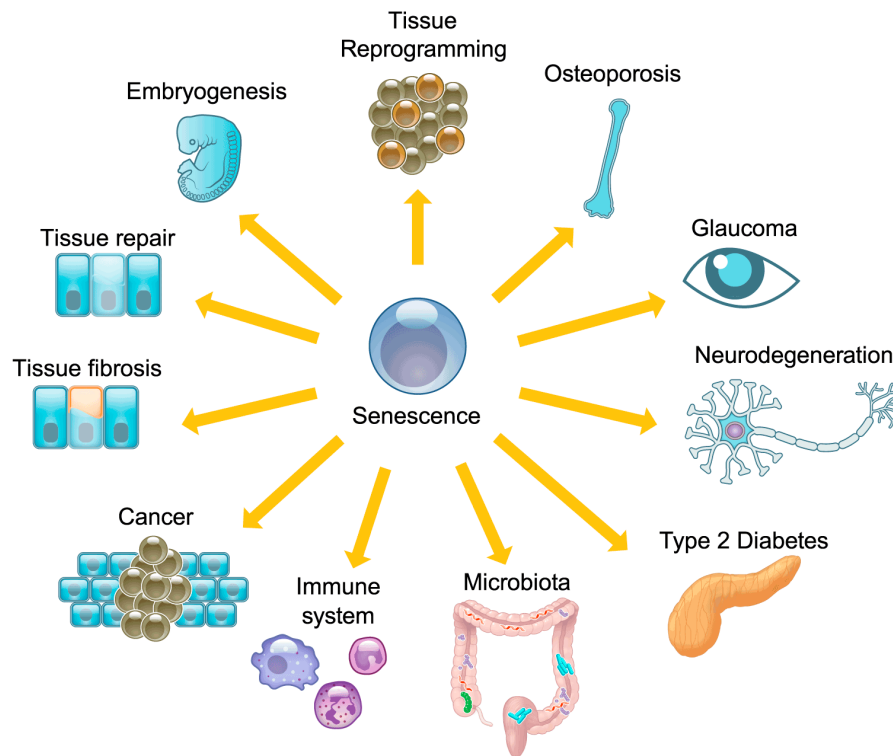


Figure 1: Cellular Senescence: Physiological role of senescence in daily life activities. The main role of senescence in young/adult organisms is to provide anticancer mechanism and promote wound healing. On other hand it contributes to age related diseases (Calcinotto et al., 2019). It is important to understand that the induction of senescence *in vitro* is different from *in vivo*. It is known that senescent cells *in vitro* remain permanent growth arrested without any proliferation, while senescence *in vivo* is quite complex. For example, nevi are considered as an *in vivo* senescent cell which eventually undergo permanent growth arrest and induce senescence for years in the organism (Michaloglou et al., 2005) on the other hand senescent cells can be rapidly engulfed by phagocytic cells, in the case of senescent tumor cells in liver carcinomas (Xue et al., 2007).

## *Cellular senescence Markers*

---

<b>Morphological changes</b>	Enlarged Flattened Morphology Increased Lysosomal activity SAHF SASP Low DNA synthesis Loss of Nuclear Integrity
<b>Molecular Markers</b>	Upregulation of p53 DNA damage response (DDR) markers Absence of proliferative markers, e.g. 5-bromodeoxyuridine (BrdU) Heterocromatin markers (H3K27me3, H3K9me3, H3.3,H.1.2) Release of SASP (IL6, IL8, IL1) Loss of Lamin B1

Table 1: Specific Molecular markers used to identify senescent cell both in vitro and in vivo.

### **1.1 Types of senescence**

In our daily life we observe some biological events, that rely on senescence namely wound healing and embryonic development. However, the contribution of senescence to wound healing is less described. Many human cells undergo senescence in response to DNA damage regardless of the genomic location. Until now there are few inducers of senescence which were successful in vitro and in vivo models

#### **1.1.1 Replicative senescence (RS)**

Until now the best explanation for replicative senescence is the shortening of telomeres which are found at the ends of chromosome. This happens because polymerases that copy the DNA template couldn't copy until the end of chromosomes. As a result telomere regions gradually shorten with each cell division and this creates a replication stress which results in induction of the cell cycle arrest called as replicative senescence (Linskens, Harley, West, Campisi, & Hayflick, 1995). Consistent with observations of Hayflick limit, many researchers have observed that human and murine fibroblast tend to undergo senescence during cell culture as they progressively lose the telomerase enzyme and face the end-replication problem. The loss of telomeric sequences elicits a DNA damage, leading to phosphorylation of Ser-139 of histone H2A.X molecules ( $\gamma$ -H2A.X) adjacent to the site of DNA damage thereby preventing genomic instability. It is thought that this phosphorylation of histone H2AX facilitates the focal assembly of checkpoint and DNA repair factors including 53BP1, MDC1/NFBD1 and NBS1, and promotes the activation by phosphorylation of the transducer kinases Chk1 and Chk2, which converge the signal on p53.

It was known already that telomere dysfunction induces growth arrest via activation of ATM/ATR (Karlseder, Broccoli, Yumin, Hardy, & De Lange, 1999; Rouse & Jackson, 2002) and eventually p53 and (in human but not mouse fibroblasts) p16 (Karlseder, 2002). However, ectopic expression of telomerase reverse transcriptase (abbreviated as TERT, or hTERT) in humans' cells can bypass Replicative senescence thereby lengthening the telomere in DNA strands. Some tumour cells can escape this senescence barrier by expressing the telomerase enzyme, which can replenish the telomeric DNA de novo (Herbig, Ferreira, Condel, Carey, & Sedivy, 2006). In other cases, alternative lengthening of telomeres can be appreciated (De Vitis, Berardinelli, & Sgura, 2018).

### **1.1.2 Oncogene Induced Senescence (OIS)**

Until last few decades what we know about oncogenes such as H-RAS<sup>V12</sup> is that they are able to transform the mammalian and rodent cell lines, but on other hand it was lately discovered by a Spanish researcher Manuel Serrano in 1997 that oncogenes are able to induce senescence when they are introduced in primary human/murine cells. One common feature shared by replicative senescence and OIS is the triggering of DNA damage response. Unlike replicative senescence, oncogene induced senescence is not dependent on telomeric DNA loss, as ectopic expression of hTERT cannot bypass oncogene Induced senescence (Wei, Wei, & Sedivy, 1999). However, the combined functional inactivation of p53 and p16 tumour suppressors is enough to bypass oncogene induced senescence (Serrano, Lin, McCurrach, Beach, & Lowe, 1997). However, in these conditions DNA damages are not solved (Di Micco et al., 2006). Examples of oncogenes that induces senescence are RAS, AKT, PI3K and MYC (Schmitt et al., 2002; Serrano et al., 1997; Zindy et al., 1998).

### **1.1.3 Oxidative stress Induced senescence (SIPS)**

Recent evidence suggests that reactive oxygen species (ROS) contribute to the pathophysiology of ageing. In addition to replicative senescence, cellular senescence can be triggered by various stressors called as Stress Induced premature senescence (SIPS). SIPS is characterized by a permanent cell cycle arrest comparable to cellular senescence. When human healthy cells are treated with Hydrogen peroxide, the cells that survive to the treatment begin to show some biomarkers of senescence such as appearance of DNA damage, acquisition of an enlarged flattened morphology, increased beta-galactosidase activity, loss of proliferative markers and increased production of ROS (Davalli, Mitic, Caporali, Lauriola, & D'Arca, 2016). Some ROS producers like Mitomycin c display senescence features in dermal fibroblasts (Alili, Diekmann, Giesen, Holtkötter, & Brenneisen, 2014). Oxidative damage accumulates in a variety of

macromolecules like lipids, DNA, or proteins and results in a progressive decline in the function of cellular processes, finally resulting in the aging phenotype (Davalli et al., 2016).

#### **1.1.4 Drug-induced accelerated senescence (DIAS)**

It is known that many chemotherapeutic drugs like Doxorubicin and cisplatin, are efficient in inducing senescence *in vitro* and *in vivo* through the induction of irreparable DNA damage (Alili et al., 2014; Muñoz-Espín et al., 2013) and display several markers of senescence.

#### **1.1.5 Epigenetically induced senescence**

Our human genome is tightly packed in nucleosomes and wrapped around histones. Any alterations at chromatin level could trigger senescence or apoptosis. It was demonstrated that treating human fibroblasts cells with HDACs inhibitors, known to cause G1 cell cycle arrest, triggers senescence (Kadosh & Struhl, 1998). It is not well understood how HDACs Inhibitors induces senescence. In 2004 Munro confirmed that HDAC Inhibitors induce senescence in human cells in a p16 dependent manner while MEF cells show a p53 dependency (Munro, Barr, Ireland, Morrison, & Parkinson, 2004). Similarly, demethylating agents like (5-aza-deoxycytidine) are known to induce senescence. Last, but not least it was shown that downregulation of p300/CBP acetyltransferase, triggers cell cycle arrest in melanocytes (Bandyopadhyay et al., 2007). It was also reported that Sirtuins (SIRT1,6) , (Class III HDACs) display anti-aging properties (Guarente, 2007; Ota et al., 2007). Inhibition of Sirtuins either by siRNA or inhibitors mediate cellular senescence in human endothelial cells (Lee, & Min, 2019; Ota et al., 2007). Another protein which could influence senescence state is Polycomb proteins G (PcG). PcG maintain the facultative heterochromatin state and regulate many developmental and differentiation processes. Polycomb proteins, exists as two forms Polycomb repressive complex 1 and 2 (PRC1 and PRC2) which belong to Polycomb protein G family. PRC2 contains EZH2, a histone lysine methyltransferase that catalyzes the histone 3 trimethylation of lysine 27 (H3K27me3) by Su(var)3-9, and Enhancer-of zeste and Trithorax (SET) domain. It is well known that downregulation of EZH2 triggers a DNA damage response with global reduction of H3K27me3 and promotes senescence. Recent studies suggested that DNA damage response is an early event in respect to heterochromatinization (Anna Fortuny et al., 2018). Furthermore, chromatin compaction appears to play an important regulatory role in DNA damage signalling. One of the earliest responses of DNA damage infliction is the recruitment of DNA damage signalling kinases, which initiates a complex cascade of events leading to cell cycle checkpoint activation. Among the many targets of these kinases, the histone variant H2A.X gets rapidly phosphorylated in large chromatin domains surrounding DSBs, giving rise to  $\gamma$ H2A.X foci (Rogakou, Pilch, Orr, Ivanova, & Bonner, 1998) which serve as a platform for

recruiting downstream checkpoint and repair factors. While this is a general response to DNA damage, several studies in yeast and mammalian cells originally showed that silenced chromatin domains were refractory to H2A.X phosphorylation (Cowell et al., 2007; J. A. Kim, Kruhlak, Dotiwala, Nussenzweig, & Haber, 2007) and hampered DNA damage checkpoint signalling (Cowell et al., 2007; Fortuny & Polo, 2018). Altogether these studies demonstrate that heterochromatin is permissive for DNA damage signalling and that heterochromatin features including histone marks and chromatin compaction exert a positive role in response to DNA damage by contributing to checkpoint activation. But still a clear picture about the heterochromatinization in senescent cells is still missing.

### 1.1.6 Paracrine senescence

Senescent cells secrete a wide variety of cytokines, chemokines and metalloproteases commonly referred as SASP. Key factors of SASP proteins are Interleukin-6 (IL-6), interleukin-8 (IL-8), interleukin-1 $\alpha$  and 1 $\beta$  and chemokines like CXCL-2, CXCL-3, and CXCL-5 which are released by senescent cells into the extracellular matrix (Coppé et al., 2010). These SASP proteins induce senescence in neighbouring cells via paracrine manner thereby allowing cells and tissues to enter senescence phase.

### 1.2 Hallmarks of Senescence

Currently there are several markers available to distinguish a senescent cell from a non-senescent cell (proliferating cell). Traditionally senescent cells are detected by the presence of low DNA replication capacity which can be detected by BrdU incorporation. The irreversible proliferation arrest is required to distinguish senescent from quiescent cells. The former are characterized also by some morphological and biological alterations that allow the discrimination between these two biological responses.

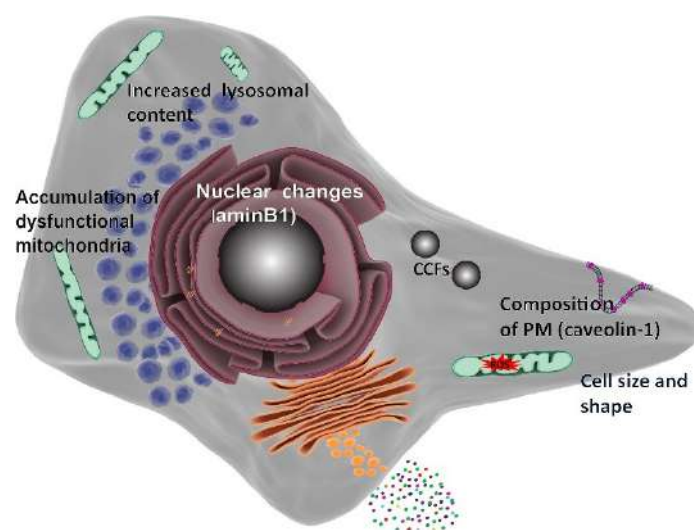


Figure 2: Hallmarks of cellular senescence. Morphological alteration loss of Lamin B1, accumulation of cytoplasmic DNA, followed by increased lysosomal content and ROS production (Hernandez-Segura, Nehme, & Demaria, 2018).

### **1.2.1 Morphological changes**

Senescent cells are usually characterized by large flattened enlarged morphology (Serrano et al., 1997) vacuolized and, occasionally, multinucleated (Wajapeyee, Serra, Zhu, Mahalingam, & Green, 2008). However, the molecular mechanism behind this is partially unknown. Moreover, differences exist regarding the morphology of senescent cells: for example, human fibroblasts transduced with RAS display flattened cell morphology, while senescence induced by *BRAFV600E* display spindle shaped morphology (Wajapeyee et al., 2008).

### **1.2.2 DNA Damage Response**

Persistent DNA damage signals are considered a major contributor to cellular senescence and organismal aging. It is well known that cells undergoing senescence triggers a DNA damage response and more precisely a DNA Double strand break response (DSBR). The DSBs created during senescence are unrepairable and which eventually leads to permanent cell cycle arrest (Campisi & d'Adda di Fagagna, 2007). Sophisticated DDR network that responds to DSBs include the recruitment of certain proteins (e.g., 53BP1 and Rad17), particular modifications like histone phosphorylation (e.g.,  $\gamma$ H2AX), or both (e.g., p-ATM), and the subsequent events (e.g., the activation of p53-p21 and/or p16-Rb signaling) to counteract DNA damage effects (Costes et al., 2007). Activated ATM orchestrates the DNA repair process by phosphorylating multiple proteins, such as H2AX and 53BP1, to form characteristic DNA foci (Campisi J et al., 2007). ATM also phosphorylates the substrates CHK2 and p53 to initiate cell-cycle arrest. This method of DNA repair is called the homologous recombination (HR) repair pathway (Lavin MF et al., 2007). Alternatively, DSBs activate non-homologous end joining (NHEJ) repair pathway which mediated by DNA-PKcs (Chung JH et al., 2018). Upon detecting DNA damage, the cell follows two routes: activation of DDR-dominant cell cycle checkpoints and cell cycle arrest to facilitate repair, or if damaged beyond repair, induction of apoptosis. In some cellular models like replicative senescence the DNA damage response is triggered as a consequence of the replication stress created by shortened telomeres or colliding forks.

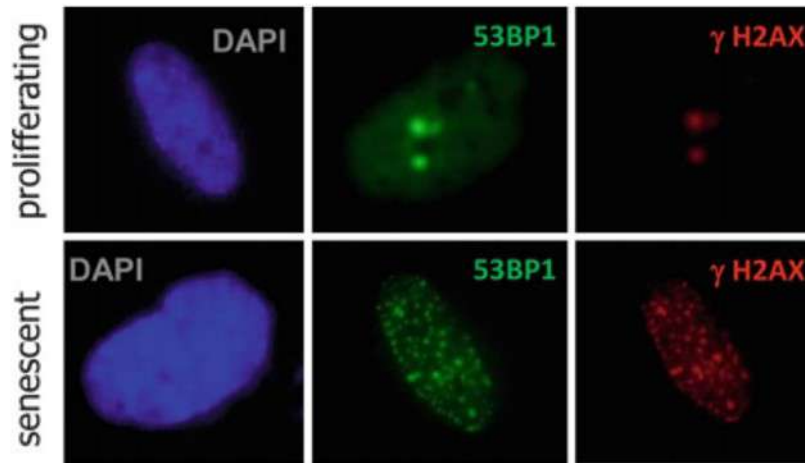


Figure 3: H2AX is commonly used as a marker of senescence in response to DNA damage (DSB). Here the human lung fibroblasts IMR90 cells (right side) are exposed to UV and Immunofluorescence is performed by using Phospho H2AX (ser139) mouse mAb (red) and a DNA damage sensor 53BP1 is stained in green. (A.carnero et al., 2013).

Another protein which is involved in DNA damage response is p53 binding protein 1 (53BP1). 53BP1 protein is recruited to the sites of DNA double strand breaks and forms microscopically visible foci (Ward, Minn, Deursen, & Chen, 2003). 53BP1 has been extensively characterized in the context of its contribution to the non-homologous rejoining (NHEJ) DNA double-strand break (DSB) repair pathway (Chapman, Taylor, & Boulton, 2012). Any defect in 53BP1 impairs DNA damage checkpoint and show defects in DNA repair . In addition to these numerous small foci, 53BP1 has also been involved in different large NBs (Nuclear Bodies) as telomere dysfunction-induced foci (TIFs) (Takai, Smogorzewska, & de Lange, 2003), DNA segments with chromatin alterations reinforcing senescence (DNA-SCARS) (Rodier et al., 2011) and finally 53BP1 nuclear bodies (53BP1 NBs). During DNA damage, cells accumulate 53BP1 NBs and disappear during mitosis and further transmitted to daughter cells, these DNA lesions are sequestered into large chromatin domains enriched in 53BP1 and other markers associated with DDR (Harrigan et al., 2011).

### 1.2.3 SAHF

During senescence, chromatin is reorganised and thus favours a global heterochromatinization also called as Senescence associated Heterochromatin foci (SAHF). SAHF are specialized domains of facultative heterochromatin that silence some proliferating -promoting genes (such as E2F target genes) in senescent cells (Narita et al., 2003). Usually SAHF appears during senescence that is induced by various stimuli such as activation of oncogenes, replication stress induced by loss of telomerase enzyme in primary cells or chemotherapeutics drugs such as

etoposide. SAHF seems to act as a tumour suppressive mechanism, as any disruption of SAHF lead to cell transformation (Narita et al., 2006). SAHF formation and senescence are not directly linked and it is not clear whether SAHF drives cellular senescence or not. Indeed, several studies have shown that senescence can occur even in the absence of SAHF formation. Some experimental studies show that SAHF formation is cell line dependant (Kosar et al., 2011), for example SAHF formation is observed in replicative senescence of IMR90 and WI 38 but less in BJ fibroblasts (Narita et al., 2003). On the opposite, some cells like murine NIH-3T3 fibroblasts display SAHF like structure in the absence of any stress (Kennedy et al., 2010); moreover, MCF10A transduced with RAS display SAHF-like structures in absence of cell-cycle arrest (Sherman, Meng, Stampfer, Gabai, & Yaglom, 2011).

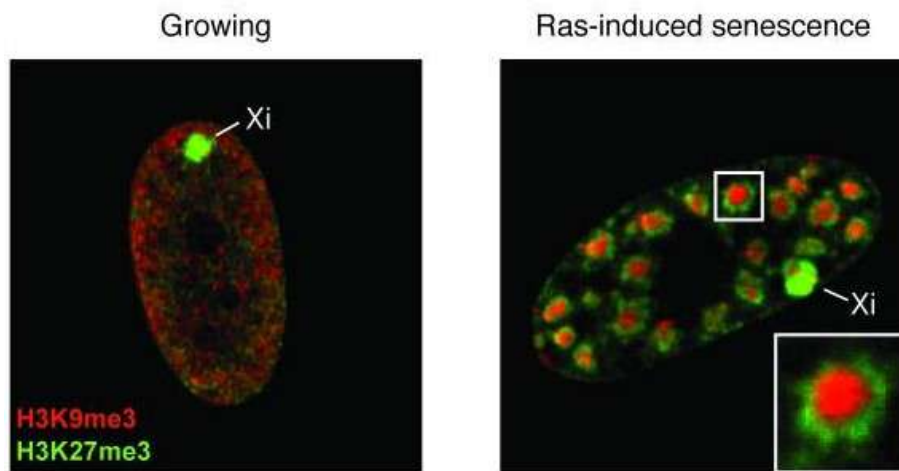


Figure 4: SAHF appearance in RAS induced senescence. Confocal images representing SAHF formation in OIS, on the left a picture repressive marks (H3K9me3 and H3K27me3) dispersed but always close to the nucleus envelope. Xi represents inactive X chromosome. On the right there is a picture represents Ras-induced senescent cell. It is possible to see that the chromatin is reorganised forming now a red core (H3K9me3) surrounded by a green ring (H3K27me3) (Narita et al., 2013).

#### 1.2.4 Changes in Nuclear architecture

Nuclear Lamina is a protein structure that surrounds the nuclear membrane on its nucleoplasm side (Y Gruenbaum et al 2003). It is made by intermediate cytoskeletal filaments of Lamin (A-C) and lamina associated proteins. It is widely accepted that alterations in nuclear lamina are linked to the onset of senescence. In particular, Lamin B1 down-regulation universally marks senescent cells (Freund, Laberge, Demaria, & Campisi, 2012) as a consequence of transcriptionally and post-transcriptionally (autophagy) mechanisms (Dou et al., 2015). Moreover, mutations in Lamin A gene have been linked to premature aging diseases. For example, point mutation in Lamin A gene that give rise to a splicing isoform called progerin

leads to a premature aging disorder called Hutchinson–Gilford Progeria Syndrome (HGPS). Like HGPS patients, cells derived from elderly people display nuclear lamina alterations. The alterations of nuclear lamina influence the chromatin architecture. In fact, knock down or knock out of Lamin B1 induces premature senescence and leads to SAHF formation in few human cell lines (Dreesen et al., 2013). However, on the opposite it is reported that also the over-expression of LMNB1 triggers senescence of human fibroblasts. It is hypothesized that the re-arrangement of chromatin territories imposed by the alteration of nuclear lamina is at the basis of a new kind of senescence imposed by epigenetic clues. However, some analysis were confirmed by ChIP or DamID showed that, interaction between nuclear lamin B1 with chromatin is abolished during OIS but H3K9me2/3 is enriched in proliferating cells (Lenain et al., 2017). On contrary, some regions carrying H3K27me3 were retained at nuclear periphery upon OIS thereby keeping senescent cells in transcriptionally repressed chromatin state (Lenain et al., 2017). Another example of strong chromatin and nuclear lamin interactions is seen in HGPS. Several studies on HGPS cells revealed that tethering of heterochromatin to the nuclear lamina is abolished (Goldman et al., 2004). HGPS cells do not display SAHF and display reduced level of heterochromatin protein H3K9me3 (Shumaker et al., 2006). In agreement with the loss of peripheral heterochromatin markers, H3K27me3 in the regions losing lamin A/C binding is also diminished in HGPS cells (McCord et al., 2013). What might be the reasons for such variation in nuclear reorganization when nuclear lamin is disrupted is unknown.

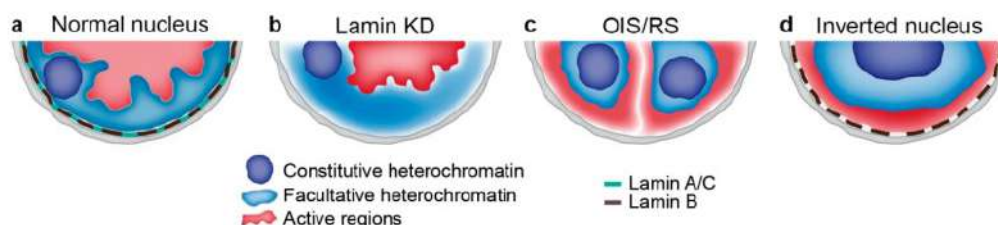


Figure 5: Schematic representation of heterochromatinization generated upon loss of NL-chromatin tethering. (a) Conventional nuclear architecture in most mammalian cell types. (b) Nuclear architecture in *Drosophila* S2 cells lacking both A- and B-type lamins. (c) Nuclear architecture upon OIS or RS. (d) “Inverted” nuclear architecture in rod photoreceptors where active regions are interacting with facultative heterochromatin.

### 1.2.5 SASP

Cells which undergo senescence secrete a wide variety of inflammatory cytokines such as IL-6, IL-8, IL-1 $\beta$ , IL-1 $\alpha$ , chemokines, proteases and growth factors which positively impacts non senescent cells in a paracrine signalling. SASP has dual roles: it stimulates neighbouring cells to undergo senescence but it also promotes the clearance from immune cells, and on other hand it promotes tumor progression (Coppé et al., 2010). SASP is required to sustain senescence but is not necessary to trigger it. In fact, inactivation of p53 bypasses senescence and restarts cell

proliferation but SASP production remains unchanged and active (Coppé et al., 2010). Further studies establish that the powerhouse of SASP is NFκB and C/EBP and cytokines regulation occurs at transcriptional and post transcriptional level. Many of cytokines mRNA were upregulated during senescence and inhibition of NFκB pathway delayed senescence as well as DNA damage response in some cellular models (Tilstra et al., 2012). The major trigger of SASP is the DNA damage response which activate NFκB pathway. In fact absence of DDR in some senescence models where p21 and p16 is overexpressed completely abolished SASP production. Release of cytokines from senescent cells is heterogenous and it influenced by the way of inducing senescence and cell lines used too. For example, expression of BRAFv600E in BJ fibroblasts to induce senescence, released a cytokine IGFBP7 and the same oncogene in Lung fibroblast IMR90 released IL-6 and IL-8 (Sherman et al., 2011).

The conditioning with the medium taken from senescent cells is strong enough to induce senescence in proliferating cells (Hubackova, Krejcikova, Bartek, & Hodny, 2012) ; however the pathways triggered by SASP-induced senescent are still unexplored. Further clarifications are needed also to understand why p53 abrogates SASP.

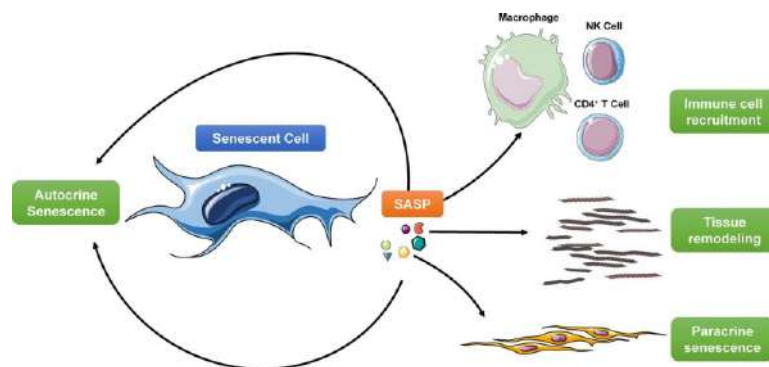


Figure 6: Senescent cell secrete some SASP proteins which mediates many cell-extrinsic functions of senescent cell, later they stimulate NK cells to clear the senescent cell (McHugh & Gil, 2018).

### 1.2.6 Senescence Associated-β-Galactosidase (SA- β Gal)

SA- β Gal was first described by the Judith Campisi group in 1995 and become one of the most popular markers of senescence. The advantage of using this marker is that it detects only senescent cells but not quiescent cells both in vitro and in vivo models. The enzymatic activity of SA-β-GAL derives from lysosomal β-galactosidase which is encoded by the GLB1 gene (Dimri et al., 1995). In normal, proliferating cells, lysosomal activity of galactosidase is detected at a pH of 4, and however in senescent cells the pH activity is increased to 6. The

increased pH activity of senescent cells is due to expansion of lysosomal activity in senescent cells. The drawback of this assay is that it stains the cells under confluency by providing a false data, more precise is required if we follow this protocol.



Figure 7: Cells staining, positive for SA-β-GAL (McHugh & Gil, 2018).

### Short Summary of current tools to detect senescence:

- **DDR:** The presence of  $\gamma$ -H2AX foci shows that there is a continuous DNA damage response which is unreparable.
- **Cell cycle arrest:** Two types of assay are normally performed to show that senescent cell is exited from cell cycle. The first is by measuring the DNA replication capacity which is done by BrdU incorporation assay. The second includes measuring the expression level of the Cell cycle inhibitors like p16 and p21.
- **SASP:** Cytokines (e.g., IL-1a, IL-6, and IL-8), chemokines (e.g., CCL2) and metalloproteinases (e.g., MMP-1 and MMP-3) are some of SASP proteins which are frequently upregulated in senescent cell. The common practice to measure SASP proteins is by ELISA, Cytokine profiling and looking at mRNA or protein level.
- **Apoptosis resistance:** The upregulation of the BCL-proteins Bcl-2, Bcl-w, or Bcl-xL has been used as a marker of senescence.
- **Metabolism:** Lack of information and poor knowledge on metabolic changes during senescence is not considered as a marker of senescence.
- **Cell morphology:** A senescent cell when visualised under normal microscope shows, enlarged and flattened cell morphology with appearance of vacuoles in the cells.
- **Increased lysosomal content:** SA-β-gal is commonly used as marker to measure lysosomal activity and one of the first tests used to assess senescence. Alternatively, SBB or its biotin-labeled analog (GL13) can be used to detect lipofuscins from old lysosomes, and LysoTrackers or orange acridine can reveal high lysosomal contents .
- **Accumulation of mitochondria:** Mitotracker to measure the membrane potential of mitochondria and electronic microscopy to evaluate their cell shape (fusion/fission) have been used in some studies.
- **Nuclear changes:** SAHF are observed as darker regions within the nucleus of senescent cells after DAPI staining and are enriched in markers of heterochromatin, such as H3K9me3 and HP1 $\alpha$ . However, this feature is not shared by all types of senescence and is not apparent in mouse cells. Alternatively, loss of LaminB1 is used also a marker of senescence.

### **1.3 Role of Senescence *In vivo***

#### **1.3.1 Replicative senescence**

Several studies have suggested that during aging process, senescent cells are accumulated. Senescent cells from skin of elderly people show an increase in SA- $\beta$ -gal activity (Dimri et al., 1995) and these cells significantly decreased telomere length (Cristofalo, Lorenzini, Allen, Torres, & Tresini, 2004). Later these studies were supported with introduction of other senescence markers like DNA damage, SAHF and SASP. Dermal fibroblasts from aged baboons showed a decreased in telomere length and increased DNA damage response when compared to young ones. DNA damage markers were known to colocalize with telomeres, and this is correlated with increase of p16<sup>INK4A</sup> levels (Herbig et al., 2006), suggesting that telomere dysfunction can create DNA damage signals leading to the onset of senescence also *in vivo*. Telomeres plays an important role in replicative senescence as cells undergo replication stress as they gradually lose telomeric DNA. However, telomeric dysfunctions also contribute to age related pathology such as Atherosclerosis and Osteoarthritis. These patients showed an increased expression of SA- $\beta$ -gal activity (Price et al., 2002). Since these studies were performed by using single senescent markers, some more additional marker should be used to confirm the above studies. In a mouse model of liver fibrosis, senescent cells were identified by positivity for SA- $\beta$ -gal, increased expression of p16<sup>INK4A</sup>, p53, p21<sup>CIP1</sup>. These senescent cells derive from activated hepatocellular stem cells and limit the progression of fibrosis (Price et al., 2002). In addition, two scientific reports have supported Hayflick that replicative senescence limits tumor progression (Cosme-Blanco et al., 2007). Both studies reported that mice lacking telomerase enzyme (mTR) showed a decreased tumor progression in the context of either one or two copies of mutant p53<sup>R172P</sup> replacing endogenous p53 (Cosme-Blanco et al., 2007) or E $\mu$ -MYC/BCL2-driven lymphomagenesis.

#### **1.3.2 Oncogene Induced Senescence *In VIVO***

Melanocytic Nevi are considered as one of the best examples of senescence *in vivo*. Melanocytic Nevi undergo a permanent cell cycle arrest that prevents them from progressing to melanoma. Although nevi can persist in the skin for years, some eventually progress and give rise to melanomas. One of the most frequently mutation found in melanoma is BRAF<sup>E600</sup>. (Davies et al., 2002) and the same oncogenic mutation is present in the majority of nevi (Pollock et al., 2003). Although the presence of oncogenic mutation in BRAF allele in nevi, these cells undergo M0 mitogenic senescence. Michaloglou et al has confirmed that BRAF *V600E* mutation in nevi have displayed increased p16 and SA- $\beta$ -gal expression. Furthermore,

nevi had showed positivity to other senescence markers such as increased number of SAHF formation and typically these nevi did not display shortened telomeres. This strongly suggests that nevi undergo OIS in vivo. These findings have been confirmed by Bennett and co-workers (Gray-Schopfer et al., 2006). Taken together, this evidence shows that nevi didn't undergo a telomere-dependent senescence when oncogenic BRAF *V600E* mutant is present (Michaloglou et al., 2005). In support to this, an experimental model has been designed by Michaloglou et al where primary melanocytes cultured in vitro underwent senescence when BRAF*V600E* is expressed. These cells initially show burst in cell proliferation followed by morphologic changes such as flattened enlarged shape, appearance of multinucleation and increased levels of SA- $\beta$ -gal (Michaloglou et al., 2005).

The studies on senescent nevi are consistent with previous observations that a mutant BRAF *V600E* in melanocytic lineage induced the formation of nevus-like lesions in zebrafish and in transgenic mouse models. Furthermore, inactivation of p53 together with oncogenic BRAF, accelerated the formation of invasive melanomas. Another study conducted by Dankort et al and Dhomen et al in 2009, demonstrated that conditional expression of mutant BRAF in the melanocytic compartment results in the development of nevus like lesions and which remain growth arrested for several months and years by displaying markers of senescence (David Dankort et al., 2009, Dhomen et al., in 2009) . However, depletion of p16INK4A did not affect the nevus formation. In contrast, loss of Pten, together with expression of BRAF resulted in melanoma, which is like metastatic melanoma of humans. These elegant models have shown that oncogenic mutation of BRAF induces nevus formation and any mutation such as loss of Pten and p53 results in melanoma progression (David Dankort et al., 2009).

### **1.3.3 Senescence during Embryogenesis**

Early findings by Hayflick suggest us that normal human cells can proliferate for a certain limited number of times before entering replicative senescence. It was considered in the past that senescence is limited only to adults' cells, but in 2013 Munoz et al discovered the role of senescence during embryogenesis focusing on inner ear and retraction of mesonephric tubules in murine species. The induction of senescence during embryogenesis was not clear, to understand better the role of senescence in embryo, p53, p21, p16 depleted mice were used. The knockout mice for p53 and p16 showed a positivity for SA- $\beta$ -Gal staining during embryogenesis and on the contrary knock out mice for p21 showed low positivity for SA- $\beta$ -Gal staining and the embryo was not developed well when compared to controls. Therefore, up-regulation of p53 and p16 pathways doesn't contribute to any role in senescence during

embryo development. Studies conducted by Munoz et al and Storer et al, provide an evidence that developmental senescence is mainly induced by the presence of p21 through a TGFβ/SMAD and PI3K/FOXO dependant, and p53-independent pathways (Muñoz-Espín et al., 2013; Storer et al., 2013). These studies showed that inhibition of senescence during embryogenesis resulted in abnormal developmental function even in the presence of apoptotic mechanism.

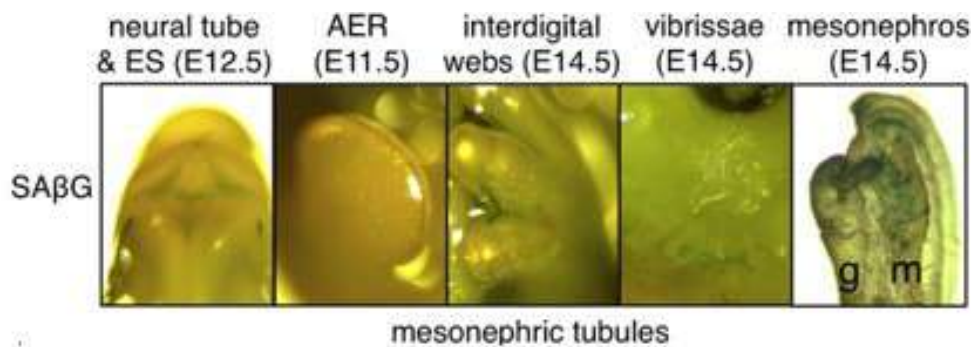


Figure 8: Cellular senescence maintains proper homeostasis during embryogenesis. Examples of senescent structures stained for a marker of senescence after embryo at the indicated stages. ES, endolymphatic sac; AER, apical ectodermal ridge (Muñoz-Espín et al., 2013).

#### 1.4 Epigenetic changes during Cellular senescence and aging

Epigenetics is a big network consists of three major events

1. DNA modifications
2. Histone modifications like histone deacetylation and acetylation or histone methylation
3. Recruitment of higher-order chromatin structures or remodelers.

Epigenetic changes are the major cause of cellular senescence and aging. Any alternations in Epigenetics would affect the transcription profiles. Alterations in Epigenetics can be induced by endogenous (e.g., intracellular signalling pathways) as well as exogenous stimuli deriving from daily life activities, food consumption and environmental exposure (like smoking, exposing to toxic chemicals, UV radiations).

Studies conducted by many groups showed that chromatin of aged people is characterized by a remodelling of chromatin as a consequence of altered histones.

Indeed, histone post-translational modifications and chromatin remodelling are very important in the recruitment and activation of DNA damage repair pathways and, therefore, protecting the genomic integrity of a cell. When there is a DNA damage response there is activation and phosphorylation of serine 139 of histone H2A variant ( $\gamma$ -H2AX), trimethylation of H3K9 and H3K27, methylation of H3K79me, acetylation of H3K9) and H3K14. These later are involved in DNA damage sensing and relaxing the chromatin.

On the opposite, dephosphorylation of H2AX, acetylation of HATs and deacetylation by HDACs on histone H3 and H4 are important to close the chromatin or restore the chromatin after DNA repair. The H3K27me3 and H3K9me3 form facultative and constitutive heterochromatin and promote gene silencing in senescent cell (Tamar Segal et al., 2018). However, this is not true that in all the cases SAHF should be appeared in senescent cells, for example fibroblasts derived from Progeria patients show no sign of SAHF. But indeed, the chromatin is also disorganised in those fibroblasts. About 70% of fibroblasts derived from HGPS patients display aberrant nuclear morphology and low levels of the heterochromatin protein HP1 $\alpha$ , which acts as adaptor between the nuclear lamina and the chromatin.

Epigenetic changes are not restricted to facultative heterochromatin regions that form the SAHF. The SAHF could be also present in telomeres and pericentromeres (R. Zhang, Chen, & Adams, 2007). During senescence, pericentric satellite DNA undergo a dramatic decondensation which is quite, independent from SAHF formation (De Cecco et al., 2013). This nuclear chromatin condensation is termed Senescence-associated distention of satellites (SADS) and which appears to be formed in senescent cells but not in proliferating cells and cancer cells (Swanson, Manning, Zhang, & Lawrence, 2013). SAHF formation is limited only to few senescent cells, while SADS formation is observed among all senescent cell types and senescence-inducing stimuli like RS, OIS, and in HGPS fibroblasts. Recently, SADS formation has been identified *in vivo* and suspected to promote tissue aging (Kosar et al., 2011).

However, the exact mechanism of SADS formation during cellular senescence remains unknown. One possible explanation could be that pericentric satellite transcripts is an early event during senescence induction that promotes genomic instability to activate cell cycle arrest. Satellite distention could also be only a consequence of the detachment of pericentromeric chromatin from LMNB1 (Swanson et al., 2013).

## **2 Oncogene Induced Senescence**

Oncogenes are well known to initiate and promote tumorigenesis. For example, activation of RAS oncogene contributed to 25% of human cancers (Fernández-Medarde & Santos, 2011). Although oncogenes have a direct effect on cell proliferation which is important for initiation of tumour progression in many human cancers, later in 1997, it was shown by Serrano and his colleagues that ectopic expression of activated oncogenes like H-RASG12V create a stress conditions where human fibroblasts undergo a permanent cell cycle arrest called as Oncogene Induced Senescence (OIS).

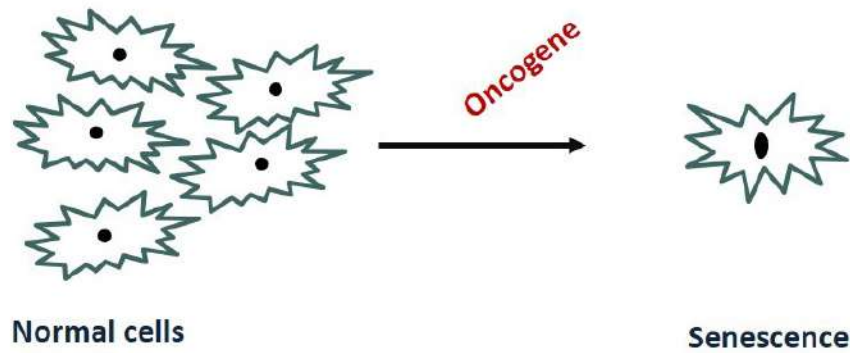


Figure 9: Schematic representation of OIS. Normal cells in the presence of oncogene undergo senescence with a decreased DNA synthesis.

OIS is independent from telomere as ectopic expression of hTERT didn't allow them to bypass senescence. The growth arrested cells resemble to replicative senescent ones by displaying markers of senescence like increase of DNA damage response, loss of Lamin B1, increased formation of SAHF, and expression of classic SA- $\beta$ -gal and flattened enlarged morphology. OIS could be triggered by some other oncogenes, such as BRAF600E, AKT, C-MYC, E2F1, TGF-BETA and cyclin E.

For example, multiple evidences indicated that increased PI3K/AKT signalling also induces cellular senescence in normal human fibroblasts. Loss of PTEN, the major negative regulator of the PI3K/AKT pathway, induced senescence in mouse embryonic fibroblasts (Astle et al., 2012). PTEN deletion also induces loss of mouse hematopoietic stem cells by induction of the senescence effectors p53, p21 and p19Arf (Yilmaz et al., 2006). Expression of constitutively active AKT induces senescence in human endothelial cells (Miyachi et al., 2004) mouse embryonic fibroblasts and mouse primary keratinocytes. The mechanisms underlying induction of senescence by AKT are poorly defined, although the accumulation of reactive oxygen species has been implicated as playing a role. A better understanding of the mechanisms of PI3K/AKT-induced senescence will be crucial for understanding the role of dysregulated PI3K/AKT signalling in cancer.

In the below table, it is reported a list of the known oncogenes that induce senescence.

<b>Oncogenes Inducing senescence</b>	<b>Pathway</b>
TGFb	Promotes Smad signaling
H-rasV12, K-rasG12V, N-rasG12D	Ras signaling
BRAF V600E	Promotes Ras signaling
c-Myc	Effector of Ras signaling — transcription and chromatin remodeling factor
Akt	PI3K/Akt signaling
$\beta$ -Catenin	Promotes Wnt signaling
PTEN (TSG)	Downregulates PI3K/Akt/mTOR signaling
Cyclin E	Activated cyclin-dependent kinase-2: promotes G1 to S phase
STAT5	Promotes JAK–STAT signaling
MEK	Promotes Ras signaling
NOTCH	TGF $\beta$ signalling

Table 2: List of oncogenes induces senescence

However, to induce OIS, in both in vitro and in vivo models, their expression levels are important, as studies revealed that senescence was induced by oncogenic Ras only when certain level of Ras is expressed. Activation of tumour suppressors proteins is a part of response triggered by senescence.

## **2.1 Factors influencing OIS**

### **Activation of Tumour suppressors during OIS**

In murine cells, the abrogation of either p53 and p16 pathways is strong enough to bypass Replicative senescence (RS). On the opposite, human fibroblast requires the contemporary ablation of p53 and p16 tumor suppressors to re-entre cell-cycle.

The blockage in the cell-cycle imposed by tumor suppressors is required to prevent the extension of DNA damage and to avoid its spreading. It culminates in the repression of E2F target genes and in the up-regulation of CDKi.

### **DNA damage response**

RAS induced senescence is associated with a DNA damage response that is due to unlimited replicative potential eventually leading to withdraw from cell cycle progression. However, inactivation of DNA damage response would allow cells to bypass senescence and favour cell transformation (Di Micco et al., 2006). Senescence induced by oncogenes was suppressed when ATM kinase is inhibited which senses DNA double strand breaks. Inhibition of ATM kinase increased tumour formation and invasion in mice. A study showed that Ubiquitin

degradation of ATM by E3 ligases like WSB1(WD repeat and SOCS box-containing protein 1) promoted cell transformation and bypassed OIS (J. J. Kim et al., 2017). An analysis on human precancerous lesions showed that DNA damage response and induction of senescence occurred concurrently. ATM and ATR (ataxia telangiectasia and Rad3-related) kinases together can activate GATA4, which is more expressed in cells undergoing senescence. GATA4 presence can activate NF- $\kappa$ B to initiate production of proinflammatory cytokines and helps in facilitating senescence, indicating its role downstream of DNA damage.

Unlike RAS, AKT promotes rapid proliferative arrest in the absence of a replicative phase and show no sign of DNA damage response. Yet the senescence induced by AKT show activation of p53 and is characterised by mTORC1-dependent thereby increasing p53 translation and inactivation of MDM2 (Astle et al., 2012) and activation of Interferon response and release of cytosolic DNA. The link between DNA damage and Interferon response are interconnected. Interferons are secreted in response to activation of pathogen-associated molecular patterns and acts as anti-viral response. Recent reports demonstrate that IFN-stimulated genes are triggered due to DNA damage response by etoposide, anticancer drugs or irradiation (Moschella et al., 2013).

DNA damage in the nucleus leads to accumulation of micronuclei (cytosolic DNA) which triggers cGAS and produce cGAMP. The product released by cGAS i.e. cGAMP binds and activates Stimulator of IFN Gene (STING). STING then recruit and activate TANK-binding kinase 1 (TBK1) and I $\kappa$ B kinase to activate IFN regulatory factor 3 (IRF3) and NF- $\kappa$ B, respectively in a phosphorylation dependant manner to turn on the production of type I interferons and cytokines (Li et al., 2015). Moreover, production of type I interferons response due to DNA damage trigger cellular senescence and depletion of the IFN  $\alpha/\beta$  receptor 1 (IFNAR1) rescues the senescence phenotypes in *Terc*<sup>-/-</sup> mice. Type I IFNs are also prosenescence and antiproliferative, as they induce DNA damage and elevate the p53 level . The cytosolic DNA mostly contains single-stranded DNA (ssDNA) (Härtlova et al., 2015; Shen et al., 2015; Erdal et al., 2017) and very few of double-stranded DNA (dsDNA) (Shen et al., 2015). ssDNA in general induces very little type I IFNs compared with dsDNA (Ishii et al., 2006) because cGAS doesn't bind ssDNA. Some studies shown that mouse embryonic fibroblasts (MEFs) from *cGas*<sup>-/-</sup> mice displayed reduced signs of senescence and underwent rapid immortalization when compared with MEFs from WT mice. Depletion of cGAS in different mouse or human cells abolished SASP production and interferon production when exposed to DNA damaging agents like including etoposide and ionizing irradiation.

Therefore, the cGAS–STING pathway provides a critical paracrine signal that is necessary for sustaining cellular senescence.

### **Activation of Autophagy during OIS**

Senescent cells are typically metabolically active forever, by displaying enlarged morphology. Originally, autophagy was thought to suppress cellular stress created during senescence and direct them for lysosomal degradation, but on other hand it was shown that autophagy promoted cellular senescence and in aging fibroblasts there is an increase of autophagic vacuoles (Capparelli et al., 2012). Autophagy and senescence are closely related, but there are many questions to be answered regarding the relationships between senescence and autophagy at a molecular level.

Autophagy is a regulatory process where majority of the cells undergo lysosomal degradation, in response for harsh conditions like starvation involved in energy homeostasis.

During senescence, autophagy related genes were upregulated like ATG5 and ATG7 and their depletion via knock out or knock down resulted in escape of senescence, like BRAF OIS is bypassed by ATG5 knock down. However, during senescent phase, a negative regulator of autophagy ie mTOR is switched off and induces senescence in cancer cells (Nam et al., 2013). The ectopic expression of ULK3 induced senescence through autophagy and its inhibition delayed OIS and markers of senescence such as SASP. Additional studies of autophagy in cancer showed that some of autophagic genes are deleted or decreased like in melanoma where the expression of ATG5 and LC3B is decreased (Liu et al., 2014) and in some cancers ATG6 ie Beclin is deleted. However, the relationship between autophagy and senescence is not clear. Autophagy is induced during senescence and its suppression of autophagic genes ATG5 and ATG7 allowed cells to escape senescence and prolonged inhibition of autophagy via knock out or knock down of ATG5 and ATG7 induced cellular senescence, because increased of ROS production and defective mitochondria (Kang et al., 2011).

### **2.2 OIS as a barrier for cancer progression**

Many groups have described the presence senescence markers in neoplastic lesions such as melanocytic nevi, lung adenomas, and hyperplastic prostate tissue (Braig et al., 2005; Michaloglou et al., 2005) indicating that senescence caused by oncogenic activation led to irreversible growth arrest by limiting uncontrolled cell proliferation and acting as barrier for tumour progression. Furthermore, evidence suggested that senescence is observed in premalignant samples but not in malignant samples (Michaloglou C et al., 2005; Collado M et al., 2005; Braig M et al., 2005). Genetic manipulations showed that activation of an oncogene is enough to induce senescence, whereas in mouse model's depletion of tumour suppressors

protein and activation of oncogene lead to aggressive tumours. These studies strongly suggest that senescence act as a barrier to protect from neoplastic transformation of cells *in vivo*.

Taking nevi, as an example several researchers tried to prove OIS acts as a barrier for tumour progression. Nevi are benign melanocytic tumours that generally lack proliferative activity. They commonly harbour BRAF mutation with a single amino acid change (V600E) accounting for most of the cases (H. Davies et al., 2002; P.M. Pollock et al., 2003). These nevi undergo permanent cell cycle arrest, by expressing higher levels of p16 which is a hallmark of OIS (Michaloglou et al., 2005). In addition, there is no sign of loss of telomeres suggesting that nevi have undergone OIS. All these results show that OIS in nevi acts as a barrier to melanoma development (W.J. Mooi et al 2006). Any further mutations in BRAF lead melanoma.

### A Link between OIS and Cancer

Early studies showed that during oncogene induced senescence, the senescence is induced by hyper replicative stress, later it is mediated by DNA double strand breaks which ultimately leads to cell cycle arrest. However, inhibition of cell cycle checkpoints in the presence of oncogenes promoted tumor progression. This provides us an information that in the presence of tumour suppressor genes, oncogenes induce senescence while absence resumes cell proliferation. More importantly, overcoming barrier of senescence would require inactivation of DNA damage pathways and some senescence independent pathways. Once the cell escapes this barrier, oncogenes promote tumor progression by acquiring additional mutations. During senescence some proteins like SASP are secreted and released into extra cellular matrix and presence of these proteins have a significant role in senescence and tumorigenesis.

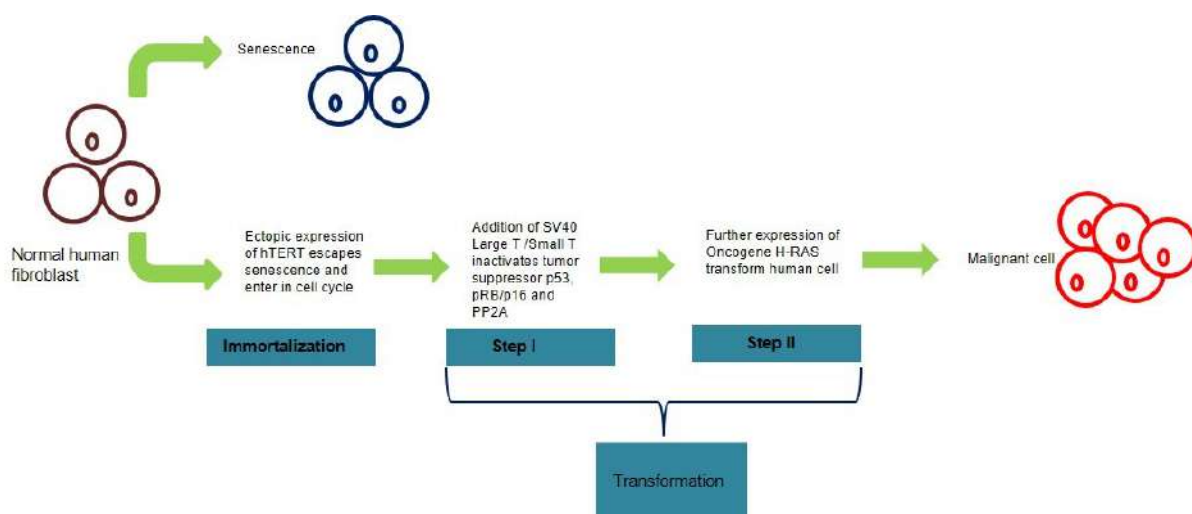


Figure 10: A schematic representation of transformation of human cell *in vitro*

### **3. Transformation**

#### **Molecular mechanisms to bypass Senescence**

Cancer is a complex genetic disease that arises by accumulating specific genetic lesions affecting oncogenes and tumor suppressor genes. These lesions hijack the transcriptional/epigenetic machineries to reprogram the transcriptional profile of the cells with the final goal of sustaining a robust proliferation, invasion and suppressing cell death. Normal human/murine cells proliferate for a limited period and they enter a stage of growth arrest called as Replicative senescence as they lose telomeric DNA which are found at the end of chromosome. To overcome this permanent growth-arrest barrier in *vitro*, researchers made several efforts to immortalize the primary cells by different methods such as ectopic expression of telomerase reverse transcriptase (abbreviated as **TERT**, or **hTERT**), viral oncogenes (Chang S et al., 1982; Rudland P et al., 1989) carcinogenic agents (Stampfer M et al., 1985; Russo J et al., 1993) and radiation (Wazer D et al., 1999).

Tumorigenesis is described as a step-by-step wise process during which the tumor cells must overcome many crises like erosion of the telomeres that are often shortened at every DNA duplication cycle due to the template requirement for DNA polymerase, escaping of DNA damage response due to the replication stress created during cell division, the restraint in blood supply, the increase in energy consumption, the resistance to pro-apoptotic stimuli and the infiltration of immune system cells (Hanahan & Weinberg, 2011).

Here I list some few genetic events that a normal cell should agree to be tumorigenic.

#### **3.1 Immortalization**

One of the hallmarks of tumor cells is the immortalized phenotype (Hanahan and Weinberg 2000). Since immortalization is a major consequence of surviving crisis, telomeres may serve to limit cell lifespan and to provide a defence against unrestrained proliferation. (Klingelutz A et al.,1999). Telomerase is a ribonucleoprotein that maintains the telomeres at the end of chromosomes and helps the cells to escape senescence barrier as a result of telomere shortening. Ectopic expression of hTERT restores functional activity of telomerase in normal human cells like fibroblasts and stabilization of telomeres leads to direct immortalization of cells in cultures (Vaziri H et al.,1998;Bodnar AG et al.,1998;Klingelutz A et al.,1999;Harada H et al 2003). However, this is not true in few cell types like keratinocytes and epithelial cells, where expression of hTERT is not sufficient to immortalize the cells and the full immortalization is achieved by the contemporary inactivation of the retinoblastoma (RB)/p16INK4A pathway. A better understanding of the immortalization process was achieved

by studying Simian Virus 40 (SV 40) Large T or Small T (Hanahan and Weinberg 2000), Adenovirus E1A and human papillomavirus E6 and E7. These viral oncoproteins target and inactivate p53 and pRB pathways, thereby allowing pre-senescent cells to escape senescence barrier like oncogene induced senescence or replicative senescence. Apart from viral oncogenes, tumor suppressor pathways are silenced through abnormal DNA methylation of a CpG islands on the promoters on those genes and there are also some genetic evidences such as overexpression of murine double minute 2 protein (HDM2), that degrade p53 protein and loss of heterozygosity of the p53 locus (JM Stommel et al.,2004). p16INK4A is often methylated in several cancers and overexpression of cyclin D1 often cause inactivation of pRB which resulted in immortalization of epithelial cells. This immortalization is independent from telomerase activity, where the length of telomeres is maintained by Alternative Lengthening of Telomeres (ALT). About 10-15% of human cancers show ALT activity to prevent erosion of telomeres.

### **3.2 Malignant Transformation**

Cancer cells are known to be immortal cells, as they overexpress hTERT or maintain telomere by ALT. Ectopic expression of hTERT in normal cells make them immortal but fail to support anchorage independent growth, contact inhibition and tumorigenesis. In order to be tumorigenic, some additional events are required like inactivation of tumour suppressor genes, activation of oncogenes and in vivo the ablation of immune system (Hanahan et al., 2011).

Since human studies in *vivo* are ethically unacceptable, the use of human cells in *in vitro* conditions represents the historically most used experimental approach (Hahn et al.,1999). Isogenic models proved to be very useful.

Transformation is a step wise process during which several genetic and epigenetic alterations cooperate to acquire the malignancy state. To understand the process of transformation, Hahn and Weinberg described a stepwise tumorigenic model system in which defined genetic changes had been introduced into normal human/murine fibroblasts in order to generate cancer cells (Hahn et al., 2002). Despite the multiple levels of tumour complexity, this genetic model approach has helped us to understand the basic principles involved in cancer development. It helps us to identify the minimal fundamental changes required in different cell types during the transformation.

Actually, at least three hits are required to achieve transformation of human cells, while in rodents two hits are enough. Cells must be immortalized; they must express an oncogene and

turn off p53 and/or p16 tumor suppressors. As a consequence of these manipulation, the tumor cells originated acquire the capability to proliferate in absence of exogenous growth factors

Some other genetic combinations have been successfully implemented in transforming human cells, like expression of mutant form of CDK4 i.e. CDK4R24C which inactivates p53 and with combination of oncogenic RAS, in epidermal keratinocytes led malignant transformation of keratinocytes, and formed tumours in immunosuppressed mice (Lazarov et al., 2002).

Recent evidence suggest that telomerase enzyme activity is not required for initial tumorigenesis under certain conditions. Seger et al demonstrated that co-expression of E1A together with RAS in BJ fibroblasts supported anchorage independent growth *in vitro*. However, these cells are not tumorigenic *in vivo*. In order to be tumorigenic Seger et al overexpressed MDM2 protein that stably degrade p53 protein. Lysates from these cells show lack of telomerase activity. However, these cells undergo crisis either after extended passaging *in vitro* (40–50 population doublings (PDs) or after expansion into culture. Cells which survive this period of crisis show telomerase activity (Seger et al., 2002). Overall, the use of genetic elements to transform human cells *in vitro* did not correspond to pathways altered in human cancer but these studies helped us to understand pathways affected in cancer should also recapitulate *in vitro* tumorigenesis. For example, to understand molecular pathways involved in Oral-Oesophageal carcinoma, Goessel et al developed a genetic model, where primary oral epithelial cells are immortalized *in vitro* with absence of viral oncoproteins, by overexpression of cyclin D1 and subsequent inactivation of p53. This immortalization is dependent on ALT mechanism but not on telomerase activation. Further expression of epithelial growth factor receptor (EGFR) together with c-myc transformed epithelial cells. This model truly copies the pathways altered in human cancer like ALT mechanism.

#### **4 Histone Deacetylases (HDACs)**

Histone acetylation and deacetylation is one of the post-translational modification of transcriptional regulation, which regulates the epigenetic state of the chromatin structure. Histone acetylation and deacetylation is reversible and tightly regulated (Martin, Kettmann, & Dequiedt, 2007). The main epigenetic regulators are the histone acetyltransferases (HATs) and the histone deacetylases (HDACs), histone methyltransferase and demethylases which have opposite functions. Usually, HDACs are found in corepressor complexes thereby removing acetyl groups from histones which results in compact chromatin structure (Delcuve, Khan, & Davie, 2012). More differential is the output of histone methylation that in some cases correlate

with transcription activation (eg H3K4me3), while in other cases mediate gene silencing (eg H3K9me3).

Until now, 18 HDACs have been identified in mammals. They are divided into four classes based on their sequence homology. The class I, II and IV are Zn<sup>2+</sup>-dependent proteins (Gregorette, Lee, & Goodson, 2004) while, the class III is NAD<sup>+</sup>- dependent. The other differences between these classes is their cellular localization and enzymatic activity (reviewed by Martin et al, 2007).

Class I consists of Histone Deacetylases 1, 2, 3 and 8 which show a high degree of sequence similarity with the yeast transcriptional regulator Rpd3. They are ubiquitously expressed and they are located into the nucleus (Martin et al., 2007).

Class II consists of HDAC 4, 5, 6, 7, 9 and 10 which are homologous to yeast Hda1 in *Saccharomyces cerevisiae*. Class II are Zn<sup>2+</sup>- dependent, highly expressed in muscles, bones, neurons, in the endothelium and in thymocytes. Their expression differs from tissue to tissue. Based on structure and function they are divided into two groups, such as Class IIa and ClassIIb. Class IIa consists of HDAC 4, 5, 7 and 9 which often travel in and out of the nucleus and are enzymatically inactive but able to repress some transcription factors which will be discussed later. The Class IIb (HDAC 6 and 10) are enzymatically active on some proteins such as tubulin (Fischle et al., 2002) and are mainly cytoplasmic.

Class III HDACs also called as Sirtuins contains SIRT1, 2, 3, 4, 5, 6, and 7 which are completely different from other classes of HDACs as they are NAD<sup>+</sup>- dependent enzymes. Sirtuins are present in nuclear, cytoplasmic and mitochondrial compartments(Haigis & Guarente, 2006).

The other Class of HDACs is Class IV(HDAC11) which has some properties of class I and of class II HDACs. Until now the role of HDAC11 is not well known (Martin et al., 2007).

### HDACs in Humans

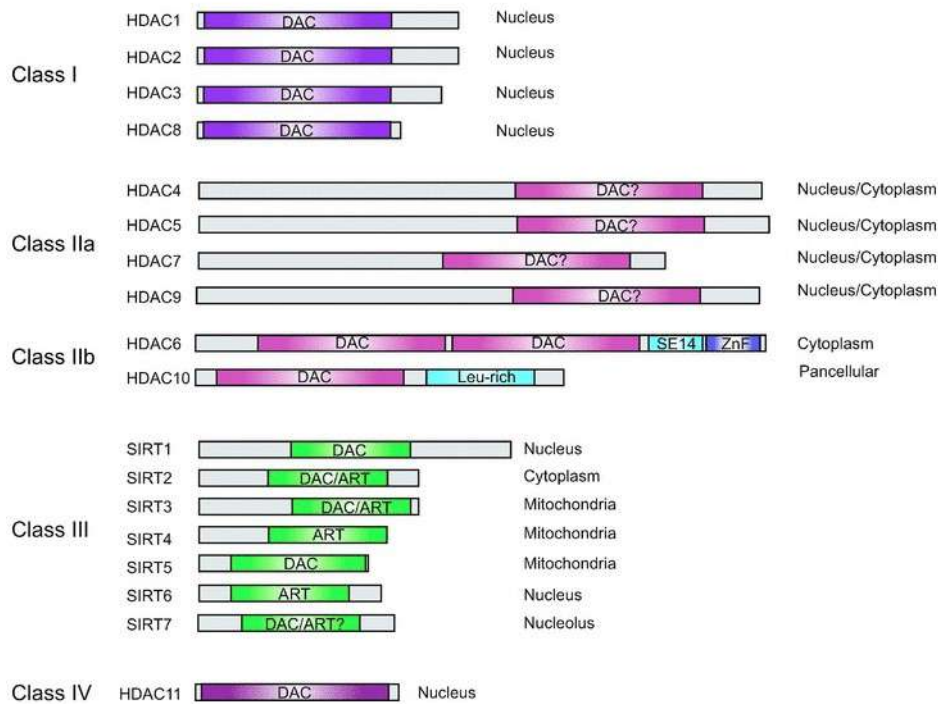


Figure 11: Histone deacetylase family subdivided into different subfamilies according to homologies to yeast prototypes (Clocchiatti A. *et al.*, 2011).

HDACs have been emerged as epigenetic regulators involved in cell growth, differentiation, and apoptotic programs (Bolden et al., 2006 ). Aberrant expression of HDACs are linked to tumour malignancy. Several literatures have demonstrated that HDACs are involved in many human cancers like breast cancer, hematological malignancies, ovarian cancer, endometrial carcinomas (Weichert W et al., 2008). High level expression of HDACs is associated with poor survival rate of patients. For example, high expression of HDAC 1, 2, and 3 cause a poor prognosis in ovarian cancer and gastric cancer patients (Weichert et al., 2008; Sudo et al., 2011) whereas high level expression of HDAC8 is seen in neuroblastoma which correlates with poor survival and advanced stage (Oehme et al.,2009; Rettig et al.,2015). HDACs are also dysregulated in multiple myeloma (MM). Overexpression of HDAC1, is correlated with inferior patient outcomes (Mithraprabhu et al., 2014) and some HDACs like HDAC4 suppress p21 expression and promote tumor survival which is clearly appreciable in colon, glioblastoma and ovarian cancer.

It is also well known that HDAC inhibitors in vitro induce apoptosis and induce cell cycle arrest in colon cancer cell lines and other cancer cell lines (Heerdt et al., 1994 ; Mariadason *et al.*,1997 ; Archer et al.,1998 ; Litvak et al., 1998 ; Mariadason et al., 2000 , 2001b ; Gurvich *et*

*al.*, 2004 ; Wilson *et al.*, 2006 ). Based on these studies, several HDAC inhibitors came into light targeting amino terminus and catalytic domain. Few of them are in clinical trials for the treatment of cancer (Rasheed *et al.*, 2007). Recently few HDAC inhibitors like SAHA are being approved for the treatment of cutaneous T cell lymphoma.

### Structure of Class IIa HDACs

Class IIa HDACs function as transcriptional repressor but they do not recognise DNA, while they interact with some transcription factors and they are recruited on specific genomic regions. There are many important differences between Class I and Class IIa HDACs which will be explained later. Class IIa HDACs are large enzymes (120-135 kDa) in comparison to the other zinc-dependent HDACs apart from HDAC6. Since the early 2000s, it took a lot of effort to understand the biological functions of Class IIa HDACs (Parra, 2015). Knock out of HDAC1, 2 in mouse models results in embryonic and perinatal lethality, (Montgomery *et al.*, 2007) whereas knock out of HDAC4 is viable but the mice die soon after the birth because of skeletal abnormalities, premature ossification and breath problems (vega 2004) .On other hand HDAC4 regulates skeletal muscle differentiation by showing repression activity on myogenic transcription factor, MEF2 (McKinsey *et al.*, 2000 ; Miska *et al.*, 2001). Mice lacking HDAC5 or HDAC9 are vital but are characterized by an exacerbated cardiac hypertrophy triggered by hormonal stress-related signals (Chang *et al.*, 2004). Moreover, HDAC9 knock-out mice are exaggeratedly sensitive to the denervation responses in skeletal muscle (Mejat *et al.*, 2005). HDAC7 *-/-* mice results in embryonic lethality due to severe defects in blood vessels; these are caused by a loss in cell-cell adhesion between endothelial cells (Chang *et al.*, 2006).

The main difference between class IIa and class I, is the presence of an extended amino terminus (N-terminal domain) which is absent in the class I (Yang & Gre, 2005) and mediates the binding with co-factors and co-regulators, like CtBP, HP-1 and TFs, like MEF2, Runx2.

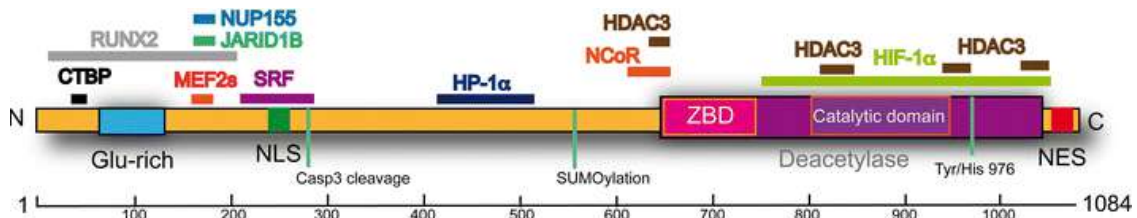


Figure 12: Schematic representation of class IIa HDACs (HDAC4). Different interactors associate with the N-terminal domain of class IIa HDACs such as CtBP, MEF2 or HP1, whereas the C-terminal domain recruits HDAC3-NCOR/SMRT complex to promote Lys deacetylation (Di Giorgio E. *et al.*, 2015).

On the N-terminus domain, there is a nuclear localisation signal (NLS) which play a crucial role in importing Class IIa HDACs into the nucleus and there is Nuclear export signal at C terminus which help to export the protein into cytoplasm. These proteins often move in and out of the nucleus and cytoplasm in a phosphorylation dependant manner, phosphorylation occurs on serine residues present in amino terminus domain. When dephosphorylated, they remain in nucleus, where class IIa HDACs associate with Class I ie HDAC3 and N-CoR/SMRT, forming an enzymatically active protein complex which influences the epigenetic state of a transcription factor.

Class IIa HDACs is enzymatically inactive and they show their function mainly in the nucleus and where they repress some transcription factors. However, cytoplasmic accumulation of Class IIa HDACs also repress few transcription factors like like HIF-1, STAT-1, MEKK2 (Clocchiatti et al., 2013) and DNAJB6/8 complex (Hageman et al, 2010). Still it is mysterious how these HDACs have catalytic activity in the cytoplasm. For example, Class IIa HDACs are nuclear in undifferentiated cells and remain cytoplasm in differentiated cells (McKinsey et al., 2001; Backs and Olson et al., 2006; Mihaylova et al., 2011).

The shuttling of Class IIa HDACs to the nucleus is supported by the presence of the NLS which bind to importin- $\alpha$ , Class IIa are exported into cytoplasm by presence of a NES to bind to CRM1. Both NLS and NES regulate the function of Class IIa HDACs. This rapid kinetics and the high reversibility of the phenomenon led scientists to speculate that the "shuttling" was mediated through phosphorylation and dephosphorylation, as this PTM (post translational modifications) is extremely quick and easily reversible by phosphatases. The goodness of this theory was confirmed in 2000 when multiple experimental evidences joined the nuclear export with the action of CaMKII (McKinsey et al, 2001). Later on, the nuclear import was associated to the activity of the phosphatase PP1 and PP2A (Martin et al 2007; Paroni et al 2008; Kozhemyakina et al 2009). CaMKII was the first known kinase that export Class IIa from the nucleus but now there are other kinases which do the same job as CAMkII. The other supervisors which have opposite action (dephosphorylation and nuclear import) were discovered much later associated to the activity of the phosphatases PP1 and PP2A. The control of phosphorylation of at least three serine residues in HDAC4: S 246, 467, 632; HDAC5: S 259,497,661 HDAC9: S 220, 451, 611 and four serine residues in HDAC7 S155, 181, 321, 446 facilitate the binding with 14-3-3 chaperones (Grozinger and Schreiber et al 2000)

The binding with the 14-3-3 chaperon proteins could mask NLS thereby preventing the interaction with importin- $\alpha$  to impede the class IIa HDACs localisation into the nucleus

(Grozinger & Schreiber, 2000) or unmask the NES and promote the direct interaction with CRM1 (McKinsey et al, 2001). Alternatively, these interactions with 14-3-3 binding site could promote an additional conformational change and the consequent exposition of the NES in the carboxy terminal region that favours nuclear export of Class IIa (Clocchiatti, Florean, & Brancolini, 2011). The mutation of the serine residues into alanine prevent the export from nucleus thereby promoting a super-repressive form of the class IIa HDACs (Clocchiatti et al., 2015) (C. L. Zhang et al., 2002). Here are three possible ways, to import Class IIa in the nucleus i) either by inhibition of the serine/threonine kinases implicated in the phosphorylation of the 14-3-3 sites, ii) the Ser to Ala mutation of these sites, or iii) the activation of phosphatases. All these favour nuclear accumulation of class IIa HDACs and confirm nuclear export of HDACs is dependent on phosphorylation and on 14-3-3 proteins (Grozinger and Schreiber et al 2000; Wang et al 2000; Nishino et al 2008; Paroni et al 2008).

The other regulators of the class IIa HDACs are phosphatases and kinases. The serine/threonine kinases involved in the HDACs shuttling are the calcium/calmodulin-dependent protein kinase family (CaMK). CaMK I and CaMK IV phosphorylate all Class IIa while CaMKII phosphorylate only HDAC4 and export them out of nucleus (T. a McKinsey, Zhang, Lu, & Olson, 2000). The calcium-mediated export of class IIa HDACs is involved in many biological processes such as myogenesis, hypertrophy and neuronal survival (Bolger and Yao et al 2005; Shalizi et al 2006; Metrich et al 2010). In 2005 Bolger and Yao observed that nuclear export of HDAC4 via CaMKII into cytoplasm showed a pro-survival role in granule cells exposed to depolarizing low potassium concentrations (Bolger and Yao, 2005). Later in 2006 it was discovered that this pro-survival effect is due to activation of MEF2 when HDAC4 is exported into cytoplasm (Shalizi et al, 2006).

Moreover PKD (Protein kinase D) a kinase activated by PKC, MARK1 (Microtubule Affinity Regulating Kinase) and MARK2 are important regulators of the Class IIa HDACs localisation (Hanks, 2003). Indeed, two studies reported that PKD1 and PKD3 phosphorylates HDAC5 and HDAC7 on 14-3-3 binding sites (Parra, Kasler, McKinsey, Olson, & Verdin, 2005). As a result, they are exported into cytoplasm inducing chromatin relaxation and activation of MEF2. In order to block nuclear export of HDAC5 a double knock out of PKD1,3 is required. PKD, MARK1 and MARK2, which belong to the same CaMK superfamily, are additional kinases involved in the regulation of class IIa HDACs shuttling (Hanks SK et al., 2003, McKinsey TA et al.,2007). MARK1 and MARK2 are constitutively active enzymes, which phosphorylate the first serine residue of the 14-3-3 binding site localized in the amino-terminal domain (Dequiedt F. *et al*, 2006). Regulation of class IIa HDACs is obtained also by further kinases such as the

Salt inducible kinase 1 and Mirk/dyrk1B kinases that consequently affect myogenic differentiation (Berdeaux R. *et al*, 2007; Deng X. *et al*, 2005). Phosphorylation is not the only post-translational modification which regulates HDACs. As a matter of fact, HDACs are also subjected to proteolytic cleavage (Paroni *et al.*, 2004), sumoylation (Gregoire & Yang, 2006) and ubiquitination (Cernotta, Clocchiatti, Florean, & Brancolini, 2011). The kinase's impact on HDACs localization can be rapidly and efficiently counteracted by phosphatases: the removal of the phosphate groups, catalyzed by PP1 or PP2A, stimulates class IIa HDACs nuclear accumulation and the treatment with some phosphatase inhibitors, such as the calyculin A and the okadaic acid, causes their cytoplasmic accumulation. (Paroni G. *et al*, 2008).

Even though Class IIa are grouped in the family of histone deacetylases they don't have a deacetylase activity as a consequence of a point mutation in the Zn binding site conserved in vertebrates. However, they can repress some transcription factors by recruiting class I HDACs and super-repressive complexes. All the class IIa HDACs are characterised by the presence of a highly conserved HDAC domain at the C-terminus but which is "inactive" or at least inactive on acetyl-lysine (Di Giorgio & Brancolini, 2016). The HDAC domain which is present at C-terminus is important for the binding with HDAC3. As a matter of fact just the SMRT/N-CoR-HDAC3 complexes which are present on the HDAC domain can give an association with HDAC activity of these proteins (Fischle *et al.*, 2002). It has been proposed that class IIa HDACs may not be real enzymes but rather they act as adaptors of repressor complexes (Parra, 2015). HDACs are able to bind acetylated lysine because of a Tyr with Histidine in their catalytic site but anyway class IIa HDACs have negligible intrinsic deacetylase activity (Bradner *et al.*, 2010).

### **Binding partners of Class IIa HDACs**

#### **MEF2 TFs**

To negatively affect the transcription, class IIa HDACs need to bind some macromolecular complexes inside the nucleus (Clocchiatti A. *et al*, 2011). As Class IIa HDACs are unable to bind DNA they need some transcription factors to interact with DNA. Different interactors associate with the N-terminal domain of class IIa HDACs, such as MEF2 (Myocyte Enhancer Factor-2), SRF (Serum Response Factor), RUNX2 (Runt Related Transcription Factor 2), CtBP (C-Terminal Binding Protein 1), or HP1 (Heterochromatin Protein 1). Until now the best binding partners with class IIa HDACs are members of the MEF2 transcription factors family, which regulate differentiation, cell growth and survival (Arnold MA. *et al*, 2007; Li L. *et al*, 2018). MEF2 proteins are members of the MADS-box (Minichromosome maintenance genes

agamous deficient and serum response factor) family of transcription factors (TFs). MEF2 is expressed as a single gene in *Caenorhabditis elegans*, *Drosophila*, and *Saccharomyces cerevisiae*, while in vertebrates (humans) there are four members of MEF2 as MEF2A, B, C and D, which are located on 15q26, 19q12, 5q14 and 1q12-q23, respectively (Potthoff MJ. and Olson EN., 2007).

MEF2 family proteins in all the species share similar N-terminus that contains a highly conserved MADS-box domain and an adjacent MEF2 domain. These domains mediate the homo- and heterodimerization of MEF2 proteins, the binding to a conserved A-T rich DNA consensus sequence, YTA(A/T)4TAR, and the interactions with transcriptional co-factors and co-regulators (Black & Olson, 1998)(T. A. McKinsey, Zhang, & Olson, 2002). The N terminus domain is well conserved among the MEF2 members, on the contrary the carboxyl-terminal regions of MEF2 factors are more divergent and acts as transcription activation domains (TADs), contain the NLS and undergoes splicing events (Potthoff & Olson, 2007) (Lu, McKinsey, Nicol, & Olson, 2000).

MEF2 proteins play a crucial role in the differentiation, morphogenesis, and maintenance of several vertebrate tissues. KO mice of *Mef2a* and *Mef2c* show neonatal and embryonic lethality whereas KO mice of *Mef2B/ Mef2D* were viable. This shows that how these proteins are important during embryogenesis and differentiation (Pon & Marra, 2016).

There are some other evidences that MEF2 is involved in the cell cycle progression by activating CDKN1A transcription. The CDK inhibitor p21 (CDKN1A) is a well-known negative regulator of cell proliferation, under the control of multiple signals. It was demonstrated that MEF2D downregulation was coupled with the reduction of CDKN1A levels, an increase in DNA synthesis and augmented cell proliferation. mRNA levels of MEF2 target genes and of CDKN1A were reduced in cells with impaired MEF2D expression (Di Giorgio, Gagliostro, Clocchiatti, & Brancolini, 2015). In particular, MEF2D binds the CDKN1A promoter at +2.1 kb from the TSS and ChIP experiments proved that HDAC7 bound preferentially the same region of the MEF2-binding site (Clocchiatti et al., 2015). The action on P21 expression made by HDAC7 and MEF2 confirm the strong cooperation between them.

Class IIa HDACs contain a conserved region among the HDACs fundamental for the MEF2 binding and these sequence correspond to the glutamine rich-region (Lu et al., 2000). HDAC7 lack of this region but the presence of two leucine permit the interaction with MEF2 (Dressel et al., 2001)

## **Class IIa HDACs in Cancer**

Class IIa HDACs are frequently upregulated in cancer. The first demonstration of HDAC4 proliferative effects comes into the light after making a knock-out mouse for HDAC4 <sup>-/-</sup>. HDAC4<sup>-/-</sup> mice die because of premature and ectopic endochondral ossification, which determines their suffocation (Vega et al 2004). This phenotype is somewhat similar to over-expression of MEF2C and RUNX2 (Vega et al 2004; Arnold et al 2007). On the contrary, HDAC4 over-expression slows-down the process of ossification and prevents chondrocytes hypertrophy (Vega et al 2004).

In 2003 Kao and colleagues demonstrated that reduced expression of HDAC4 in HeLa cells by siRNA, lead them to a decrease in cell viability. Later it was reported that, HDAC4 and p53 co-localized upon DNA damage response (Basile V et al 2005). By using immunoprecipitation assay, they found that HDAC4 interacts with p53 (Kao GD et al 2003). However, some studies reported an opposite effect concerning with reduced levels of HDAC4 decreased cell viability. For example, in urothelial cancer cells, inhibition of HDAC4 expression delayed cell proliferation but not decreased cell growth (Kaletsch A, et al 2018). A study conducted by Cadot and colleagues investigated the effects of HDAC4 on cell cycle progression by making a knock-out / knock-down of HDAC4 in normal and tumor cells. The knockdown of HDAC4 in HeLa cells negatively impacted the cell cycle progression leading to mitotic arrest and apoptosis. During apoptosis, HDAC4 (Paroni et al 2004) and HDAC7 (Scott FL et al 2008) are cleaved by caspases.

In some cancers like gastric cancer, HDAC4 typically acts as an oncogene (Kang et al 2014). HDAC4 mediates the repression of p21 and silencing of HDAC4 resulted in decrease of cell proliferation in gastric cancer cell lines by increasing p21 levels and arresting the cells in G1. HDAC4 silencing in those gastric cancer cell lines also increased autophagy and apoptosis rate; suggesting that most HDAC4-mediated effects are due to p21 de-regulation (Kang et al, 2014). Repression of p21 by HDAC4 is dependent on SP1 transcription factor, which were recruited to Sp1/Sp3 binding site of the p21<sup>WAF1/CIP1</sup> promotor (Mottet D et al 2009). As HDAC4 is enzymatically inactive, some additional binding partners are needed to mediate the repression of p21<sup>WAF1/CIP1</sup> expression. One of the binding partners with Class IIa HDACs are Class I which are present at the catalytic site and probably may be recruited to the site (Fischle W et al 2002). Later it was proved that HDAC4 associates with the HDAC3-NCoR/SMRT complex to mediate the suppression of p21<sup>WAF1/CIP1</sup> expression in colon cancer cells. Another study conducted by Geng et al in non-small cell lung cancer showed that when cells exposed to

irradiation (IR), HDAC4 translocate from cytoplasm to nucleus. Treating the cells with pan-HDAC inhibitors (panobinostat) reversed the location of HDAC4 in response to IR (Geng L et al 2006). It is interesting to address one question, in the presence of DNA damage response whether inhibiting HDAC4 leads to cytoplasmic accumulation.? To answer this a selective class IIa HDAC inhibitors are required. Panobinostat exported HDAC4 even in the presence of irradiation (IR), this could be due inhibition of HDAC3. A study reported that NLS independent nuclear import of HDAC4. The N terminus part of MEF2 interact with HDAC4(aa 1-208) and deletion of MEF2 binding site in HDAC4 domain abrogated interaction with MEF2 (Chan et al 2003).

Studies from Stronach et al. showed that there is a link between the HDAC4 and resistance of platinum-based DNA damaging drugs. They have screened 16 tumor biopsies of ovarian cancer, before and after the development of resistance to platinum-based drugs. Curiously 44% of platinum resistant tumour biopsies showed a huge upregulation of HDAC4 (Stronach EA et al 2011). This resistance could be due to acetylation status of STAT1. Silencing of HDAC4 in platinum-resistant cell lines increased acetylation of STAT1 (Stronach EA et al 2011) and cells were sensitive to the treatment of cisplatin.

Presence of high-level expression of HDAC7 in lung cancer correlates with a poor survival rate in patients. This is because of deacetylation of STAT3 by HDAC7 results in inhibition of STAT3 activity. However, knock down of HDAC7 in endothelial cells effected the migration properties by decreasing angiogenesis (Mottet D et al 2007). In pancreatic tumours, there is a high expression of HDAC7 in the cytoplasm (Ouaïssi M et al 2008). Presence of high-levels of HDAC7 and HDAC9 contributes to a poor prognosis in acute lymphoblastic leukaemia (ALL) (Moreno DA et al 2010). HDAC7 regulates cell proliferation in tumour cell by upregulating strong oncogene MYC and downregulating tumour suppressor proteins like p21 and p27. On other hand in B-cell malignancies there is a low expression of HDAC7. Overexpression of HDAC7 in these cells leads to downregulation of c-Myc and promotes apoptosis (Barneda-Zahonero B et al 2015). Silencing of HDAC7 led to withdraw from cell cycle and triggered senescence (Zhu C et al 2011).

Another protein that is frequently upregulated in cancer is HDAC9. In breast cancer cell lines presence of high level of HDAC9 decrease apoptosis and increase cell proliferation. A recent study from Di Giorgio et al 2019, demonstrated that presence of high level of HDAC9 in high grade leiomyosarcoma contribute to a worse survival rate in patients. Simultaneously, knock

out of HDAC9 in those cell lines resulted in triggering apoptosis by extrinsic pathways. This is because HDAC9 repress FAS gene, an initiator of apoptosis (Di Giorgio et al 2019).

A spliced isoform of HDAC9 i.e. MITR (lacking c-terminus) is expressed in lung, skeletal muscle and in adult and fetal brain, although they are considerably more abundant in fetal tissue (Petrie K. *et al* 2003). Further inspections in hematopoietic cell lines show that HDAC9 isoforms are differentially expressed in the B cell lineage and cell lines derived from B cell tumors. HDAC9 is generally expressed in pre-B cell acute lymphoblastic leukemia cell lines, B cell lymphoma cell lines and in the plasma cell line U-266. HDAC9 is also expressed in some T cells and in particular in T cell leukemia cell line MOLT-3 express MITR.

However, all these studies show that Class IIa HDACs are involved in oncogenesis process. Therefore, further novel compounds/inhibitors should be generated targeting specific domains which are present on HDAC sites.

## Material and Methods

### Cell cultures and reagents

The human foreskin fibroblasts BJ/TERT cells received from CRO AVIANO were cultured in Earle's salts minimal essential medium (EMEM) and human leiomyosarcoma cell lines SK-LMS-1 were cultivated in Dulbecco modified Eagle medium (DMEM) (Euroclone, Milan, Italy) and completed with 10% FBS, L-glutamine (2 mM), penicillin (100 U·mL<sup>-1</sup>), and streptomycin (100 µg·mL<sup>-1</sup>) (Lonza, Basel, Switzerland). In addition EMEM is supplemented with nonessential amino acids (HyClone, Little Chalfont, UK ). All the cells were grown at normoxic conditions at 37 °C with 5% of CO<sub>2</sub>. Cells expressing the inducible form of Estrogen receptor were grown in a medium without phenol red and the serum is stripped with charcoal. All transgenes which are pre-transformed and transformed were cultured in EMEM.

### BrdU (Bromodeoxyuridine) assay

Cells were grown for 3h with 100µM BrdU and then fixed with 3% paraformaldehyde and permeabilized with 0.1% Triton X-100. Incubation with HCl (1N) for 10 min on ice permits to break open the DNA structure of the labelled cells. This is followed by HCl treatment (2N) for 10 min at RT and then the cells are incubated at 37°C for 20 min. After acid washes, borate buffer (0.2M) is added to buffer the cells before the incubation of the mouse anti-BrdU antibody (Sigma-Aldrich). Secondary antibodies (AlexaFluor 488 or 533) were used for the detection. Nuclei were stained with Hoechst 33258 (Sigma-Aldrich).

### Invasion and random motility assays

To understand the transformation process in vitro we have performed Invasion assay and Soft agar Assay. For soft agar assay, equal volumes of 1.2% agar and DMEM were mixed to generate 0.6% base agar. A total of  $0.5 \cdot 10^5$ /ml sarcoma cells were seeded in 0.3% top agar and incubated at 37°C. The cells were grown for 21 days changing the culture medium twice per week. Foci were evidenced with MTT staining and counted by using ImageJ.

For invasion assay, each well of the invasion chamber (CLS3428, Corning) was coated with 200µl of Matrigel matrix coating solution (Cultrex, Trevigen). Next, a cell suspension of  $0.5 \cdot 10^5$ /ml cells in 0.1% FBS-DMEM was added. As chemoattractant, 20% FBS-DMEM was added in each lower chamber. As a control 0.1% FBS-DMEM was used to evaluate random invasion. After 16h cells were fixed and stained with Hoechst. 5 random field were counted. Random motility was analysed by time-lapse video microscopy, as previously described (Cernotta N. *et al*, 2011).

### **Cloning and Plasmid construction, transfections, retroviral infections**

The stable expression of pWZL/HDAC4-WT and mutants, pWZL-Neo/E1A (1–143) and pBABE-Puro/myristoylated AKT1 (myr-AKT1) expressing plasmids were generated by cloning. pWZL-HDAC4-TM $\Delta$ MEF2 was generated in two steps. The N-terminus (aa 1 to 166 and aa 184 to 221) was generated by PCR and cloned into pcDNA3.1 (*EcoRI/ BamHI* and *BamHI/Sall*). Finally, fragment 1-221 was subcloned into pWZL-HDAC4-TM-GFP restricted by using *Eco-Sall* (Di Giorgio *et al* 2013). pCW-Puro/HDAC4 and H-RAS/G12V plasmids were generated by subcloning with a PCR amplification and digested with restriction enzymes and cloned into DOX-inducible pCW-Cas9 plasmid (#50661 Addgene, Cambridge MA, USA). pMXPIE-Puro HDAC4-WT/TM, H-RAS/G12V were obtained by subcloning with a PCR method the ORF into the 4 hydroxy-tamoxifen (4-OHT)- inducible pMXPIE plasmid (Toledo *et al* 2008). Apple 53bp1 truncated (69531) plasmid was purchased from Addgene and subcloned into pWZL hygro vector by digesting with restriction enzyme (*BamHI/Sall*). pBabe puro H2B GFP (26790) was purchased from Addgene. pLKO plasmids (15 and 27) expressing shRNAs directed against hMEF2D were obtained from Sigma-Aldrich. For lentivirus-based knock-down, HEK-293T cells were used and transfected with 1.8  $\mu$ g of VSV-G, 5  $\mu$ g of  $\Delta$ 8.9 and 8  $\mu$ g of pLKO plasmids. After 12 hours of transfections, virus is collected later 24 hours at 37 °C and diluted with new medium and infected the cells. Later, the cells are selected for puromycin resistance. Retroviral infections were performed at 32 °C and virus is collected after 48 hours and used to infect the cells (Di Giorgio *et al* 2013).

### **Immunoblotting**

The protein sample preparation required a first SDS denaturing cell lysis in presence of protease and phosphatase inhibitors and of  $\beta$ -mercaptoethanol to reduce the intra and inter-molecular disulfide bonds. Protein samples were sonicated and heated in boiling water for 5 min before the electrophoresis. Proteins were then transferred to a 0.2 $\mu$ m pore-sized nitrocellulose membrane (Protran, Amersham) by an electroblotting device. Blocking of non-specific binding was achieved through incubation with non-fat dry milk in tris-buffered saline (TBS) with the 0.1% of Tween 20. Blots were incubated with primary antibodies (1h at RT or overnight at 4°C). After washes, blots were incubated with peroxidase-conjugated goat anti-rabbit or goat anti-mouse (Sigma-Aldrich) for 1h at RT. Secondary antibodies (Sigma-Aldrich) were developed with Super Signal West Dura (Pierce Waltham). For primary antibody stripping, blots were incubated for 30 min at 60°C in stripping solution (62.5mM Tris-HCl pH 6.8, 2% SDS) containing 100mM  $\beta$ -mercaptoethanol (Sigma-Aldrich).

### **RNA extraction and quantitative qRT-PCR**

Cells were lysed and homogenized directly on the culture dish by using TRI-REAGENT (Sigma-Aldrich). 1.0 µg of the total isolated RNA was retro-transcribed by using 100 units of M-MLV (Moloney Murine Leukemia Virus) Reverse transcriptase (Life Technologies). qRT-PCRs were performed using the Bio-Rad CFX96 real-time PCR detection system and SYBR green (KAPA Biosystems) technology. Data were analysed by comparative threshold cycle using the expression levels of two housekeeping genes, HPRT (hypoxanthine phosphoribosyl transferase) and GAPDH as normalizer genes. All reactions were done in triplicates.

### **Antibodies**

Antibodies used were against HDAC4 is produced in the laboratory (Paroni *et al* 2004) (MEF2D (BD Bioscience), H3K27ac (ab4729; Abcam, Cambridge, MA, USA). H3K27me3 (ab195477, Abcam)  $\gamma$ H2AX (9718, Cell Signalling, Leiden, The Netherlands), TP53 (DO-7; Dako, Santa Clara, CA, USA), LT SV40 (sc-147, Santa Cruz), Lamin B1 (ab16048, Abcam), p21 (CP74, Sigma), RACK1 (sc-17754, Santa Cruz, Dallas, TX, USA), GFP (Paroni *et al* 2004).

### **Immunofluorescence and *in vivo* time lapse assay**

Cells were seeded at  $0.8 \times 10^5$ /ml and then they are fixed with 3% paraformaldehyde and permeabilized with 0.1% Triton X-100. Secondary antibodies used were Alexa Fluor conjugated 488, 546 and 633 (Molecular Probes). Actin was labeled with Phalloidin-AF546 (Molecular Probes). Nuclei were stained with Hoechst 33258 (Sigma). Imaging was performed with a Leica confocal scanner SP equipped with a 488  $\lambda$  Ar laser and a 543 to 633  $\lambda$  HeNe laser. For *in vivo* time lapse assay, cells expressing H2B GFP and apple 53BP1 truncated were seeded on a time lapse petridish and further processed for time lapse assay.

### **CRISPR/Cas9 technology**

CRISPR/Cas9 technology was applied to generate HDAC4 knock out clones in SKLMS-1. Two sgRNA (CACCGCCGATGCCCGAGTTGCAGGT, CACCGTAGGGAATGCCGGGCTGTT) were lentivirally delivered and positive clones were selected. After selections, clones were screened by PCR and immunoblot. Sanger sequencing was applied for the final validation

### **SA- $\beta$ -gal assay**

For SA- $\beta$ -gal assay, cells were fixed in a solution of 2% formaldehyde/0.2% glutaraldehyde and stained with staining solution: 40 mM citric acid/Na phosphate buffer, 5 mM  $K_4[Fe(CN)_6] \cdot 3H_2O$ , 5 mM  $K_3[Fe(CN)_6]$ , 150 mM sodium chloride, 2 mM magnesium chloride and 1 mg  $\cdot$  mL<sup>-1</sup> X-gal (Debacq-Chainiaux *et al.*, 2009). Staining was performed for

16 h at 37 °C and cells were imaged under bright-field microscope (Leica). To quantify SA- $\beta$ -gal activity, the percentage of positively stained blue cells versus total cells were counted (300–400 cells in total were counted per each round).

### **Matrigel plug assay**

A total of 1600 cells were seeded in a Matrigel solution which composes of 20  $\mu$ L 0.1% FBS-EMEM, 60  $\mu$ L Matrigel. The cells are seeded on coverslips in 35-mm tissue culture plates. After 30 min of incubation at 37 °C, cells were supplied with EMEM of 20% FBS. After 4-days of incubation, coverslips were fixed and processed for Immunofluorescence analysis.

### **Transcriptome profiling and data analysis**

Total RNA was isolated using Direct-zol RNA mini prep (Zymo Research). Preparation and hybridization of cRNA samples were performed at Cogentech (Milan, Italy, <https://www.cogentech.it/>). Labeled cRNAs were hybridized on Affymetrix GeneChip Human Clariom S arrays. Differentially expressed genes (DEGs) were selected based on 1.5 cut-off in the fold changes. Analysis was performed as previously described (Di Giorgio *et al* 2013; Picco *et al* 2014). Gene set enrichment analysis (GSEA) (Subramanian *et al* 2005) and the MSigDB database (<http://software.broadinstitute.org/gsea/index.jsp>) (Liberzon *et al* 2015) were used to investigate statistical association between genes modulated by HDAC4-TM or RAS and genes perturbed by other conditions.

### **Data retrieval and analysis**

The transcriptional profiles of the three isogenic transformation models were obtained by re-analyzing the datasets GSE17941 (Hirsch *et al* 2010), GSE72530 (Malysheva *et al* 2016) and GSE120040 (Paluvai *et al* 2018) deposited as raw files in GEO (Gene Expression Omnibus). The CEL files were processed with affy package in R (Gauthier *et al* 2004). Multiple callings coming from redundant probes were reduced to a single signal per gene by using Unigene ID centered CDFs (Chip Description Files) retrieved from the Molecular and Behavioral Neuroscience Institute Microarray Lab (URL:[http://brainarray.mbni.med.umich.edu/Brainarray/ Database/ CustomCDF/genomic\\_curated\\_CDF.asp](http://brainarray.mbni.med.umich.edu/Brainarray/Database/CustomCDF/genomic_curated_CDF.asp)) (Dai *et al* 2005). RMA algorithm was used for normalization (Irizarry *et al* 2003). In the three datasets selected, the hybridization was done on three different Affymetrix chips (platforms HG-U133A\_2, HuGene-1\_0-st-v1 and Clariom.S). For the identification of differentially expressed genes (DEGs), the limma package (Ritchie *et al* 2015) was used. The calling of significance was based on a 1.5 fold change/FDR<0.05 criteria. In each dataset, the transformation model represented by pre-transformed BJ cells expressing RAS G12V (GSE17941) or c-MYC (GSE72530) or HDAC4

(GSE120040) was compared to the pre-transformation model which is represented by BJ fibroblasts expressing hTERT, LT and ST SV40 genes.

### **Enrichment analysis**

The “HALLMARK” collection of 50 gene sets deposited in the Molecular Signatures Database (MSigDB) (subject) was interrogated with the three DEG lists generated (query). The MSigDB analysis tool (Broad Institute (<http://www.broadinstitute.org/gsea/msigdb/index.jsp>) algorithm was used to score the overlap between queries and subjects. The identified hits were ranked by the enrichment score and the p-value (FDR < 0.05) (Daly et al 2003, Subramanian et al 2005).

### **Generation of the signatures of transformation**

The signature of the induced genes includes three genes that were significantly upregulated in the three selected models of transformation. The signature of the repressed genes includes 13 genes commonly down-regulated in the three models of transformation. This signature was further sub-divided in sub-signatures A and B, where A includes 6 genes that do not belong to the HALLMARK gene sets “inflammation” and “interferon response” and B includes the other 7 genes.

### **Analysis of survival**

mRNA expression data coming from RNAseq studies and normalized by the expectation-maximization (RSEM) method and patients’ clinical data about 32 cancer studies were retrieved from TCGA, using the R package *cgdsr* (Ritchie et al 2015). Hits corresponding to patients with incomplete expression or survival data were discarded. The Kaplan-Meier survival analysis was performed by using the survival package in R (Jacobsen A et al 2015).

### **Estimation of the contribution/perturbation of the immune infiltration to the survival analysis**

The infiltration of immune cells in the tumor biopsies was evaluated by using MCP counter method (Becht et al 2016). Briefly, immunological signatures were retrieved by using the R package *MCPcounter*. The previously described dataset of 11424 samples was interrogated with these signatures and each sample was associated to the median value of expression of each signature. According to these values, patients were segregated in two groups and the Kaplan-Meier method was applied to calculate the survival rate. To evaluate the contribution/disturbance of the inflammatory infiltrate to the prediction of survival based on the transformation signatures, patients were divided in 4 groups accordingly to the expression levels of genes belonging to the *MCPcounter* signatures and to the transformation signatures: high-high (high levels of both), high-low (high MCP/low transformation), low-low (low levels of both) or low-high (low MCP-high transformation). The ‘*survfit*’ function and the

“survdiff” function were used to generate the Kaplan-Meier curves and to calculate the significance.

### **Statistics**

For experimental data Student t-test was employed. Mann-Whitney test was applied when normality could not be assumed.  $p < 0.05$  was chosen as statistical limit of significance. For comparisons between samples  $> 2$  Anova test was applied, coupled to Krustal-Wallis and Dunn's Multiple Comparison Test. We marked with \*  $p < 0.05$ , \*\*  $p < 0.01$ , \*\*\*  $p < 0.001$ . Unless otherwise indicated, all the data in the figures were represented as arithmetic means + the standard deviations from at least three independent experiments.

## Results

### 6.1 Senescence Induced by HDAC4

#### **Expression of nuclear mutant of HDAC4 in BJ-hTERT fibroblasts triggers senescence**

To investigate the role of HDAC4 in human fibroblasts, we used foreskin derived BJ fibroblasts, which are immortalized with hTERT. Presence of hTERT in the cells allow them to bypass replicative senescence. A set of conserved serine residues, once phosphorylated act as docking sites for 14-3-3 binding sites and mediate export of HDAC4 from the nucleus into the cytoplasm, thereby limiting repressive potential of deacetylase. Since HDAC4 often travels in and out of the nucleus in a phosphorylation-dependent manner, a nuclear mutant of HDAC4 (HDAC4-TM) was generated (Di Giorgio *et al* 2013) which is defective in 14-3-3 binding sites. Dephosphorylation of 14-3-3 binding sites or Ser/Ala mutations or the activation of phosphatases allow strong nuclear accumulation of HDAC4 protein.

Expression of HDAC4-TM in NIH 3T3 cells induces cell transformation and is capable to form tumors when injected in nude mice (Di Giorgio *et al* 2013). However, nuclear accumulation of HDAC4 shows a strong repressive activity on MEF2 transcription factor, and additional nuclear mutants were tested i) which lack MEF2 binding site (HDAC4-TM $\Delta$ MEF2), ii) and a mutant which has a mutation on nuclear export signal (HDAC4-L1062A), which reside in the nucleus similarly to the HDAC4-TM (Di Giorgio *et al* 2013) show less transcriptional repressive activity on MEF2 (Figure 13A).

BJ-hTERT fibroblasts were infected retrovirally with all the mutants of HDAC4 and as positive control also with RAS and AKT. Expression of strong oncogenes like RAS, MYC and AKT in normal human fibroblasts induces senescence and this is described in the part of introduction (Oncogene induced Senescence). After positive selection of retroviral infections, HDAC4-TM triggers senescence which is similar to RAS and AKT. Presence of senescence was confirmed by SA- $\beta$ -gal staining, a marker of senescence (Figure 13B). While other two nuclear mutants HDAC4-TM $\Delta$ MEF2 and HDAC4L1062A show moderate staining to SA- $\beta$ -gal, HDAC4 WT is largely cytoplasmic and didn't contribute to senescence like negative control GFP. One reason could be HDAC4 TM is able to bind for a longer time to the chromatin in respect both to the wild-type form and to a nuclear resident form of HDAC4 mutated in the *nes* (L1062A, Paroni *et al*, 2008).

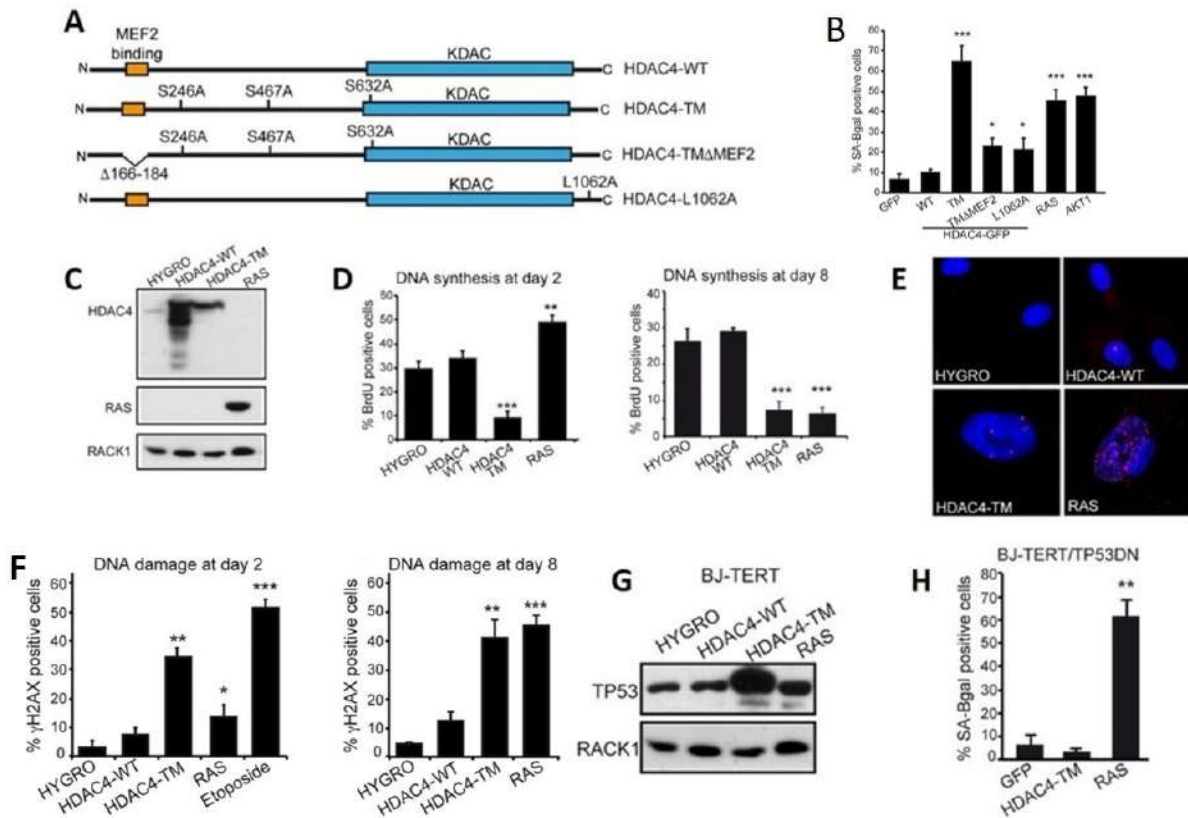


Figure 13: Expression of HDAC4-TM in BJ-hTERT fibroblasts triggers senescence. (A) Schematic representation of HDAC4 mutants used in this study. Phosphorylated serine residues, binding sites for 14-3-3 proteins are indicated. (B) AKT,RAS two well known oncogenes were used. Quantitative analysis of SA- $\beta$ -gal positive cells. Data is expressed as means SD,  $n = 3$ . Student  $t$ -test: \* $P < 0.05$ , \*\* $P < 0.01$ , \*\*\* $P < 0.005$ . (C) Immunoblot was performed after 48 hours of treatment with tamoxifen. RACK1 was used as a loading control. (D) Analysis of cell proliferation assay at DAY 2 and DAY 8, as scored after BrdU staining at the indicated times. Data are expressed as means  $\pm$  SD,  $n = 4$ . Student  $t$ -test: \*\* $P < 0.01$ , \*\*\* $P < 0.005$ . (E) Cells were treated for 2 hours with Etoposide (10 $\mu$ m) and fixed and stained with H2A.X antibody: two phenotypes were observed (i) nuclei in HDAC4-TM and RAS-expressing cells were larger than in control and HDAC4-WT cells; (ii) nuclei of TM cells showed fewer but bigger H2AX-positive foci than RAS cells. (F) A DNA damage analysis was performed at day 2 and day 8. HDAC4-TM showed early induction of DNA damage at day 2, while RAS expressing cells, showed a DNA damage response after 8 days of induction (G) BJ-hTERT fibroblasts expressing HDAC4-TM showed huge activation of p53 when compared with RAS at day8 . (H) Quantitative analysis SA-  $\beta$ -gal staining for cells expressing dominant negative of p53.

As HDAC4-TM cells undergo senescence, an inducible system is required. We have generated all the transgenes fused to Estrogen receptor alpha (Figure 13C). Presence of tamoxifen induces the expression of transgenes. After adding tamoxifen to the cells, we analysed cell proliferation assay at different time periods (day2 and day8). HDAC4-TM blocked DNA synthesis at day2 and showed low DNA replication capacity (which is detected by BrdU incorporation) and stained positive for SA- $\beta$ -gal, while HRAS on day2 is in proliferative phase

and showed negative staining for SA- $\beta$ -gal and positivity for BrdU incorporation. As reported by others, longer induction of HRAS causes cell-cycle arrest and senescence (Figure 13D).

To exclude any contribution of tamoxifen to senescence, we generated a TET-ON doxycycline inducible system. In the presence of doxycycline HDAC4-TM triggered a permanent growth arrest similar to RAS and AKT which was confirmed by staining of SA- $\beta$ -gal (Data not shown here, included in the paper Paluvai et al 2018).

The major difference between RAS and HDAC4-TM is early induction of cell cycle arrest, which is clearly seen in HDAC4-TM. As RAS expressing cells show a boost in cell proliferation during initial days and later undergo senescence due to replication stress created by RAS. Therefore, two different time periods (day2 and day8) were chosen to analyse the DNA damage response triggered by two oncogenes (Figure 13F-G). After 2 days of induction with tamoxifen, HDAC4-TM-expressing cells showed an accumulation of DNA damage, while RAS expressing cells, showed a DNA damage response after 8 days of induction with tamoxifen (Figure 13E). Our single cell analysis showed that  $\gamma$ H2AX-positive foci formed by HDAC4-TM are bigger than RAS, while nuclei of HDAC4-TM and RAS are quite bigger than control and HDAC4 WT cells (Paluvai et al 2018).

During cellular senescence, there is a constant activation of DNA damage response which ultimately activates p53. Cells expressing nuclear mutant of HDAC4 show stabilization of p53 in response to DNA damage. After 2 days of induction with tamoxifen, an Immunoblot was performed on the cells expressing HDAC4-TM and cells expressing RAS at day 8. As shown in figure 13G there is a massive upregulation of p53 in HDAC4-TM cells at day 2, when compared to RAS expressing cells at day 8 (Figure 13G).

To investigate the contribution of p53 in HDAC4-TM-induced senescence, p53 responses were abrogated by expressing a dominant negative form of p53 (R175H) (Figure 13H) (Gualberto *et al* 1998). The dominant negative effect was clearly appreciable on p53-target genes such as *DEC1* and *GADD45A* (Paluvai et al 2018). Later, cells expressing BJ-hTERT/p53DN GFP together with HDAC4-TM and RAS were generated. Depletion of p53 in HDAC4-TM expressing cells resulted in bypass of senescence (Figure 12H) while RAS underwent senescence even in the presence of DN of p53. This suggests us that further hits are required to escape RAS but not HDAC4-TM induced senescence (Brookes *et al* 2002; Huot *et al* 2002).

To sum up, HDAC4-TM induces senescence in BJ-hTERT fibroblasts and this senescence is dependent on p53 activation. Abrogation of p53 in BJ-hTERT HDAC4-TM cells resulted in escape of senescence and enter in cell cycle progression.

## **Oncogenic mediated Transformation**

Oncogenes have two different roles in human cells, they can induce senescence and are able to transform the cells. In order to transform human cells multiple hits are required as in respect to murine cells they are more resistant to transformation process. Transformation of human/murine cell can be achieved by presence of viral oncogenes like SV40, E1A or exposing them to carcinogens.

### **6.2 Transformation of BJ-hTERT fibroblasts by HDAC4-TM**

Class IIa HDACs are often dysregulated in human cancer and promote tumorigenesis *in vivo*. To prove the oncogenic properties of HDAC4 an *in vitro* transformation assay was performed. As HDAC4-TM cells escape senescence in the presence of DN environment of p53, an *in vitro* transformation assay was performed to observe transformation process in the absence of p53 (Paluvai et al 2018). Presence of DN p53(p53 R175H) in HDAC4-TM cells poorly supported oncogenic transformation, this suggest us that why human cells are resistant to oncogenesis and why further genetic alterations pathways are required to transform the cells.

Next BJ-hTERT fibroblasts were pre-transformed by viral oncogene Simian Virus 40 (SV40). It was reported by many groups that SV40-Large-T-antigen pre-transforms human cells and immortalise them. A pool of cells were generated with a combination of BJ-hTERT/SV40-LT alone and with a combination of HDAC4-WT, HDAC4-TM and RAS (Figure 14A). Presence of Large T antigen in the cells allowed them to escape senescence and stained negative for SA- $\beta$ -gal assay a marker of senescence (Figure 14B-C). After growing the cells for 21 days with 20% FBS, cells were stained with MTT to visualise the foci formation (Figure 14D). The diameter of each foci was measured (according to Cifone and Fidler.,1980 model) and classified them into three groups based on their diameter of foci formation like 0-50 $\mu$ m, 100-150 $\mu$ m and >150 $\mu$ m (Figure 14E). HDAC4-TM and RAS showed colonies more frequently smaller than 50- $\mu$ m diameter and very rarely big colonies of diameter >150 $\mu$ m appeared (Figure 14E). More interestingly small colonies were also observed in HDAC4-WT (Figure 14D). Based on our experimental data, HDAC4-TM and RAS transformed the cells but a mild transformation was supported by HDAC4-WT.

To confirm that cells were malignant in the presence of HDAC4-TM we performed an Matrigel Invasion assay to score the random motility and invasiveness. As expected HDAC4-TM increased the random motility. Both HDAC4-TM and RAS promoted invasiveness when compared with BJ-hTERT LT (Paluvai et al 2018).

Next, in order to achieve full transformation, we have introduced Small T antigen together with Large T antigen (Figure 14F). Expression of Large T antigen and small T drastically enhanced transformation. Next clones were generated with a combination of both T antigens together with HDAC4-WT, HDAC4-TM and RAS as a positive control. After growing for 21 days in soft agar, cells were stained with MTT to score the foci formation (Figure 14G).

After staining with MTT, we have divided them into three groups similar to Large T expressing clones alone (Figure 14H). Quantitative analysis proved that the expression of the Small T antigen together with Large T antigen increased efficiency of number of foci and increased the size of foci dimensions (Figure 14H). The combinations of SV40 T antigens increased the efficiency of transformation when compared with the presence of Large T antigen only. We have noticed that HDAC4-TM increased the efficiency of invasiveness in soft agar which we could clearly see with their branching out in soft agar. HDAC4 WT also supported anchorage independent growth but at a less potent when compared with HDAC4-TM. This shows that HDAC4 favours cell transformation but nuclear mutant of HDAC4 achieves an enhanced transformation efficiency.

To confirm the invasiveness properties elicited by HDAC4-TM and RAS we have performed Random motility and Invasion assay. This experiment supports that HDAC4-TM is invasive (Paluvai et al 2018). Later we performed Matrigel assay on cells expressing BJ-hTERT LT/ST and HDAC4-TM and RAS. For this experiment we seeded cells on Matrigel surface to provide 3D growth. Only the cells which are invasive supported 3D growth and Immunofluorescence was performed by staining cytoskeleton with actin using phalloidin 546 (Figure 14I). Hence both HDAC4-TM and RAS supported the growth in Matrigel showing strong invasiveness behaviour.

All our data suggest us that HDAC4 acts like an oncogene by inducing senescence in primary fibroblasts (BJ-hTERT) and capable to transform the cells.

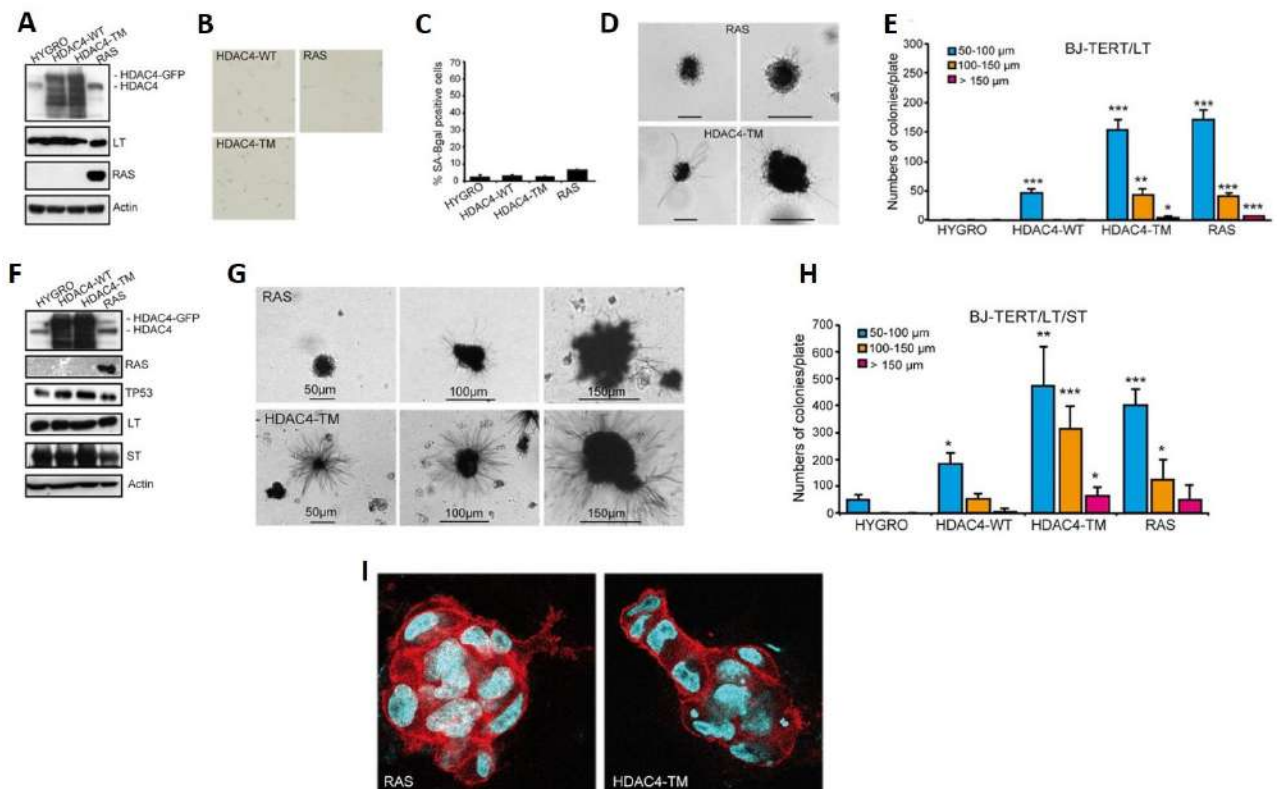


Figure 14: Presence of SV40 LT/ST in cells leads to cellular transformation. (A) Immunoblot analysis of presence of Large T (LT) in BJ-hTERT cells. Actin was used as loading control. (B) BJ-hTERT LT cells were stained for SA-β-gal activity as a marker of senescence. Scale bar: 50 μm. (C) Quantitative analysis of SA-β-gal positivity from experiments described in (B). Data are expressed as means SD, n = 3. Student t-test: \*P < 0.05, \*\*P < 0.01, \*\*\*P < 0.005. (D) The colonies were stained and visualized with MMT. Scale bars are indicated as 50 μm and 100 μm. (E) Quantitative analysis of soft agar foci formation by BJ-hTERT LT together with a combination of HDAC4-WT, TM, and RAS related to figure D. Data are expressed as means SD, n = 4. Student t-test: \*P < 0.05, \*\*P < 0.01, \*\*\*P < 0.005. (F) Immunoblot analysis of BJ-hTERT LT/ST expressing Hygro, HDAC4-WT, HDAC4-TM and RAS. HDAC4 was tagged with GFP and the recombinant proteins detected with an anti-GFP antibody. Actin was used as loading control. (G) The colonies of BJ-hTERT LT/ST together with HDAC4WT, HDAC4-TM and RAS were stained and visualized with MMT and divided into three categories based on size of foci formation. (H) Quantitative analysis of soft agar foci formation of BJ-hTERT LT/ST and with a combination of HDAC4-WT, TM, and RAS related to Fig B. Data are expressed as means SD, n = 4. Student t-test: \*P < 0.05, \*\*P < 0.01, \*\*\*P < 0.005. (I) Confocal images representing the cells grown under 3D condition in a Matrigel surface. BJ-hTERT LT/ST HDAC4-TM, RAS and Hygro were seeded on a Matrigel plug. Immunofluorescence was performed by staining the Nuclei using Hoechst 33342 and actin filaments were stained with phalloidin-Alexa 546.

### **Gene Expression profiling studies further helped in understanding the transformation process initiated by HDAC4-TM**

To understand the transformation process elicited by HDAC4-TM and RAS a transcriptomic analysis was performed. We have compared transcriptomes of BJ-hTERT LT/ST together with BJ-hTERT LT/ST HDAC4-TM and BJ-hTERT LT/ST RAS. DEGs were analysed relative to BJ-hTERT LT/ST cells. We have found that 920 genes were affected during transformation process induced by HDAC4-TM and 892 genes under RAS. In both HDAC4-TM and RAS, the number of repressed genes is higher than induced genes. Since HDAC4 is an Epigenetic repressor that favours transcriptional gene silencing, more attention is paid on repressed genes during transformation by both oncogenes. Nearly 156 genes were repressed by both oncogenes (HDAC4-TM and RAS) while RAS repressed 400 genes while HDAC4-TM repressed 450 genes (Figure 15A). Interestingly most of the genes that are repressed (downregulated) during transformation process are Interferon genes and inflammatory response (Figure 15B) It is known that oncogenes inhibit the function of interferon response during transformation process by inhibiting STAT1 and STAT2 pathways. Next we have analysed genes downregulated by HDAC4-TM alone and found that Epithelial-mesenchymal transition, Hypoxia and Myogenesis are effectively downregulated (Figure 15D). The high number of genes regulating cell adhesion, cellular movements and morphological structure, as disclosed by the Gene Ontology analysis, could explain us the phenotype of colonies formed by HDAC4-TM in soft agar (Figure 15D). Finally, by looking at transcriptomic analysis of BJ-hTERT LT/ST HDAC4-TM cells we have concluded that the transformation process initiated by HDAC4-TM is similar to other oncogenes.

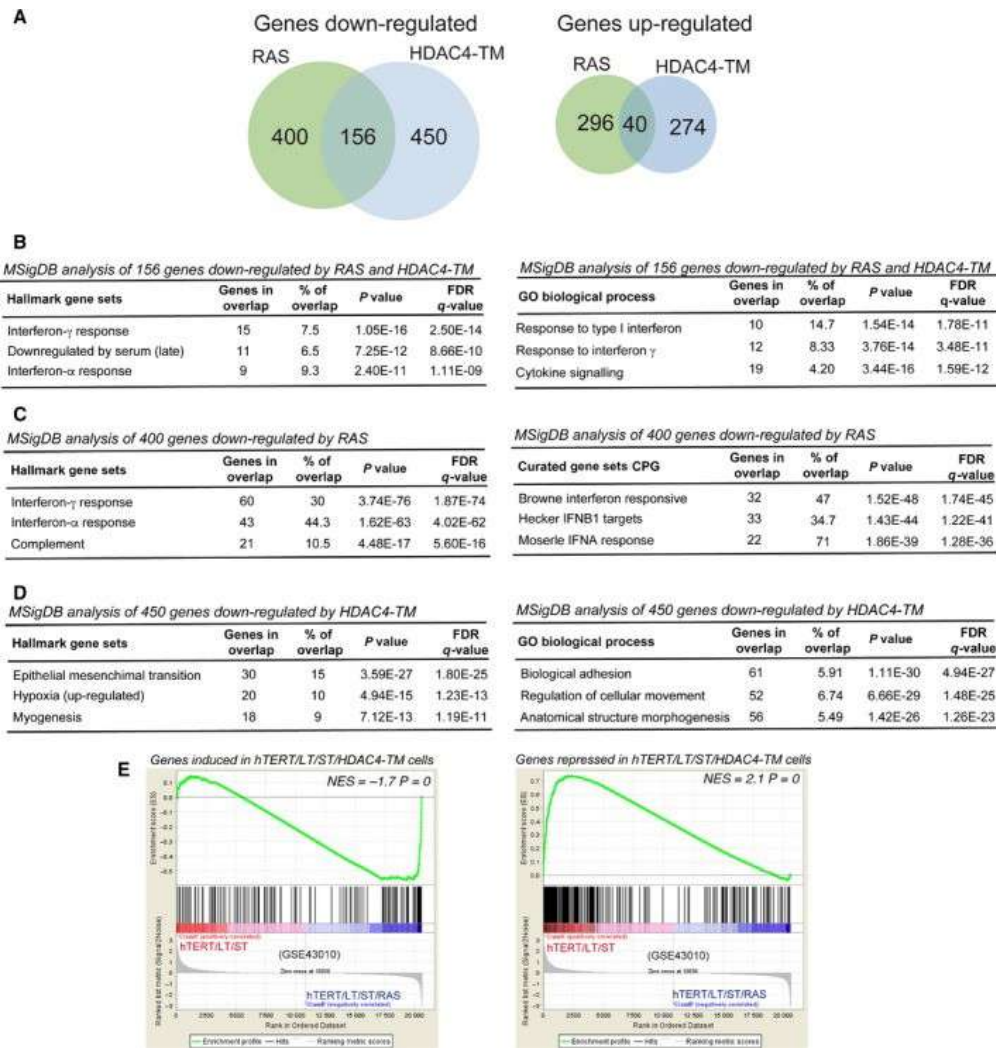


Figure 15: Transcriptomic analysis of BJ-hTERT LT/ST RAS and HDAC4-TM. (A) A venn diagram representing number of genes up and down regulated in BJ-hTERT LT/ST RAS and BJ-hTERT LT/ST HDAC4-TM cells with comparing to BJ-hTERT LT/ST HYGRO. (B) GSEA for 156 genes commonly downregulated by HDAC4-TM and RAS using hallmark and GO biological process gene sets. (C) GSEA for 400 genes specifically downregulated by RAS alone using hallmark and curated gene sets. (D) GSEA for 450 genes specifically downregulated by HDAC4-TM alone using hallmark and GO biological process gene sets. (E) GSEA plots showing significant enrichment for HDAC4-regulated genes in a BJ transformation model (GSE43010), considering both HDAC4-positively regulated genes (left) and HDAC4-repressed genes (right).

### Analysis of the transcriptional profiles in three different models of *in vitro* transformation

In order to understand the cellular and molecular pathways during the transformation process a transcriptomic analysis of BJ-*hTERT/ST/LT/HDAC4S246A*, *S467A*, *S632A(HDAC4-TM)* (GSE120040) is compared with other two strong oncogenes like BJ-*hTERT/ST/LT/MYC* (GSE72530) and BJ-*hTERT/ST/LT/HRASG12V* (GSE17941) in respect to BJ-*hTERT/ST/LT*. Our transcriptomic analysis showed that the number of repressed genes are more than induced

genes in all three oncogenes. Overall, 519 and 634 genes were respectively up-regulated and down-regulated by MYC, while 556 and 595 by RAS and finally, 551 and 979 by HDAC4 (Figure 16A-B).

A limited number of genes were commonly dysregulated during oncogenic transformation process and only 3 genes were commonly upregulated (Figure 16A) while 22 genes were commonly downregulated by three oncogenes (HDAC4-TM, RAS, MYC) (Figure 16B). Although the number of genes that were commonly shared by three oncogenes is limited, yet they could influence cell behavior and cell transformation by some common pathways. To understand this we have performed Gene Set Enrichment Analysis (GSEA) using the hallmark MSigDB gene sets and we found out that 14 different gene sets were commonly up-regulated by RAS, MYC and HDAC4 (Figure 16C) and for the down-regulated genes there were 23 gene sets (Figure 16D). Individual hallmarks for both upregulated and downregulated genes during transformation process were listed (Di Giorgio et al 2019, submitted to IJMS).

The genes that were commonly upregulated during *in vitro* transformation are *DOCK4*, *G0S2*, *SRPX* and Interferon and Inflammatory are the gene set downregulated during *in vitro* transformation, as listed in below (table 2).

For the commonly downregulated genes, we divided our signature into two categories A and B. The downregulated signature A includes genes (*CDH11*, *DKK1*, *GREM1*, *MYLK*, *SPRY2*) which does not belong to neither inflammatory and interferon gene sets listed in below table. While signature B represents genes related to inflammatory-immune responses (*ARID5B*, *DUSP4*, *ELF1*, *LPAR1*, *MX1*, *SOCS2*, *TNFRSF11B*).

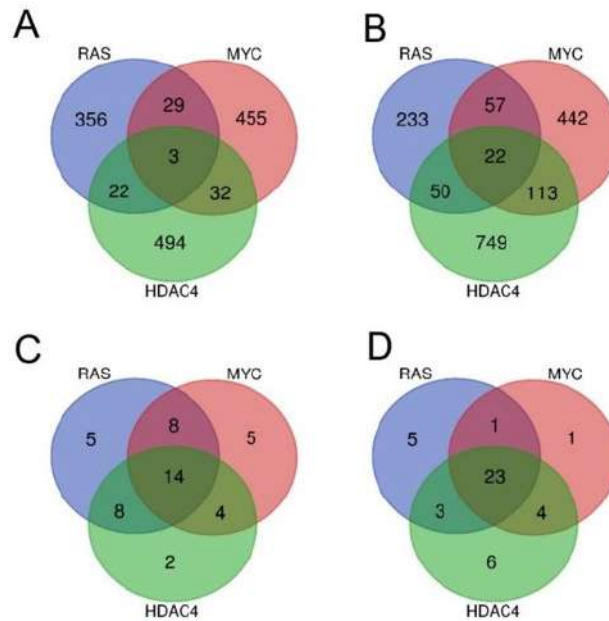


Table 2

GENE	SIGNATURE	HALLMARK
DOCK4	Up-regulated	Complement/Spindle
G0S2	Up-regulated	TNF-NFKB/KRAS
SRPX	Up-regulated	Hypoxia
CDH11	Down-regulated A	EMT/APICAL
DKK1	Down-regulated A	EMT
GREM1	Down-regulated A	EMT
MYLK	Down-regulated A	Adipogenesis/Myogenesis/EMT
SPRY2	Down-regulated A	KRAS
ARID5B	Down-regulated B	Androgen/IFNg
DUSP4	Down-regulated B	TNF $\alpha$ -NFKB
ELF1	Down-regulated B	IFN $\alpha$ /ESTROGEN
LPAR1	Down-regulated B	Inflammation/UV
MX1	Down-regulated B	IFN $\alpha$ /IFNg
SOC3	Down-regulated B	IL2-STAT5
TNFRSF11B	Down-regulated B	EMT/APICAL

Figure 16: Analysis of the transcriptional profiles in three different models of *in vitro* transformation. (A) Venn diagram showing the number of genes upregulated during *in vitro* transformation process in BJ/hTERT/LT/ST cells expressing RAS, MYC or HDAC4 as indicated. (B) Venn diagram showing the number of genes down regulated during *in vitro* transformation process in BJ/hTERT/LT/ST cells expressing RAS, MYC or HDAC4 as indicated. (C) Venn diagram showing the number of different hallmarks gene sets significantly upregulated by RAS, MYC and HDAC4. (D) Venn diagram showing the number of different hallmarks gene sets significantly down regulated by RAS, MYC and HDAC4. Venn diagrams were generated by using Bioinformatic software indicated below <http://bioinformatics.psb.ugent.be/webtools/Venn/>.

Table 2 Common up-regulated and down-regulated genes during *in vitro* transformation process.

### **A link between *in vitro* transformation and cancer**

Can *in vitro* models predict cancer? To address this, we have interrogated our up-regulated signatures (*DOCK4*, *G0S2*, *SRPX*) on survival data of 32 cancer types deposited in the Cancer Genome Atlas (TCGA).

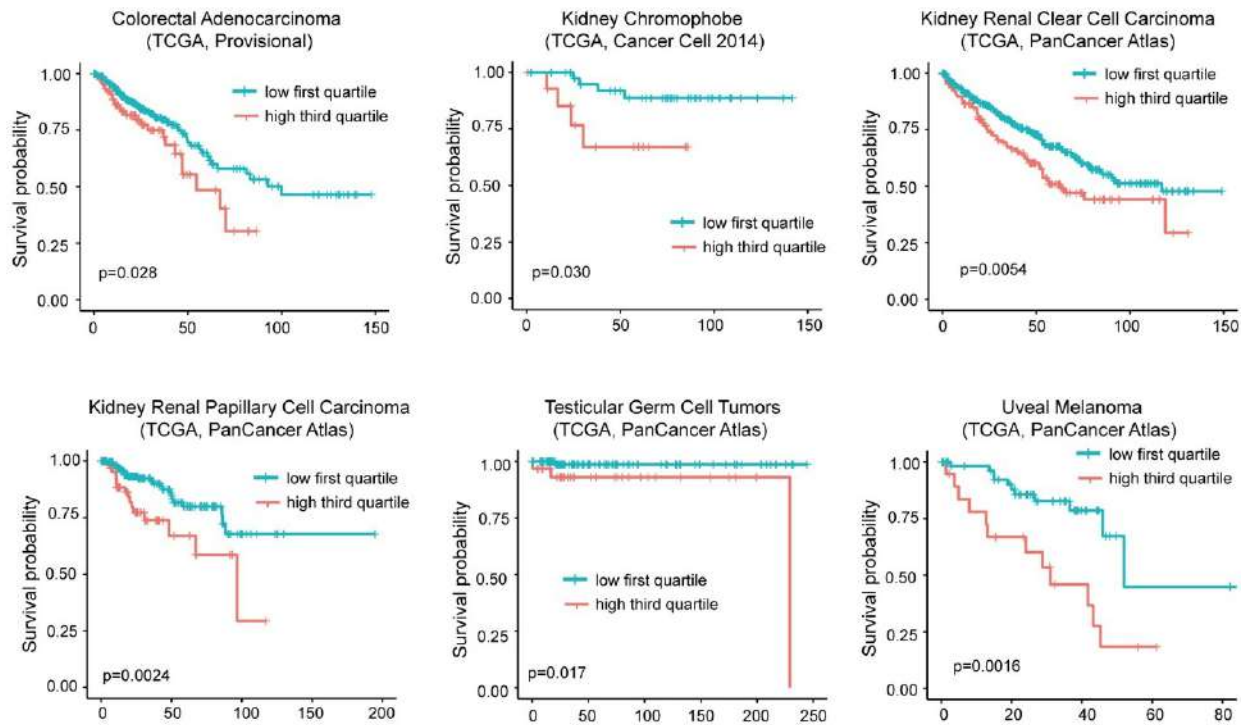
Genes upregulated during *in vitro* transformation contribute to a worst survival rate in patients. For the up-regulated genes, we grouped patients into two groups: ones characterized by high expression of our signature (above the third quartile) and the ones with repressed signature (below the third quartile). As Figure 17A shows that presence of high mRNA levels of *DOCK4*, *G0S2*, *SRPX* gene in 6 different cancer types like colorectal adenocarcinoma, kidney chromophobe, kidney renal clear cell carcinoma, kidney renal papillary cell carcinoma, testicular germ cell tumors and uveal melanoma contributed to worst survival rate.

On other hand high levels of the signature of up-regulated genes positively influenced a better survival rate in adrenocortical carcinoma (ACC) (Figure 17B). In ACC, very frequently *G0S2* is hypermethylated and the presence of low levels of *G0S2* mRNA expression characterize tumors with *G0S2* hypermethylation. Although low levels of *G0S2* contribute to 40% of ACC and independently predicts shorter disease-free and overall survival, the role of this gene in adrenocortical biology is still unknown. To confirm this data, we repeated survival analysis just by excluding *G0S2* gene. In this case the positive correlation with ACC survival was abolished (Figure 17C).

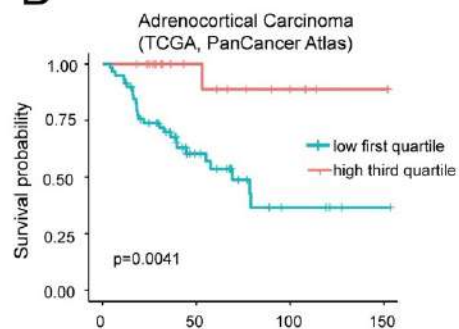
To verify whether *G0S2* is the key gene in predicting patients' survival, we repeated the analysis for *DOCK4* and *SRPX* alone. High levels of *DOCK4* expression showed a negative impact on survival in 5 different tumors (colorectal, kidney chromophobe, brain low grade glioma, stomach adenocarcinoma and uveal melanoma) and with a better prognosis in two cancer types (mesothelioma and skin cutaneous melanoma) (Eros Di Giorgio et al 2019). Same analysis was repeated for *SRPX*, this showed a dramatic effect on patient survival in 7 different cancer types (bladder, colorectal, head and neck squamous carcinoma, kidney renal clear cell and papillary carcinomas, thyroid carcinoma and uterus corpus endometrial carcinoma) while it predicted a better outcome in melanoma. This suggests us that 3 commonly up-regulated genes could act independently to influence cancer behavior.

## The RAS/MYC/HDAC4 up-regulated signature

**A**



**B**



**C**

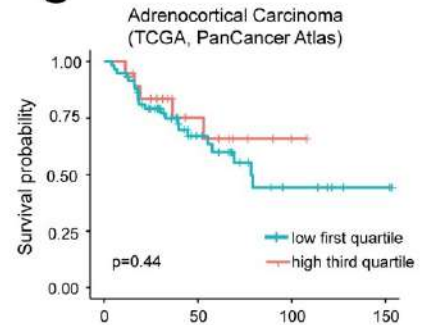


Figure 17: Presence of high mRNA levels of upregulated genes during *in vitro* transformation process influence patients' survival. (A) Kaplan-Meier survival analysis related to the three up-regulated genes *DOCK4*, *G0S2*, *SRPX*. All cases were analyzed and clustered into two groups according to *DOCK4*, *G0S2* and *SRPX* expression levels (high levels > the third quartile). Cases were: colorectal adenocarcinoma (all n=382, high expressing n=95), kidney chromophobe (all n=65, high expressing n=16), kidney renal clear cell carcinoma (all n=510, high expressing n=127), kidney renal papillary cell carcinoma (all n=283, high expressing n=70), testicular germ cell tumors (all n=149, high expressing n=37) and uveal melanoma (all n=80, high expressing n=20). (B) Kaplan-Meier survival analysis related to *G0S2* in adrenocortical carcinoma (ACC). High level expression (above the third quartile) of *G0S2* in ACC were in n 19 cases. All cases were n=78. (C) Kaplan-Meier survival analysis related to *DOCK4* and *SRPX* in ACC. High level expression (> the third quartile) of *DOCK4* and *SRPX* were in n 19 cases, all cases were n=78.

### **Genes repressed during *in vitro* transformation and patients' survival**

Next, we analyzed the TCGA survival data represented in the table 2. Using our repressed signature A we divided patients into two groups according to the median value of expression of the signature. Only in two cancer types, high levels of our signature correlated with an increased survival rate, while in six cancer types high levels of the same signature correlates with reduced survival (data not shown). On other hand a quite opposite result was observed with the repressed signature B that groups inflammatory and interferon genes. Presence of low levels of signature B correlate with a worst prognosis, at least this is evident in few cases like kidney chromophobe carcinoma, kidney clear cell carcinoma, sarcoma, skin cutaneous melanoma and uterine carcinosarcoma (Figure 18A). On contrary, low levels of this signature predict a better outcome in patients with brain lower grade glioma and ovarian serous cystadenocarcinoma (Figure 18B).

As a final analysis we have evaluated the presence of tumor infiltrating immune cells and the repressed inflammatory B signature on overall survival. To approach this, we have analyzed 3 tumors (LGG, skin cutaneous melanoma and sarcoma) showing a significant correlation between immune cell infiltrates and overall survival (Figure 19). In LGG, the presence of high levels of immune cells (T cells) and signature B represent a poor prognosis (Figure 19B/C/G) while in sarcoma the presence of immune cells infiltrate positively correlates with increased survival rate even in the presence of low levels of signature B (Figure 19E-G). In contrast, in skin cutaneous melanoma low levels of expression of the B signature are enough to reduce the overall survival (Figure 19A/C/D/F/G). In melanoma the best prognosis is observed in the presence of high expression of the signature and the concomitant presence of immune cells, particularly T cells, NK, CD8 T cells and cytotoxic lymphocytes.

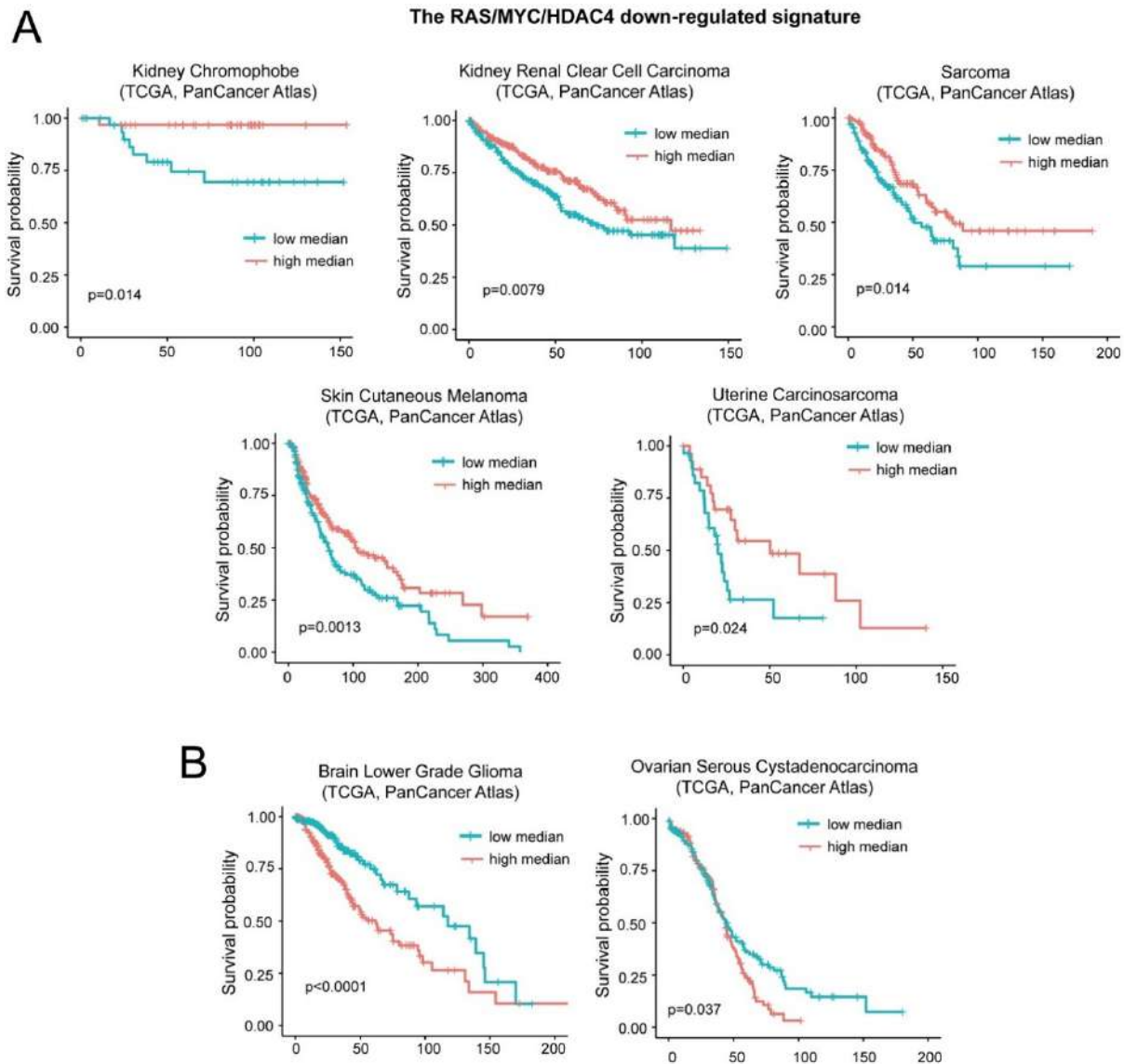


Figure 18: TCGA survival data on genes repressed during *in vitro* transformation. (A) Kaplan-Meier survival analysis related to the immune/inflammatory signature. All cases were analyzed and clustered into two groups according to median expression levels (high levels > the median). Cases were: kidney chromophobe (all n=65, high expressing n=32), kidney renal clear cell carcinoma (all n=510, high expressing n=255), sarcoma (all n=253, high expressing n=126), skin cutaneous melanoma (all n=443, high expressing n=221) and uterine carcinosarcoma (all n=57, high expressing n=28). (B) Kaplan-Meier survival analysis related to the immune/inflammatory signature. All cases were analyzed and clustered into two groups according to median expression levels (high levels > the median). Cases were: brain low grade gliomas (all n=514, high expressing n=257) and ovarian serous cystadenocarcinoma (all n=300, high expressing n=150).

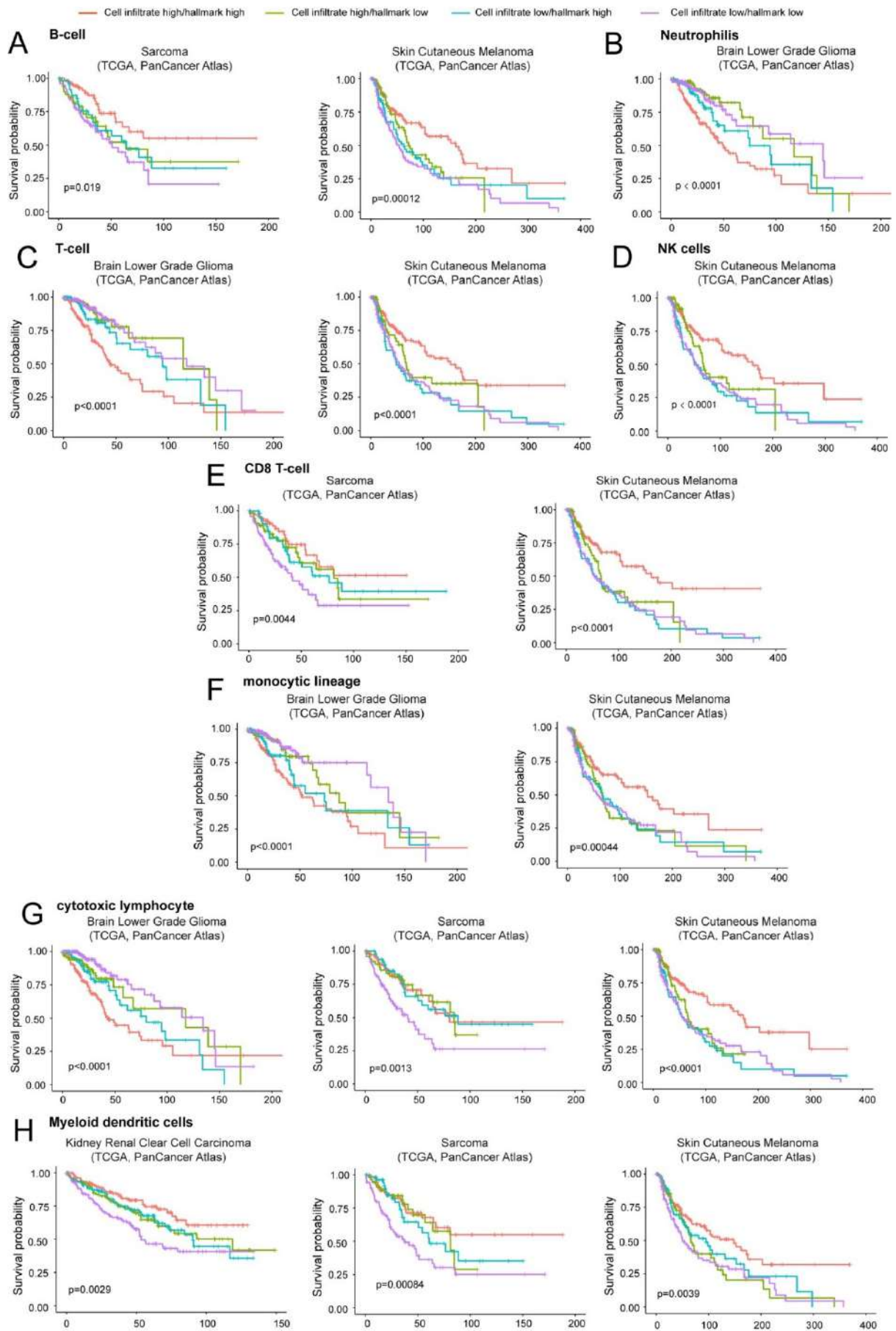


Figure 19: The contribution of tumor infiltrating immune/inflammatory cells to overall survival. Kaplan-Meier survival analysis related to the immune/inflammatory signature and the infiltration of different immune/inflammatory cells. Infiltrating immune/inflammatory cells were defined as described in materials and methods. Patients were grouped high/high (high levels of both infiltrating cells and immune signature), high/low (high levels of infiltrating cells and low levels of the immune signature), low/high (low levels of infiltrating cells and high levels of the immune signature) and as low/low (low levels of both infiltrating cells and immune signature). The four groups were generated according to median expression levels of the two signatures. Cases: (A) Sarcoma (all=253, high/high=75, high/low=51, low/high=51, low/low=76) and skin cutaneous melanoma (all=428, high/high=133, high/low=82, low/high=82, low/low=131). (B) Brain low grade glioma (all=512, high/high=155, high/low=102, low/high=101, low/low=154). (C) Brain low grade glioma (all=512, high/high=164, high/low=92, low/high=92, low/low=164) and skin cutaneous melanoma (all=428, high/high=148, high/low=66, low/high=67, low/low=147). (D) Skin cutaneous melanoma (all=428, high/high=143, high/low=72, low/high=72, low/low=141). (E) Sarcoma (all=253, high/high=70, high/low=56, low/high=56, low/low=71) and skin cutaneous melanoma (all=428, high/high=136, high/low=77, low/high=79, low/low=136). (F) Brain low grade glioma (all=512, high/high=164, high/low=93, low/high=92, low/low=163) and skin cutaneous melanoma (all=428, high/high=140, high/low=73, low/high=75, low/low=140). (G) Brain low grade glioma (all=512, high/high=153, high/low=104, low/high=103, low/low=152), sarcoma (all=253, high/high=74, high/low=52, low/high=52, low/low=75) and skin cutaneous melanoma (all=428, high/high=142, high/low=74, low/high=73, low/low=139). (H) kidney renal clear cell carcinoma (all=510, high/high=132, high/low=123, low/high=123, low/low=132), sarcoma (all=253, high/high=70, high/low=56, low/high=56, low/low=71) and skin cutaneous melanoma (all=428, high/high=126, high/low=89, low/high=89, low/low=124).

### **6.3 Senescence Induced by HDAC4 knock out in cellular models**

#### **HDAC4 is downregulated during Oncogene Induced senescence in a GSK3 $\beta$ dependant mechanism**

The relationships between HDAC4 and the induction of senescence is unclear. To investigate the contribution of class IIa HDACs to senescence and senescence escape, we generated an inducible model of senescence by expressing RAS and AKT in an inducible manner (doxycycline) in BJ-hTERT cells. In cells undergoing OIS, class IIa HDACs levels decrease except for HDCA9 (Figure 20A). The induction of senescence is accompanied by the phosphorylation of  $\gamma$ H2A.X (a marker of DNA damage) and by the appearance of SA- $\beta$ -gal positive cells (a marker of senescence). Class IIa HDACs activity were scored in different models of senescence and in tissues from aged mice; among the different conditions only HDAC4 was de-regulated (data not shown). We therefore decided to focus more attention on HDAC4 for further studies. The downregulation of HDAC4 is due to UPS degradation, since HDAC4 levels are restored by the proteasome inhibitor MG132 but not by inhibiting autophagy (Data not shown). The UPS mediated degradation of HDAC4 was proved in the past to be

GSK3 $\beta$  dependent (Cernotta et al, 2011). We confirmed that the degradation of HDAC4 during senescence is mediated by GSK3 $\beta$  by silencing GSK3 $\beta$  in BJ-hTERT RAS cells (doxycycline) at day 8 (when they reach senescence). The silencing of GSK3 $\beta$  in senescent cells do not positively impact on the senescence of these cells but it is enough to restore HDAC4 levels as confirmed by immunoblot (Figure 20B).

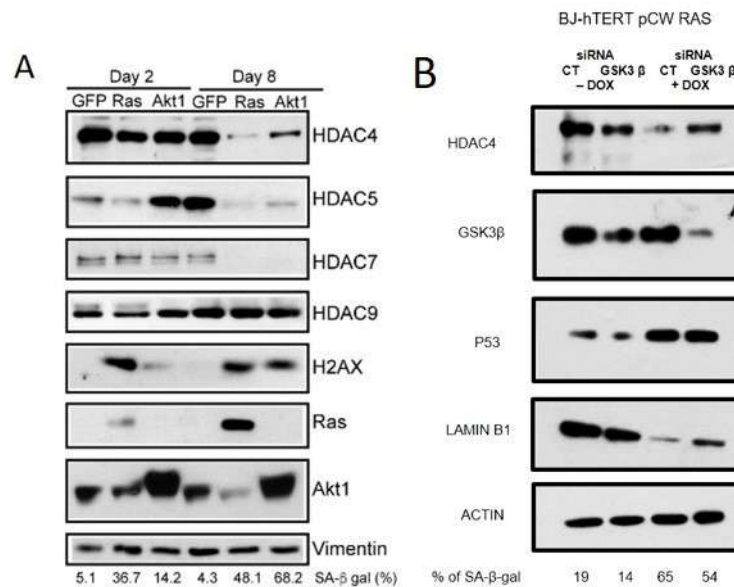


Figure 20: HDAC4 are regulated during cellular senescence. (A) Immunoblot analysis of different class IIa HDACs during OIS at day2 and at day8 in BJ-hTERT fibroblastss and percentage of SA-  $\beta$ -gal is indicated in the below lane (B). Immunoblot analysis of siRNA GSK3 $\beta$  in the absence and presence of doxycycline. Presence of doxycycline triggers OIS, leading to degradation of HDAC4 by GSK3 $\beta$  dependant. siRNA of GSK3 $\beta$  in the presence of doxycycline, recovered the stability of HDAC4 which is lost during OIS and percentatge of SA-  $\beta$ -gal is indicated in the below lane

### Knock out of HDAC4 triggers senescence in SK-LMS-1

To better investigate the role of HDAC4 in regulating senescence, we made a knock-out of HDAC4 in low grade sarcoma cells (SK-LMS-1). Depletion of HDAC4 in these cells altered cellular and nuclear morphology, triggered permanent cell cycle arrest and the cells stained positive for SA- $\beta$ -gal assay a marker of senescence (Figure 21A-C) and showed an increase in DNA damage response as when compared with WT HDAC4 and confirmed by gH2A.X positivity (Figure 21D). Moreover, as these cells undergo senescence in the absence of HDAC4, they lost their tumorigenic properties. We have generated different KO clones by using 2 different sgRNA guides (guide 1: 76 and 1231, guide 2: 205 and 1254) (Figure 21A)

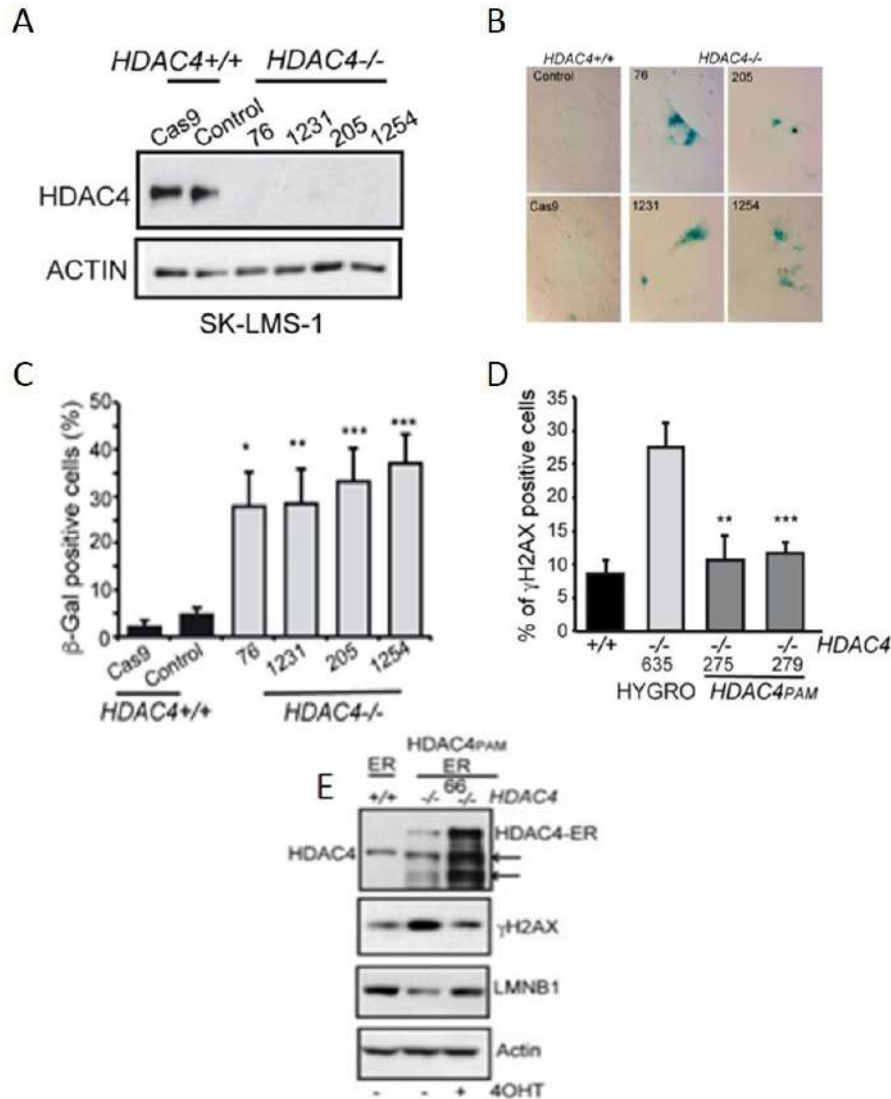


Figure 21: Generation of knock-out cells by using CRISPR CAS9 technology. (A) Immunoblot analysis showing 4 knock out clones of HDAC4 as generated by using CRISPR/Cas9 technology in SL-LMS-1 cells. (B) Microscopic pictures of indicated cells stained for a marker of senescence (SA-β-gal assay). (C) Quantitative analysis of SA-β-gal positivity described in Figure B. Data are expressed as means SD, n = 3. Student t-test: \*P < 0.05, \*\*P < 0.01, \*\*\*P < 0.005. (D) Quantitative analysis of cells positive for γH2A.X. Data are presented as percentages of cells. (E) Immunoblot analysis of an inducible Cas9 resistant HDAC4 knock-out clone. Absence of tamoxifen removes HDAC4 in SK-LMS-1 cell line, thereby cells undergo senescence by activation of γH2A.X in response to DNA damage, cells in the presence of tamoxifen recover HDAC4 protein and start to proliferate.

As the cells in the absence of HDAC4 undergo senescence, we decided to generate a knock-out clone that can express an inducible Cas9-resistant HDAC4. By using CRISPR/Cas9 technology, we have generated an inducible cas9 knockout clone of SKLMS1 that is HDAC4<sup>-/-</sup> in absence of tamoxifen and in the presence of tamoxifen induces HDAC4 protein thereby allowing cells to proliferate (clone 66). The re-expression of HDAC4 rescues the senescent

phenotype as the levels of Lamin B1 are recovered as well as the magnitude of DNA damage is reduced ( $\gamma$ H2A.X) (Figure 21E).

### **Adoption of a DNA damage sensor in *in vivo* microscopy**

Absence of HDAC4 in SK-LMS-1 triggered a DNA damage response. To investigate the onset of this response and the relationships with the cell cycle we engineered SK-LMS-1 cells in order to monitor *in vivo* the appearance of lesions in the DNA and the progression through the cell cycle. We transduced SK-LMS-1 HDAC4<sup>-/-</sup> cells that re-express HDAC4 in an inducible manner (clone 66) with H2B-GFP (to track mitosis) and apple-53BP1 truncated protein as a double strand breaks reporter (53BP1 localizes to sites of double-strand breaks).

To validate these probes, we treated SK-LMS-1-WT with etoposide (10 $\mu$ m) for 2 hours and then we performed an immunofluorescence assay using antibody against 53BP1. Cells treated with etoposide display accumulation of 53BP1 spots (Figure 22A). In our immunofluorescence analysis we have observed that some cells display bigger foci and some display small foci of 53BP1. Hence, we quantified the immunofluorescence results. Cells not treated with DNA damaging agents were divided into two groups based on foci dimension as small and large, as previously noted (Julian Spies et al.,2019). Figure 22B shows accumulation of 53BP1 in small and larger spots which should represent sites of DNA damage. This result also indicates that SK-LMS-1 suffer of an endogenous amount of DNA damage.

Since removal of HDAC4 in SK-LM-1 causes the progressive accumulation of DNA damage and activation of  $\gamma$ H2A.X, we used SK-LMS-1 inducible clone 66 HDAC4<sup>-/-</sup> to investigate DNA damage response and mitosis in *in vivo* by time-lapse microscopy. For this purpose we retrovirally infected clone 66 KO HDAC4 with H2B-GFP and apple-53BP1 truncated probes to follow mitosis and DNA damage (Figure 22C).

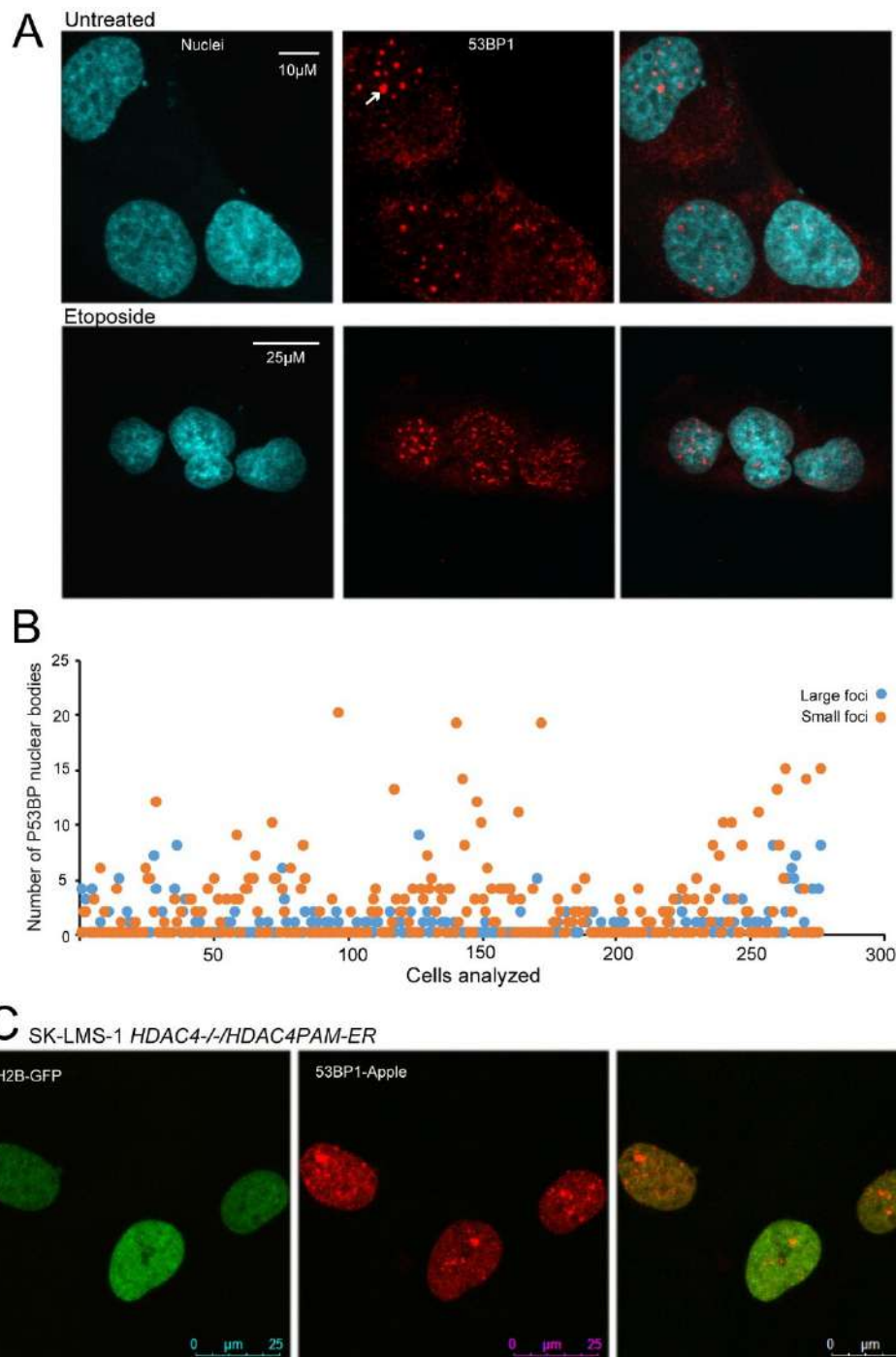


Figure 22: Development of a single cell DNA damage reporter and a mitosis sensor (Apple-53BP1 truncated and H2B-GFP). (A) Immunofluorescence analysis of SK-LMS-1 cells untreated and treated with etoposide showing accumulation of 53BP1 in foci (indicated by arrow) sites of DNA damage. Nuclei of the cells were stained with Hoechst 33342 and 53BP1 is stained with secondary antibody conjugated to Alexa546. (B) Dot plot representation of SK-LMS-1 WT treated with etoposide showing accumulation of small and large foci of 53BP1 in each cell. An average of 270 cells were counted. (C) Sk-LMS-1/HDAC4<sup>-/-</sup> cells were retrovirally infected with H2B-GFP and apple-53BP1. Immunofluorescence was performed to see the positivity of cells for the probes in the presence of 4OHT which sustains HDAC4 expression.

### **SK-LMS-1 HDAC4<sup>-/-</sup> cells accumulate a DNA damage response in a time frame**

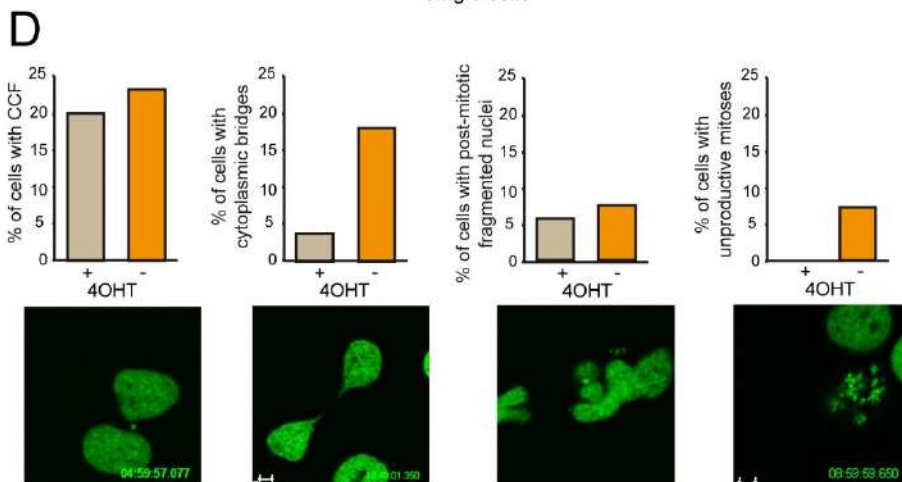
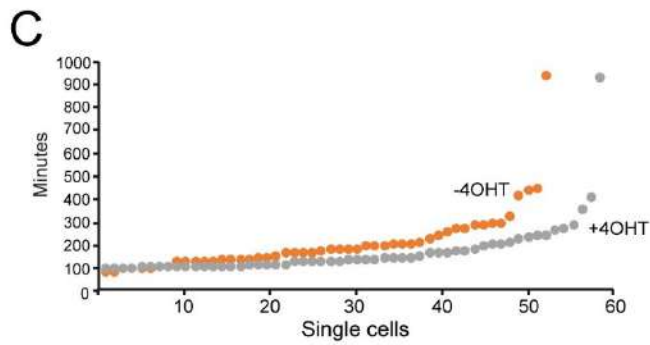
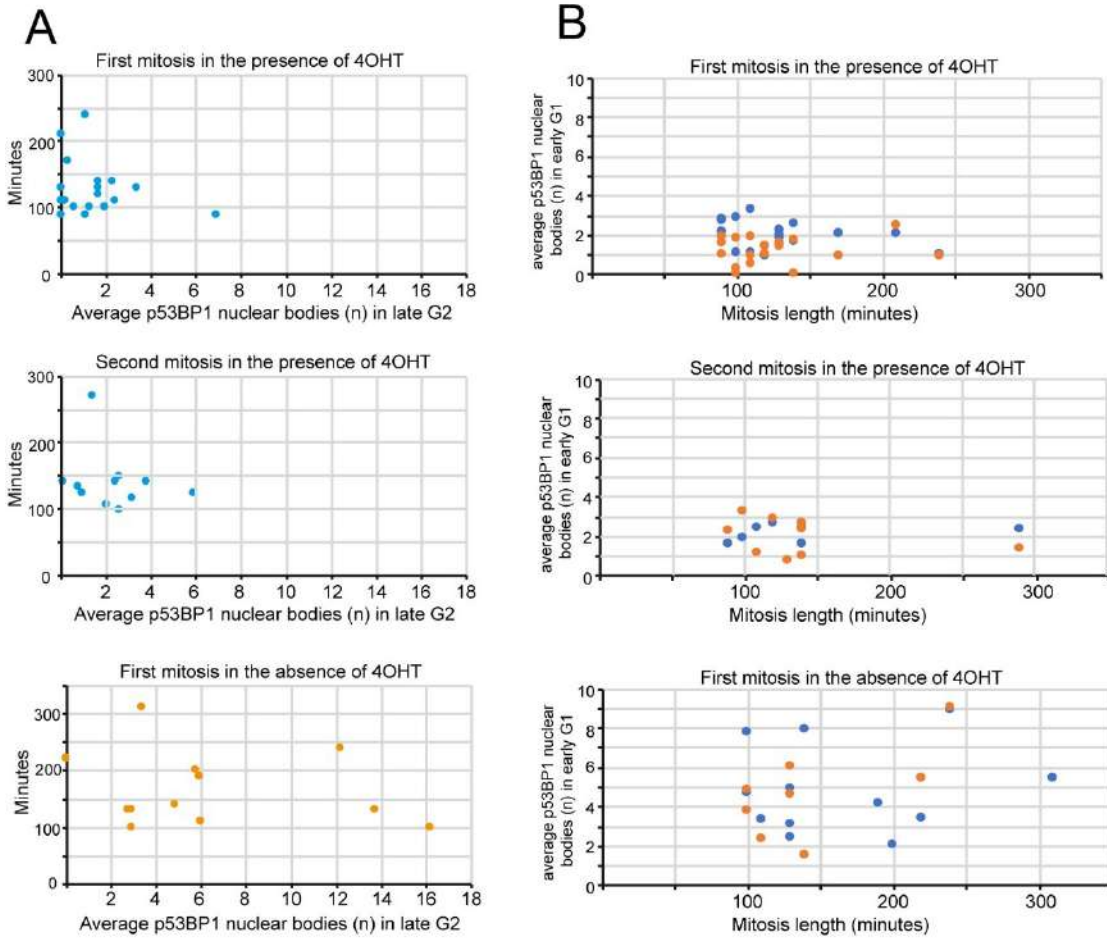
HDAC4<sup>-/-</sup> clone 66 expressing H2B-GFP and apple 53BP1 was subjected to *in vivo* time-lapse microscopy. Figure 23E shows that cells in the presence of HDAC4 (+4OHT) spontaneously accumulate DNA damage, frequently in the G2 phase of the cell cycle. Although apple-P53BP1 does not allow the monitoring of DNA lesions during mitosis, the two daughter cells emerging in G1 show lower number of DNA lesions. This result suggests that in the presence of HDAC4 spontaneous DNA lesions in SK-LMS-1 cells are possibly resolved in G2. Frequently these cells enter two times in mitosis under the time of analysis (72 hours). Each arrow on the heatmap indicates the mitosis taken by the cell.

The heatmaps measuring the accumulation of 53BP1 nuclear bodies clearly evidence an increase in the DNA lesions of in the absence of HDAC4 (-4OHT). Although peaks of lesions accumulate in G2 they also spread throughout the cell cycle. Under this increased amount of DNA damage cells rarely enter a second mitosis during the time of the analysis (Figure 23E). In summary the increase of the DNA damage seems to be an early response to the removal of HDAC4.

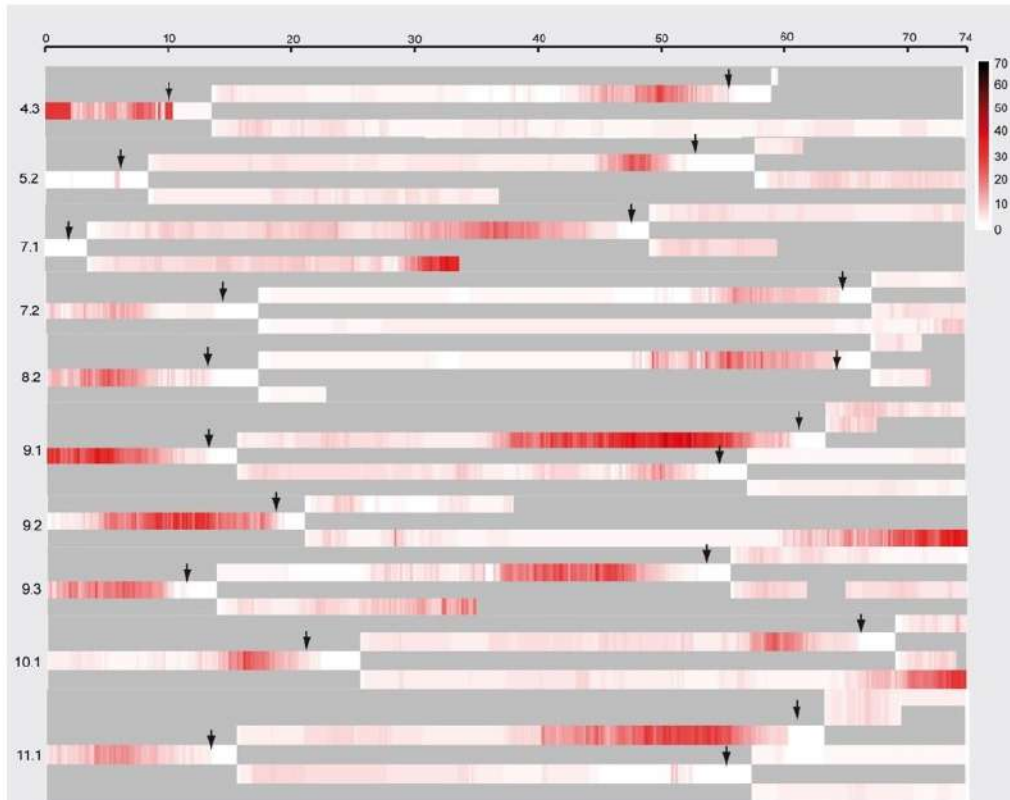
Next we analyzed in more detail the relationships between mitosis, HDAC4 and DNA damage. Figure 23A shows that in the presence of HDAC4 nuclear bodies of P53BP1 are well resolved before entering mitosis and, with the exception of two cases the mitotic length is quite constant average length  $127 \pm 39.34$  minutes on average. Similar number were observed with the second mitosis ( $139.09 \pm 53.37$  minutes). When the activity of HDAC4 was abrogated by the removal of 4OHT, the number of P53BP1 nuclear bodies accumulating in late G2 increased and in parallel the duration of mitosis increased ( $166.67 \pm 65.55$  minutes).

We also analyzed the relationships between P53BP1 nuclear bodies and the emerging of the two daughters' cells in early G1 (Figure 23B). Also in early G1 the absence of HDAC4 provokes an overall increase in the number of P53BP1 nuclear bodies in the daughter cells. Next we performed another to time-lapse to confirm the difference in the mitosis length in a larger number of cells. Figure 23C demonstrate that in the absence of HDAC4 SK-LMS-1 cells spend a longer time in mitosis. Monitoring the nuclear morphology *in vivo* using the GFP-H2B we also observed that the presence of CCF (Chromatin Cytoplasmic Fragments), of nuclear cytoplasmic bridges and of aberrant mitosis are all increased in the absence of HDAC4 (Fig. 23D).

In summary these results suggest that HDAC4 prevents the accumulation of lesion in the DNA and in its absence the accumulation of these lesions can impact on the progression through the mitosis.



E



F

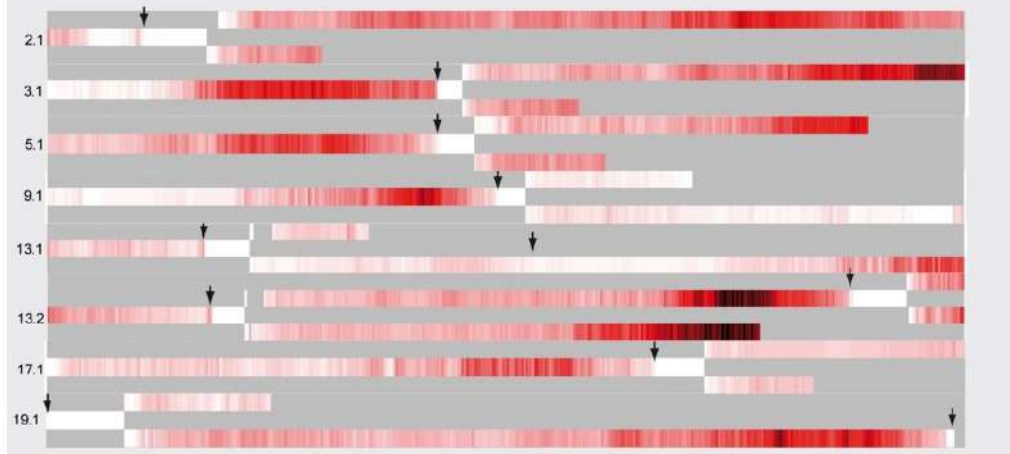


Figure 23: A serial *in vivo* time-lapse microscopic imaging of SK-LMS-1 HDAC4<sup>-/-</sup> ko clone66 expressing H2B GFP and apple 53BP1 trunc probes in the presence/absence of 4OHT. (A) A dot plot representing accumulation of 53BP1 nuclear bodies in late G2. In the presence of 4OHT cells accumulated very few nuclear bodies of 53BP1 when compared with absence of 4OHT. (B) A dot plot representing in the presence of 4OHT mother cell accumulate 2-4 nuclear bodies of 53BP1 (on average), during two conservative mitosis eventually leading offspring's (blue spots) to accumulate few nuclear bodies of 53BP1, while in the absence of 4OHT mother cell accumulated huge DNA damage response which negatively impacted on mitosis and showed single mitosis. In the absence of 4OHT both mother and daughter cell accumulated huge nuclear bodies 53BP1 nuclear bodies. (C)

Cells in the absence of 4OHT showed a delay in cell proliferation and took time to duplicate when compared with in the presence of 4OHT. (D) Mitotic defects in the absence of 4OHT, show accumulation of micronuclei, cytoplasmic bridge and unproductive mitosis.

### HDAC4 silencing by siRNA triggers senescence in different cell lines

In order to further exclude the off targets of CRISPR/Cas9 technology, we used small interfering RNA (siRNA) technology to silence HDAC4 protein in several cellular models like BJ-hTERT/LT/RAS transformed cells and WM115 (metastatic melanoma).

Silencing of HDAC4 in these cell lines triggers a mild induction of senescence as scored by means of percentage of  $\beta$ -gal positivity. Silenced cells similarly to knocked-out cells are characterized by the reduction of Lamin B1 levels, accumulation of P53 and accumulation of  $\gamma$ H2AX.

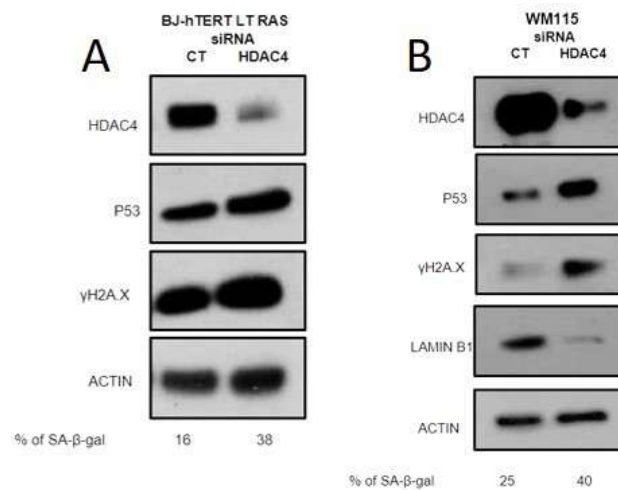


Figure 24: Knockdown of HDAC4 in few cellular models. (A) Immunoblot analysis showing siRNA interference HDAC4 in BJ-hTERT LT/RAS resulted in induction of senescence by activating p53 and accumulating phosphorylation of  $\gamma$ H2A.X. (B) Immunoblot analysis showing siRNA of HDAC4 in metastatic melanoma induced senescence by triggering p53 and  $\gamma$ H2A.X and decreasing Lamin B1 levels.

To summarize knock out of HDAC4 or siRNA of HDAC4 triggers a DNA damage response thereby allowing the cells to enter a state a permanent irreversible growth arrest. Our time lapse analysis showed that absence of HDAC4 in the SK-LMS-1 cell lines showed a mitotic defect with unreparable DNA damage. This DNA damage response could be due to some epigenetic stress created by HDAC4 absence or due to presence of high acetylated histones (Payel Sen et al 2019).

## Discussion

Normal human cells/murine cells in response to strong oncogenic signals enter into a state of irreversible cell cycle growth arrest called Oncogene Induced senescence (OIS) (Serrano *et al* 1997). Activation of OIS depends on tumor suppressor proteins like pRB/p53 pathways and their response to DNA damage (Serrano *et al* 1997). The escape from senescence barrier seems to be required step for oncogenesis. The epigenetic resetting represents a novel hallmark in the transformation process (Bradner *et al* 2017). At each step of tumor progression, from initiation to evolution, epigenetic plasticity is necessary to fuel new waves of transcription (Koschmann *et al* 2017). Among the epigenetic regulators, class IIa HDACs represent novel promising druggable targets in consideration of the increasing number of evidences of their oncogenic properties. Here we described for the first time the capability of HDAC4 to drive oncogenic transformation in human cells. Differently from the transformation of murine cells, human fibroblasts require a step-by-step oncogenic conversion that allow the escape from apoptotic and pro-senescent stimuli. The over-expression of a nuclear mutant of HDAC4 (HDAC4-TM) in primary fibroblasts triggers premature senescence earlier than RAS and WT form of HDAC4 showed no sign of senescence. Although the levels of p16 have been shown to be an important determinant for RAS-induced senescence (Benanti and Galloway *et al* 2004), HDAC4-TM induced senescence is strongly dependent on p53.

The senescence induced by HDAC4-TM is rapid with early signs of DNA damage and with the activation of p53. Depletion of p53 in cells expressing HDAC4-TM results in escape of senescence, and further mutations leads to malignant transformation. On contrary, inactivation of p53 in RAS induced senescence is frequently reported to be not sufficient to escape the cell-cycle arrest (Di Micco *et al* 2006).

Some senescence features of HDAC4-TM are commonly shared with AKT (Astle *et al* 2012). Presence of AKT in the normal cells triggers rapid cell cycle arrest similarly to HDAC4-TM but seems to not evoke a DNA damage response (Astle *et al* 2012), differently from RAS and HDAC4-TM

The contemporary inactivation of p53 and p16/Rb pathways achieved by the transduction of the cells with SV40 LT allows the transformation of HDAC4-TM cells. HDAC4 expressing cells achieve full transformation in the presence of small T and Large T, probably because through the inhibition of PP2A phosphatase (Hahn *et al* 2002). In this condition also the WT form of HDAC4 displays oncogenic properties

Transcriptomic analysis of HDAC4-TM and RAS transformed evidenced that both the oncogenes require the repression of Interferon-related genes, as previously reported

(Battcock et al 2006; Christian et al 2009; Noser et al 2007). It was previously reported that some of the Interferon genes act as tumour suppressor during oncogenic transformation process (Tanaka N et al 1994). Later further studies confirmed that absence of Interferon genes mediates cellular transformation; for example, IRF-/- MEF cells expressing oncogenes like RAS were readily transformed but not MEF WT type . Another study revealed that ectopic expression of IRF-1 reduced tumorigenic properties of oncogene induced transformation and tumour cells *in vitro* and *in vivo* (Takaoka A et al 2008). Other pathways altered by HDAC4 during transformation are mostly related adaptation to hypoxia, adhesion, motility and differentiation processes. Further investigations of these signalling pathways are required to prove the direct involvement of HDAC4 in their regulation.

Next we have compared our signature with other two oncogenes like RAS and c-MYC which favour in *in vitro* transformation in BJ-hTERT SV40 LT/ST. Differently from what reported by others, we found out that most of the tumorigenic properties driven by the three oncogenes relies on the activation of some common molecular pathways (like inhibition of interferon response) but not on the activation and repression of the same genes.

By checking the commonly regulated genes, we found out that very few genes upregulated during in *in vitro* transformation and these genes contribute to a worst survival rate in some cancers. On opposite most of the genes that are downregulated during *in vitro* transformation are Interferon and Inflammatory genes. Switching off the Interferon and the inflammatory responses provide a double advantage to the transformed cells, both in a cell autonomous and non-autonomous manner. Repression of Interferon genes favor the transformation process, by limiting tumor suppressive actions (such as apoptosis/escaping senescence), and it can influence the tumor microenvironment and the immune response. In some *in vivo* experiments on murine models of cancer have reported that, the initial step of tumorigenesis provides an strong inflammatory environment which promote cancers in later events. All our results justify the inclusion of HDAC4 in the group of two historically well-known oncogenes for being similarly able to repress IFN genes during the transformation process.

Epigenetic dysregulation is a hallmark of senescence and aging. Recent studies in diverse species and cell types have highlighted the pervasiveness of age-associated changes in transcription factor binding, histone marks, heterochromatin formation, and DNA methylation (Benayoun et al 2015; Zampieri et al 2015) that contribute to changes in gene expression. Indeed, gene expression has been shown to change drastically during aging by reorganising chromatin structure (Baumgart et al 2014). In particularly we focused on one aspect of epigenetic regulation of HDAC4 which was not known for its role in oncogenesis and aging.

Expression of HDAC4-TM in BJ-hTERT induces senescence while knock out of HDAC4 / knock down of HDAC4 in low grade leiomyosarcoma triggers DNA damage, eventually leading to senescence. The absence of HDAC4 in SK-LMS-1 triggers a DNA damage response and may recruit some chromatin modifiers like acetylation which could affect DNA repair. This suggests that an accumulation of DNA damage and loss of HDAC4 repression may underlie age-associated epigenomic changes. Further studies are required to answer, the link between HDAC4 and DNA damage. The fruitful strategies could be developing a specific inhibitors or block HDAC function in combination with other standard treatments, like radiation and chemotherapy, to maximize the killing of cancer cells.

## Bibliography:

- Acosta, J. C., Banito, A., Wuestefeld, T., Georgilis, A., Morton, J. P., Athineos, D., Gil, J. (2014). Europe PMC Funders Group Europe PMC Funders Author Manuscripts A complex secretory program orchestrated by the inflammasome controls paracrine senescence, *15*(8), 978–990. <https://doi.org/10.1038/ncb2784.A>
- Alili, L., Diekmann, J., Giesen, M., Holtkötter, O., & Brenneisen, P. (2014). A drug-induced accelerated senescence (DIAS) is a possibility to study aging in time lapse. *Age*, *36*(3), 1329–1343. <https://doi.org/10.1007/s11357-014-9658-8>
- Astle, M. V., Hannan, K. M., Ng, P. Y., Lee, R. S., George, A. J., Hsu, A. K., ... Pearson, R. B. (2012). AKT induces senescence in human cells via mTORC1 and p53 in the absence of DNA damage: Implications for targeting mTOR during malignancy. *Oncogene*. <https://doi.org/10.1038/onc.2011.394>
- Bandyopadhyay, D., Curry, J. L., Lin, Q., Richards, H. W., Chen, D., Hornsby, P. J., ... Medrano, E. E. (2007). Dynamic assembly of chromatin complexes during cellular senescence: Implications for the growth arrest of human melanocytic nevi. *Aging Cell*, *6*(4), 577–591. <https://doi.org/10.1111/j.1474-9726.2007.00308.x>
- Black, B. L., & Olson, E. N. (1998). Transcriptional Control of Muscle Development By Myocyte Enhancer Factor-2 (Mef2) Proteins. *Annu. Rev. Cell Dev. Biol*, *14*, 167–196. <https://doi.org/10.1146/annurev.cellbio.14.1.167>
- Bradner, J. E., West, N., Grachan, M. L., Greenberg, E. F., Haggarty, S. J., Warnow, T., & Mazitschek, R. (2010). NIH Public Access, *6*(3), 238–243. <https://doi.org/10.1038/nchembio.313.Chemical>
- Braig, M., Lee, S., Loddenkemper, C., Rudolph, C., Peters, A. H. F. M., Schlegelberger, B., ... Schmitt, C. A. (2005). Oncogene-induced senescence as an initial barrier in lymphoma development. *Nature*, *436*(7051), 660–665. <https://doi.org/10.1038/nature03841>
- Burton, D. G. A., & Krizhanovsky, V. (2014). Physiological and pathological consequences of cellular senescence. *Cellular and Molecular Life Sciences*, *71*(22), 4373–4386. <https://doi.org/10.1007/s00018-014-1691-3>
- Calcinotto, A., Kohli, J., Zagato, E., Pellegrini, L., Demaria, M., & Alimonti, A. (2019). Cellular senescence: Aging, cancer, and injury. *Physiological Reviews*, *99*(2), 1047–1078. <https://doi.org/10.1152/physrev.00020.2018>
- Campisi, J., & d'Adda di Fagagna, F. (2007). Cellular senescence: when bad things happen to good cells. *Nature Reviews Molecular Cell Biology*, *8*(9), 729–740.

<https://doi.org/10.1038/nrm2233>

- Capparelli, C., Guido, C., Whitaker-Menezes, D., Bonuccelli, G., Balliet, R., Pestell, T. G., ... Lisanti, M. P. (2012). Autophagy and senescence in cancer-associated fibroblasts metabolically supports tumor growth and metastasis, via glycolysis and ketone production. *Cell Cycle*, *11*(12), 2285–2302. <https://doi.org/10.4161/cc.20718>
- Cernotta, N., Clocchiatti, A., Florean, C., & Brancolini, C. (2011). Ubiquitin-dependent degradation of HDAC4, a new regulator of random cell motility. *Molecular Biology of the Cell*, *22*(2), 278–289. <https://doi.org/10.1091/mbc.E10-07-0616>
- Chang, A. L. S. (2016). Expanding Our Understanding of Human Skin Aging. *Journal of Investigative Dermatology*, *136*(5), 897–899. <https://doi.org/10.1016/j.jid.2016.02.020>
- Chapman, J. R., Taylor, M. R. G., & Boulton, S. J. (2012). Playing the End Game: DNA Double-Strand Break Repair Pathway Choice. *Molecular Cell*, *47*(4), 497–510. <https://doi.org/10.1016/j.molcel.2012.07.029>
- Clocchiatti, A., Di Giorgio, E., Viviani, G., Streuli, C., Sgorbissa, A., Picco, R., ... Brancolini, C. (2015). The MEF2-HDAC axis controls proliferation of mammary epithelial cells and acini formation in vitro. *Journal of Cell Science*, *128*(21), 3961–3976. <https://doi.org/10.1242/jcs.170357>
- Clocchiatti, A., Florean, C., & Brancolini, C. (2011). Class IIa HDACs: From important roles in differentiation to possible implications in tumourigenesis. *Journal of Cellular and Molecular Medicine*. <https://doi.org/10.1111/j.1582-4934.2011.01321.x>
- Collado, M., Gil, J., Efeyan, A., Guerra, C., Schuhmacher, A. J., Barradas, M., ... Serrano, M. (2005). Tumour biology: Senescence in premalignant tumours. *Nature*, *436*(7051), 642. <https://doi.org/10.1038/436642a>
- Coppé, J. P., Patil, C. K., Rodier, F., Krtolica, A., Beauséjour, C. M., Parrinello, S., ... Campisi, J. (2010). A human-like senescence-associated secretory phenotype is conserved in mouse cells dependent on physiological oxygen. *PLoS ONE*, *5*(2). <https://doi.org/10.1371/journal.pone.0009188>
- Cosme-Blanco, W., Shen, M. F., Lazar, A. J. F., Pathak, S., Lozano, G., Multani, A. S., & Chang, S. (2007). Telomere dysfunction suppresses spontaneous tumorigenesis in vivo by initiating p53-dependent cellular senescence. *EMBO Reports*, *8*(5), 497–503. <https://doi.org/10.1038/sj.embor.7400937>
- Cowell, I. G., Sunter, N. J., Singh, P. B., Austin, C. A., Durkacz, B. W., & Tilby, M. J. (2007).  $\gamma$ H2AX foci form preferentially in euchromatin after ionising-radiation. *PLoS ONE*, *2*(10), 1–8. <https://doi.org/10.1371/journal.pone.0001057>

- Cristofalo, V. J., Lorenzini, A., Allen, R. G., Torres, C., & Tresini, M. (2004). Replicative senescence: a critical review. *Mechanisms of Ageing and Development*, *125*(10–11), 827–848. <https://doi.org/10.1016/j.mad.2004.07.010>
- Davalli, P., Mitic, T., Caporali, A., Lauriola, A., & D’Arca, D. (2016). ROS, Cell Senescence, and Novel Molecular Mechanisms in Aging and Age-Related Diseases. *Oxidative Medicine and Cellular Longevity*, *2016*, 1–18. <https://doi.org/10.1155/2016/3565127>
- Davies, H., Edkins, S., Clegg, S., Teague, J., Woffendin, H., Garnett, M. J., ... Futreal, P. A. (2002). Mutations of the BRAF gene in human cancer. *Nature*, *417*, 949–954. <https://doi.org/10.1038/nature00766>
- De Cecco, M., Criscione, S. W., Peckham, E. J., Hillenmeyer, S., Hamm, E. A., Manivannan, J., ... Sedivy, J. M. (2013). Genomes of replicatively senescent cells undergo global epigenetic changes leading to gene silencing and activation of transposable elements. *Aging Cell*, *12*(2), 247–256. <https://doi.org/10.1111/accel.12047>
- De Vitis, M., Berardinelli, F., & Sgura, A. (2018). Telomere length maintenance in cancer: At the crossroad between telomerase and alternative lengthening of telomeres (ALT). *International Journal of Molecular Sciences*, *19*(2). <https://doi.org/10.3390/ijms19020606>
- Delcuve, G. P., Khan, D. H., & Davie, J. R. (2012). Roles of histone deacetylases in epigenetic regulation: emerging paradigms from studies with inhibitors. *Clinical Epigenetics*, *4*(1), 5. <https://doi.org/10.1186/1868-7083-4-5>
- Di Giorgio, E., & Brancolini, C. (2016). Regulation of class IIa HDAC activities: it is not only matter of subcellular localization. *Epigenomics*, *8*(2), 251–269. <https://doi.org/10.2217/epi.15.106>
- Di Giorgio, E., Gagliostro, E., Clocchiatti, A., & Brancolini, C. (2015). The control operated by the cell cycle machinery on MEF2 stability contributes to the downregulation of CDKN1A and entry into S phase. *Molecular and Cellular Biology*, *35*(9), 1633–1647. <https://doi.org/10.1128/MCB.01461-14>
- Di Micco, R., Fumagalli, M., Cicalese, A., Piccinin, S., Gasparini, P., Luise, C., ... D’Adda Di Fagagna, F. (2006). Oncogene-induced senescence is a DNA damage response triggered by DNA hyper-replication. *Nature*. <https://doi.org/10.1038/nature05327>
- Dimri, G. P., Lee, X., Basile, G., Acosta, M., Scott, G., Roskelley, C., ... Campisi, J. (1995). A biomarker that identifies senescent human cells in culture and in aging skin in vivo. *Proceedings of the National Academy of Sciences of the United States of America*,

- 92(20), 9363–9367. <https://doi.org/10.1073/pnas.92.20.9363>
- Dou, Z., Xu, C., Donahue, G., Shimi, T., Pan, J. A., Zhu, J., ... Berger, S. L. (2015). Autophagy mediates degradation of nuclear lamina. *Nature*, 527(7576), 105–109. <https://doi.org/10.1038/nature15548>
- Dreesen, O., Chojnowski, A., Ong, P. F., Zhao, T. Y., Common, J. E., Lunny, D., ... Colman, A. (2013). Lamin B1 fluctuations have differential effects on cellular proliferation and senescence. *Journal of Cell Biology*, 200(5), 605–617. <https://doi.org/10.1083/jcb.201206121>
- Dressel, U., Bailey, P. J., Wang, S. C. M., Downes, M., Evans, R. M., & Muscat, G. E. O. (2001). A Dynamic Role for HDAC7 in MEF2-mediated Muscle Differentiation. *Journal of Biological Chemistry*, 276(20), 17007–17013. <https://doi.org/10.1074/jbc.M101508200>
- Fernández-Medarde, A., & Santos, E. (2011). Ras in cancer and developmental diseases. *Genes and Cancer*, 2(3), 344–358. <https://doi.org/10.1177/1947601911411084>
- Firsanov, D. V., Solovjeva, L. V., & Svetlova, M. P. (2011). H2AX phosphorylation at the sites of DNA double-strand breaks in cultivated mammalian cells and tissues. *Clinical Epigenetics*, 2(2), 283–297. <https://doi.org/10.1007/s13148-011-0044-4>
- Fischle, W., Dequiedt, F., Hendzel, M. J., Guenther, M. G., Lazar, M. A., Voelter, W., ... Tg, A. (2002). Enzymatic Activity Associated with Class II HDACs Is Dependent on a Multiprotein Complex Containing HDAC3 and SMRT / N-CoR. *Molecular Cell*, 9, 45–57.
- Fortuny, A., & Polo, S. E. (2018). The response to DNA damage in heterochromatin domains. *Chromosoma*, 127(3), 291–300. <https://doi.org/10.1007/s00412-018-0669-6>
- Freund, A., Laberge, R.-M., Demaria, M., & Campisi, J. (2012). Lamin B1 loss is a senescence-associated biomarker. *Molecular Biology of the Cell*. <https://doi.org/10.1091/mbc.E11-10-0884>
- Goldman, R. D., Shumaker, D. K., Erdos, M. R., Eriksson, M., Goldman, A. E., Gordon, L. B., ... Collins, F. S. (2004). Accumulation of mutant lamin A causes progressive changes in nuclear architecture in Hutchinson–Gilford progeria syndrome. *Proceedings of the National Academy of Sciences*, 101(24), 8963–8968. <https://doi.org/10.1073/pnas.0402943101>
- Gray-Schopfer, V. C., Cheong, S. C., Chong, H., Chow, J., Moss, T., Abdel-Malek, Z. A., ... Bennett, D. C. (2006). Cellular senescence in naevi and immortalisation in melanoma: A role for p16? *British Journal of Cancer*, 95(4), 496–505.

<https://doi.org/10.1038/sj.bjc.6603283>

- Gregoire, S., & Yang, X.-J. (2006). Association with Class Iia Histone Deacetylases Upregulates the Sumoylation of MEF2 Transcription Factors. *Molecular and Cellular Biology*, 26(8), 3335–3335. <https://doi.org/10.1128/mcb.26.8.3335.2006>
- Gregoretto, I. V., Lee, Y. M., & Goodson, H. V. (2004). Molecular evolution of the histone deacetylase family: Functional implications of phylogenetic analysis. *Journal of Molecular Biology*, 338(1), 17–31. <https://doi.org/10.1016/j.jmb.2004.02.006>
- Grozinger, C. M., & Schreiber, S. L. (2000). Regulation of histone deacetylase 4 and 5 and transcriptional activity by 14-3-3-dependent cellular localization. *Proceedings of the National Academy of Sciences of the United States of America*, 97(14), 7835–7840. <https://doi.org/10.1073/pnas.140199597>
- Guarente, L. (2007). Sirtuins in aging and disease. *Cold Spring Harbor Symposia on Quantitative Biology*, 72, 483–488. <https://doi.org/10.1101/sqb.2007.72.024>
- Haigis, M. C., & Guarente, L. P. (2006). Mammalian sirtuins--emerging roles in physiology, aging, and calorie restriction. *Genes & Development*, 20(21), 2913–2921. <https://doi.org/10.1101/gad.1467506>
- Hanahan, D., & Weinberg, R. A. (2011). Hallmarks of Cancer: The Next Generation. *Cell*, 144(5), 646–674. <https://doi.org/10.1016/j.cell.2011.02.013>
- Hanks, S. K. (2003). Genomic analysis of the eukaryotic protein kinase superfamily: a perspective. *Genome Biology*, 4(5), 111. <https://doi.org/10.1186/gb-2003-4-5-111>
- Harrigan, J. A., Belotserkovskaya, R., Coates, J., Dimitrova, D. S., Polo, S. E., Bradshaw, C. R., ... Jackson, S. P. (2011). Replication stress induces 53BP1-containing OPT domains in G1 cells. *Journal of Cell Biology*, 193(1), 97–108. <https://doi.org/10.1083/jcb.201011083>
- HAYFLICK, L., & MOORHEAD, P. S. (1961). The serial cultivation of human diploid cell strains. *Experimental Cell Research*, 25(3), 585–621. [https://doi.org/10.1016/0014-4827\(61\)90192-6](https://doi.org/10.1016/0014-4827(61)90192-6)
- Herbig, U., Ferreira, M., Condel, L., Carey, D., & Sedivy, J. M. (2006). Cellular senescence in aging primates. *Science*, 311(5765), 1257. <https://doi.org/10.1126/science.1122446>
- Hernandez-Segura, A., Nehme, J., & Demaria, M. (2018). Hallmarks of Cellular Senescence. *Trends in Cell Biology*, 28(6), 436–453. <https://doi.org/10.1016/j.tcb.2018.02.001>
- Hubackova, S., Krejcikova, K., Bartek, J., & Hodny, Z. (2012). IL1-and TGFβ-Nox4 signaling, oxidative stress and DNA damage response are shared features of replicative, oncogene-induced, and drug-induced paracrine “Bystander senescence.” *Aging*, 4(12),

932–951. <https://doi.org/10.18632/aging.100520>

- Ivanov, A., Pawlikowski, J., Manoharan, I., van Tuyn, J., Nelson, D. M., Rai, T. S., ... Adams, P. D. (2013). Lysosome-mediated processing of chromatin in senescence. *The Journal of Cell Biology*, 202(1), 129–143. <https://doi.org/10.1083/jcb.201212110>
- Kadosh, D., & Struhl, K. (1998). Histone deacetylase activity of Rpd3 is important for transcriptional repression in vivo. *Genes & Development*, 12(6), 797–805. <https://doi.org/10.1101/gad.12.6.797>
- Karlseder, J. (2002). Senescence Induced by Altered Telomere State, Not Telomere Loss. *Science*, 295(5564), 2446–2449. <https://doi.org/10.1126/science.1069523>
- Karlseder, J., Broccoli, D., Yumin, D., Hardy, S., & De Lange, T. (1999). p53- and ATM-dependent apoptosis induced by telomeres lacking TRF2. *Science*, 283(5406), 1321–1325. <https://doi.org/10.1126/science.283.5406.1321>
- Kennedy, A. L., McBryan, T., Enders, G. H., Johnson, F. B., Zhang, R., & Adams, P. D. (2010). Senescent mouse cells fail to overtly regulate the HIRA histone chaperone and do not form robust Senescence Associated Heterochromatin Foci. *Cell Division*, 5, 1–11. <https://doi.org/10.1186/1747-1028-5-16>
- Kim, J. A., Kruhlak, M., Dotiwala, F., Nussenzweig, A., & Haber, J. E. (2007). Heterochromatin is refractory to  $\gamma$ -H2AX modification in yeast and mammals. *Journal of Cell Biology*, 178(2), 209–218. <https://doi.org/10.1083/jcb.200612031>
- Kim, J. J., Lee, S. B., Yi, S. Y., Han, S. A., Kim, S. H., Lee, J. M., ... Lou, Z. (2017). WSB1 overcomes oncogene-induced senescence by targeting ATM for degradation. *Cell Research*, 27(2), 274–293. <https://doi.org/10.1038/cr.2016.148>
- Kosar, M., Bartkova, J., Hubackova, S., Hodny, Z., Lukas, J., & Bartek, J. (2011). Senescence-associated heterochromatin foci are dispensable for cellular senescence, occur in a cell type- And insult-dependent manner, and follow expression of p16ink4a. *Cell Cycle*, 10(3), 457–468. <https://doi.org/10.4161/cc.10.3.14707>
- Kuilman, T., & Peeper, D. S. (2009). Senescence-messaging secretome: SMS-ing cellular stress. *Nature Reviews Cancer*, 9(2), 81–94. <https://doi.org/10.1038/nrc2560>
- Lee, S. H., Lee, J. H., Lee, H. Y., & Min, K. J. (2019). Sirtuin signaling in cellular senescence and aging. *BMB Reports*, 52(1), 24–34. <https://doi.org/10.5483/BMBRep.2019.52.1.290>
- Lenain, C., De Graaf, C. A., Pagie, L., Visser, N. L., De Haas, M., De Vries, S. S., ... Peeper, D. S. (2017). Massive reshaping of genome-nuclear lamina interactions during oncogene-induced senescence. *Genome Research*, 27(10), 1634–1644.

<https://doi.org/10.1101/gr.225763.117>

- Li, H., Fu, Y. X., Wu, Q., Zhou, Y., Crossman, D. K., Yang, P., ... Mountz, J. D. (2015). Interferon-induced mechanosensing defects impede apoptotic cell clearance in lupus. *Journal of Clinical Investigation*, *125*(7), 2877–2890. <https://doi.org/10.1172/JCI81059>
- Linskens, M., Harley, C., West, M., Campisi, J., & Hayflick, L. (1995). Replicative senescence and cell death. *Science*, *267*(5194), 17–17. <https://doi.org/10.1126/science.7848496>
- Lu, J., McKinsey, T. A., Nicol, R. L., & Olson, E. N. (2000). Signal-dependent activation of the MEF2 transcription factor by dissociation from histone deacetylases. *Proceedings of the National Academy of Sciences of the United States of America*, *97*(8), 4070–4075. <https://doi.org/10.1073/pnas.080064097>
- Martin, M., Kettmann, R., & Dequiedt, F. (2007). Class IIa histone deacetylases: Regulating the regulators. *Oncogene*. <https://doi.org/10.1038/sj.onc.1210613>
- Mattson, M. P., & Arumugam, T. V. (2018). Hallmarks of Brain Aging: Adaptive and Pathological Modification by Metabolic States. *Cell Metabolism*, *27*(6), 1176–1199. <https://doi.org/10.1016/j.cmet.2018.05.011>
- McCord, R. P., Nazario-Toole, A., Zhang, H., Chines, P. S., Zhan, Y., Erdos, M. R., ... Cao, K. (2013). Correlated alterations in genome organization, histone methylation, and DNA-lamin A/C interactions in Hutchinson-Gilford progeria syndrome. *Genome Research*, *23*(2), 260–269. <https://doi.org/10.1101/gr.138032.112>
- McHugh, D., & Gil, J. (2018). Senescence and aging: Causes, consequences, and therapeutic avenues. *Journal of Cell Biology*, *217*(1), 65–77. <https://doi.org/10.1083/jcb.201708092>
- McKinsey, T. A., Zhang, C. L., & Olson, E. N. (2002). MEF2: A calcium-dependent regulator of cell division, differentiation and death. *Trends in Biochemical Sciences*, *27*(1), 40–47. [https://doi.org/10.1016/S0968-0004\(01\)02031-X](https://doi.org/10.1016/S0968-0004(01)02031-X)
- McKinsey, T. a, Zhang, C. L., Lu, J., & Olson, E. N. (2000). Signal-dependent nuclear export of a histone deacetylase regulates muscle differentiation. *Nature*, *408*(6808), 106–111. <https://doi.org/10.1038/35040593>
- Michaloglou, C., Vredeveld, L. C. W., Soengas, M. S., Denoyelle, C., Kuilman, T., Van Der Horst, C. M. A. M., ... Peeper, D. S. (2005). BRAFE600-associated senescence-like cell cycle arrest of human naevi. *Nature*, *436*(7051), 720–724. <https://doi.org/10.1038/nature03890>
- Miyauchi, H., Minamino, T., Tateno, K., Kunieda, T., Toko, H., & Komuro, I. (2004). Akt negatively regulates the in vitro lifespan of human endothelial cells via a p53/p21-

- dependent pathway. *EMBO Journal*, 23(1), 212–220.  
<https://doi.org/10.1038/sj.emboj.7600045>
- Moschella, F., Torelli, G. F., Valentini, M., Urbani, F., Buccione, C., Petrucci, M. T., ... Proietti, E. (2013). Cyclophosphamide induces a type I interferon-Associated sterile inflammatory response signature in cancer patients' blood cells: Implications for cancer chemoimmunotherapy. *Clinical Cancer Research*, 19(15), 4249–4261.  
<https://doi.org/10.1158/1078-0432.CCR-12-3666>
- Muñoz-Espín, D., Cañamero, M., Maraver, A., Gómez-López, G., Contreras, J., Murillo-Cuesta, S., ... Serrano, M. (2013). XProgrammed cell senescence during mammalian embryonic development. *Cell*, 155(5), 1104. <https://doi.org/10.1016/j.cell.2013.10.019>
- Munro, J., Barr, N. I., Ireland, H., Morrison, V., & Parkinson, E. K. (2004). Histone deacetylase inhibitors induce a senescence-like state in human cells by a p16-dependent mechanism that is independent of a mitotic clock. *Experimental Cell Research*, 295(2), 525–538. <https://doi.org/10.1016/j.yexcr.2004.01.017>
- Narita, M., Narita, M., Krizhanovsky, V., Nuñez, S., Chicas, A., Hearn, S. A., ... Lowe, S. W. (2006). A Novel Role for High-Mobility Group A Proteins in Cellular Senescence and Heterochromatin Formation. *Cell*, 126(3), 503–514.  
<https://doi.org/10.1016/j.cell.2006.05.052>
- Narita, M., Nuñez, S., Heard, E., Narita, M., Lin, A. W., Hearn, S. A., ... Lowe, S. W. (2003). Rb-mediated heterochromatin formation and silencing of E2F target genes during cellular senescence. *Cell*, 113(6), 703–716. [https://doi.org/10.1016/S0092-8674\(03\)00401-X](https://doi.org/10.1016/S0092-8674(03)00401-X)
- Nelson, G., Wordsworth, J., Wang, C., Jurk, D., Lawless, C., Martin-Ruiz, C., & von Zglinicki, T. (2012). A senescent cell bystander effect: Senescence-induced senescence. *Aging Cell*, 11(2), 345–349. <https://doi.org/10.1111/j.1474-9726.2012.00795.x>
- Ota, H., Akishita, M., Eto, M., Iijima, K., Kaneki, M., & Ouchi, Y. (2007). Sirt1 modulates premature senescence-like phenotype in human endothelial cells. *Journal of Molecular and Cellular Cardiology*, 43(5), 571–579. <https://doi.org/10.1016/j.yjmcc.2007.08.008>
- Parra, M. (2015). Class IIa HDACs - New insights into their functions in physiology and pathology. *FEBS Journal*, 282(9), 1736–1744. <https://doi.org/10.1111/febs.13061>
- Parra, M., Kasler, H., McKinsey, T. A., Olson, E. N., & Verdin, E. (2005). Protein kinase D1 phosphorylates HDAC7 and induces its nuclear export after T-cell receptor activation. *Journal of Biological Chemistry*, 280(14), 13762–13770.  
<https://doi.org/10.1074/jbc.M413396200>

- Pollock, P. M., Harper, U. L., Hansen, K. S., Yudt, L. M., Stark, M., Robbins, C. M., ... Meltzer, P. S. (2003). High frequency of BRAF mutations in nevi. *Nature Genetics*, 33(1), 19–20. <https://doi.org/10.1038/ng1054>
- Pon, J. R., & Marra, M. A. (2016). MEF2 transcription factors: developmental regulators and emerging cancer genes. *Oncotarget*, 7(3), 2297–2312. <https://doi.org/10.18632/oncotarget.6223>
- Potthoff, M. J., & Olson, E. N. (2007). MEF2: a central regulator of diverse developmental programs. *Development*, 134(23), 4131–4140. <https://doi.org/10.1242/dev.008367>
- Price, J. S., Waters, J. G., Darrah, C., Pennington, C., Edwards, D. R., Donell, S. T., & Clark, I. M. (2002). The role of chondrocyte senescence in osteoarthritis. *Aging Cell*, 1(1), 57–65. <https://doi.org/10.1046/j.1474-9728.2002.00008.x>
- Rodier, F., Muñoz, D. P., Teachenor, R., Chu, V., Le, O., Bhaumik, D., ... Campisi, J. (2011). DNA-SCARS: Distinct nuclear structures that sustain damage-induced senescence growth arrest and inflammatory cytokine secretion. *Journal of Cell Science*, 124(1), 68–81. <https://doi.org/10.1242/jcs.071340>
- Rogakou, E. P., Pilch, D. R., Orr, A. H., Ivanova, V. S., & Bonner, W. M. (1998). DNA double-stranded breaks induce histone H2AX phosphorylation on serine 139. *Journal of Biological Chemistry*, 273(10), 5858–5868. <https://doi.org/10.1074/jbc.273.10.5858>
- Rouse, J., & Jackson, S. P. (2002). Interfaces between the detection, signaling, and repair of DNA damage. *Science*, 297(5581), 547–551. <https://doi.org/10.1126/science.1074740>
- Schmitt, C. A., Fridman, J. S., Yang, M., Lee, S., Baranov, E., Hoffman, R. M., & Lowe, S. W. (2002). A Senescence Program Controlled by p53 and p16INK4a Contributes to the Outcome of Cancer Therapy. *Cell*, 109(3), 335–346. [https://doi.org/10.1016/S0092-8674\(02\)00734-1](https://doi.org/10.1016/S0092-8674(02)00734-1)
- Serrano, M., Lin, A. W., McCurrach, M. E., Beach, D., & Lowe, S. W. (1997). Oncogenic ras provokes premature cell senescence associated with accumulation of p53 and p16(INK4a). *Cell*. [https://doi.org/10.1016/S0092-8674\(00\)81902-9](https://doi.org/10.1016/S0092-8674(00)81902-9)
- Sherman, M. Y., Meng, L., Stampfer, M., Gabai, V. L., & Yaglom, J. A. (2011). Oncogenes induce senescence with incomplete growth arrest and suppress the DNA damage response in immortalized cells. *Aging Cell*, 10(6), 949–961. <https://doi.org/10.1111/j.1474-9726.2011.00736.x>
- Shumaker, D. K., Dechat, T., Kohlmaier, A., Adam, S. A., Bozovsky, M. R., Erdos, M. R., ... Goldman, R. D. (2006). Mutant nuclear lamin A leads to progressive alterations of epigenetic control in premature aging. *Proceedings of the National Academy of Sciences*

- of the United States of America*, 103(23), 8703–8708.  
<https://doi.org/10.1073/pnas.0602569103>
- Sousa-Victor, P., Gutarra, S., García-Prat, L., Rodríguez-Ubreva, J., Ortet, L., Ruiz-Bonilla, V., ... Muñoz-Cánoves, P. (2014). Geriatric muscle stem cells switch reversible quiescence into senescence. *Nature*, 506(7488), 316–321.  
<https://doi.org/10.1038/nature13013>
- Storer, M., Mas, A., Robert-Moreno, A., Pecoraro, M., Ortells, M. C., Di Giacomo, V., ... Keyes, W. M. (2013). Senescence Is a Developmental Mechanism that Contributes to Embryonic Growth and Patterning. *Cell*, 155(5), 1119–1130.  
<https://doi.org/10.1016/j.cell.2013.10.041>
- Swanson, E. C., Manning, B., Zhang, H., & Lawrence, J. B. (2013). Higher-order unfolding of satellite heterochromatin is a consistent and early event in cell senescence. *Journal of Cell Biology*, 203(6), 929–942. <https://doi.org/10.1083/jcb.201306073>
- Takai, H., Smogorzewska, A., & de Lange, T. (2003). DNA Damage Foci at Dysfunctional Telomeres. *Current Biology*, 13(17), 1549–1556. [https://doi.org/10.1016/S0960-9822\(03\)00542-6](https://doi.org/10.1016/S0960-9822(03)00542-6)
- Tilstra, J. S., Robinson, A. R., Wang, J., Gregg, S. Q., Clauson, C. L., Reay, D. P., ... Robbins, P. D. (2012). NF-κB inhibition delays DNA damage-induced senescence and aging in mice. *The Journal of Clinical Investigation*, 122(7), 2601–2612.  
<https://doi.org/10.1172/JCI45785>
- Wajapeyee, N., Serra, R. W., Zhu, X., Mahalingam, M., & Green, M. R. (2008). Oncogenic BRAF Induces Senescence and Apoptosis through Pathways Mediated by the Secreted Protein IGFBP7. *Cell*, 132(3), 363–374. <https://doi.org/10.1016/j.cell.2007.12.032>
- Ward, I. M., Minn, K., Deursen, J. Van, & Chen, J. (2003). p53 Binding Protein 53BP1 Is Required for DNA Damage Responses and Tumor Suppression in Mice These include : p53 Binding Protein 53BP1 Is Required for DNA Damage Responses and Tumor Suppression in Mice Downloaded from <http://mcb.asm.org/> on September 28 , 23(7), 2556–2563. <https://doi.org/10.1128/MCB.23.7.2556>
- Wei, S., Wei, S., & Sedivy, J. M. (1999). Expression of catalytically active telomerase does not prevent premature senescence caused by overexpression of oncogenic Ha-Ras in normal human fibroblasts. *Cancer Research*, 59(7), 1539–1543. Retrieved from <http://www.ncbi.nlm.nih.gov/pubmed/10197626>
- Yang, X., & Gre, S. (2005). Class II Histone Deacetylases : from Sequence to Function , Regulation , and Clinical Implication MINIREVIEW Class II Histone Deacetylases :

- from Sequence to Function , Regulation , and Clinical Implication. *Molecular and Cellular Biology*, 25(8), 2873–2884. <https://doi.org/10.1128/MCB.25.8.2873>
- Yilmaz, Ö. H., Valdez, R., Theisen, B. K., Guo, W., Ferguson, D. O., Wu, H., & Morrison, S. J. (2006). Pten dependence distinguishes haematopoietic stem cells from leukaemia-initiating cells. *Nature*, 441(7092), 475–482. <https://doi.org/10.1038/nature04703>
- Zhang, C. L., McKinsey, T. A., Chang, S., Antos, C. L., Hill, J. A., & Olson, E. N. (2002). Class II histone deacetylases act as signal-responsive repressors of cardiac hypertrophy. *Cell*, 110(4), 479–488. [https://doi.org/10.1016/S0092-8674\(02\)00861-9](https://doi.org/10.1016/S0092-8674(02)00861-9)
- Zhang, R., Chen, W., & Adams, P. D. (2007). Molecular Dissection of Formation of Senescence-Associated Heterochromatin Foci. *Molecular and Cellular Biology*, 27(6), 2343–2358. <https://doi.org/10.1128/mcb.02019-06>
- Zindy, F., Eischen, C. M., Randle, D. H., Kamijo, T., Cleveland, J. L., Sherr, C. J., & Roussel, M. F. (1998). Myc signaling via the ARF tumor suppressor regulates p53-dependent apoptosis and immortalization. *Genes & Development*, 12(15), 2424–2433. <https://doi.org/10.1101/gad.12.15.2424>

# Unscheduled HDAC4 repressive activity in human fibroblasts triggers TP53-dependent senescence and favors cell transformation

Harikrishnareddy Paluvai, Eros Di Giorgio and Claudio Brancolini

Department of Medicine, Università degli Studi di Udine, Italy

## Keywords

AKT; class IIa HDACs; MEF2; OIS; pRB; RAS

## Correspondence

C. Brancolini, Department of Medicine, Università degli Studi di Udine, P.le Kolbe 4 – 33100 Udine, Italy  
Tel: + 39 0432 494382  
E-mail: claudio.brancolini@uniud.it

Harikrishnareddy Paluvai and Eros Di Giorgio contributed equally to this article.

(Received 14 June 2018, revised 13 September 2018, accepted 2 October 2018, available online 14 November 2018)

doi:10.1002/1878-0261.12392

Expression of the class IIa HDACs is frequently altered in different human cancers. In mouse models these transcriptional repressors can trigger transformation, acting as bona fide oncogenes. Whether class IIa HDACs also exhibit transforming activities in human cells is currently unknown. We infected primary human fibroblasts with retroviruses to investigate the transforming activity of HDAC4 in cooperation with well-known oncogenes. We have discovered that HDAC4 triple mutant (S246A, S467A, S632A) (HDAC4-TM), a nuclear resident version of the deacetylase, triggers TP53 stabilization and OIS (oncogene-induced senescence). Unlike RAS, HDAC4-induced OIS was TP53-dependent and characterized by rapid cell cycle arrest and accumulation of an unusual pattern of  $\gamma$ H2AX-positive foci. The inactivation of both TP53 and of the retinoblastoma (pRb) tumor suppressors, as induced by the viral oncogenes large and small T of SV40, triggers anchorage-independent growth in RAS, HDAC4-TM and, to a lesser extent, in HDAC4-wild type (WT)-expressing cells. Our results suggest an oncogenic function of class IIa HDACs in human cells, and justify further efforts to discover and evaluate isoform-specific inhibitors of these epigenetic regulators from a therapeutic perspective.

## 1. Introduction

The remodeling of transcriptional programs is a key aspect of tumorigenic processes (Bradner *et al.*, 2017). Oncogenes and tumor suppressor genes can influence transcription directly by acting as transcription factors (TFs) or indirectly by supervising signaling pathways that control the transcriptional machinery (Bradner *et al.*, 2017). Transcriptional remodeling requires epigenetic

changes and the involvement of chromatin modifiers (Brien *et al.*, 2016; Yang *et al.*, 2012). Epigenetic plasticity is emerging as an important hallmark of cancer. At each step of tumor progression, from initiation to evolution, epigenetic plasticity is necessary to fuel new waves of transcription (Koschmann *et al.*, 2017).

Histone modifications contribute to chromatin remodeling and to the epigenetic signature. Dysfunctions in enzymes controlling these post-transcriptional

## Abbreviations

4-OHT, 4 hydroxy-tamoxifen; BrdU, bromodeoxyuridine; DDR, DNA damage response; DEG, differentially expressed genes; DMEM, Dulbecco's modified Eagle's medium; DN, dominant negative; EMEM, Earle's salts minimal essential medium; ENG, engrailed; ER, estrogen receptor alpha; GSEA, gene set enrichment analysis; HDAC4-TM, HDAC4 triple mutant (S246A, S467A, S632A); HDAC, histone deacetylase; HPRT, hypoxanthine phosphoribosyltransferase 1; IFN, interferon; LT, large T antigen; MEF2, myocyte enhancer factor; MTT, 3-(4,5-dimethylthiazol-2-yl)-2,5-diphenyltetrazolium bromide; myr-AKT1, myristoylated AKT1; OIS, oncogene-induced senescence; pRB, retinoblastoma protein; PTM, post-transcriptional modification; SASP, senescence-associated secretory phenotype; ST, small T antigen; TERT, telomerase catalytic subunit; TF, transcription factor; WT, wild type.

modifications (PTMs) can affect the tumorigenic process (Cheng *et al.*, 2017a,b; Montero-Conde *et al.*, 2017). Both pro-tumorigenic and tumor-suppressive activities have been reported for some epigenetic regulators, which reflects the importance of the specific cellular context (Beira *et al.*, 2018; Chen *et al.*, 2018; Koschmann *et al.*, 2017; Wang *et al.*, 2017).

In addition to alterations in epigenetic regulators, mutations in histones can trigger the tumorigenic process. Oncogenic mutations in H3.3 genes encoding K27M and G34R/V have been characterized in pediatric high-grade gliomas (Fontebasso *et al.*, 2014; Khuong-Quang *et al.*, 2012; Schwartzentruber *et al.*, 2012; Taylor *et al.*, 2014).

Histone deacetylases (HDACs) are important erasers of epigenetic marks. HDAC can be subdivided into five subclasses (I, IIa, IIb, III and IV). Class IIa includes four members (HDAC4/5/7/9) characterized by a poor deacetylase activity, phosphorylation-dependent nuclear/cytoplasmic shuttling and an extended amino-terminal region devoted to TFs and co-repressor binding (Martin *et al.*, 2007). The C-terminal deacetylase domain is required to interact with the SMRT/N-CoR/HDAC3 complex, which confers the KDAC activity (Lahm *et al.*, 2007). Important partners of class IIa HDACs are members of the MEF2 (myocyte enhancer factors) family of TFs (Clocchiatti *et al.*, 2013a,b; Di Giorgio and Brancolini, 2016). There is evidence from several reports of the altered expression of class IIa in human cancer (Barneda-Zahonero and Parra, 2012; Clocchiatti *et al.*, 2011). Furthermore, *in vitro* and *in vivo* studies have proved the oncogenic role of HDAC4 (Di Giorgio *et al.*, 2013; Peruzzo *et al.*, 2016), HDAC7 (Di Giorgio *et al.*, 2013; Lei *et al.*, 2017; Rad *et al.*, 2010) and HDAC9 (Gil *et al.*, 2016) in different murine models. Since human cells behave differently from rodent cells and, in general, require more genetic alterations to acquire a neoplastic phenotype (Boehm *et al.*, 2005), whether these deacetylases can transform human cells is currently unknown.

*In vitro* oncogenic transformation of normal cells represents an invaluable model to prove tumor-suppressive or oncogenic functions of a specific gene (Funes *et al.*, 2014). The robustness of the assay is corroborated by the correlation between the *in vitro* transforming activities of the tested genes and their implications in human cancers (Boehm and Hahn, 2005; Boehm *et al.*, 2005; Maya-Mendoza *et al.*, 2015; Seger *et al.*, 2002). Moreover, these *in vitro* generated transformed cells can provide alternatives to costly mouse models, as well as genetically defined environments for testing anticancer therapies (Balani *et al.*, 2017). In this manuscript we investigated the ability of

HDAC4 to cooperate with well-known oncogenes to transform human fibroblasts.

## 2. Materials and methods

### 2.1. Cell cultures and reagents

The BJ/TERT cells were cultured in Earle's salts minimal essential medium (EMEM) (Euroclone, Milan, Italy) completed with nonessential amino acids (HyClone, Little Chalfont, UK). Media were supplemented with 10% FBS, L-glutamine (2 mM), penicillin (100 U·mL<sup>-1</sup>), and streptomycin (100 µg·mL<sup>-1</sup>) (Lonza, Basel, Switzerland). Cells expressing the inducible form of the transgenes were grown in medium without phenol red. For S-phase analysis, cells were grown for 3 h with 50 µM bromodeoxyuridine (BrdU, Sigma). Mouse anti-BrdU (Sigma, St. Louis, MO, USA) was used as the primary antibody in the immunofluorescent assays. Nuclei were stained with Hoechst 33258 (Sigma).

### 2.2. Invasion and soft agar assays

For invasion assay, each well of the invasion chamber (CLS3428, Corning, New York, NY, USA) was coated with 200 µL of Matrigel matrix coating solution (Cultrex, Trevigen, Gaithersburg, MD USA). Next, a cell suspension of 30 000 cells in 0.1% FBS-Dulbecco's modified Eagle's medium (DMEM) was added. As chemoattractant, 20% FBS-DMEM was added in each lower chamber. As a control, 0.1% FBS-DMEM was used to evaluate random invasion. For soft agar assays, equal volumes of 1.2% agar and DMEM were mixed to generate 0.6% base agar. A total of 0.8 × 10<sup>5</sup> cells were seeded in 0.3% top agar, followed by incubation at 37 °C in humidified conditions. The cells were grown for 21 days and visualized by MTT [3-(4,5-dimethylthiazol-2-yl)-2,5-diphenyltetrazolium bromide] staining. Images were taken with a DN6000 Leica microscope that allows the the number and the diameter of the foci to be counted.

### 2.3. Plasmid construction, transfections, retroviral infections

The pWZL/HDAC4-WT and mutants, pWZL-Neo/E1A (1–143) and pBABE-Puro/myristoylated AKT1 (myr-AKT1)-expressing plasmids were previously described (Aistle *et al.*, 2012; Deng *et al.*, 2005; Di Giorgio *et al.*, 2013). pCW-Puro/HDAC4 and H-RAS/G12V plasmids were obtained by subcloning with a PCR method, HDAC4 and H-RAS/G12V into the all-in-one DOX-inducible pCW-Cas9 plasmid (#50661

Addgene, Cambridge MA, USA). pMXPIE-Puro HDAC4-WT/TM, H-RAS/G12V were obtained by sub-cloning with a PCR method the ORF into the 4 hydroxy-tamoxifen (4-OHT)- inducible pMXPIE plasmid (Toledo *et al.*, 2008). The plasmids used to silence MEF2D and plasmids encoding for MEF2D-FLAG and MEF2-Engrailed FLAG (MEF2-ENG) were previously described (Di Giorgio *et al.*, 2015, 2017). For lentivirus-based knock-down, HEK-293T cells were transfected with 1.8  $\mu\text{g}$  of VSV-G, 5  $\mu\text{g}$  of  $\Delta 8.9$  and 8  $\mu\text{g}$  of pLKO plasmids. After 36 h at 37 °C, virions were collected and opportunely diluted in fresh medium. Retroviral infections were performed as previously described (Di Giorgio *et al.*, 2017).

#### 2.4. RNA extraction and quantitative qRT-PCR

Cells were lysed using Tri-Reagent (Molecular Research Center, Cincinnati, OH USA). A total of 1  $\mu\text{g}$  of total RNA was retrotranscribed using 100 U of Moloney murine leukemia virus reverse transcriptase (Invitrogen, Carlsbad, CA, USA). qRT-PCR analyses were performed using Bio-Rad CFX96 and SYBR green technology (Resnova, Roma, Italy). The data were analyzed by a comparative threshold cycle using the  $\beta 2$  microglobulin gene and hypoxanthine phosphoribosyltransferase 1 (HPRT) as normalizer genes. All reactions were done in triplicate.

#### 2.5. Antibodies

Antibodies used were against MEF2D (BD Bioscience), H3K27ac (ab4729; Abcam, Cambridge, MA, USA), H3K27me3 (ab195477, Abcam) HDAC4 (Paroni *et al.*, 2004),  $\gamma$ H2AX (9718, Cell Signalling, Leiden, The Netherlands), TP53 (DO-7; Dako, Santa Clara, CA, USA), LT SV40 (sc-147, Santa Cruz), Lamin B1 (ab16048, Abcam), p21 (CP74, Sigma), RACK1 (sc-17754, Santa Cruz, Dallas, TX, USA), GFP (Paroni *et al.*, 2004).

#### 2.6. Immunofluorescence and immunoblotting

Immunofluorescence and immunoblotting were performed as previously described (Di Giorgio *et al.*, 2017). Briefly, cells were fixed with 3% paraformaldehyde and permeabilized with 0.1% Triton X-100. Secondary antibodies were conjugated to Alexa Fluor 488, 546 and 633 (Molecular Probes, Eugene, OR, USA). Cells were imaged with a Leica confocal microscopy (LSM) SP2 and SP8. After SDS/PAGE and immunoblotting, cell lysates were incubated with primary antibodies. HRP-conjugated secondary antibodies

were from Sigma-Aldrich and blots were developed with Super Signal West Dura (ThermoFisher Scientific, Waltham, MA, USA).

#### 2.7. SA- $\beta$ -gal assay

For SA- $\beta$ -gal assay, cells were fixed in a solution of 2% formaldehyde/0.2% glutaraldehyde and stained with staining solution: 40 mM citric acid/Na phosphate buffer, 5 mM  $\text{K}_4[\text{Fe}(\text{CN})_6]3\text{H}_2\text{O}$ , 5 mM  $\text{K}_3[\text{Fe}(\text{CN})_6]$ , 150 mM sodium chloride, 2 mM magnesium chloride and 1  $\text{mg}\cdot\text{mL}^{-1}$  X-gal (Debacq-Chainiaux *et al.*, 2009). Staining was performed for 16 h at 37 °C and cells were imaged under bright-field microscope (Leica). To quantify SA- $\beta$ -gal activity, the percentage of positively stained blue cells versus total cells were counted (300–400 cells in total were counted per each round).

#### 2.8. Matrigel plug assay

A total of 1600 cells were suspended in a Matrigel solution (20  $\mu\text{L}$  0.1% FBS-EMEM, 60  $\mu\text{L}$  Matrigel) and plated on coverslips in 35-mm tissue culture plates. After 30 min of incubation at 37 °C, cells were fed with EMEM–20% FBS. Following a 4-day incubation, coverslips were fixed and processed for fluorescence analysis.

#### 2.9. Transcriptome profiling and data analysis

Total RNA was isolated using Direct-zol RNA mini prep (Zymo Research). Preparation and hybridization of cRNA samples were performed at Cogentech (Milan, Italy, <https://www.cogentech.it/>). Labeled cRNAs were hybridized on Affymetrix GeneChip Human Clariom S arrays. Differentially expressed genes (DEGs) were selected based on 1.5 cut-off in the fold changes. Analysis was performed as previously described (Di Giorgio *et al.*, 2013; Picco *et al.*, 2014). Gene set enrichment analysis (GSEA) (Subramanian *et al.*, 2005) and the MSigDB database (<http://software.broadinstitute.org/gsea/index.jsp>) (Liberzon *et al.*, 2015) were used to investigate statistical association between genes modulated by HDAC4-TM or RAS and genes perturbed by other conditions.

#### 2.10. Statistics

For experimental data, a Student *t*-test was used. A *P*-value of 0.05 was chosen as the statistical limit of significance. Unless otherwise indicated, data in the figures are arithmetic means and standard deviations from at least three independent experiments: \**P* < 0.05, \*\**P* < 0.01, \*\*\**P* < 0.005.

**Fig. 1.** The HDAC4 expression in human fibroblasts. (A) Schematic representation of the different HDAC4 versions used in this study. Phosphorylated serine residues, binding sites for 14-3-3 proteins are indicated. (B) Immunoblot analysis using the indicated antibodies in BJ/TERT expressing the indicated transgenes. Vimentin was used as loading control. (C) Normal human diploid fibroblasts (BJ) expressing the telomerase catalytic subunit (TERT) infected with retrovirus expressing the indicated genes and stained for senescence-associated  $\beta$ -galactosidase (SA- $\beta$ -gal) marker. Scale bar: 50  $\mu$ m. (D) Quantitative analysis of SA- $\beta$ -gal positivity from experiments described in (C). Data are expressed as means  $\pm$  SD,  $n = 3$ . Student t-test: \* $P < 0.05$ , \*\*\* $P < 0.005$ . (E) Immunoblot analysis using the indicated antibodies in BJ/TERT expressing the indicated transgenes following treatment with 4-OHT for 48 h. RACK1 was used as loading control. (F) Analysis of cells synthesizing DNA, as scored after BrdU staining at the indicated times. Data are expressed as means  $\pm$  SD,  $n = 4$ . Student t-test: \*\* $P < 0.01$ , \*\*\* $P < 0.005$ . (G) BJ-TERT expressing the indicated transgenes after 8 days of induction were stained for SA- $\beta$ -gal activity. Scale bar: 50  $\mu$ m. (H) Quantitative analysis of SA- $\beta$ -gal positivity from experiments described in (G). Data are expressed as means  $\pm$  SD,  $n = 4$ . \*\*\* $P < 0.005$ . (I) Immunoblot analysis using the indicated antibodies in BJ/TERT expressing the indicated transgenes following treatment with doxycycline for 48 h. Vimentin was used as loading control. (J) Quantitative analysis of SA- $\beta$ -gal positivity in BJ-TERT cells expressing doxycycline-inducible versions of the indicated transgenes after 8 days of induction. Data are expressed as means  $\pm$  SD,  $n = 3$ . Student t-test: \* $P < 0.05$ , \*\* $P < 0.01$ , \*\*\* $P < 0.005$ .

### 3. Results

#### 3.1. Nuclear resident HDAC4 induces senescence in human fibroblasts (BJ-TERT)

To explore the contribution of HDAC4 to the transformation process we used skin-derived BJ fibroblasts, immortalized with the telomerase catalytic subunit (TERT). Since HDAC4 is subjected to intense nuclear export following phosphorylation-mediated 14-3-3 binding, we took advantage from a Ser/Ala mutated version in the three 14-3-3 binding sites (HDAC4-TM). This mutant exhibits stronger repressive activity and is sufficient to transform NIH-3T3 murine fibroblasts (Di Giorgio *et al.*, 2013). Additional HDAC4 mutants tested were a nuclear resident form lacking the MEF2-binding site (HDAC4-TM $\Delta$ MEF2) and a mutant in the nuclear export sequence (HDAC4-L1062A), which similarly to the TM, accumulate in the nucleus (Fig. 1A) (Di Giorgio *et al.*, 2013).

All HDAC4 versions were expressed in BJ-TERT fibroblasts after retroviral infections. We also used well-known oncogenes such as RAS (H-RAS-G12V) and AKT1 (myr-AKT1), for comparison. Expression of the different transgenes was verified by immunoblot (Fig. 1B).

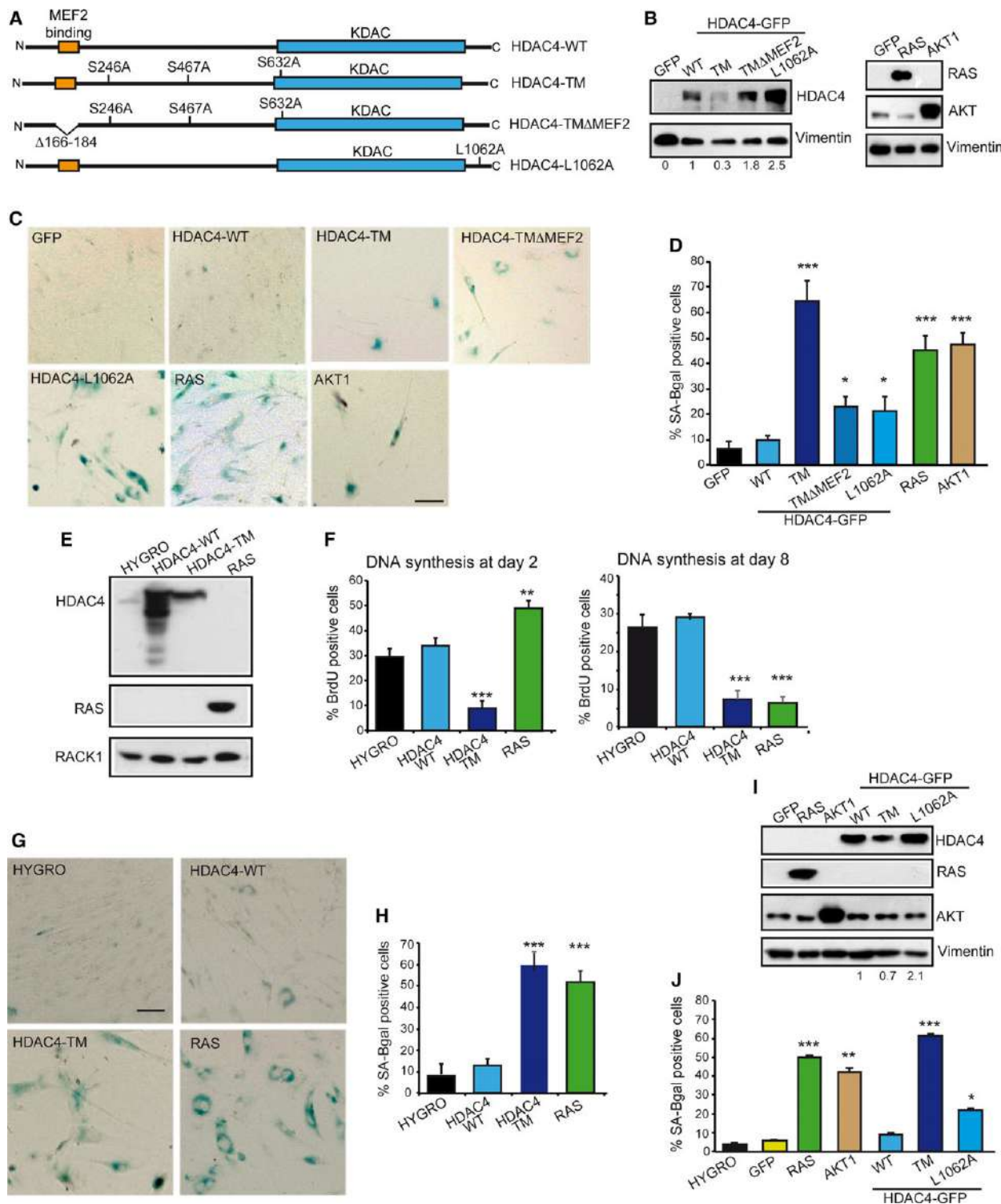
Non-transformed human fibroblasts respond to the introduction of oncogenes by activating OIS (Aste *et al.*, 2012; Kennedy *et al.*, 2011; Serrano *et al.*, 1997). Hence, we evaluated the presence of cells positive for SA- $\beta$ -galactosidase activity (Fig. 1C). After selection, few cells were recovered when nuclear localized forms of HDAC4 were expressed. The few cells expressing HDAC4-TM were positive on SA- $\beta$ -gal staining, with a score comparable to RAS and AKT1 (Fig. 1D). Cells expressing two nuclear mutants of HDAC4 such as L1062A (Paroni *et al.*, 2004) and TM $\Delta$ MEF2 (Di Giorgio *et al.*, 2013) were only moderately positive on SA- $\beta$ -gal staining (Fig. 1D). Both

mutants accumulate into the nucleus with a rate comparable to HDAC4-TM but are less strongly bound to chromatin (Paroni *et al.*, 2007). SA- $\beta$ -gal positivity was not relevant in cells expressing HDAC4-WT (which is largely cytoplasmic in BJ/TERT cells) or the negative control GFP (Fig. 1D).

To characterize the massive induction of senescence, we generated an estrogen receptor alpha (ER)-inducible version of HDAC4-TM, HDAC4-WT and H-RAS/G12V. HDAC4-TM was expressed less compared with the wild type (Fig. 1E), possibly because of the proteasome-dependent nuclear degradation of HDAC4 (Cernotta *et al.*, 2011). Next, we analyzed cell proliferation 2 or 8 days after transgene induction (Fig. 1F). HDAC4-TM triggered a rapid block in DNA synthesis. By contrast, RAS initially enhanced cell proliferation; only after 8 days of induction DNA synthesis was blocked. When the presence of SA- $\beta$ -gal-positive cells was investigated, only the induction of HDAC4-TM and RAS stimulated SA- $\beta$ -gal activity (illustrated in Fig. 1G and quantified in Fig. 1H). Finally, to corroborate these data and to exclude a contribution of tamoxifen to the process of senescence, we used a second inducible system. The different transgenes were efficiently induced by the doxycycline-inducible system (Fig. 1I). The SA- $\beta$ -gal staining confirmed that the induction of HDAC4-TM triggers senescence with rates comparable to RAS and AKT1 (Fig. 1J). In summary, nuclear resident HDAC4 can trigger senescence in immortalized human fibroblasts. In contrast to RAS, an early proliferative block characterizes HDAC4-TM-induced senescence.

#### 3.2. DNA damage in HDAC4-TM-induced senescence

OIS in RAS-overexpressing cells is triggered by the accumulation of unrepaired damaged DNA caused by unscheduled DNA synthesis (Di Micco *et al.*, 2006).



Hence, we compared by time course the kinetics of accumulation of  $\gamma$ H2AX-positive cells in cells expressing HDAC4-TM/ER, HDAC4-WT/ER and

H-RAS-G12V/ER. As early as 2 days after transgene induction, HDAC4-TM-expressing cells showed an accumulation of DNA damage (Fig. 2A). In contrast,

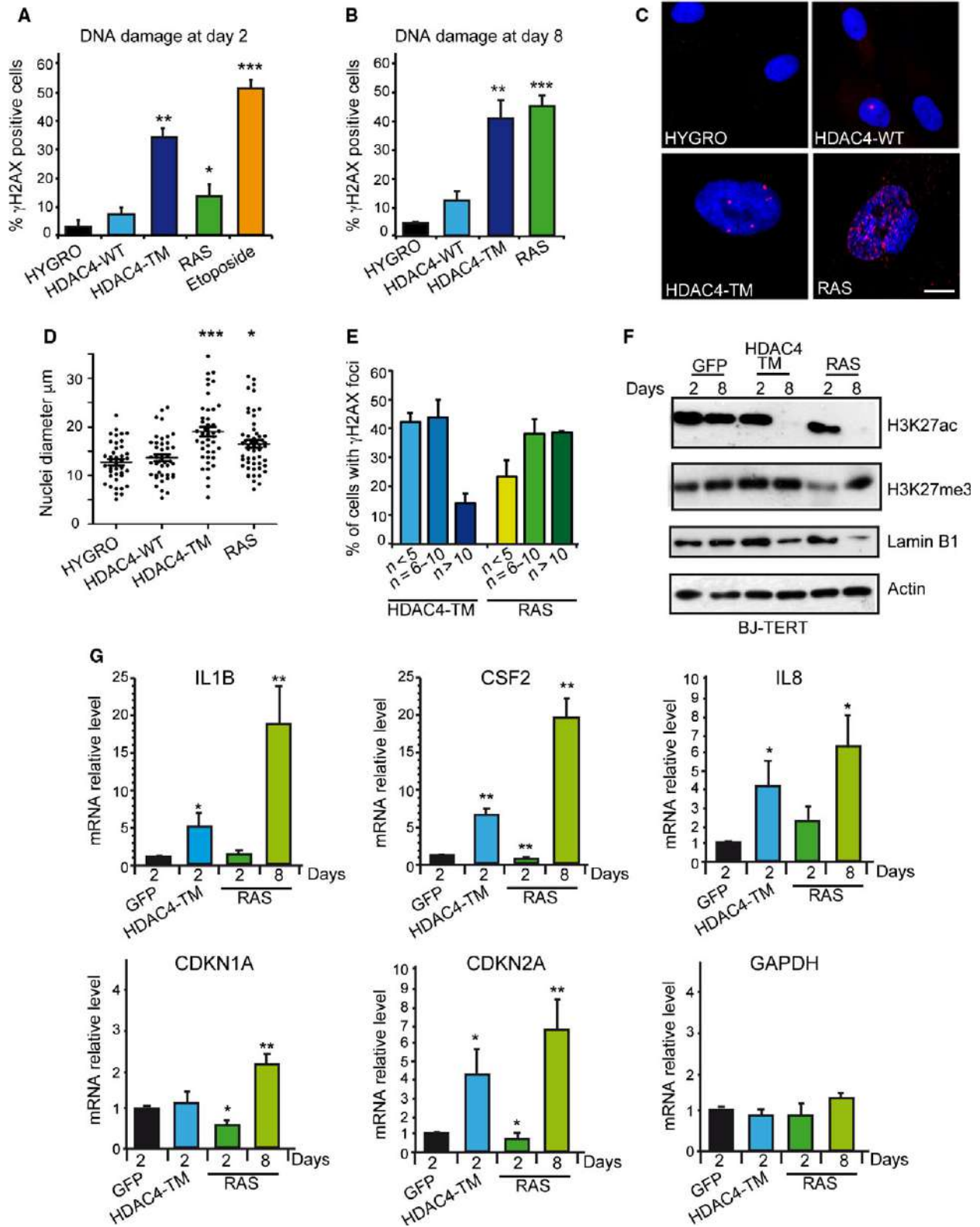


**Fig. 2.** HDAC4-induced senescence is characterized by DNA damage. (A) Quantitative analysis of the immunofluorescence staining for  $\gamma$ H2AX after 2 days of induction of the indicated transgenes in BJ-TERT cells. Data are expressed as means  $\pm$  SD,  $n = 4$ . Student *t*-test: \* $P < 0.05$ , \*\* $P < 0.01$ , \*\*\* $P < 0.005$ . (B) Quantitative analysis of the immunofluorescence staining for  $\gamma$ H2AX after 8 days of induction of the indicated transgenes in BJ-TERT cells. Data are expressed as means  $\pm$  SD,  $n = 4$ . Student *t*-test: \*\* $P < 0.01$ , \*\*\* $P < 0.005$ . (C) Immunofluorescence picture of  $\gamma$ H2AX positivity after 8 days of induction of the indicated transgenes. Nuclei were stained with Hoechst 33342. Scale bar: 5  $\mu$ m. (D) Quantitative analysis of nuclear dimension in BJ-TERT cells following 8 days of induction of the different transgenes. Measures were obtained with IMAGEJ. At least 50 nuclei were scored for each condition. The means and the 1<sup>st</sup> and 3<sup>rd</sup> quartiles are indicated. \* $P < 0.05$ , \*\*\* $P < 0.005$ . (E) Percentage of  $\gamma$ H2AX-positive cells with the indicated numbers of  $\gamma$ H2AX foci in the nuclei of BJ-TERT cells, after 8 days of expression of the indicated transgenes. (F) Immunoblot analysis using the indicated antibodies in BJ-TERT cells expressing the different transgenes for 2 or 8 days. Actin was used as loading control. (G) mRNA expression levels of the indicated genes, as measured by qRT-PCR in BJ/TERT cells expressing the different transgenes following treatment for the indicated days with 4-OHT. Data are expressed as means  $\pm$  SD,  $n = 3$ . Student *t*-test: \* $P < 0.05$ , \*\* $P < 0.01$ .

in RAS-expressing cells, DNA damage became consistent only after 8 days of induction with tamoxifen (Fig. 2B). A few  $\gamma$ H2AX-positive cells were also observed in the case of HDAC4-WT (Fig. 2B). When immunofluorescence was analyzed in more detail, two phenotypes appeared evident: (a) nuclei in TM- and RAS-expressing cells were larger than in control and HDAC4-WT cells; (b) nuclei of TM cells showed fewer but bigger  $\gamma$ H2AX-positive foci than did RAS cells (Fig. 2C). Quantitative analysis confirmed this observation (Fig. 2D,E).

Next, we evaluated the epigenetic modifications induced by the different transgenes. The global levels of histone H3 lysine 27 acetylation (H3K27ac), a marker of open and transcriptional active chromatin, and of H3K27me3, a marker of facultative heterochromatin, were evaluated after 2 and 8 days of transgene induction. We also evaluated the levels of Lamin B1, which is down-regulated during senescence (Freund *et al.*, 2012). Whereas H3K27ac and Lamin B1 showed a similar behavior in TM and RAS cells, with a dramatic decrease at day 8 (Fig. 2F), the pattern of H3K27me3 was different between the two senescence responses. Only in RAS cells did a transient reduction occur at day 2, as recently observed (Ito *et al.*, 2018).

Senescent cells produce and release a range of cytokines, chemokines and proteases in the extracellular environment: the senescence-associated secretory phenotype (SASP) (Coppé *et al.*, 2008). Hence, we compared the kinetics of appearance of senescence and SASP after HDAC4-TM or RAS induction by analyzing the expression levels of SASP components (*IL1B*, *IL8* and *CSF2*) and those of the CDK inhibitors *CDKN1A* and *CDKN2A*, key regulators of the senescent response. QRT-PCR analysis proved that HDAC4-TM anticipated the appearance of senescence with respect to RAS (Fig. 2G) in terms of SASP and *CDKN2A* induction. In RAS-expressing cells this response was only evident after 8 days of induction.

### 3.3. HDAC4-induced senescence depends on TP53 activation

The induction of DNA damage in TM-expressing cells prompted us to investigate the contribution of TP53. Immunoblot analysis performed after 8 days of transgene induction demonstrated a strong up-regulation of TP53 levels in TM cells (Fig. 3A). To investigate the contribution of TP53 in TM-induced senescence, we generated BJ-TERT cells expressing TP53 mutant R175H (Fig. 3B). This mutant is frequently found in human cancers and acts as a dominant negative (TP53DN) (Gualberto *et al.*, 1998). The DN effect was shown on the TP53-target genes *DEC1* and *GADD45A* (Fig. 3C). Subsequently, we generated BJ-TERT/TP53 cells expressing HDAC4-TM, RAS or GFP as control. Immunoblot analysis confirmed the expression of the different transgenes and showed that Lamin B1 was not down-regulated in TM cells, thus suggesting the escape from senescence (Fig. 3D). SA- $\beta$ -gal activity (Fig. 3E) and the relative quantitative analysis (Fig. 3F) confirmed the failure of TM in triggering senescence, once the TP53 response was blunted. In contrast, in RAS-expressing cells, suppression of TP53 activities was not sufficient to block the occurrence of senescence (Fig. 3E,F), as previously observed (Serano *et al.*, 1997).

These experiments demonstrate that HDAC4-TM triggers senescence, which is markedly different from RAS, since it is characterized by: (a) an early proliferative block, (b) an early and peculiar induction of DNA damage and (c) a strong TP53-dependency.

### 3.4. Down-regulation of MEF2 transcription is sufficient to promote senescence

HDAC4 can interact with several proteins, among which MEF2 TFs represent important partners (Clocchiatti *et al.*, 2013a). Since HDAC4-TM deleted in the

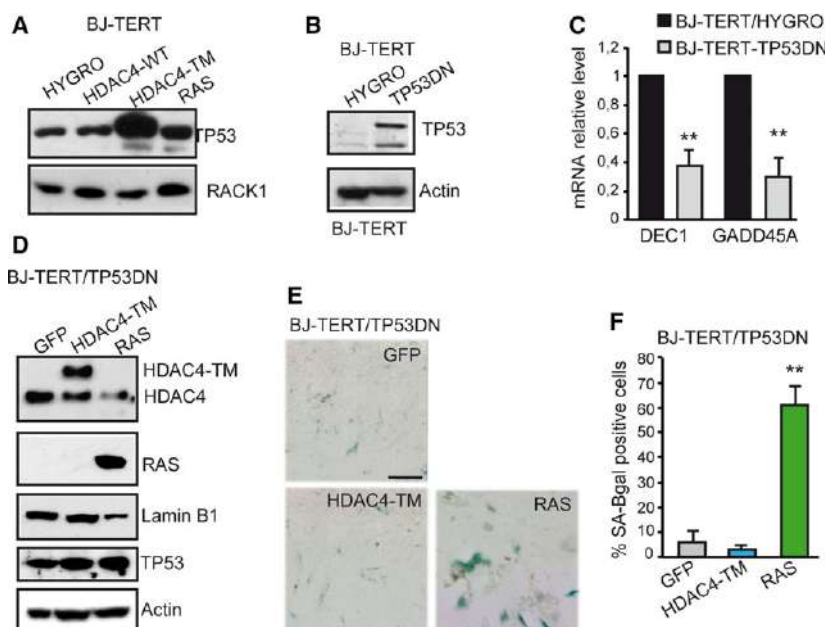


**Fig. 3.** The HDAC4-induced senescence is characterized by TP53 activation. (A) TP53 levels in BJ-TERT cells expressing the indicated transgenes for 8 days. RACK1 was used as loading control. (B) Immunoblot analysis proving the generation of BJ-TERT cells expressing the DN TP53. Actin was used as loading control. (C) qRT-PCR analysis evaluating the expression of two TP53 target genes in the different BJ-TERT cell lines as indicated. mRNA levels are relative to BJ-TERT/HYGRO cells. Data are expressed as means  $\pm$  SD,  $n = 3$ .  $**P < 0.01$ . (D) Immunoblot analysis evaluating the levels of indicated proteins in BJ-TERT cells after 8 days of 4-OHT treatment. The HDAC4-TM is expressed as fusion with GFP. Actin was used as loading control. (E) BJ-TERT/TP53DN expressing the indicated transgenes and stained for SA- $\beta$ -gal activity. Scale bar: 50  $\mu$ m. (F) Quantitative analysis of SA- $\beta$ -gal positivity from experiments described in (F). Data are expressed as means  $\pm$  SD,  $n = 4$ .  $**P < 0.01$ .

MEF2-binding region triggers senescence less potently compared with HDAC4-TM (Fig. 1C), we hypothesized that the induction of senescence could be partially due to the repression of these TFs. To clarify this point, we generated BJ-TERT cells expressing MEF2-ENG, a repressive version of these TFs in which the C-terminal MEF2 activation domain is substituted by the Engrailed repressor domain (Arnold *et al.*, 2007). Cells overexpressing MEF2D or HYGRO were used as controls (Fig. 4A). Appearance of senescence was clearly observed in BJ-TERT-MEF2/ENG cells but not in the controls (Fig. 4B). To alternatively down-regulate the expression of MEF2-target genes, we silenced the expression of MEF2D using a shRNA (Fig. 4C). MEF2D downregulation triggered a senescence response, characterized by a strong impairment in S-phase entry (Fig. 4D) and the accumulation of SA- $\beta$ -gal-positive cells (Fig. 4E and quantitative analysis in Fig. 4F). Finally, similarly to HDAC4-TM, senescence in response to MEF2 transcriptional repression is TP53-dependent. BJ-TERT-TP53DN cells expressing RAS entered into senescence, whereas SA- $\beta$ -gal-positive cells were not detected when MEF2-ENG was introduced (Fig. 4G and quantitative analysis in Fig. 4H).

### 3.5. HDAC4-mediated repression cooperates with SV40-LT in transforming human fibroblasts

To prove that BJ/TERT cells expressing the nuclear version of HDAC4 enter senescence as part of a protective response against an oncogenic dysfunction, it is imperative to prove that HDAC4 provides some transforming properties. Since anchorage-independent growth is a clear marker of cellular transformation, we initially decided to monitor this feature in BJ/TERT/TP53DN/HDAC4-TM cells that escape senescence. We also analyzed the effect of the overexpression of HDAC4-WT, MEF2-ENG and RAS.

Expression of the different transgenes was verified by immunoblot (Fig. 5A) and soft agar assays were performed to evaluate the anchorage-independent growth. In none of the engineered cell lines was growth in soft agar detectable (Fig. 5B). This result indicates that HDAC4-TM- or MEF2-mediated gene repression cannot sustain anchorage-independent growth once senescence is suppressed by TP53 mutations.

The SV40 large T antigen (LT) can inactivate two major tumor suppressor genes, p53 and retinoblastoma protein (pRb) (Hahn *et al.*, 2002). In several

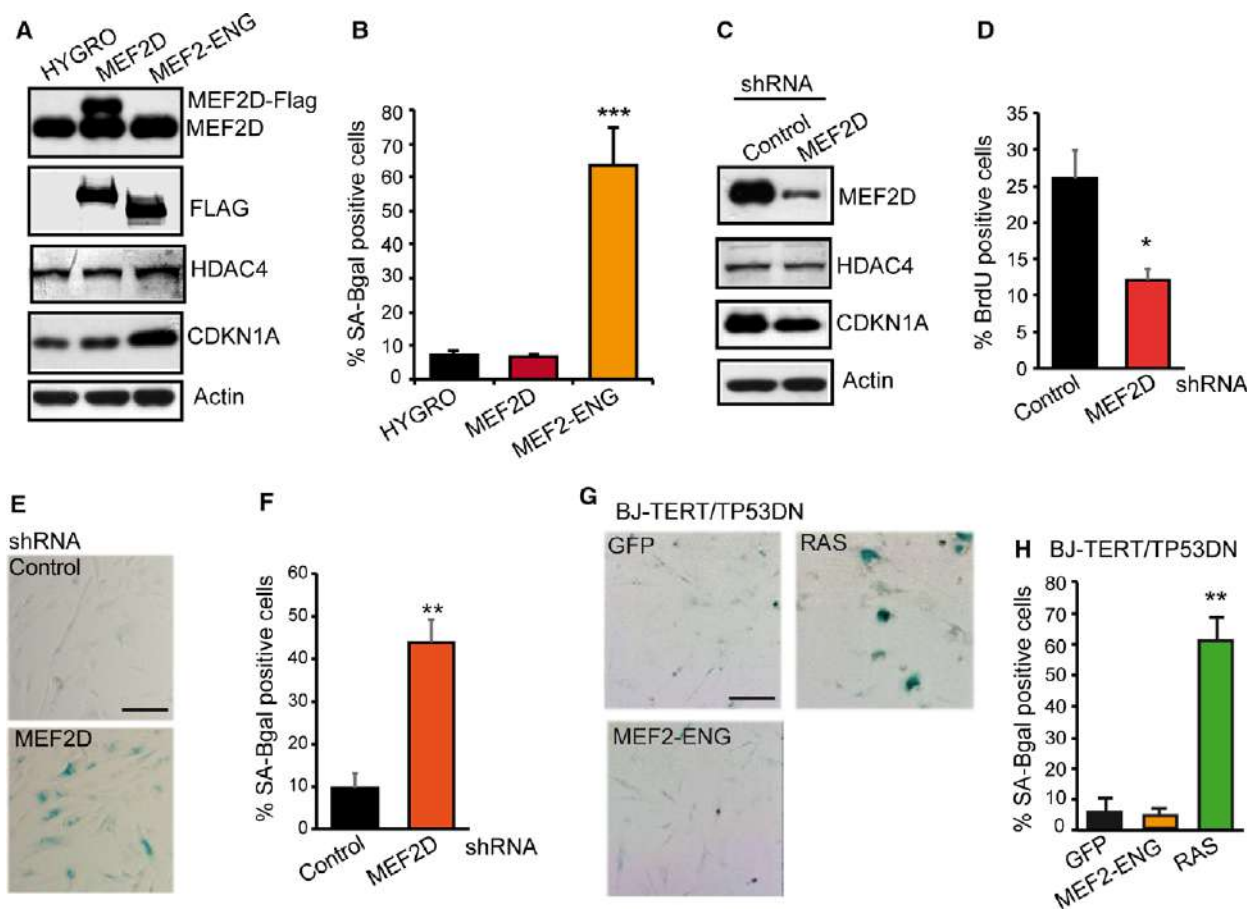


**Fig. 4.** Myocyte enhancer factor transcriptional activity counteracts senescence. (A) Immunoblot analysis evaluating the levels of the indicated proteins in BJ-TERT cells. MEF2D and MEF2-ENG contain a Flag epitope. Actin was used as loading control. (B) Quantitative analysis of SA- $\beta$ -gal positivity in BJ-TERT cells expressing the indicated transgenes. (C) Immunoblot analysis of MEF2D, HDAC4 and CDKN1A levels in BJ-TERT cells expressing the control shRNA or a shRNA against MEF2D. shRNA was delivered by lentiviral infection. Actin was used as loading control. (D) Analysis of DNA synthesis, as scored after BrdU staining in BJ-TERT cells expressing the two shRNA. Data are expressed as means  $\pm$  SD,  $n = 3$ . \* $P < 0.05$ . (E) BJ-TERT expressing the indicated shRNA were stained for SA- $\beta$ -gal activity. Scale bar: 50  $\mu$ m. (F) Quantitative analysis of SA- $\beta$ -gal positivity from experiments described in (E). Data are expressed as means  $\pm$  SD,  $n = 4$ . \*\* $P < 0.01$ . (G) BJ-TERT/TP53 expressing the indicated transgene were stained for SA- $\beta$ -gal activity. Scale bar: 50  $\mu$ m. (H) Quantitative analysis of SA- $\beta$ -gal positivity from experiments described in (G). Data are expressed as means  $\pm$  SD,  $n = 4$ . \*\*\* $P < 0.005$ .

experiments LT has proved to cooperate in the transformation of human cells (Hahn *et al.*, 1999). Hence, we generated BJ-TERT/LT cells (Fig. 5C) to evaluate oncogenic cooperation with HDAC4-TM, HDAC4-WT and RAS as a control (Fig. 5D). In contrast to TP53DN, LT expression suppressed OIS by RAS (Fig. 5E and quantitative analysis in Fig. 5F). Growth in soft agar was performed and the appearance of foci was scored 21 days later. We also evaluated the size distribution of the colonies (Fig. 5G) using already published criteria (Cifone and Fidler, 1980). Small colonies with a 50- $\mu$ m diameter or less were frequently observed in RAS- and HDAC4-TM-expressing cells (Fig. 5H). Rarely, larger colonies with a diameter of 100–150  $\mu$ m were present. Interestingly, foci of small

dimensions were also observed when TERT/LT/HDAC4-WT were co-expressed. Analysis of the transformation efficiency confirmed that HDAC4-TM and RAS showed comparable activities. A much weaker transforming effect was observed for HDAC4-WT (Fig. 5I).

To confirm the induction of a transformed phenotype we evaluated random motility and invasiveness using the Matrigel invasion assay. Figure 5J shows that only HDAC4-TM enhanced random cell motility but both RAS and HDAC4-TM strongly promoted invasiveness in TERT/LT human cells (Fig. 5K).

To have a full transformation of human fibroblasts, both the LT and the SV40 small T antigen (ST) must be co-expressed with TERT and RAS (Hahn *et al.*,

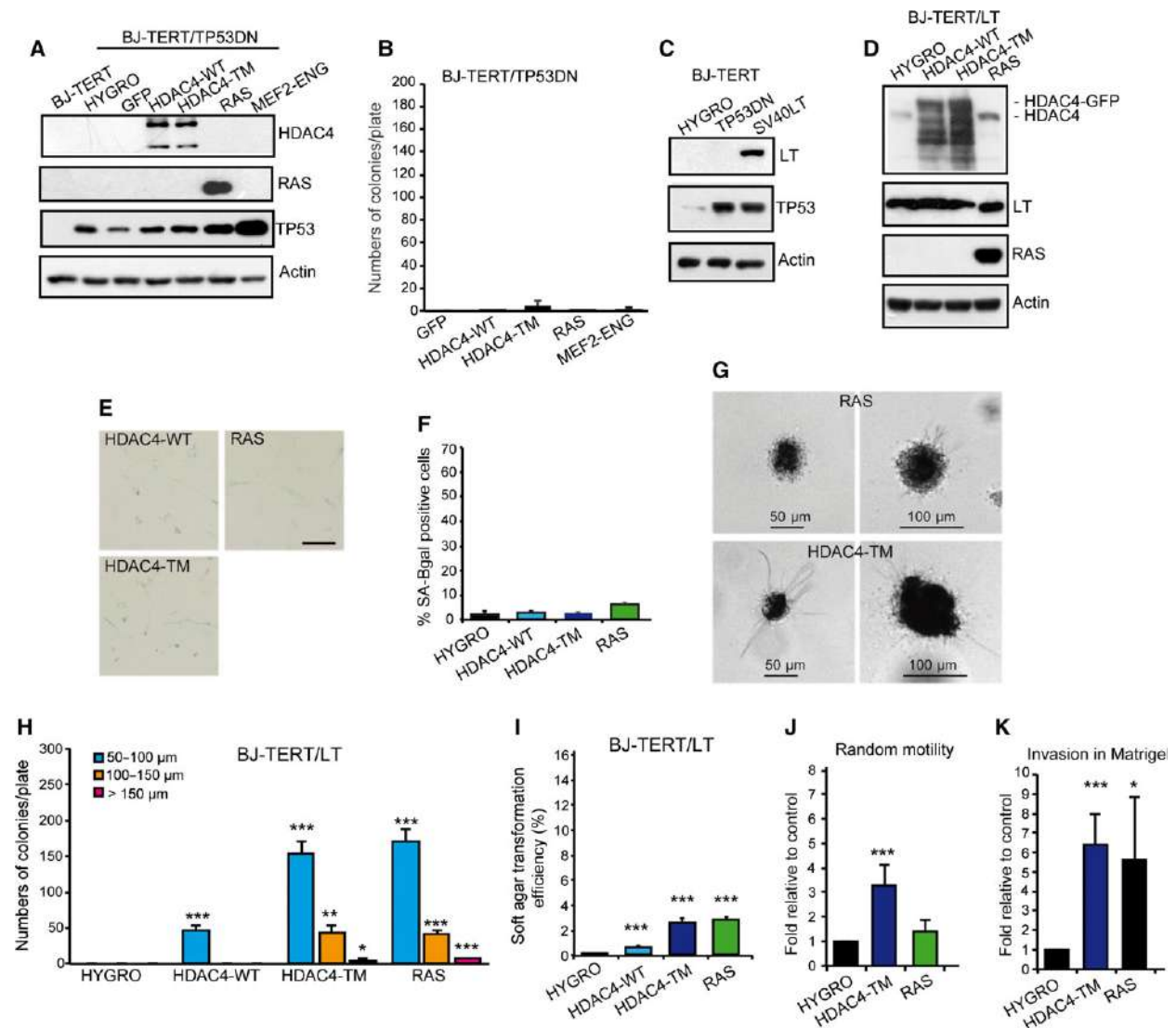


**Fig. 5.** The HDAC4-TM cooperates with SV40 LT in sustaining a transformed phenotype. (A) Immunoblot analysis of indicated proteins as expressed in BJ-TERT/TP53DN cells infected with retrovirus encoding the indicated genes. HDAC4 was expressed as fusion with GFP and the recombinant proteins detected with an anti-GFP antibody. Actin was used as loading control. (B) Growth in soft agar of the BJ-TERT/TP53 cells expressing the indicated transgene. After staining with MTT, foci with diameter  $> 50 \mu\text{m}$  were counted. Data are expressed as means  $\pm$  SD,  $n = 3$ . Student  $t$ -test:  $*P < 0.05$ ,  $**P < 0.01$ ,  $***P < 0.005$ . (C) Immunoblot analysis of indicated proteins as expressed in BJ-TERT cells infected with retrovirus encoding the indicated genes. Actin was used as loading control. (D) Immunoblot analysis of indicated proteins as expressed in BJ-TERT/LT cells infected with retrovirus encoding the indicated genes. HDAC4 was expressed as fusion with GFP and the recombinant proteins detected with an anti-GFP antibody. Actin was used as loading control. (E) BJ-TERT/LT cells expressing the indicated transgenes were stained for SA- $\beta$ -gal activity. Scale bar:  $50 \mu\text{m}$ . (F) Quantitative analysis of SA- $\beta$ -gal positivity from experiments described in (E). Data are expressed as means  $\pm$  SD,  $n = 3$ . Student  $t$ -test:  $*P < 0.05$ ,  $**P < 0.01$ ,  $***P < 0.005$ . (G) Representative images of MMT positive soft agar foci of BJ-TERT/LT cells expressing HDAC4-TM or RAS. Scale bars are indicated. (H) Quantitative analysis of soft agar foci of BJ-TERT/LT cells expressing the indicated transgenes grouped for foci dimensions related to (G). Data are expressed as means  $\pm$  SD,  $n = 4$ . Student  $t$ -test:  $*P < 0.05$ ,  $**P < 0.01$ ,  $***P < 0.005$ . (I) Soft agar transformation efficiency represents the total number of foci generated by BJ-TERT/LT cells expressing the indicated transgenes, divided by the total number of seeded cells. Data are expressed as means  $\pm$  SD,  $n = 4$ .  $***P < 0.005$ . (J) Motility properties of BJ-TERT/LT cells expressing RAS, HDAC4-TM or HYGRO as control. Data are expressed as means  $\pm$  SD,  $n = 3$ .  $***P < 0.005$ . (K) Invasive properties, as measured by Matrigel invasion assay of BJ-TERT/LT cells expressing RAS, HDAC4-TM or Hygro as control. Data are expressed as means  $\pm$  SD,  $n = 3$ .  $*P < 0.05$ ,  $***P < 0.005$ .

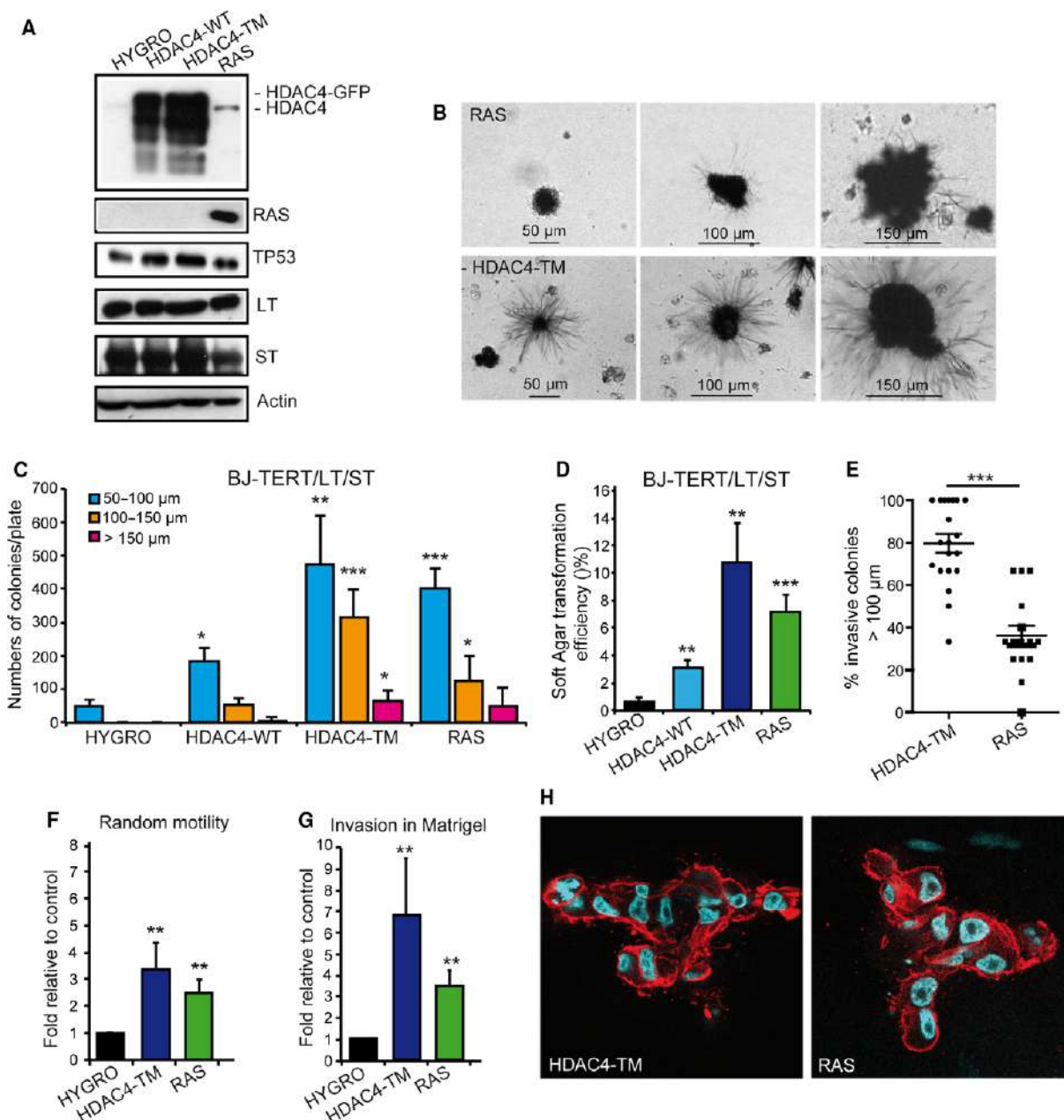


**Fig. 6.** The HDAC4-TM cooperates with SV40 LT in sustaining a transformed phenotype. (A) Immunoblot analysis of indicated proteins as expressed in BJ-TERT/LT/ST cells infected with retrovirus encoding the indicated genes. HDAC4 was expressed as fusion with GFP and the recombinant proteins detected with an anti-GFP antibody. Actin was used as loading control. (B) Representative images of MMT-positive soft agar foci of BJ-TERT/LT/ST cells expressing HDAC4-TM or RAS. Scale bars are indicated. (C) Quantitative analysis of soft agar foci of BJ-TERT/LT/ST cells expressing the indicated transgenes grouped for foci dimensions related to Fig. 6B. Data are expressed as means  $\pm$  SD,  $n = 4$ . Student  $t$ -test: \* $P < 0.05$ , \*\* $P < 0.01$ , \*\*\* $P < 0.005$ . (D) Soft agar transformation efficiency represents the total number of foci generated by BJ-TERT/LT/ST cells expressing the indicated transgenes divided by the total number of seeded cells. Data are expressed as means  $\pm$  SD,  $n = 4$ . \*\* $P < 0.01$ , \*\*\* $P < 0.005$ . (E) Percentage of invasive soft agar foci. Foci were scored for the presence of cells showing extensive growth in the surrounding agar. The means and the 1st and 3rd quartiles are indicated.  $n = 19$  (HDAC4-TM) and  $n = 15$  (RAS). \*\*\* $P < 0.005$ . (F) Motility properties of BJ-TERT/LT/ST cells expressing RAS, HDAC4-TM or Hygro as control. Data are expressed as means  $\pm$  SD,  $n = 3$ . Student  $t$ -test: \*\*\* $P < 0.01$ . (G) Invasive properties, as measured by Matrigel invasion assay of BJ-TERT/LT/ST cells expressing RAS, HDAC4-TM or Hygro as control. Data are expressed as means  $\pm$  SD,  $n = 3$ . \*\* $P < 0.01$ . (H) Confocal images representing the equatorial section of BJ-TERT/LT/ST cells expressing RAS or HDAC4-TM grown in Matrigel plugs. Nuclei were visualized using Hoechst 33342 and actin filaments with phalloidin-Alexa 546.

2002). Hence, we generated human fibroblasts expressing the combination of TERT/LT/ST together with HDAC4-WT, HDAC4-TM or RAS as a positive control of transformation. Immunoblot analysis verified the expression of the different transgenes (Fig. 6A). Next, soft agar assay was performed and after 21 days, colonies were stained with MTT and foci were counted and grouped for dimensions as exemplified (Fig. 6B). Quantitative analysis proved that the expression of the ST increased the number of foci and particularly their dimensions (Fig. 6C) as well as the transformation efficiency (compare Fig. 6D with Fig. 5I). Interestingly, cells expressing HDAC4-TM frequently show extensive invasion and some branching into the agar (Fig. 6B). Quantitative analysis confirmed the invasive properties of foci generated by HDAC4-TM (Fig. 6E). Here, again, growth in soft agar was also observed when HDAC4-WT was expressed, although with reduced efficiency compared with HDAC4-TM (Fig. 6C,D).

To confirm the invasive properties of TERT/LT/ST/HDAC4-TM cells we performed the Matrigel invasion assay. Random cell motility and invasion were measured (Fig. 6F,G). These experiments confirmed the strong invasive behavior of HDAC4-TM-expressing cells.

Finally, we analyzed TERT/LT/ST cells expressing HYGRO, RAS and HDAC4-TM in three-dimensional Matrigel plugs. Only cells expressing RAS or HDAC4-TM exhibited robust growth and invasion into the matrix (Fig. 6H).

### 3.6. Common and specific transcriptomic adaptations characterize RAS and HDAC4-TM transformed cells

To gain insight into the molecular mechanisms responsible for the RAS- and HDAC4-TM-mediated oncogenic transformation, we performed gene expression profile studies. The transcriptomes of TERT/LT/ST/HYGRO, TERT/LT/ST/RAS and TERT/LT/ST/HDAC4-TM were compared. DEGs were analyzed relative to TERT/LT/ST/HYGRO cells. Figure 7A shows that RAS and HDAC4-TM influence the expression of a comparable number of genes (respectively 892 and 920). In both cases, the number of repressed genes is more than the double that of the induced ones. Moreover, HDAC4-TM and RAS have a larger pool (15.5%,  $n = 156$  genes) of all the repressed genes in common, in contrast to 6.5% ( $n = 40$ ) of up-regulated genes. Since HDAC4 is a transcriptional repressor, we focused our analysis on the repressed genes. The 156 commonly repressed genes turned out to be highly enriched for elements of the

interferon (IFN) pathways (Fig. 7B). In addition and in agreement with the transformed state of these cells, a subset of the commonly silenced genes belong to the category of genes repressed by serum/growth factors (Fig. 7B). Next, we evaluated RAS- and HDAC4-TM-specific repressive signatures. IFN and, in general, inflammatory signatures were prevalent among genes ( $n = 400$ ) specifically repressed by RAS (Fig. 7C). In contrast, genes that are specifically repressed by HDAC4-TM are involved in more heterogeneous regulative processes, including the epithelial-mesenchymal transition, the hypoxia response and differentiation/morphogenesis (Fig. 7D). The high number of genes regulating cell adhesion and migration, as disclosed by the Gene Ontology analysis, could explain the peculiar phenotype of the soft agar colonies generated by TERT/LT/ST/HDAC4-TM cells (Fig. 6).

Finally, the comparison of the transcriptomic profiles indicated that the transformation phenotype elicited by HDAC4-TM in TERT/LT/ST cells resembles adaptations in gene expression previously described in other models of human fibroblast transformation (Fig. 7E).

## 4. Discussion

In this manuscript we used human fibroblasts to evaluate the oncogenic cooperative properties of HDAC4. The transforming potential of class IIa HDACs has been shown in different murine models (Di Giorgio *et al.*, 2013; Gil *et al.*, 2016; Lei *et al.*, 2017; Peruzzo *et al.*, 2016; Rad *et al.*, 2010). However, since there are substantial interspecies differences in the biology of cell transformation (Boehm *et al.*, 2005), we decided to verify the oncogenic properties of HDAC4 in human cells.

The combined expression of HDAC4-TM with the viral oncogene LT and much more strongly with LT and ST viral oncogenes can sustain growth in soft agar, similarly to RAS oncogene. Although at reduced levels, HDAC4-WT can also promote anchorage-independent growth when co-expressed with LT and ST.

The ability of LT to cooperate with HDAC4 strongly indicates that inactivation of the pRb and TP53 tumor suppressor pathways is required to unleash the HDAC4-transforming potential. However, in the absence of ST, the growth is not robust and foci are less frequently observed and of small size. This behavior was previously reported in the case of RAS (Hahn *et al.*, 2002).

ST is required to increase dramatically the anchorage-independent growth of both HDAC4 and RAS. ST-transforming activities rely on the binding and inhibition of some isoforms of the serine-threonine

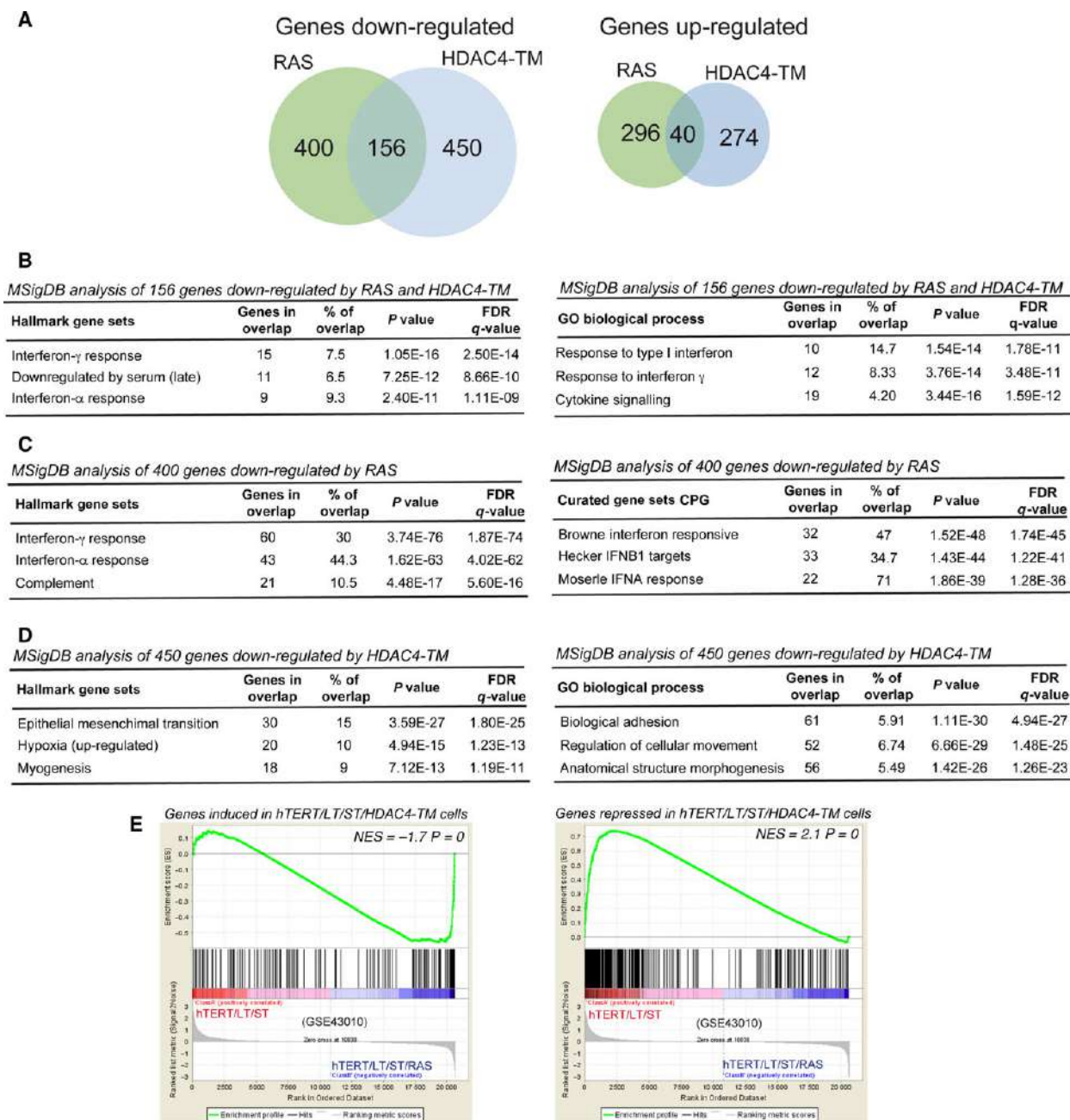


**Fig. 7.** Gene expression profiles of RAS and HDAC4-TM transformed human fibroblasts. (A) Pie-chart indicating the number of genes significantly up- and down-regulated in TERT/LT/ST/RAS and TERT/LT/ST/HDAC4-TM cells compared with TERT/LT/ST/HYGRO cells. (B) GSEA for the 156 genes commonly repressed by RAS and HDAC4-TM using the hallmark and the GO/biological process MSigDB gene sets. (C) GSEA for the 400 genes specifically repressed by RAS using the hallmark and the curated (CPG) MSigDB gene sets. (D) GSEA for the 450 genes specifically repressed by HDAC4-TM using the hallmark and the GO/biological process MSigDB gene sets. (E) GSEA plots showing significant enrichment for HDAC4-regulated genes in a BJ transformation model (GSE43010), considering both HDAC4-positively regulated genes (left) and HDAC4-repressed genes (right).

phosphatase, PP2A (Hahn *et al.*, 2002). PP2A can dephosphorylate and regulate several targets, thus making it difficult to hypothesize which pathway could

synergize with HDAC4. Recently, it has been shown that the PAK1-YAP axis can mediate ST-transforming activity (Nguyen *et al.*, 2014). Interestingly, a

contribution of HDAC4 in mediating YAP-repressive activity has been reported (Wang *et al.*, 2014).

Transcriptomic analysis has revealed that HDAC4-TM and RAS trigger the transformation processes via both common and peculiar adaptive responses. Repression of genes marking the IFN responses was commonly found in RAS- and HDAC4-TM-transformed cells. IFN and inflammatory signaling were highly enriched also among genes specifically repressed by RAS. Although it is well known that RAS and its downstream elements suppress the IFN-induced antiviral responses and favor virus spreading (Battcock *et al.*, 2006; Christian *et al.*, 2009; Noser *et al.*, 2007), how this repressive wave could impact on the *in vitro* transformation process is less clear (Christian *et al.*, 2012). Gene signatures specifically influenced by HDAC4-TM are more heterogeneous and involve adaptation to hypoxia, adhesion, motility and differentiation processes. It is possible that RAS more potently suppresses the IFN responses compared with HDAC4-TM, which instead represses additional pathways.

The ability of HDAC4-TM to regulate genes involved in adhesion and motility was confirmed in the morphological analysis of soft agar foci as well as in the results obtained with Matrigel invasion and evasion assays. These results indicate that HDAC4-expressing cells exhibit a strong invasive phenotype, further supported by previous studies on the invasive, migrating and metastatic activities of class IIa HDACs (Cao *et al.*, 2017; Cernotta *et al.*, 2011; Di Giorgio *et al.*, 2013; Fabian *et al.*, 2016; Mottet *et al.*, 2007).

Normal cells in response to oncogenic signals enter into senescence, a state of irreversible/permanent growth arrest that prevents cells from undergoing further cell divisions, defined as OIS (Serrano *et al.*, 1997). Activation of OIS depends on the pRB and/or TP53 tumor suppressor pathways (Serrano *et al.*, 1997). We have proved that HDAC4-TM, in TERT-immortalized human fibroblasts, can activate senescence. This senescent response can be also triggered by other class IIa HDACs such as HDAC7, when localized into the nucleus (Supporting Information Fig. S1). Since the expression of HDAC4-TM in the opportune genetic environment (LT/ST co-expression) can transform cells, and since the senescent response is p53-dependent, we can define senescence triggered by HDAC4-TM as OIS. However, OIS induced by RAS cannot be reversed by simply blocking TP53 activity, but requires the suppression of pRB, possibly through the CDK inhibitor p16 (Serrano *et al.*, 1997). The difference between HDAC4-TM and RAS can be appreciated also at the earliest stages of their induction. RAS triggers hyperproliferation and S-phase-associated DNA damage response

(DDR). The oncogene-dependent increase in proliferation leads to accumulation of incomplete replication intermediates, resulting in DNA damage and activation of the DDR (Di Micco *et al.*, 2006).

In contrast, HDAC4-TM triggers suddenly growth arrest, senescence and SASP, which could be caused by the rapid activation of TP53. The absence of the hyperproliferative response correlates with the failure to trigger H3K27 global demethylation, as observed in RAS-expressing cells.

#### 4.1. How can HDAC4-TM trigger TP53 stabilization and senescence?

Induction of DNA damage, marked by  $\gamma$ H2AX positivity, was observed. In contrast to RAS, the number of  $\gamma$ H2AX spots per cell was reduced in HDAC4-TM cells. Hence, the induction of DNA damage and TP53 activation seems to involve different pathways compared with the replication stress induced by RAS. Previous reports have described correlations between HDAC4 and the DNA damage response, and also with TP53 regulation (Cadot *et al.*, 2009; Marampon *et al.*, 2017). Unfortunately, these preliminary observations have not led to further studies and currently the correlations between class IIa HDACs and the DNA damage response remain unknown.

Although RAS-induced OIS is among the foremost pathways, alternative OIS pathways exist. PI3K/AKT-induced senescence is characterized by TP53 and CDKN1A induction in the absence of overt DNA damage. mTORC1-dependent regulation of TP53 translation and stabilization of TP53 protein, as a result of MDM2 nucleolar localization and inactivation, is the mechanism activated in this senescent response (Aistle *et al.*, 2012; Kennedy *et al.*, 2011). Importantly, similarly to HDAC4, AKT promotes a rapid proliferative arrest in the absence of hyperproliferation (Aistle *et al.*, 2012; Kennedy *et al.*, 2011).

Interestingly, in certain cancer types, particularly in leiomyosarcomas, class IIa HDACs and PI3K/AKT can regulate common genetic programs that are under the influence of MEF2 TFs. Class IIa HDAC binds MEF2 on target promoters and favors the establishment of a closed chromatin configuration (Di Giorgio *et al.*, 2017). In contrast, PI3K/AKT can trigger polyubiquitylation and degradation of certain MEF2 isoforms (Di Giorgio *et al.*, 2015). As MEF2s are possible common targets of these pathways, it is important to underline that the repression of MEF2 TFs is required for the OIS response triggered by HDAC4 and that the knock-down of MEF2D is sufficient to trigger senescence.

## 5. Conclusions

Our results provide further evidence concerning the contribution, as cooperating oncogenes, of class IIa HDACs in human cancer. This finding is encouraging for further investigations aimed at discovering and evaluating inhibitors of these epigenetic regulators as anticancer drugs.

## Acknowledgements

We thank Dr. Peiqing Sun and Dr. R. B. Pearson for kindly providing plasmids encoding E1A (1-143) and myr-AKT1. We also thanks Dr. Raffaella Picco for the initial bioinformatics analysis. This study was supported by AIRC Associazione Italiana per la Ricerca sul Cancro, IG 15640 and COLONACT regione FVG to C.B. E.D.G. received an AIRC fellowship (Volontari Jesolo).

## Authors' contributions

CB and EDG designed the study. HP and EDG performed the experiments. CB wrote and revised the manuscript. All authors read and approved the final manuscript.

## References

- Arnold MA, Kim Y, Czubyrt MP, Phan D, McAnally J, Qi X, Shelton JM, Richardson JA, Bassel-Duby R and Olson EN (2007) MEF2C transcription factor controls chondrocyte hypertrophy and bone development. *Dev Cell* **12**, 377–389.
- Astle MV, Hannan KM, Ng PY, Lee RS, George AJ, Hsu AK, Haupt Y, Hannan RD and Pearson RB (2012) AKT induces senescence in human cells via MTORC1 and P53 in the absence of DNA damage: implications for targeting MTOR during malignancy. *Oncogene* **31**, 1949–1962.
- Balani S, Nguyen LV and Eaves CJ (2017) Modeling the process of human tumorigenesis. *Nat Commun* **8**, 15422.
- Barneda-Zahonero B and Parra M (2012) Histone deacetylases and cancer. *Molecular Oncology*, **6**, 579–589.
- Battcock SM, Collier TW, Zu D, Hirasawa K (2006) Negative regulation of the alpha interferon-induced antiviral response by the Ras/Raf/MEK pathway. *J Virol* **80**, 4422–4430.
- Beira JV, Torres J and Paro R (2018) Signalling crosstalk during early tumorigenesis in the absence of polycomb silencing. *PLoS Genet* **14**, e1007187.
- Boehm JS, Hahn WC (2005) Understanding transformation: progress and gaps. *Curr Opin Genet Dev* **15**: 13–17.
- Boehm JS, Hession MT, Bulmer SE and Hahn WC (2005) Transformation of human and murine fibroblasts without viral oncoproteins. *Mol Cell Biol* **25**, 6464–6474.
- Bradner JE, Hnisz D and Young RA (2017) Transcriptional addiction in cancer. *Cell* **168**, 629–643.
- Brien GL, Valerio DG and Armstrong SA (2016) Exploiting the epigenome to control cancer-promoting gene-expression programs. *Cancer Cell* **29**, 464–476.
- Cadot B, Brunetti M, Coppari S, Fedeli S, De Rinaldis E, Dello Russo C, Gallinari P, De Francesco R, Steinkühler C and Filocamo G (2009) Loss of histone deacetylase 4 causes segregation defects during mitosis of P53-deficient human tumor cells. *Cancer Res* **69**, 6074–6082.
- Cao C, Vasilatos SN, Bhargava R, Fine JL, Oesterreich S, Davidson NE and Huang Y (2017) Functional interaction of histone deacetylase 5 (HDAC5) and lysine-specific demethylase 1 (LSD1) promotes breast cancer progression. *Oncogene* **36**, 133–145.
- Cernotta N, Clocchiatti A, Florean C and Brancolini C (2011) Ubiquitin-dependent degradation of HDAC4, a new regulator of random cell motility. *Mol Biol Cell* **22**, 278–289.
- Chen L, Alexe G, Dharia NV, Ross L, Iniguez AB, Conway AS, Wang EJ, Veschi V, Lam N, Qi J, Gustafson WC et al. (2018) CRISPR-Cas9 screen reveals a MYCN-amplified neuroblastoma dependency on EZH2. *J Clin Invest*. **125**, 446–462.
- Cheng X, Hao Y, Shu W, Zhao M, Zhao C, Yuan W, Peng X et al. (2017b) Cell cycle-dependent degradation of the methyltransferase SETD3 attenuates cell proliferation and liver tumorigenesis. *J Biol Chem* **292**, 9022–9033.
- Cheng G, Liu F, Asai T, Lai F, Man N, Xu H, Chen S et al. (2017a) Loss of P300 accelerates MDS-associated leukemogenesis. *Leukemia* **31**, 1382–1390.
- Christian SL, Collier TW, Zu D, Licursi M, Hough CM and Hirasawa K (2009) Activated Ras/MEK inhibits the antiviral response of alpha interferon by reducing STAT2 levels. *J Virol* **83**, 6717–6726.
- Christian SL, Zu D, Licursi M, Komatsu Y, Pongnopparat T, Codner DA, Hirasawa K (2012) Suppression of IFN-induced transcription underlies IFN defects generated by activated Ras/MEK in human cancer cells. *PLoS ONE* **7**, e44267.
- Cifone MA and Fidler IJ (1980) Correlation of patterns of anchorage-independent growth with in vivo behavior of cells from a murine fibrosarcoma. *Proc Natl Acad Sci USA* **2**, 1039–1043.
- Clocchiatti A, Di Giorgio E, Demarchi F, Brancolini C (2013a) Beside the MEF2 Axis: unconventional functions of HDAC4. *Cell Signal* **25**, 269–276.
- Clocchiatti A, Di Giorgio E, Ingrao S, Meyer-Almes FJ, Tripodo C and Brancolini C (2013b) Class IIa HDACs repressive activities on MEF2-dependent transcription are associated with poor prognosis of ER+ breast tumors. *FASEB Journal* **27**, 942–954.

- Clocchiatti A, Florean C, Brancolini C (2011) Class IIa HDACs: from important roles in differentiation to possible implications in tumorigenesis. *J Cell Mol Med* **15**, 1833–1846.
- Coppé JP, Patil CK, Francis Rodier Y, Sun DP, Muñoz JG, Nelson PS, Desprez PY and Campisi J (2008) Senescence-associated secretory phenotypes reveal cell-nonautonomous functions of oncogenic RAS and the P53 tumor suppressor. *PLoS Biol* **6**, 2853–2868.
- Debacq-Chainiaux F, Erusalimsky JD, Campisi J and Toussaint O (2009) Protocols to detect senescence-associated beta-galactosidase (SA-Bgal) activity, a biomarker of senescent cells in culture and in vivo. *Nat Protoc* **4**, 1798–1806.
- Deng Q, Li Y, Tedesco D, Liao R, Fuhrmann G and Sun P (2005) The ability of E1A to rescue Ras-induced premature senescence and confer transformation relies on inactivation of both P300/CBP and Rb family proteins. *Cancer Res* **65**, 8298–8307.
- Di Giorgio E, Brancolini C (2016) Regulation of class IIa HDAC activities: it is not only matter of subcellular localization. *Epigenomics* **8**, 251–269.
- Di Giorgio E, Clocchiatti A, Piccinin S, Sgorbissa A, Viviani G, Peruzzo P, Romeo S *et al.* (2013) MEF2 is a converging hub for histone deacetylase 4 and phosphatidylinositol 3-kinase/Akt-induced transformation. *Mol Cell Biol* **33**, 4473–4491.
- Di Giorgio E, Franforte E, Cefalù S, Rossi S, Dei TA, Brenca M, Polano M *et al.* (2017) The co-existence of transcriptional activator and transcriptional repressor MEF2 complexes influences tumor aggressiveness. *PLoS Genet* **13**, e1006752.
- Di Giorgio E, Gagliostro E, Clocchiatti A and Brancolini C (2015) The control operated by the cell cycle machinery on MEF2 stability contributes to the downregulation of CDKN1A and entry into S phase. *Mol Cell Biol* **35**, 1633–1647.
- Di Micco R, Fumagalli M, Cicalese A, Piccinin S, Gasparini P, Luise C, Schurra C *et al.* (2006) Oncogene-induced senescence is a DNA damage response triggered by DNA hyper-replication. *Nature* **444**, 638–642.
- Fabian J, Opitz D, Althoff K, Lodrini M, Volland R, Beckers A, de Preter K *et al.* (2016) MYCN and HDAC5 transcriptionally repress CD9 to trigger invasion and metastasis in neuroblastoma. *Oncotarget* **7**, 66344–66359.
- Fontebasso AM, Papillon-Cavanagh S, Schwartzentruber J, Nikbakht H, Gerges N, Fiset PO, Bechet D *et al.* (2014) Recurrent somatic mutations in ACVR1 in pediatric midline high-grade astrocytoma. *Nat Genet* **5**, 462–466.
- Freund A, Laberge R-M, Demaria M and Campisi J (2012) Lamin B1 loss is a senescence-associated biomarker. *Mol Biol Cell* **11**, 2066–2075.
- Funes JM, Henderson S, Kaufman R, Flanagan JM, Robson M, Pedley B, Moncada S, Boshoff C (2014) Oncogenic transformation of mesenchymal stem cells decreases Nrf2 expression favoring in vivo tumor growth and poorer survival. *Mol Cancer* **13**, 20.
- Gil VS, Bhagat G, Howell L, Zhang J, Kim CH, Stengel S, Vega F, Zelent A and Petrie K (2016) Deregulated expression of HDAC9 in B cells promotes development of lymphoproliferative disease and lymphoma in mice. *Dis Models Mech* **12**, 1483–1495.
- Gualberto A, Aldape K, Kozakiewicz K and Tlsty TD (1998) An oncogenic form of P53 confers a dominant, gain-of-function phenotype that disrupts spindle checkpoint control. *Proc Natl Acad Sci USA* **95**, 5166–5171.
- Hahn WC, Counter CM, Lundberg AS, Beijersbergen RL, Brooks MW, Weinberg RA (1999) Creation of human tumour cells with defined genetic elements. *Nature* **400**, 464–468.
- Hahn WC, Dessain SK, Brooks MW, King JE, Elenbaas B, Sabatini DM, DeCaprio JA and Weinberg RA (2002) Enumeration of the simian virus 40 early region elements necessary for human cell transformation. *Mol Cell Biol* **7**, 2111–2123.
- Ito T, Teo YV, Evans SA, Neretti N and Sedivy JM (2018) Regulation of cellular senescence by polycomb chromatin modifiers through distinct DNA damage- and histone methylation-dependent pathways. *Cell Rep* **22**, 3480–3492.
- Kennedy AL, Morton JP, Manoharan I, Nelson DM, Jamieson NB, Pawlikowski JS, McBryan T *et al.* (2011) Activation of the PIK3CA/AKT pathway suppresses senescence induced by an activated RAS oncogene to promote tumorigenesis. *Mol Cell* **42**, 36–49.
- Khuong-Quang DA, Buczkowicz P, Rakopoulos P, Liu XY, Fontebasso AM, Bouffet E, Bartels U *et al.* (2012) K27M mutation in histone H3.3 defines clinically and biologically distinct subgroups of pediatric diffuse intrinsic Pontine gliomas. *Acta Neuropathol* **3**, 439–447.
- Koschmann C, Nunez FJ, Mendez F, Brosnan-Cashman JA, Meeker AK, Lowenstein PR and Castro MG (2017) Mutated chromatin regulatory factors as tumor drivers in cancer. *Cancer Res* **2**, 227–233.
- Lahm A, Paolini C, Pallaoro M, Nardi MC, Jones P, Neddermann P, Sambucini S *et al.* (2007) Unraveling the hidden catalytic activity of vertebrate class IIa histone deacetylases. *Proc Natl Acad Sci USA* **104**, 17335–17340.
- Lei Y, Liu L, Zhang S, Guo S, Li X, Wang J, Bo S *et al.* (2017) Hdac7 promotes lung tumorigenesis by inhibiting Stat3 activation. *Mol Cancer* **16**, 170.
- Liberzon A, Birger C, Thorvaldsdóttir H, Ghandi M, Mesirov JP and Tamayo P (2015) The molecular

- signatures database hallmark gene set collection. *Cell Syst* **1**, 417–425.
- Marampon F, Megiorni F, Camero S, Crescioli C, McDowell HP, Sferra R, Vetusch A *et al.* (2017) HDAC4 and HDAC6 sustain DNA double strand break repair and stem-like phenotype by promoting radioresistance in glioblastoma cells. *Cancer Lett* **397**, 1–11.
- Martin M, Kettmann R and Dequiedt F (2007) Class IIa histone deacetylases: regulating the regulators. *Oncogene* **26**, 5450–5467.
- Maya-Mendoza A, Ostrakova J, Kosar M, Hall A, Duskova P, Mistrik M, Merchut-Maya JM *et al.* (2015) Myc and Ras oncogenes engage different energy metabolism programs and evoke distinct patterns of oxidative and DNA replication stress. *Mol Oncol* **9**, 601–616.
- Montero-Conde C, Leandro-Garcia LJ, Chen X, Oler G, Ruiz-Llorente S, Ryder M, Landa I *et al.* (2017) Transposon mutagenesis identifies chromatin modifiers cooperating with *Ras* in thyroid tumorigenesis and detects *ATXN7* as a cancer gene. *Proc Natl Acad Sci USA* **114**, E4951–E4960.
- Mottet D, Bellahcène A, Pirotte S, Waltregny D, Deroanne C, Lamour V, Lidereau R and Castronovo V (2007) Histone deacetylase 7 silencing alters endothelial cell migration, a key step in angiogenesis. *Circ Res* **12**, 1237–1246.
- Nguyen HT, Hong X, Tan S, Chen Q, Chan L, Fivaz M, Cohen SM and Mathijs Voorhoeve P (2014) Viral small T oncoproteins transform cells by alleviating hippo-pathway-mediated inhibition of the YAP proto-oncogene. *Cell Rep* **8**, 707–713.
- Noser JA, Mael AA, Sakuma R, Ohmine S, Marcato P, Lee PWK and Ikeda Y (2007) The RAS/Raf1/MEK/ERK signaling pathway facilitates VSV-mediated oncolysis: implication for the defective interferon response in cancer cells. *Mol Ther* **8**, 1531–1536.
- Paroni G, Fontanini A, Cernotta N, Foti C, Gupta MP, Yang X-J, Fasino D and Brancolini C (2007) Dephosphorylation and Caspase processing generate distinct nuclear pools of histone deacetylase 4. *Mol Cell Biol* **19**, 6718–6732.
- Paroni G, Mizzau M, Henderson C, Del Sal G, Schneider C and Brancolini C (2004) Caspase-dependent regulation of histone deacetylase 4 nuclear-cytoplasmic shuttling promotes apoptosis. *Mol Biol Cell* **15**, 2804–2818.
- Peruzzo P, Comelli M, Di Giorgio E, Franforte E, Mavelli I and Brancolini C (2016) Transformation by different oncogenes relies on specific metabolic adaptations. *Cell Cycle* **15**, 2656–2668.
- Picco R, Tomasella A, Fogolari F, Brancolini C (2014) Transcriptomic analysis unveils correlations between regulative apoptotic caspases and genes of cholesterol homeostasis in human brain. *PLoS One* **9**, e110610.
- Rad R, Rad L, Wang W, Cadinanos J, Vassiliou G, Rice S, Campos LS *et al.* (2010) PiggyBac transposon mutagenesis: a tool for cancer gene discovery in mice. *Science* **330**, 1104–1107.
- Schwartzentruber J, Korshunov A, Liu XY, Jones DT, Pfaff E, Jacob K, Sturm D *et al.* (2012) Driver mutations in histone H3.3 and chromatin remodelling genes in paediatric glioblastoma. *Nature* **482**, 226–231.
- Seger YR, García-Cao M, Piccinin S, Cunsolo CL, Doglioni C, Blasco MA, Hannon GJ and Maestro R (2002) Transformation of normal human cells in the absence of telomerase activation. *Cancer Cell* **5**, 401–413.
- Serrano M, Lin AW, McCurrach ME, Beach D and Lowe SW (1997) Oncogenic Ras provokes premature cell senescence associated with accumulation of P53 and P16(INK4a). *Cell* **88**, 593–602.
- Subramanian A, Tamayo P, Mootha VK, Mukherjee S, Ebert BL, Gillette MA, Paulovich A *et al.* (2005) Gene set enrichment analysis: a knowledge-based approach for interpreting genome-wide expression profiles. *Proc Natl Acad Sci USA* **102**, 15545–15550.
- Taylor KR, Mackay A, Truffaux N, Butterfield YS, Morozova O, Philippe C, Castel D *et al.* (2014) Recurrent activating ACVR1 mutations in diffuse intrinsic Pontine glioma. *Nat Genet* **5**, 457–461.
- Toledo LI, Murga M, Gutierrez-Martinez P, Soria R and Fernandez-Capetillo O (2008) ATR signaling can drive cells into senescence in the absence of DNA breaks. *Genes Dev* **3**, 297–302.
- Wang Y, Guoqing H, Liu F, Wang X, Mingfu W, Schwarz JJ and Zhou J (2014) Deletion of yes-associated protein (YAP) specifically in cardiac and vascular smooth muscle cells reveals a crucial role for YAP in mouse cardiovascular development. *Circ Res* **6**, 957–965.
- Wang Y, Hou N, Cheng X, Zhang J, Tan X, Zhang C, Tang Y, Teng Y and Yang X (2017) Ezh2 acts as a tumor suppressor in Kras-driven lung adenocarcinoma. *International Journal of Biological Sciences*. **5**, 652–659.
- Yang W, Xia Y, Hawke D, Li X, Liang J, Xing D, Aldape K, Tony Hunter WK, Yung A and Zhimin L (2012) PKM2 phosphorylates histone H3 and promotes gene transcription and tumorigenesis. *Cell* **4**, 685–696.

## Supporting information

Additional supporting information may be found online in the Supporting Information section at the end of the article.

**Fig. S1.** HDAC7-S/A triggers senescence similarly to HDAC4-TM.



Article

# Genetic Programs Driving Oncogenic Transformation: Lessons from In Vitro Models

Eros Di Giorgio, Harikrishnareddy Paluvai, Raffaella Picco and Claudio Brancolini \*

Department of Medicine, Università degli Studi di Udine, P.le Kolbe 4, 33100 Udine, Italy; eros.digiorgio@uniud.it (E.D.G.); hari.paluvai@student.unisi.it (H.P.); raf.picco@uniud.it (R.P.)

\* Correspondence: claudio.brancolini@uniud.it; Tel.: +39-0432-494382

Received: 30 October 2019; Accepted: 11 December 2019; Published: 12 December 2019



**Abstract:** Cancer complexity relies on the intracellular pleiotropy of oncogenes/tumor suppressors and in the strong interplay between tumors and micro- and macro-environments. Here we followed a reductionist approach, by analyzing the transcriptional adaptations induced by three oncogenes (*RAS*, *MYC*, and *HDAC4*) in an isogenic transformation process. Common pathways, in place of common genes became dysregulated. From our analysis it emerges that, during the process of transformation, tumor cells cultured in vitro prime some signaling pathways suitable for coping with the blood supply restriction, metabolic adaptations, infiltration of immune cells, and for acquiring the morphological plasticity needed during the metastatic phase. Finally, we identified two signatures of genes commonly regulated by the three oncogenes that successfully predict the outcome of patients affected by different cancer types. These results emphasize that, in spite of the heterogeneous mutational burden among different cancers and even within the same tumor, some common hubs do exist. Their location, at the intersection of the various signaling pathways, makes a therapeutic approach exploitable.

**Keywords:** *RAS*; *MYC*; *HDAC4*; *G0S2*; *DOCK4*; *SRPX* interferon; inflammation; TCGA

## 1. Introduction

Cancer is a complex disease that arises through the accumulation of specific genetic lesions, affecting oncogenes and tumor suppressor genes. These lesions hijack transcriptional/epigenetic machineries to reprogram the gene expression profile of the cells [1]. The final goal is to sustain a robust proliferation, invasion, and the suppression of cell death programs. The tumorigenic process is the consequence of the adaptations that tumor cells must achieve to overcome different crises. Escaping senescence, suppressing apoptosis, resolving starvation from blood supply, impinging the metabolic circuits, and evading immune surveillance represent the major achieved adaptations [2].

Cancer cells are part of a complex ecosystem. Together with fibroblasts, endothelial and the immune cells constitute and organize the tumor microenvironment [3]. These cells establish different interactions that are transduced and maintained by interconnected networks of signals. To unveil this complexity, system biology approaches can be adopted to integrate genomic and epigenomic data collected from tumor biopsies [4,5]. Moreover, the initial assumption of considering cancer as the expansion of a monoclonal population has been recently replaced by the evidence obtained by single-cell sequencing [6]. In each cancer, several subclones can co-exist and can expand or contract as a function of their fitness [6].

Within this complexity, it is important to define the crucial events that can be target for a therapeutic intervention. The social impact of the tumorigenic process must prompt us to focus all efforts in unveiling the key oncogenic additions for each different tumor type.

Historically, *in vitro* transformation models have provided the first approach to understand the tumorigenic process [7]. The identification of oncogenes and tumor suppressor genes and the demonstration of the cooperation among oncogenes represent the major accomplishments of these model systems. Traditionally, rodent cells have been largely used. However, transformation of murine cells and human cells greatly differ [8]. Human cells are more resistant to oncogenic transformation and require more events [9]. *In vitro* transformation approaches frequently adopt viral oncoproteins to switch off important tumor suppressor genes, such as RB and TP53. Nevertheless, transformation of human cells can also be obtained in absence of viral genes [10]. An innovative version of the *in vitro* transformation studies is represented by the generation of human organoids. Under a 3D growth condition and a selected microenvironment, these primary cells can be engineered *in vitro*, using CRISPR/Cas9 genome editing approaches, to recapitulate the key oncogenic lesions of the primary tumors [11].

Importantly, *in vitro* tumorigenic models must find validation *in vivo*. The resetting of the transcriptomic output represents the major tool through which cancer cells modulate their plasticity and adapt to the microenvironment. Hence, in this manuscript, we have compared the transcriptional profiles of three different isogenic models of *in vitro* transformation. Our goal is to demonstrate a correspondence between the *in vitro* transformation process and cancer development in patients. Moreover, we would like to define a minimal gene signature, shared among different transformation models, that could represent a useful tool to unveil the Achilles' heel of many cancers.

## 2. Results

### 2.1. *In Vitro* Transformation of Human Fibroblasts Achieved by Different Oncogenes Leads to the Activation of Both Distinct and Common Genetic Programs

*In vitro* transformation of human cells requires a limited number of genetic changes [7]. Viral genes such as the SV40 early region, which encodes both the large T and small t oncoproteins, in combination with the catalytic subunit of the telomerase (hTERT) have been commonly used to drive the immortalization and to circumvent senescence of normal human fibroblasts and kidney cells [12]. The subsequent introduction of strong oncogenes such as *RAS* or *MYC* triggers the cellular transformation. These cells are characterized by an anchorage independent growth and by the ability to generate tumors when injected in immunocompromised mice [12,13].

Here, we deeply investigated the strength of the transcriptome reprogramming, triggered during the *in vitro* transformation process, in predicting the outcome of different human cancers. With this aim we compared the gene expression profiles of human foreskin fibroblasts expressing *hTERT*, the early region of SV40 and subsequently transduced with *HRAS/G12V* [13], *MYC* [14], or an oncogenic nuclear resident form of *HDAC4* (*HDAC4-TM*) [13,15]. These oncogenes have been chosen for their heterogeneity. As frequently reported for other oncogenic combinations [12,13], when mutations, amplifications, or transcript dysregulations of these oncogenes were analyzed in different human cancers, the co-occurrence of their alterations appears to be restricted to a small number of cases. In Figure 1, we report the oncoprint of TCGA PanCancer ATLAS datasets selected among some of the most frequent solid tumors. We included breast, colorectal, lung, prostate, stomach, and uterine cancers (Figure 1). As expected, point mutations in *RAS* are not common in breast and prostate cancer [16]. Interestingly, genetic alterations in *HDAC4* are more frequent in uterine and stomach cancers, with a conspicuous incidence of truncations and point mutations of still unknown impact on the activities of this deacetylase (Figure 1).

The simultaneous dysregulations of *HDAC4*, *MYC*, and *RAS* oncogenes are relatively rare. There are some co-occurrences between *HDAC4* and *MYC* or *HDAC4* and *RAS* as well as between *MYC* and *RAS*. Most frequently, patients carry alterations only in one of the three oncogenes (Figure 1). This evidence suggests that the three oncogenes can act through completely distinct and non-complementary mechanisms or through at least partially overlapping pathways.

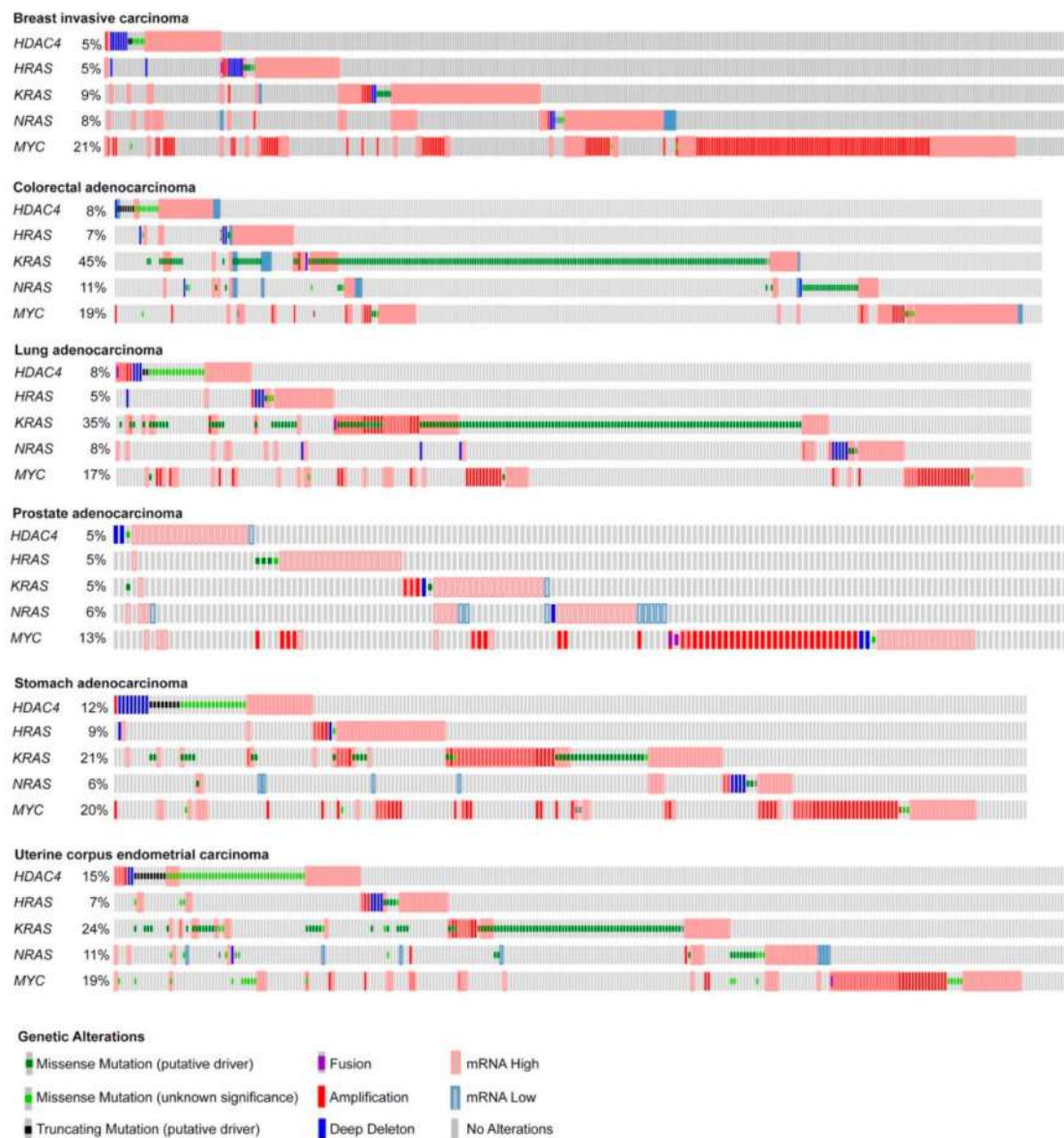


**Figure 1.** Summary of the genetic alterations reported for *HRAS*, *KRAS*, *NRAS*, *MYC*, and *HDAC4* in some human cancers. Oncoprints of *HDAC4*, *HRAS*, *KRAS*, *NRAS*, and *MYC* mutations and alterations in the indicated tumor types. Images were cropped to highlight the alterations. Data were obtained from the TCGA database. The heatmap was generated through cBioPortal (<http://www.cbioportal.org>). The different genetic alterations are indicated by the provided color code.

## 2.2. *RAS*, *MYC*, and *HDAC4*-Mediated Oncogenic Transformation Is Marked by the Dysregulation of Common Pathways Rather Than of Common Genes.

To prove the above enounced concept, we interrogated the gene expression profiles of BJ-*hTERT/ST/LT/MYC* [14], BJ-*hTERT/ST/LT/HRASG12V* [13], and BJ-*hTERT/ST/LT/HDAC4-S246A, S467A, S632A* [15], relatively to the isogenic pre-transformed control cells, expressing the SV40 LT and ST or the entire early region.

By adopting as cut-off criteria 1.5-fold change and  $FDR < 0.05$ , we obtained six signatures of genes regulated by the three oncogenes. Overall, 519 and 634 transcripts were respectively upregulated and downregulated by *MYC*, 556 and 595 by *RAS* and finally, 551 and 979 by *HDAC4*.

Few genes turned out to be commonly dysregulated by the three oncogenes. Only three genes were upregulated either in RAS, MYC, and HDAC4 transformed cells (Figure 2A), while 22 were the commonly repressed genes (Figure 2B).

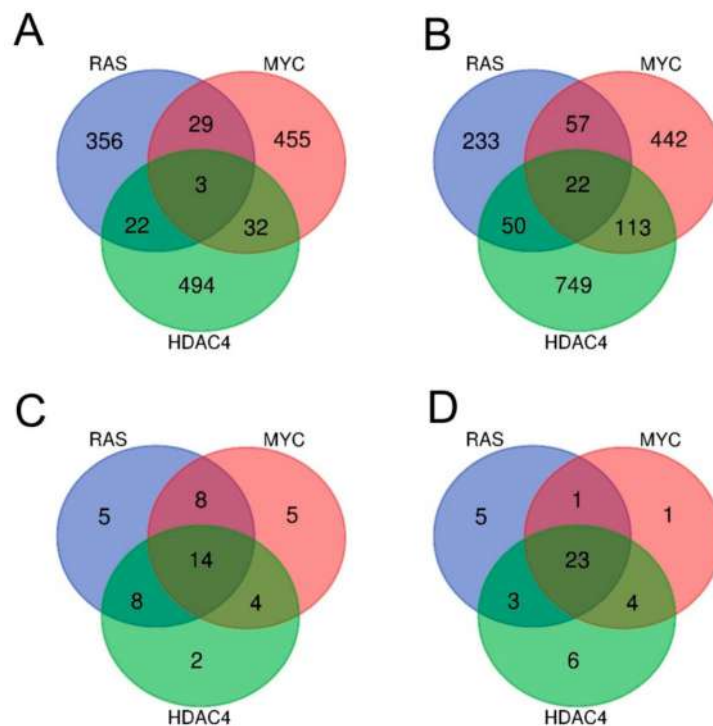


**Figure 2.** Analysis of the transcriptional profiles in three different models of in vitro transformation. (A) Venn diagram showing the number of transcripts upregulated during the transformation process in BJ/hTERT/LT/ST cells expressing RAS, MYC, or HDAC4 as indicated. (B) Venn diagram showing the number of transcripts downregulated during the transformation process in BJ/hTERT/LT/ST cells expressing RAS, MYC, or HDAC4 as indicated. (C) Venn diagram showing the number of different hallmarks gene sets significantly upregulated by RAS, MYC, and HDAC4. (D) Venn diagram showing the number of different hallmarks gene sets significantly downregulated by RAS, MYC, and HDAC4. All the Venn diagrams were created by using this software <http://bioinformatics.psb.ugent.be/webtools/Venn/>.

Although the commonly dysregulated genes are rare, the three oncogenes could influence the same pathways through alterations of different genes, operating at different steps of the same pathway. To prove this hypothesis, we applied the Gene Set Enrichment Analysis (GSEA) algorithm to compare the six signatures obtained to the MSigDB HALLMARK gene sets [17,18]. The “HALLMARKS” is a collection of 50 gene sets; each of them groups genes that display coordinate expression and represent well-defined biological processes. Tables SIA–SIC summarize the statistically significant genes sets identified by the analysis for the upregulated genes and Tables SIIA–SIIC for the downregulated genes. Venn diagrams show that the three oncogenes share several gene sets, which control important biological functions related to the transformation process. For the upregulated genes, 14 different gene sets were commonly regulated by RAS, MYC, and HDAC4 (Figure 2C). For the repressed genes this number increased up to 23 (Figure 2D).

In summary, although the number of genes commonly regulated in the three models of in vitro transformation is small, the pathways and the biological processes under the influences of HDAC4, RAS, and MYC testify a convergence towards common strategies of hijacking specific cellular responses.

### 2.3. Identification of the Pathway Reprogramming Core that Defines the Common Trait of the in Vitro Transformation Process

Having found that the three transformation models influence common gene sets, we next analyzed which genes were under the regulation of the three oncogenes in the different gene sets.

Figure 3 shows the result of such analysis for the upregulated genes. As above mentioned, only three genes (*DOCK4*, *G0S2*, *SRPX*) were commonly induced by the three oncogenes. These genes are represented in more than one gene set. The Venn diagrams illustrate also the common genes among two models of in vitro transformation (Figure 3). Interestingly, the gene set “p53 pathway” includes all the three genes. Although no other genes were in common between RAS and MYC or RAS and HDAC4, all genes ( $n = 9$ ) were in common between MYC and HDAC4. This observation suggests that HDAC4 and MYC share similar strategies to dysregulate the p53 pathway. Another relevant gene set is the “inflammatory response”. Here common genes were not identified. However, this cellular response is equally modulated by all three oncogenes, with a similar number of genes. Some of them are in common between RAS and HDAC4 ( $n = 2$ ), RAS and MYC ( $n = 2$ ), and MYC and HDAC4 ( $n = 3$ ). In the case of the gene set “glycolysis” several genes are under the influence of RAS and a good overlap is observed with MYC ( $n = 5$ ). By contrast, HDAC4 shows a peculiar influence on this metabolic gene set, possibly reflecting its non-conventional activities on the metabolism of the transformed cells [19].

When we analyzed the repressed genes, the number of statistically significant hallmarks gene sets was higher ( $n = 23$ ) (Figure 4 and Tables SIIA–SIIC). The gene set “epithelial-mesenchymal transition” scored the highest number of common hubs ( $n = 5$ ). In addition, a significant number of genes were similarly dysregulated by RAS and HDAC4 ( $n = 7$ ) and by MYC and HDAC4 ( $n = 5$ ). The EMT gene set was the most statistically significant enriched gene set in the RAS and HDAC4 transformed cells, whereas in MYC-transformed it scored the fourth position. An opposite behavior was observed for the gene set “complement”. The total number of genes regulated was 46 but only 2 genes were in common between RAS and MYC and HDAC4 and MYC. This observation indicates that the complement pathway is targeted through alternative mechanisms in the three models of in vitro transformation.

Other statistically significant repressed gene sets are the *interferon- $\alpha$*  (IFN $\alpha$ ) and the *interferon- $\gamma$*  (IFN $\gamma$ ) responses. In RAS-transformed cells they resulted the second and the third top hits, respectively, whereas in MYC-transformed cells the second and the first. Finally, in the case of HDAC4 they scored as the seventh and the third hits.

Only three genes were commonly repressed in the IFNs hallmarks gene sets: *ARID5B*, *ELF1*, and *MX1*. The last was present in both the IFN $\alpha$  and the IFN $\gamma$  gene sets. When RAS and MYC were compared, 20 genes were in common for the IFN $\gamma$  response and 15 in the case of the IFN $\alpha$ . On the other side, *HDAC4* shows stronger similarities with *MYC*. Nine genes belonging to IFN $\gamma$  and to IFN $\alpha$  gene sets were in common between MYC and HDAC4 in IFN $\gamma$  as well as in IFN $\alpha$  gene sets. Few similarities were found between *HDAC4* and *RAS*, with only a gene in common for IFN $\gamma$  (Figure 4).

In summary, this analysis indicates the IFN $\alpha$  and IFN $\gamma$  signaling are significantly and robustly repressed in different models of in vitro transformation. This can be due to: (i) the key role that the repression of the pathways plays in the transformation process, as previously reported [20–24]; (ii) a certain degree of purifying selection that supervise the conservation of IFN signaling [25].

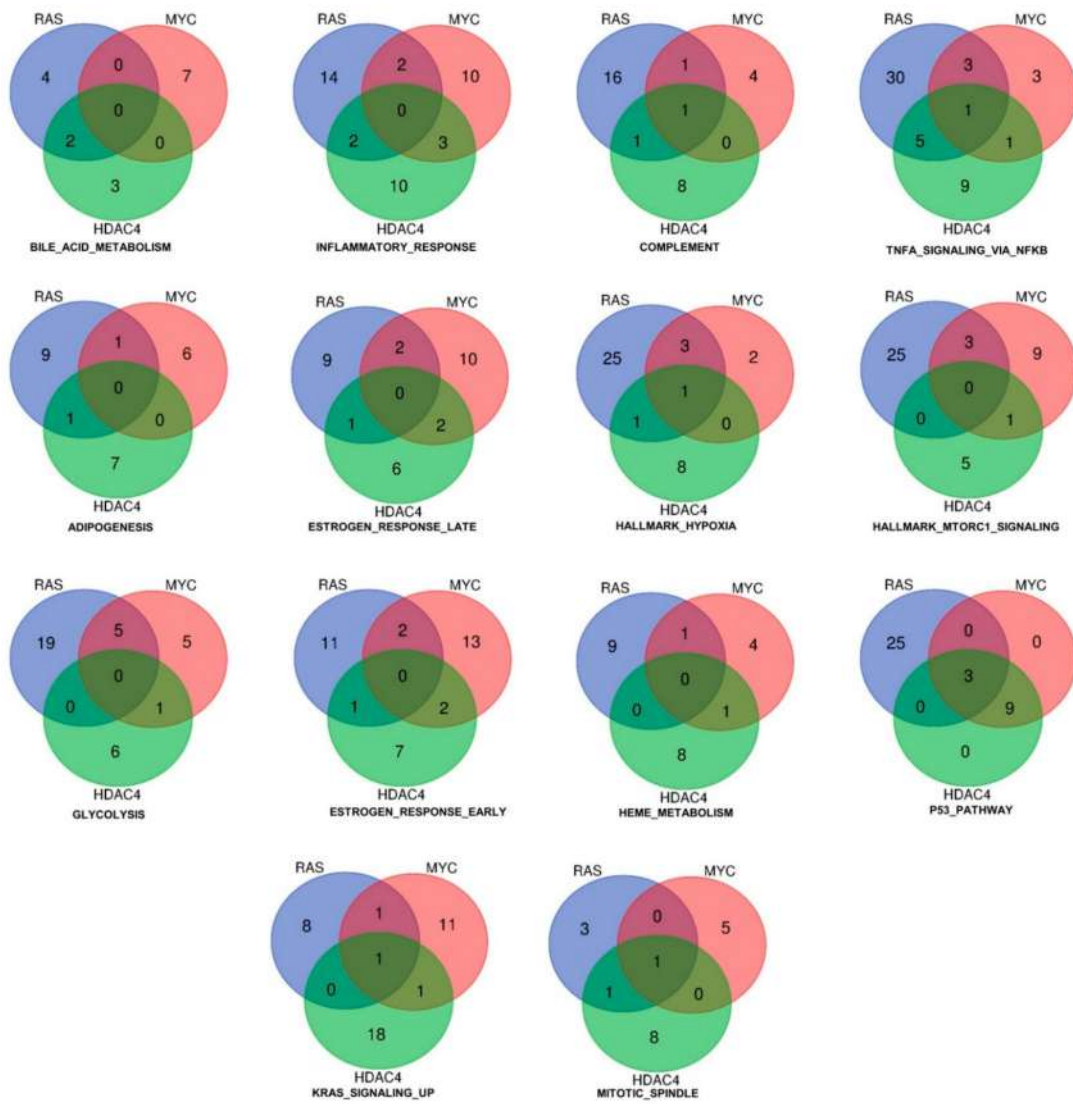


**Figure 3.** Hallmarks and genes commonly upregulated by the three oncogenes (HDAC4, RAS, MYC) during the in vitro transformation process. Venn diagram showing different sets of hallmarks and the number of upregulated genes, which are shared by HDAC4, RAS, and MYC.

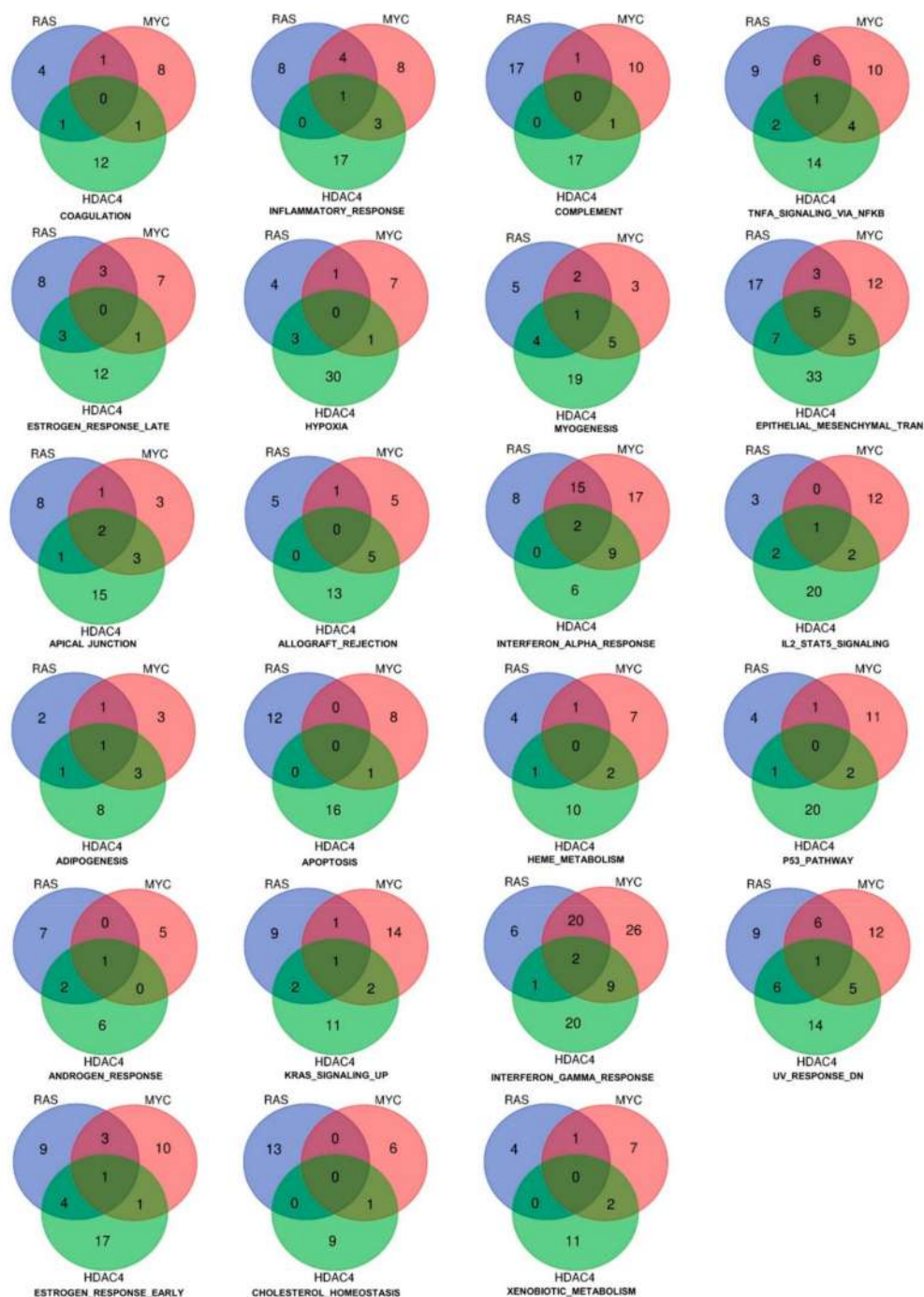


**Figure 4.** Hallmarks and genes commonly downregulated by three oncogenes (HDAC4, RAS, MYC) during the in vitro transformation process. Venn diagram showing different sets of hallmarks and number of downregulated genes that were commonly shared by HDAC4, RAS, and MYC.

2.4. Definition of the Minimal Signatures Regulated during in Vitro Transformation

The final goal of our approach is to verify if the pathways dysregulated during the in vitro transformation can predict the outcome of malignant cancers in patients. For this reason, we extracted three signatures: Two for the repressed and one for upregulated genes (Table 1). Both signatures are made up of genes commonly and significantly upregulated or downregulated by the three oncogenes.

**Table 1.** List of the common genes and of the relative signatures modulated during the in vitro transformation process.

GENE	SIGNATURE	HALLMARK
<i>DOCK4</i>	Upregulated	Complement/Spindle
<i>G0S2</i>	Upregulated	TNF-NFKB/KRAS
<i>SRPX</i>	Upregulated	Hypoxia
<i>CDH11</i>	Downregulated A	EMT/APICAL
<i>DKK1</i>	Downregulated A	EMT
<i>GREM1</i>	Downregulated A	EMT
<i>MYLK</i>	Downregulated A	Adipogenesis/Myogenesis/EMT
<i>SPRY2</i>	Downregulated A	KRAS
<i>ARID5B</i>	Downregulated B	Androgen/IFN $\gamma$
<i>DUSP4</i>	Downregulated B	TNF $\alpha$ -NFKB
<i>ELF1</i>	Downregulated B	IFN $\alpha$ /ESTROGEN
<i>LPAR1</i>	Downregulated B	Inflammation/UV
<i>MX1</i>	Downregulated B	IFN $\alpha$ /IFN $\gamma$
<i>SOCS2</i>	Downregulated B	IL2-STAT5
<i>TNFRSF11B</i>	Downregulated B	EMT/APICAL

The signature of the upregulated genes groups *DOCK4*, *G0S2*, and *SRPX* (Table 1). *DOCK4* encodes for a guanine nucleotide exchange factors that participates in the regulation of cell adhesion and membrane trafficking [26,27]. It is reported to be mutated in cancer [26] and to influence cancer aggressiveness through the modulation of WNT and TGF- $\beta$  pathways [28,29]. Since also anti-proliferative activities have been reported, its oncogenic potential seems to be context specific [30,31].

*G0S2* (G0/G1 switch gene 2) encodes for a potent inhibitor of adipose triglyceride lipase. In this manner, *G0S2* acts as a master regulator of the tissue-specific balance of triglyceride storage vs. mobilization [32]. Correlations with cancer are unclear with anti-proliferative effects described by some reports [33–35]. Finally, *SRPX* (sushi repeat containing protein X-linked), known also as *ETX1* or *DRS*, was initially isolated as deleted in patients with X-linked retinitis pigmentosa [36], as well as downregulated by *v-src* [37]. A tumor suppressive activity for *SRPX* was proposed [38]. Moreover, its expression seems to be downregulated in different aggressive cancers [39–41].

For the repressed genes we selected two different signatures. The first signature (repressed signature A) includes five genes (*CDH11*, *DKK1*, *GREM1*, *MYLK*, *SPRY2*). These genes do not belong to the inflammatory and interferon gene sets (Table 1). A second signature of genes (repressed signature B) groups the remaining commonly repressed genes that belong to inflammatory-immune responses (*ARID5B*, *DUSP4*, *ELF1*, *LPAR1*, *MX1*, *SOCS2*, *TNFRSF11B*).

### 2.5. High mRNA Levels of the Upregulated Genes Correlate with Reduced Patients' Survival in a Group of Different Tumors

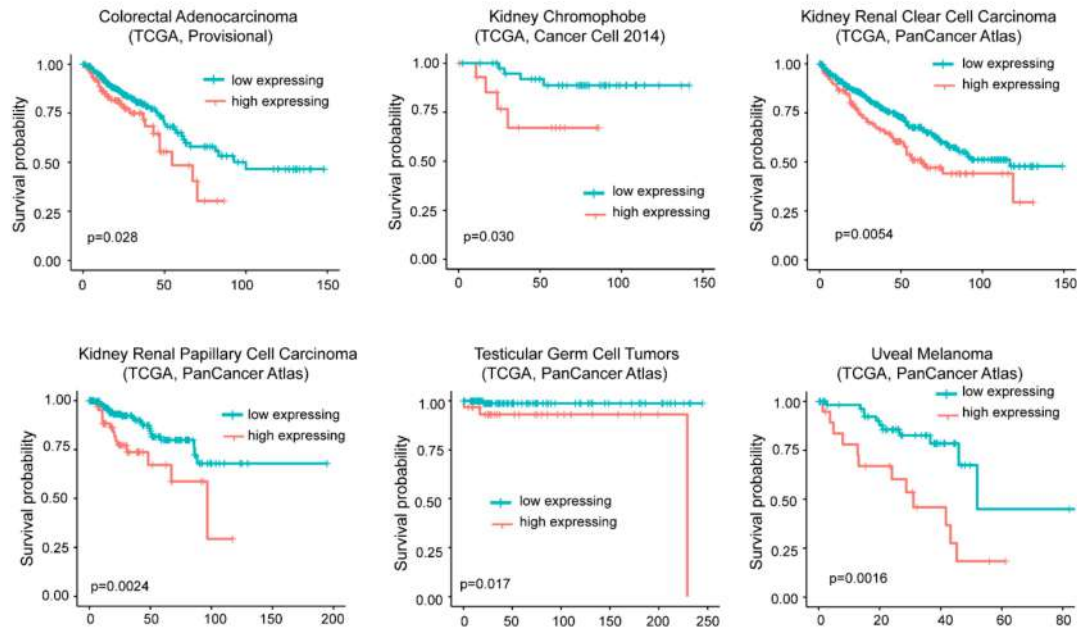
In order to understand if the identified signatures can predict cancer aggressiveness and patients' outcome, they were used to interrogate the survival data of 32 cancer types deposited in the Cancer Genome Atlas (TCGA).

For the upregulated genes, we segregated the patients in two groups. The first group is characterized by high expression levels of the signature (above the third quartile). The second group is characterized by moderated upregulation, unperturbed or repressed expression of the signature (below the third quartile). Figure 5A illustrates that in six different cancer types (colorectal adenocarcinoma, kidney chromophobe, kidney renal clear cell carcinoma, kidney renal papillary cell carcinoma, testicular

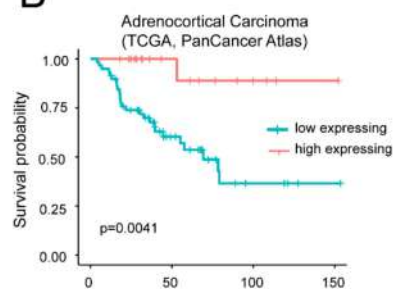
germ cell tumors, and uveal melanoma) high levels of *DOCK4*, *G0S2*, and *SRPX* significantly correlate with a worst survival.

#### The RAS/MYC/HDAC4 up-regulated signature

### A



### B



### C

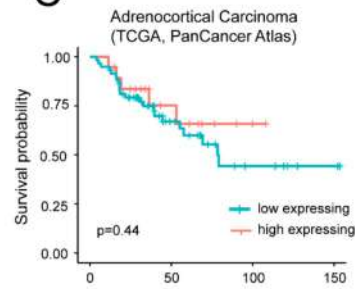


**Figure 5.** High mRNA levels of upregulated genes during in vitro transformation process influence patients' survival. (A) Kaplan-Meier survival analysis related to the three upregulated genes *DOCK4*, *G0S2*, *SRPX*. All cases were analyzed and clustered into two groups according to *DOCK4*, *G0S2*, and *SRPX* expression levels. High levels of expression group (> the third quartile/high expressing) compared to all other cases (< the third quartile/low expressing). Cases were: Colorectal adenocarcinoma (all  $n = 382$ , high expressing  $n = 95$ ), kidney chromophobe (all  $n = 65$ , high expressing  $n = 16$ ), kidney renal clear cell carcinoma (all  $n = 510$ , high expressing  $n = 127$ ), kidney renal papillary cell carcinoma (all  $n = 283$ , high expressing  $n = 70$ ), testicular germ cell tumors (all  $n = 149$ , high expressing  $n = 37$ ), and uveal melanoma (all  $n = 80$ , high expressing  $n = 20$ ). (B) Kaplan-Meier survival analysis related to *G0S2* in adrenocortical carcinoma (ACC). High level expression (above the third quartile) of *G0S2* in ACC were observed in 19 cases. All cases were  $n = 78$ . (C) Kaplan-Meier survival analysis related to *DOCK4* and *SRPX* in ACC. High level expression (> the third quartile) of *DOCK4* and *SRPX* were observed in 19 cases, all cases were  $n = 78$ .

On the opposite high levels of the signature predicts a better overall survival in adrenocortical carcinoma (ACC) (Figure 5B). This behavior could depend on *G0S2*. In fact in ACC, which is a rare, aggressive malignancy, *G0S2* hypermethylation is a hallmark of rapidly recurrent or fatal disease, amenable to targeted assessment using routine molecular diagnostics [35]. Very low levels of *G0S2*

mRNA expression characterize tumors with *GOS2* hypermethylation. Although low *GOS2* expression marks 40% of ACC and independently predicts shorter disease-free and overall survival, the role of this gene in adrenocortical biology is still unknown [42]. To confirm this data, we repeated the survival analysis without the *GOS2* gene. In this case the positive correlation with ACC survival was abrogated (Figure 5C). For the remaining 25 cancer types the signature failed to predict any patients' survival.

### 2.6. High Levels of *DOCK4*, *GOS2*, and *SRPX* Expression Are Related to Worse Survival in Similar but also Different Tumor Types

The influence of *GOS2* methylation on cancer mortality is peculiar of ACC. As expected from the in vitro transformation models, in many other tumors ( $n = 9$ ) high levels of *GOS2* mRNA are indicative of a reduced survival (Figure 6).

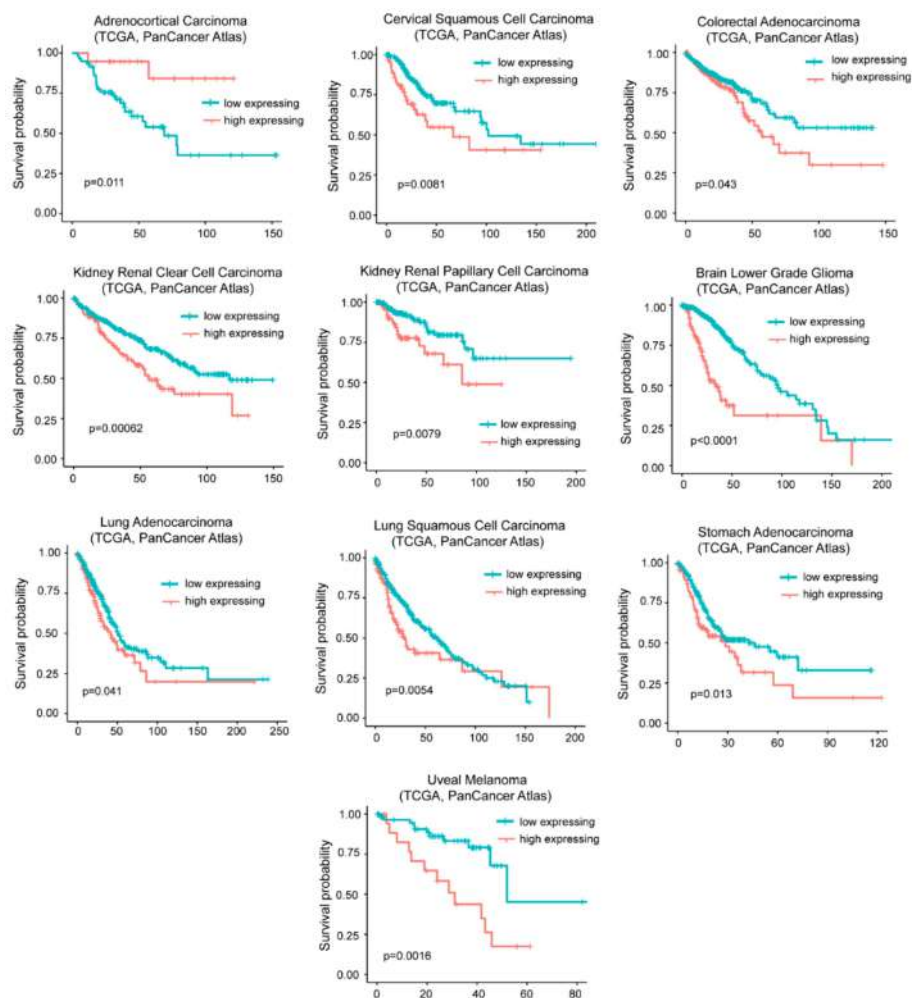


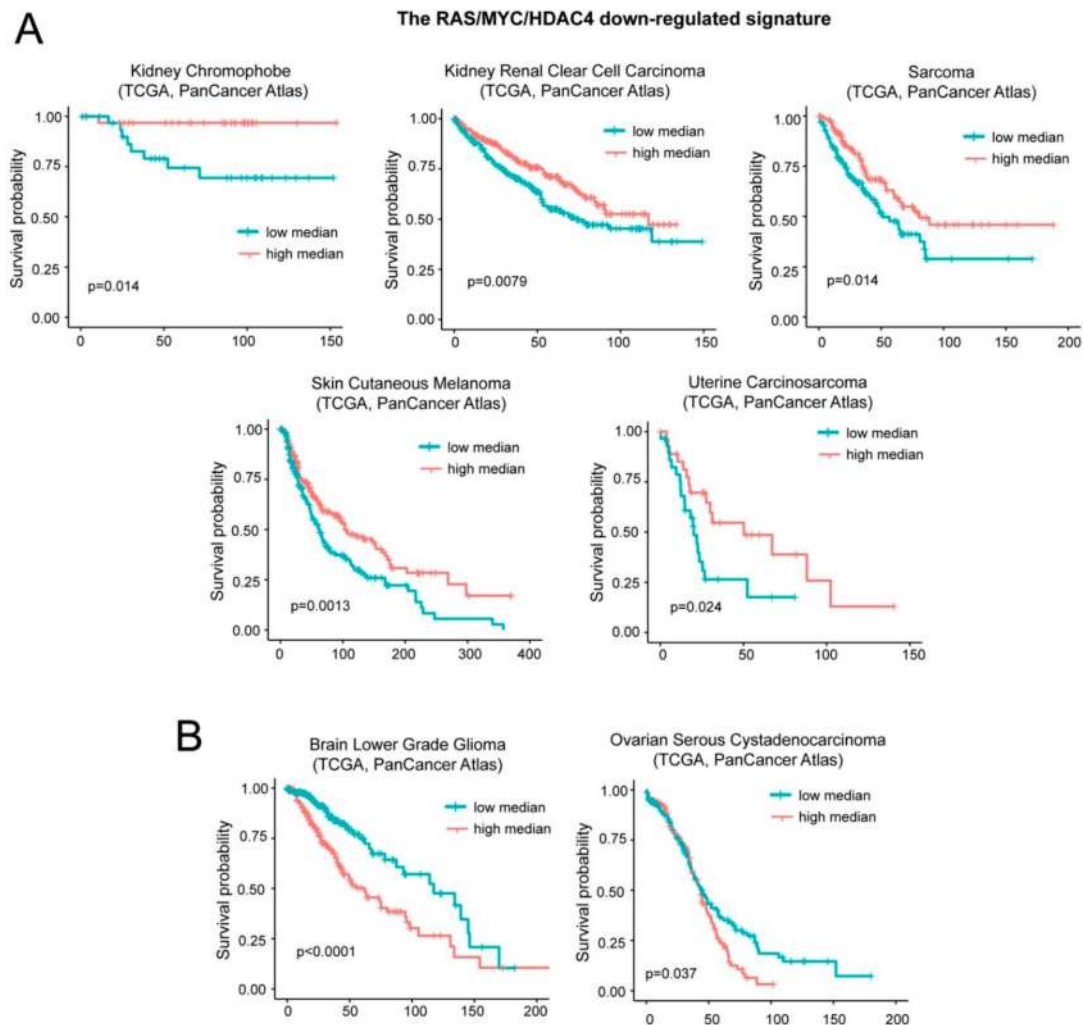
**Figure 6.** High levels of *GOS2* expression correlate with reduced survival in different cancer types. TCGA survival data analysis on tumors grouped for high levels of *GOS2* expression alone (> the third quartile/high expressing) compared to all other cases (< the third quartile/low expressing). Cases were: Adrenocortical carcinoma (all  $n = 78$ , high expressing  $n = 19$ ), cervical squamous cell carcinoma (all  $n = 294$ , high expressing  $n = 73$ ), colorectal adenocarcinoma (all  $n = 592$ , high expressing  $n = 148$ ), kidney renal clear cell carcinoma (all  $n = 510$ , high expressing  $n = 127$ ), kidney renal papillary cell carcinoma (all  $n = 283$ , high expressing  $n = 70$ ), brain low grade glioma (all  $n = 514$ , high expressing  $n = 128$ ), lung adenocarcinoma (all  $n = 510$ , high expressing  $n = 127$ ), lung squamous cell carcinoma (all  $n = 484$ , high expressing  $n = 121$ ), stomach carcinoma (all  $n = 412$ , high expressing  $n = 103$ ), and uveal melanoma (all  $n = 80$ , high expressing  $n = 20$ ).

To verify whether *GOS2* is the key gene in predicting patients' survival, we repeated the analysis for *DOCK4* and *SRPX*. High levels of *DOCK4* correlates with a reduced survival in five different tumors (colorectal, kidney chromophobe, brain low grade glioma, stomach adenocarcinoma, and uveal melanoma) and with a better prognosis in two cancer types (mesothelioma and skin cutaneous melanoma) (Figure S1). Increased levels of *SRPX* correlates with an increased hazardous rate in seven different cancer types (bladder, colorectal, head and neck squamous carcinoma, kidney renal clear cell and papillary carcinomas, thyroid carcinoma, and uterus corpus endometrial carcinoma). Conversely, it predicts a better outcome in melanoma (Figure S2). This analysis suggests that the three upregulated genes could exert independent activities to influence cancer aggressiveness.

### 2.7. A Group of Genes Repressed during in Vitro Transformation Predicts Patients' Survival.

Next, we interrogated the TCGA survival data with the repressed signature A. The patients were segregated in two groups accordingly to the median value of expression of the signature. In two different cancer types, high levels of the signature correlate with increased survival, while in other six cancer types high levels of the same signature correlate with reduced survival. Hence, we discarded this signature for further analysis.

A different result was obtained with the repressed signature B that groups inflammatory and interferon genes. Low levels of the repressed signature correlate with a worst prognosis in five cases: Kidney chromophobe carcinoma, kidney clear cell carcinoma, sarcoma, skin cutaneous melanoma, and uterine carcinosarcoma (Figure 7A). On the opposite, low levels of this signature predict a better outcome in patients with brain lower grade glioma and ovarian serous cystadenocarcinoma (Figure 7B). For simplicity we named this signature "oncogene-repressed inflammatory signature".



### *2.8. Inflammatory Genes Repressed during the in Vitro Transformation Process and Tissue-Infiltrating Immune Cells*

Tumors are characterized by a variegated abundance of tissue infiltrating immune cells, which can influence the prognosis [43]. Since the oncogene-repressed inflammatory signature comprises many inflammatory genes, our in vivo analysis could be influenced by the presence of tumor infiltrating immune cells. Recent studies have shown that the abundance of immune cells in tissue transcriptomic data can be predicted by specific mRNA signatures [44].

We applied the microenvironment cell populations-counter (MCP-counter) to evaluate the contribution of different immune cells to the survival outcomes of patients analyzed for the oncogene-repressed inflammatory signature. With the exclusion of kidney chromophobe, uterine carcinosarcoma, and ovarian serous cystadenocarcinoma, in the other cancer types the survival was also influenced by the presence of immune cells, although with different outcomes (Figures S3 and S4). Prognosis of skin cutaneous melanoma, sarcoma, and brain low grade glioma (LGG) is influenced by the infiltration of different subtypes of immune cells. These tumors behave differentially, with only LGG showing a worst outcome. On the contrary, the better outcome of kidney renal cell carcinoma results significantly and specifically associated with the presence of myeloid dendritic cells (Figure S4).

In conclusion, although in some tumor types the repression of the inflammatory signature and the resulting reduced patients' survival can be specifically ascribed to the transcriptional reprogramming of the neoplastic cells; in other tumors, we cannot exclude a contribution of the immune cells. These cells may have been isolated along with the tumor tissue and thus contribute to the transcriptional landscape as reported by the TCGA data.

### *2.9. Oncogene-Repressed Inflammatory Signature Provides an Additional Contribution to Overall Survival*

As a final analysis, we decided to evaluate the impact on patients' survival of both the tumor infiltrating immune cells and of the expression levels of the oncogene-repressed inflammatory signature. The analysis was restricted to tumor types that showed significant correlations between the overall survival and the presence of the immune cell infiltrates (Figures S3 and S4).

The three tumor types analyzed were LGG, skin cutaneous melanoma, and sarcoma (Figure 8). In LGG, the coexistence of high levels of expression of the oncogene-repressed inflammatory signature and the presence of immune cells, particularly of T cells, cytotoxic lymphocytes and neutrophils represent a negative prognostic condition (Figure 8B,C,G). In agreement with our data, strong correlations between the risk score and T cells, macrophage-related immune response, as well as the expression of immunomodulators were recently reported in LGGs [3,45].

Interestingly, in sarcoma and melanoma tumors where high levels of the oncogene-repressed inflammatory signature correlate with an increased survival, two different behaviors can be appreciated. In sarcoma the presence of immune cells is dominant. In fact, when immune cell infiltrates (particularly CD8 T cells and cytotoxic lymphocytes) are observed, increased survival is maintained, also in the presence of low levels of the oncogene-repressed inflammatory signature (Figure 8E,G). In contrast, in skin cutaneous melanoma low expression levels of the signature are sufficient to reduce the overall survival (Figure 8A,C,D,F,G). In melanoma, the best prognosis is observed in the presence of high expression of the oncogene-repressed inflammatory signature and the concomitant presence of immune cells, particularly T cells, NK, CD8 T cells, and cytotoxic lymphocytes.

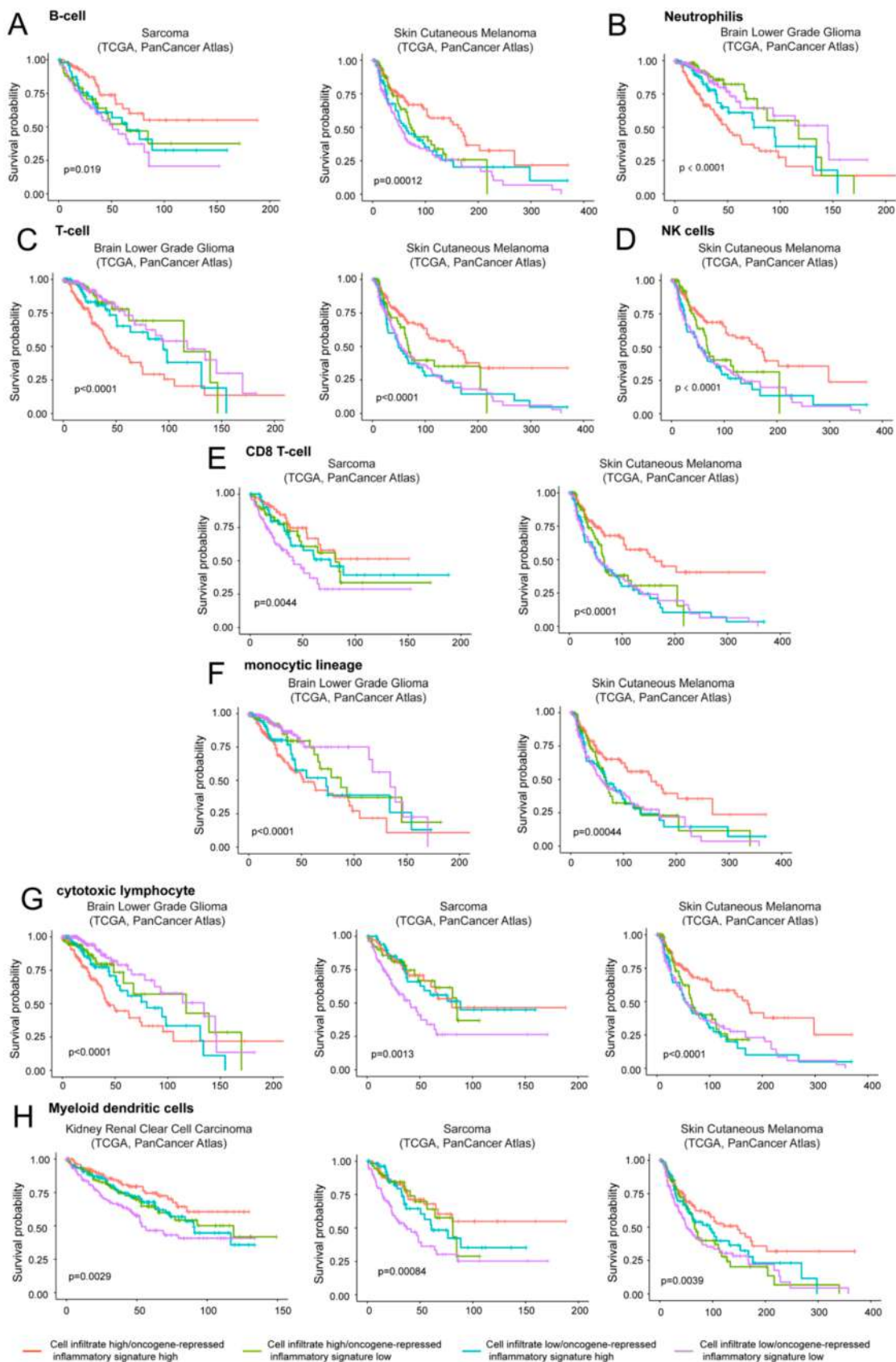


**Figure 8.** The contribution of infiltrating immune/inflammatory cells to overall survival. Kaplan-Meier survival analysis related to the immune/inflammatory signature and the infiltration of different

immune/inflammatory cells. Infiltrating immune/inflammatory cells were defined as described in materials and methods. Patients were grouped high/high (high levels of both infiltrating cells and immune signature), high/low (high levels of infiltrating cells and low levels of the oncogene-repressed inflammatory signature), low/high (low levels of infiltrating cells and high levels of the oncogene-repressed inflammatory signature), and as low/low (low levels of both infiltrating cells and of the oncogene-repressed inflammatory signature). The four groups were generated according to median expression levels of the two signatures. Cases: (A) Sarcoma (all = 253, high/high = 75, high/low = 51, low/high = 51, low/low = 76) and skin cutaneous melanoma (all = 428, high/high = 133, high/low = 82, low/high = 82, low/low = 131). (B) Brain low grade glioma (all = 512, high/high = 155, high/low = 102, low/high = 101, low/low = 154). (C) Brain low grade glioma (all = 512, high/high = 164, high/low = 92, low/high = 92, low/low = 164) and skin cutaneous melanoma (all = 428, high/high = 148, high/low = 66, low/high = 67, low/low = 147). (D) Skin cutaneous melanoma (all = 428, high/high = 143, high/low = 72, low/high = 72, low/low = 141). (E) Sarcoma (all = 253, high/high = 70, high/low = 56, low/high = 56, low/low = 71) and skin cutaneous melanoma (all = 428, high/high = 136, high/low = 77, low/high = 79, low/low = 136). (F) Brain low grade glioma (all = 512, high/high = 164, high/low = 93, low/high = 92, low/low = 163) and skin cutaneous melanoma (all = 428, high/high = 140, high/low = 73, low/high = 75, low/low = 140). (G) Brain low grade glioma (all = 512, high/high = 153, high/low = 104, low/high = 103, low/low = 152), sarcoma (all = 253, high/high = 74, high/low = 52, low/high = 52, low/low = 75) and skin cutaneous melanoma (all = 428, high/high = 142, high/low = 74, low/high = 73, low/low = 139). (H) Kidney renal clear cell carcinoma (all = 510, high/high = 132, high/low = 123, low/high = 123, low/low = 132), sarcoma (all = 253, high/high = 70, high/low = 56, low/high = 56, low/low = 71) and skin cutaneous melanoma (all = 428, high/high = 126, high/low = 89, low/high = 89, low/low = 124).

### 3. Discussion

In this manuscript, we compared three isogenic models of *in vitro* transformation and we identified minimal signatures that characterize the transformation process. We figured out that most of the oncogenic programs driven by the three oncogenes rely on the activation of common pathways. Curiously, these pathways seem to be activated through alternative/complimentary mechanisms, as the modulated transcripts deeply differ and overlap only partially. This could be expected as RAS and MYC in cancer establish a cooperation based on the integration rather than on the intersection of their genetic programs [46]. Moreover, this evidence suggests that the third selected oncogene, HDAC4, triggers a different transformation process, as suggested previously [19,47–50]. However, even if through alternative roads, the three oncogenes converge on some common hubs [2].

A minimal signature of three upregulated transcripts identified through our analysis successfully predict worse prognosis in some cancers. Among these genes emerges *G0S2*. This inhibitor of adipose triglyceride lipase governs lipolysis and fatty acid (FA) availability. *G0S2* is abundantly expressed in adipose tissue and *G0S2* transgenic mice experience difficulties in shifting from carbohydrate to FA oxidation during fasting [51]. *In vivo* studies have indicated that *G0S2* could ensure the usage of glycogen-derived glucose as the primary source of rapid energy output [32,51]. This influence could be relevant for the metabolic adaptation of cancer cells. However, preliminary studies have provided conflicting data on a role of *G0S2* in cancer cells [34,52–54]. Our discovery about the existence of strong correlations between *G0S2* levels and patients' survival in different cancers suggests the needing of a more extensive investigation about the impact of this gene on the metabolism and proliferation of transformed cells.

Repression of interferon-inducible genes is a well-known feature of the RAS-dependent transformation process [55–59]. Similarly, correlations between MYC and interferon have been known since a long time. Initially, it was discovered that IFNs can regulate MYC expression [60,61]. Subsequently, a suppressive activity of MYC on IFN signaling was reported [62]. This repressive influence was further proved by transcriptomic studies [63–67]. The recent discovery that the targeting of MYC through an epigenetic therapy provides an important advantage for an efficient immunotherapy could represent an important clinical perspective of all these studies [68,69].

Our results justify the inclusion of HDAC4 in the group that comprises two historically oncogenes for being similarly able to repress IFN genes during the transformation process. In the *in vitro* model of transformation, the presence of SV40 genes—which promote the expression of the interferon response [70]—could overestimate the repressive influence of the cellular oncogenes on this pathway. Nevertheless, alterations of the interferon genes were observed also *in vivo* and independently from the presence of the immune cells (Figure 8). Switching off the IFN and the inflammatory responses could provide a double advantage to the transformed cells, both in a cell autonomous and non-autonomous manner. It can favor the transformation process, by limiting tumor suppressive actions (such as apoptosis), and it can influence the tumor microenvironment and the immune response [71]. *In vivo* experiments on murine models of cancer have clarified that, in the initial tumorigenic steps, a strong inflammatory environment is promoted by the cancer cells themselves [72]. The release of chemokines, cytokines, and growth factors, as a consequence of the DNA damage accumulated during the early transformation process, promotes the infiltration and proliferation of immune cells that set up the first line of anti-cancer extracellular responses [73]. When full transformation is achieved, cancer cells drive a strong anti-inflammatory response, through intracellular clues—such as the activation of the IL10-Stat3 pathway and the release of extracellular molecules—which recall immune suppressor cells [74]. The balance of the anti-tumor response is then further compromised by the effect of the stroma and of the microenvironment, with the involvements of cancer associated fibroblasts (CAFs) and of tumor associated macrophages (TAMs).

It is curious that these two steps are exactly recapitulated during the *in vitro* transformation, with the arising of a type I IFN response during oncogene induced senescence or in the steps that come immediately before the full oncogenic conversion. After this step, the anti-inflammatory responses become predominant, as examined in this manuscript. The concept that some of these key features are triggered also in cancer cells cultured in petri dish suggests that the microenvironment acts by sculpting pathways that are already well established and poised in tumor cells in face of intracellular survival needs [75].

In conclusion, our analysis evidences that different oncogenes use common pathways to reach malignancy and to set up a barrier against the immune aggression.

## 4. Materials and Methods

### 4.1. Data Retrieval and Analysis

The transcriptional profiles of the three isogenic transformation models were obtained by re-analyzing the datasets GSE17941 [13], GSE72530 [14], and GSE120040 [15] deposited as raw files in GEO (Gene Expression Omnibus). The CEL files were processed with affy package in R [76]. Multiple callings coming from redundant probes were reduced to a single signal per gene by using Unigene ID centered CDFs (Chip Description Files) retrieved from the Molecular and Behavioral Neuroscience Institute Microarray Lab (URL: [http://brainarray.mbni.med.umich.edu/Brainarray/Database/CustomCDF/genomic\\_curated\\_CDF.asp](http://brainarray.mbni.med.umich.edu/Brainarray/Database/CustomCDF/genomic_curated_CDF.asp)) [77]. RMA algorithm was used for normalization [78]. In the three datasets selected, the hybridization was done on three different Affymetrix chips (platforms HG-U133A\_2, HuGene-1\_0-st-v1 and Clariom\_S). For the identification of differentially expressed genes (DEGs), the limma package [79] was used. The calling of significance was based on a 1.5-fold change/FDR < 0.05 criteria. In each dataset, the transformation model represented by pre-transformed BJ cells expressing RAS G12V (GSE17941) or MYC (GSE72530) or HDAC4 (GSE120040) was compared to the pre-transformation model which is represented by BJ fibroblasts expressing hTERT, LT, and ST SV40 genes.

### 4.2. Enrichment Analysis

The “HALLMARK” collection of 50 gene sets deposited in the Molecular Signatures Database (MSigDB) (subject) was interrogated with the three DEG lists generated (query). The MSigDB analysis

tool (Broad Institute (<http://www.broadinstitute.org/gsea/msigdb/index.jsp>) algorithm was used to score the overlap between queries and subjects. The identified hits were ranked by the enrichment score and the *p*-value (FDR < 0.05) [17,18].

#### 4.3. Generation of the Signatures of Transformation

The signature of the induced genes includes three genes that were significantly upregulated in the three selected models of transformation. The signature of the repressed genes includes 13 genes commonly downregulated in the three models of transformation. This signature was further sub-divided in sub-signatures A and B, where A includes six genes that do not belong to the HALLMARK gene sets “inflammation” and “interferon response” and B includes the other seven genes.

#### 4.4. Analysis of Survival

mRNA expression data coming from RNAseq studies and normalized by the expectation-maximization (RSEM) method and patients' clinical data about 32 cancer studies were retrieved from TCGA, using the R package *cgdsr* [80]. Hits corresponding to patients with incomplete expression or survival data were discarded. The final created dataset groups 11,424 samples belonging to individual censored patients, distributed as follows: Adrenocortical Carcinoma (ACC, *n* = 93), Bladder Urothelial Carcinoma (BLCA, *n* = 411), Breast Invasive Carcinoma (BRCA, *n* = 1108), Cervical Squamous Cell Carcinoma (CESC, *n* = 310), Cholangiocarcinoma (CHOL, *n* = 51), Colorectal Adenocarcinoma (COADREAD, *n* = 640), Diffuse Large B-Cell Lymphoma (DLBC, *n* = 48), Esophageal Carcinoma (ESCA, *n* = 186), Glioblastoma Multiforme (GBM, *n* = 615), Head and Neck Squamous Cell Carcinoma (HNSC, *n* = 530), Kidney Chromophobe (KICH, *n* = 66), Kidney Renal Clear Cell Carcinoma (KIRC, *n* = 538), Kidney Renal Papillary Cell Carcinoma (KIRP, *n* = 293), Acute Myeloid Leukemia (LAML, *n* = 200), Brain Lower Grade Glioma (LGG, *n* = 530), Liver Hepatocellular Carcinoma (LIHC, *n* = 442), Lung Adenocarcinoma (LUAD, *n* = 588), Lung Squamous Cell Carcinoma (LUSC, *n* = 511), Mesothelioma (MESO, *n* = 87), Ovarian Serous Cystadenocarcinoma (OV, *n* = 609), Pancreatic Adenocarcinoma (PAAD, *n* = 186), Pheochromocytoma and Paraganglioma (PCPG, *n* = 178), Prostate Adenocarcinoma (PRAD, *n* = 499), Sarcoma (SARC, *n* = 265), Skin Cutaneous Melanoma (SKCM, *n* = 480), Stomach Adenocarcinoma (STAD, *n* = 478), Testicular Germ Cell Cancer (TGCT, *n* = 156), Thyroid Carcinoma (THCA, *n* = 516), Thymoma (THYM, *n* = 124), Uterine Corpus Endometrial Carcinoma (UCEC, *n* = 549), Uterine Carcinosarcoma (UCS, *n* = 57), Uveal Melanoma (UVM, *n* = 80). For each sample/patient, the median expression values of the investigated signatures were calculated. According to these values, patients were divided in two groups characterized by high or low expression of the signatures. The Kaplan-Meier survival analysis was performed by using the survival package in R [81].

#### 4.5. Estimation of the Contribution/Perturbation of the Immune Infiltration to the Survival Analysis

The infiltration of immune cells in the tumor biopsies was evaluated by using MCP counter method [44]. Briefly, immunological signatures were retrieved by using the R package *MCPcounter*. The previously described dataset of 11,424 samples was interrogated with these signatures [44] and each sample was associated to the median value of expression of each signature. According to these values, patients were segregated in two groups and the Kaplan-Meier method was applied to calculate the survival rate.

To evaluate the contribution/disturbance of the inflammatory infiltrate to the prediction of survival based on the transformation signatures, patients were divided into four groups accordingly to the expression levels of genes belonging to the *MCPcounter* signatures and to the transformation signatures: High-high (high levels of both), high-low (high MCP/low transformation), low-low (low levels of both), or low-high (low MCP-high transformation).

The ‘*survfit*’ function and the ‘*survdif*’ function were used to generate the Kaplan-Meier curves and to calculate the significance.

**Supplementary Materials:** The following are available online at <http://www.mdpi.com/1422-0067/20/24/6283/s1>.

**Author Contributions:** E.D.G. Methodology, investigation, formal analysis, writing—original draft preparation; R.P. Methodology, investigation, data curation, formal analysis; H.P. Writing—original draft preparation, methodology, visualization; C.B. Conceptualization, writing—original draft preparation, writing—review and editing, visualization, supervision, project administration, funding acquisition.

**Funding:** This study was supported by COLONACT from LR 17/2014 regione Friuli Venezia-Giulia and European Union, European Regional Development Fund and Interreg V-A Italia-Austria 2014-2020 ITAT1054 (Program EPIC CUP G24I19001250007) to C.B.

**Conflicts of Interest:** The authors declare no conflict of interest.

## References

1. You, J.S.; Jones, P.A. Cancer Genetics and Epigenetics: Two Sides of the Same Coin? *Cancer Cell* **2012**, *22*, 9–20. [[CrossRef](#)] [[PubMed](#)]
2. Hanahan, D.; Weinberg, R.A. Hallmarks of Cancer: The Next Generation. *Cell* **2011**, *144*, 646–674. [[CrossRef](#)] [[PubMed](#)]
3. Thorsson, V.; Gibbs, D.L.; Brown, S.D.; Wolf, D.; Bortone, D.S.; Ou Yang, T.-H.; Porta-Pardo, E.; Gao, G.F.; Plaisier, C.L.; Eddy, J.A.; et al. The Immune Landscape of Cancer. *Immunity* **2018**, *48*, 812–830. [[CrossRef](#)] [[PubMed](#)]
4. Sompairac, N.; Nazarov, P.V.; Czerwinska, U.; Cantini, L.; Biton, A.; Molkenov, A.; Zhumadilov, Z.; Barillot, E.; Radvanyi, F.; Gorban, A.; et al. Independent Component Analysis for Unraveling the Complexity of Cancer Omics Datasets. *Int. J. Mol. Sci.* **2019**, *20*, 4414. [[CrossRef](#)] [[PubMed](#)]
5. Laubenbacher, R.; Hower, V.; Jarrah, A.; Torti, S.V.; Shulaev, V.; Mendes, P.; Torti, F.M.; Akman, S. A systems biology view of cancer. *Biochim. Biophys. Acta Rev. Cancer* **2009**, *1796*, 129–139. [[CrossRef](#)]
6. Kuipers, J.; Jahn, K.; Beerenwinkel, N. Biochimica et Biophysica Acta Advances in understanding tumour evolution through single-cell sequencing. *BBA Rev. Cancer* **2017**, *1867*, 127–138.
7. Hahn, W.C.; Counter, C.M.; Lundberg, A.S.; Beijersbergen, R.L.; Brooks, M.W.; Weinberg, R.A. Creation of human tumour cells with defined genetic elements. *Nature* **1999**, *400*, 464–468. [[CrossRef](#)]
8. Knudson, A.G. Two genetic hits (more or less) to cancer. *Nat. Rev. Cancer* **2001**, *1*, 637–641. [[CrossRef](#)]
9. Rangarajan, A.; Weinberg, R.A. Comparative biology of mouse versus human cells: Modelling human cancer in mice. *Nat. Rev. Cancer* **2003**, *3*, 952–959. [[CrossRef](#)]
10. Boehm, J.S.; Hession, M.T.; Bulmer, S.E.; Hahn, W.C. Transformation of Human and Murine Fibroblasts without Viral Oncoproteins. *Mol. Cell. Biol.* **2005**, *25*, 6464–6474. [[CrossRef](#)]
11. Drost, J.; van Boxtel, R.; Blokzijl, F.; Mizutani, T.; Sasaki, N.; Sasselli, V.; de Ligt, J.; Behjati, S.; Grolleman, J.E.; van Wezel, T.; et al. Use of CRISPR-modified human stem cell organoids to study the origin of mutational signatures in cancer. *Science* **2017**, *358*, 234–238. [[CrossRef](#)] [[PubMed](#)]
12. Hahn, W.C.; Weinberg, R.A. Rules for Making Human Tumor Cells. *N. Engl. J. Med.* **2002**, *347*, 1593–1603. [[CrossRef](#)] [[PubMed](#)]
13. Hirsch, H.A.; Iliopoulos, D.; Joshi, A.; Zhang, Y.; Jaeger, S.A.; Bulyk, M.; Tschlis, P.N.; Shirley Liu, X.; Struhl, K. A Transcriptional Signature and Common Gene Networks Link Cancer with Lipid Metabolism and Diverse Human Diseases. *Cancer Cell* **2010**, *17*, 348–361. [[CrossRef](#)] [[PubMed](#)]
14. Malysheva, V.; Mendoza-parra, M.A.; Saleem, M.M.; Gronemeyer, H. Reconstruction of gene regulatory networks reveals chromatin remodelers and key transcription factors in tumorigenesis. *Genome Med.* **2016**, *8*, 57. [[CrossRef](#)] [[PubMed](#)]
15. Paluvai, H.; Di Giorgio, E.; Brancolini, C. Unscheduled HDAC4 repressive activity in human fibroblasts triggers TP53-dependent senescence and favors cell transformation. *Mol. Oncol.* **2018**, *12*, 2165–2181. [[CrossRef](#)] [[PubMed](#)]
16. Makridakis, N.M.; Caldas Ferraz, L.F.; Reichardt, J.K.V. Genomic analysis of cancer tissue reveals that somatic mutations commonly occur in a specific motif. *Hum. Mutat.* **2009**, *30*, 39–48. [[CrossRef](#)] [[PubMed](#)]
17. Daly, M.J.; Patterson, N.; Mesirov, J.P.; Golub, T.R.; Tamayo, P.; Spiegelman, B. PGC-1 $\alpha$ -responsive genes involved in oxidative phosphorylation are coordinately downregulated in human diabetes. *Nat. Genet.* **2003**, *34*, 267–273.

18. Subramanian, A.; Tamayo, P.; Mootha, V.K.; Mukherjee, S.; Ebert, B.L.; Gillette, M.A.; Paulovich, A.; Pomeroy, S.L.; Golub, T.R.; Lander, E.S.; et al. Gene set enrichment analysis: A knowledge-based approach for interpreting genome-wide expression profiles. *Proc. Natl. Acad. Sci. USA* **2005**, *102*, 15545–15550. [[CrossRef](#)]
19. Peruzzo, P.; Comelli, M.; Di Giorgio, E.; Franforte, E.; Mavelli, I.; Brancolini, C. Transformation by different oncogenes relies on specific metabolic adaptations. *Cell Cycle* **2016**, *15*, 2656–2668. [[CrossRef](#)]
20. Perucho, M.; Esteban, M. Inhibitory effect of interferon on the genetic and oncogenic transformation by viral and cellular genes. *J. Virol.* **1985**, *54*, 229–232.
21. Samid, D.; Flessate, D.M.; Friedman, R.M. Interferon-induced revertants of ras-transformed cells: Resistance to transformation by specific oncogenes and retransformation by 5-azacytidine. *Mol. Cell. Biol.* **1987**, *7*, 2196–2200. [[CrossRef](#)] [[PubMed](#)]
22. Kim, T.Y.; Lee, K.-H.; Chang, S.; Chung, C.; Lee, H.-W.; Yim, J.; Kim, T.K. Oncogenic Potential of a Dominant Negative Mutant of Interferon Regulatory Factor 3. *J. Biol. Chem.* **2003**, *278*, 15272–15278. [[CrossRef](#)] [[PubMed](#)]
23. Critchley-Thorne, R.J.; Yan, N.; Nacu, S.; Weber, J.; Holmes, S.P.; Lee, P.P. Down-Regulation of the Interferon Signaling Pathway in T Lymphocytes from Patients with Metastatic Melanoma. *PLoS Med.* **2007**, *4*, e176. [[CrossRef](#)] [[PubMed](#)]
24. Katlinskaya, Y.V.; Katlinski, K.V.; Yu, Q.; Ortiz, A.; Beiting, D.P.; Brice, A.; Davar, D.; Sanders, C.; Kirkwood, J.M.; Rui, H.; et al. Suppression of Type I Interferon Signaling Overcomes Oncogene-Induced Senescence and Mediates Melanoma Development and Progression. *Cell Rep.* **2016**, *15*, 171–180. [[CrossRef](#)] [[PubMed](#)]
25. Manry, J.; Laval, G.; Patin, E.; Fornarino, S.; Itan, Y.; Fumagalli, M.; Sironi, M.; Tichit, M.; Bouchier, C.; Casanova, J.-L.; et al. Evolutionary genetic dissection of human interferons. *J. Exp. Med.* **2011**, *208*, 2747–2759. [[CrossRef](#)] [[PubMed](#)]
26. Yajnik, V.; Paulding, C.; Sordella, R.; McClatchey, A.I.; Saito, M.; Wahrer, D.C.R.; Reynolds, P.; Bell, D.W.; Lake, R.; van den Heuvel, S.; et al. DOCK4, a GTPase activator, is disrupted during tumorigenesis. *Cell* **2003**, *112*, 673–684. [[CrossRef](#)]
27. Kawada, K.; Upadhyay, G.; Ferandon, S.; Janarthanan, S.; Hall, M.; Vilardaga, J.-P.; Yajnik, V. Cell Migration Is Regulated by Platelet-Derived Growth Factor Receptor Endocytosis. *Mol. Cell. Biol.* **2009**, *29*, 4508–4518. [[CrossRef](#)]
28. Yu, J.; Tai, Y.; Jin, Y.; Hammell, M.C.; Wilkinson, J.E.; Roe, J.; Vakoc, C.R.; Van Aelst, L. TGF- $\beta$ /Smad signaling through DOCK4 facilitates lung adenocarcinoma metastasis. *Genes Dev.* **2015**, *29*, 250–261. [[CrossRef](#)]
29. Westbrook, J.A.; Wood, S.L.; Cairns, D.A.; McMahon, K.; Gahlaut, R.; Thygesen, H.; Shires, M.; Roberts, S.; Marshall, H.; Oliva, M.R.; et al. Identification and validation of DOCK4 as a potential biomarker for risk of bone metastasis development in patients with early breast cancer. *J. Pathol.* **2019**, *247*, 381–391. [[CrossRef](#)]
30. Debruyne, D.N.; Turchi, L.; Fareh, M.; Almairac, F.; Virolle, V. DOCK4 promotes loss of proliferation in glioblastoma progenitor cells through nuclear beta-catenin accumulation and subsequent miR-302-367 cluster expression. *Nat. Publ. Gr.* **2017**, *37*, 241–254. [[CrossRef](#)]
31. Sundaravel, S.; Kuo, W.-L.; Jeong, J.J.; Choudhary, G.S.; Gordon-Mitchell, S.; Liu, H.; Bhagat, T.D.; McGraw, K.L.; Gurbuxani, S.; List, A.F.; et al. Loss of Function of DOCK4 in Myelodysplastic Syndromes Stem Cells is Restored by Inhibitors of DOCK4 Signaling Networks. *Clin. Cancer Res.* **2019**, *25*, 5638–5649. [[CrossRef](#)] [[PubMed](#)]
32. Coleman, R.A.; Hesselink, M.K. Recent advances in lipid droplet biology. *Biochim. Biophys. Acta Mol. Cell Biol. Lipids* **2017**, *1862*, 1129–1130. [[CrossRef](#)] [[PubMed](#)]
33. Zhu, M.; Liu, C.; Cheng, C. REACTIN: Regulatory activity inference of transcription factors underlying human diseases with application to breast cancer. *BMC Genom.* **2013**, *14*, 504. [[CrossRef](#)] [[PubMed](#)]
34. Yim, C.Y.; Sekula, D.J.; Hever-Jardine, M.P.; Liu, X.; Warzecha, J.M.; Tam, J.; Freemantle, S.J.; Dmitrovsky, E.; Spinella, M.J. G0S2 Suppresses Oncogenic Transformation by Repressing a MYC-Regulated Transcriptional Program. *Cancer Res.* **2016**, *76*, 1204–1213. [[CrossRef](#)] [[PubMed](#)]
35. Mohan, D.R.; Lerario, A.M.; Else, T.; Mukherjee, B.; Almeida, M.Q.; Vinco, M.; Rege, J.; Mariani, B.M.P.; Zerbini, M.C.N.; Mendonca, B.B.; et al. Targeted Assessment of G0S2 Methylation Identifies a Rapidly Recurrent, Routinely Fatal Molecular Subtype of Adrenocortical Carcinoma. *Clin. Cancer Res.* **2019**, *25*, 3276–3288. [[CrossRef](#)] [[PubMed](#)]

36. Meindl, A.; Carvalho, M.R.; Herrmann, K.; Lorenz, B.; Achatz, H.; Lorenz, B.; Apfelstedt-Sylla, E.; Wittwer, B.; Ross, M.; Meitinger, T. A gene (SRPX) encoding a sushi-repeat-containing protein is deleted in patients with X-linked retinitis pigmentosa. *Hum. Mol. Genet.* **1995**, *4*, 2339–2346. [[CrossRef](#)]
37. Jing, P.; Kazuyoshi, N.; Masuo, Y.; Hirokazu, I.; Qin, L.; Kiyomasa, O.; Naohisa, Y.; Akira, H. Isolation of a novel gene down-regulated by v-src. *FEBS Lett.* **1996**, *383*, 21–25. [[CrossRef](#)]
38. Yamashita, A.; Hakura, A.; Inoue, H. Suppression of anchorage-independent growth of human cancer cell lines by the drs gene. *Oncogene* **1999**, *18*, 4777–4787. [[CrossRef](#)]
39. Shimakage, M.; Kawahara, K.; Kikkawa, N.; Sasagawa, T.; Yutsudo, M.; Inoue, H. Down-regulation of drs mRNA in human colon adenocarcinomas. *Int. J. Cancer* **2000**, *87*, 5–11. [[CrossRef](#)]
40. Kim, C.J.; Shimakage, M.; Kushima, R.; Mukaiho, K.; Shinka, T.; Okada, Y.; Inoue, H. Down-regulation of drs mRNA in human prostate carcinomas. *Hum. Pathol.* **2003**, *34*, 654–657. [[CrossRef](#)]
41. Shimakage, M.; Inoue, N.; Ohshima, K.; Kawahara, K.; Yamamoto, N.; Oka, T.; Tambe, Y.; Yasui, K.; Matsumoto, K.; Yutsudo, M.; et al. Downregulation of drs mRNA expression is associated with the progression of adult T-cell leukemia/lymphoma. *Int. J. Oncol.* **2007**, *30*, 1343–1348. [[CrossRef](#)] [[PubMed](#)]
42. Else, T.; Kim, A.C.; Sabolch, A.; Raymond, V.M.; Kandathil, A.; Caoili, E.M.; Jolly, S.; Miller, B.S.; Giordano, T.J.; Hammer, G.D. Adrenocortical Carcinoma. *Endocr. Rev.* **2014**, *35*, 282–326. [[CrossRef](#)] [[PubMed](#)]
43. Finotello, F.; Trajanoski, Z. Quantifying tumor-infiltrating immune cells from transcriptomics data. *Cancer Immunol. Immunother.* **2018**, *67*, 1031–1040. [[CrossRef](#)] [[PubMed](#)]
44. Becht, E.; Giraldo, N.A.; Lacroix, L.; Buttard, B.; Elarouci, N.; Petitprez, F.; Selves, J.; Laurent-puig, P.; Sautès-fridman, C.; Fridman, W.H.; et al. Estimating the population abundance of tissue-infiltrating immune and stromal cell populations using gene expression. *Genome Biol.* **2016**, *17*, 218. [[CrossRef](#)] [[PubMed](#)]
45. Qian, Z.; Li, Y.; Fan, X.; Zhang, C.; Wang, Y.; Jiang, T.; Liu, X. Molecular and clinical characterization of IDH associated immune signature in lower-grade gliomas. *Oncoimmunology* **2018**, *7*, e1434466. [[CrossRef](#)] [[PubMed](#)]
46. Ischenko, I.; Zhi, J.; Moll, U.M.; Nemajerova, A.; Petrenko, O. Direct reprogramming by oncogenic Ras and Myc. *Proc. Natl. Acad. Sci. USA* **2013**, *110*, 3937–3942. [[CrossRef](#)]
47. Di Giorgio, E.; Clocchiatti, A.; Piccinin, S.; Sgorbissa, A.; Viviani, G.; Peruzzo, P.; Romeo, S.; Rossi, S.; Dei Tos, A.P.; Maestro, R.; et al. MEF2 is a converging hub for histone deacetylase 4 and phosphatidylinositol 3-kinase/Akt-induced transformation. *Mol. Cell. Biol.* **2013**, *33*, 4473–4491. [[CrossRef](#)]
48. Di Giorgio, E.; Franforte, E.; Cefalù, S.; Rossi, S.; Dei Tos, A.P.; Brenca, M.; Polano, M.; Maestro, R.; Paluvai, H.; Picco, R.; et al. The co-existence of transcriptional activator and transcriptional repressor MEF2 complexes influences tumor aggressiveness. *PLoS Genet.* **2017**, *13*, e1006752. [[CrossRef](#)]
49. Di Giorgio, E.; Gagliostro, E.; Clocchiatti, A.; Brancolini, C. The Control Operated by the Cell Cycle Machinery on MEF2 Stability Contributes to the Downregulation of CDKN1A and Entry into S Phase. *Mol. Cell. Biol.* **2015**, *35*, 1633–1647. [[CrossRef](#)]
50. Di Giorgio, E.; Brancolini, C. Regulation of class IIa HDAC activities: It is not only matter of subcellular localization. *Epigenomics* **2016**, *8*, 251–269. [[CrossRef](#)]
51. Heckmann, B.L.; Zhang, X.; Xie, X.; Saarinen, A.; Lu, X.; Yang, X.; Liu, J. Defective Adipose Lipolysis and Altered Global Energy Metabolism in Mice with Adipose Overexpression of the Lipolytic Inhibitor G 0/G 1 Switch Gene 2 (G0S2). *J. Biol. Chem.* **2014**, *289*, 1905–1916. [[CrossRef](#)] [[PubMed](#)]
52. Yim, C.Y.; Bikorimana, E.; Khan, E.; Warzecha, J.M.; Shin, L.; Rodriguez, J.; Dmitrovsky, E.; Freemantle, S.J.; Spinella, M.J. G0S2 represses PI3K/mTOR signaling and increases sensitivity to PI3K/mTOR pathway inhibitors in breast cancer. *Cell Cycle* **2017**, *16*, 2146–2155. [[CrossRef](#)] [[PubMed](#)]
53. Fukunaga, T.; Fujita, Y.; Kishima, H.; Yamashita, T. Methylation dependent down-regulation of G0S2 leads to suppression of invasion and improved prognosis of IDH1-mutant glioma. *PLoS ONE* **2018**, *13*, e0206552. [[CrossRef](#)] [[PubMed](#)]
54. Cho, E.; Kwon, Y.-J.; Ye, D.-J.; Baek, H.-S.; Kwon, T.-U.; Choi, H.-K.; Chun, Y.-J. G0/G1 Switch 2 Induces Cell Survival and Metastasis through Integrin-Mediated Signal Transduction in Human Invasive Breast Cancer Cells. *Biomol. Ther.* **2019**, *12*, 1–12. [[CrossRef](#)]
55. Balachandran, S.; Porosnicu, M.; Barber, G.N. Oncolytic activity of vesicular stomatitis virus is effective against tumors exhibiting aberrant p53, Ras, or myc function and involves the induction of apoptosis. *J. Virol.* **2001**, *75*, 3474–3479. [[CrossRef](#)]

56. Klampfer, L.; Huang, J.; Corner, G.; Mariadason, J.; Arango, D.; Sasazuki, T.; Shirasawa, S.; Augenlicht, L. Oncogenic Ki-Ras Inhibits the Expression of Interferon-responsive Genes through Inhibition of STAT1 and STAT2 Expression. *J. Biol. Chem.* **2003**, *278*, 46278–46287. [[CrossRef](#)]
57. Battcock, S.M.; Collier, T.W.; Zu, D.; Hirasawa, K. Negative regulation of the alpha interferon-induced antiviral response by the Ras/Raf/MEK pathway. *J. Virol.* **2006**, *80*, 4422–4430. [[CrossRef](#)]
58. Komatsu, Y.; Christian, S.L.; Ho, N.; Pongnopparat, T.; Licursi, M.; Hirasawa, K. Oncogenic Ras inhibits IRF1 to promote viral oncolysis. *Oncogene* **2015**, *34*, 3985–3993. [[CrossRef](#)]
59. Komatsu, Y.; Hirasawa, K.; Christian, S.L. Global gene analysis identifying genes commonly regulated by the Ras/Raf/MEK and type I IFN pathways. *Genom. Data* **2015**, *4*, 84–87. [[CrossRef](#)]
60. Jonak, G.J.; Knight, E. Selective reduction of c-myc mRNA in Daudi cells by human beta interferon. *Proc. Natl. Acad. Sci. USA* **1984**, *81*, 1747–1750. [[CrossRef](#)]
61. Dani, C.; Mechti, N.; Piechaczyk, M.; Lebleu, B.; Jeanteur, P.; Blanchard, J.M. Increased rate of degradation of c-myc mRNA in interferon-treated Daudi cells. *Proc. Natl. Acad. Sci. USA* **1985**, *82*, 4896–4899. [[CrossRef](#)] [[PubMed](#)]
62. Schlee, M.; Hölzel, M.; Bernard, S.; Mailhammer, R.; Schuhmacher, M.; Reschke, J.; Eick, D.; Marinkovic, D.; Wirth, T.; Rosenwald, A.; et al. c-MYC activation impairs the NF- $\kappa$ B and the interferon response: Implications for the pathogenesis of Burkitt's lymphoma. *Int. J. Cancer* **2007**, *120*, 1387–1395. [[CrossRef](#)] [[PubMed](#)]
63. Schlee, M.; Schuhmacher, M.; Hölzel, M.; Laux, G.; Bornkamm, G.W. c-MYC Impairs Immunogenicity of Human B Cells. *Adv. Cancer Res.* **2007**, *97*, 167–188. [[PubMed](#)]
64. Polioudakis, D.; Bhinge, A.A.; Killion, P.J.; Lee, B.; Abell, N.S.; Iyer, V.R. A Myc-microRNA network promotes exit from quiescence by suppressing the interferon response and cell-cycle arrest genes. *Nucleic Acids Res.* **2013**, *41*, 2239–2254. [[CrossRef](#)]
65. Wee, Z.N.; Li, Z.; Lee, P.L.; Lee, S.T.; Lim, Y.P.; Yu, Q. EZH2-Mediated Inactivation of IFN- $\gamma$ -JAK-STAT1 Signaling Is an Effective Therapeutic Target in MYC-Driven Prostate Cancer. *Cell Rep.* **2014**, *8*, 204–216. [[CrossRef](#)]
66. Kim, T.W.; Hong, S.; Lin, Y.; Murat, E.; Joo, H.; Kim, T.; Pascual, V.; Liu, Y. Transcriptional Repression of IFN Regulatory Factor 7 by MYC Is Critical for Type I IFN Production in Human Plasmacytoid Dendritic Cells. *J. Immunol.* **2016**, *197*, 3348–3359. [[CrossRef](#)]
67. Layer, J.P.; Kronmüller, M.T.; Quast, T.; Boorn-Konijnenberg, D.V.D.; Effern, M.; Hinze, D.; Althoff, K.; Schramm, A.; Westermann, F.; Peifer, M.; et al. Amplification of N-Myc is associated with a T-cell-poor microenvironment in metastatic neuroblastoma restraining interferon pathway activity and chemokine expression. *Oncoimmunology* **2017**, *6*, e1320626. [[CrossRef](#)]
68. Zou, J.; Zhuang, M.; Yu, X.; Li, N.; Mao, R.; Wang, Z.; Wang, J.; Wang, X.; Zhou, H.; Zhang, L.; et al. MYC inhibition increases PD-L1 expression induced by IFN- $\gamma$  in hepatocellular carcinoma cells. *Mol. Immunol.* **2018**, *101*, 203–209. [[CrossRef](#)]
69. Topper, M.J.; Vaz, M.; Chiappinelli, K.B.; DeStefano Shields, C.E.; Niknafs, N.; Yen, R.C.; Wenzel, A.; Hicks, J.; Ballew, M.; Stone, M.; et al. Epigenetic Therapy Ties MYC Depletion to Reversing Immune Evasion and Treating Lung Cancer. *Cell* **2017**, *171*, 1284–1300. [[CrossRef](#)]
70. Rathi, A.V.; Cantalupo, P.G.; Sarkar, S.N.; Pipas, J.M. Induction of interferon-stimulated genes by Simian virus 40 T antigens. *Virology* **2010**, *406*, 202–211. [[CrossRef](#)]
71. Nozawa, H.; Oda, E.; Nakao, K.; Ishihara, M.; Ueda, S.; Yokochi, T.; Ogasawara, K.; Nakatsuru, Y.; Shimizu, S.; Ohira, Y.; et al. Loss of transcription factor IRF-1 affects tumor susceptibility in mice carrying the Ha-ras transgene or nullizygosity for p53. *Genes Dev.* **1999**, *13*, 1240–1245. [[CrossRef](#)] [[PubMed](#)]
72. Sica, A.; Allavena, P.; Mantovani, A. Cancer related inflammation: The macrophage connection. *Cancer Lett.* **2008**, *267*, 204–215. [[CrossRef](#)] [[PubMed](#)]
73. Nagarsheth, N.; Wicha, M.S.; Zou, W. Chemokines in the cancer microenvironment and their relevance in cancer immunotherapy. *Nat. Rev. Immunol.* **2017**, *17*, 559–572. [[CrossRef](#)] [[PubMed](#)]
74. Chow, M.T.; Luster, A.D. Chemokines in Cancer. *Cancer Immunol. Res.* **2014**, *2*, 1125–1131. [[CrossRef](#)] [[PubMed](#)]
75. Spranger, S.; Gajewski, T.F. Impact of oncogenic pathways on evasion of antitumour immune responses. *Nat. Rev. Cancer* **2018**, *18*, 139–147. [[CrossRef](#)] [[PubMed](#)]

76. Gauthier, L.R.; Charrin, B.C.; Borrell-Pagès, M.; Dompierre, J.P.; Rangone, H.; Cordelières, F.P.; De Mey, J.; MacDonald, M.E.; Leßmann, V.; Humbert, S.; et al. Huntingtin Controls Neurotrophic Support and Survival of Neurons by Enhancing BDNF Vesicular Transport along Microtubules. *Cell* **2004**, *118*, 127–138. [[CrossRef](#)]
77. Dai, M. Evolving gene/transcript definitions significantly alter the interpretation of GeneChip data. *Nucleic Acids Res.* **2005**, *33*, e175. [[CrossRef](#)]
78. Irizarry, R.A. Exploration, normalization, and summaries of high density oligonucleotide array probe level data. *Biostatistics* **2003**, *4*, 249–264. [[CrossRef](#)]
79. Ritchie, M.E.; Phipson, B.; Wu, D.; Hu, Y.; Law, C.W.; Shi, W.; Smyth, G.K. limma powers differential expression analyses for RNA-sequencing and microarray studies. *Nucleic Acids Res.* **2015**, *43*, e47. [[CrossRef](#)]
80. Jacobsen, A. Cgdsr: R-Based API for Accessing the MSKCC Cancer Genomics Data Server (CGDS). Version 1.3.0. Available online: <http://CRAN.R-project.org/package=cgdsr> (accessed on 30 October 2019).
81. Therneau, T. A package for survival analysis. In S. Version 2.44-1.1. Available online: <https://CRAN.R-project.org/package=survival> (accessed on 30 October 2019).



© 2019 by the authors. Licensee MDPI, Basel, Switzerland. This article is an open access article distributed under the terms and conditions of the Creative Commons Attribution (CC BY) license (<http://creativecommons.org/licenses/by/4.0/>).

# Different class IIa HDACs repressive complexes regulate specific epigenetic responses related to cell survival in leiomyosarcoma cells

Eros Di Giorgio , Emiliano Dalla, Elisa Franforte, Harikrishnareddy Paluvai, Martina Minisini, Matteo Trevisanut, Raffaella Picco and Claudio Brancolini\*

Department of Medicine, Università degli Studi di Udine. P.le Kolbe 4, 33100 Udine, Italy

Received June 13, 2019; Revised October 28, 2019; Editorial Decision November 12, 2019; Accepted November 13, 2019

## ABSTRACT

Transcriptional networks supervising class IIa HDAC expression are poorly defined. Here we demonstrate that MEF2D is the key factor controlling HDAC9 transcription. This control, which is part of a negative feed-back loop during muscle differentiation, is hijacked in cancer. In leiomyosarcomas the MEF2D/HDAC9 vicious circuit sustains proliferation and cell survival, through the repression of the death receptor FAS. Comprehensive genome-wide studies demonstrate that HDAC4 and HDAC9 control different genetic programs and show both specific and common genomic binding sites. Although the number of MEF2-target genes commonly regulated is similar, only HDAC4 represses many additional genes that are not MEF2D targets. As expected, HDAC4<sup>-/-</sup> and HDAC9<sup>-/-</sup> cells increase H3K27ac levels around the TSS of the respective repressed genes. However, these genes rarely show binding of the HDACs at their promoters. Frequently HDAC4 and HDAC9 bind intergenic regions. We demonstrate that these regions, recognized by MEF2D/HDAC4/HDAC9 repressive complexes, show the features of active enhancers. In these regions HDAC4 and HDAC9 can differentially influence H3K27 acetylation. Our studies describe new layers of class IIa HDACs regulation, including a dominant positional effect, and can contribute to explain the pleiotropic actions of MEF2 TFs.

## INTRODUCTION

Class IIa HDACs are important regulators of different adaptive and differentiative responses. During embryonic development, these deacetylases influence specific differentiation pathways and tissue morphogenesis (1–3). In vertebrates HDAC4, HDAC5, HDAC7 and HDAC9 consti-

tute the class IIa subfamily. Because of the Tyr/His substitution in the catalytic site, they exhibit a negligible lysine-deacetylase activity (2,3). However, the deacetylase domain, through the recruitment of the NCOR1/NCOR2/HDAC3 complex, can influence histones modifications, including acetylation (4–6). The repressive influence of class IIa HDACs can also be exploited independently from HDAC3 recruitment. In fact MITR, a HDAC9 splicing variant, can still repress transcription in the absence of the deacetylase domain (7). The amino-terminus of class IIa HDACs is dedicated to the binding of different transcription factors (TFs), among which MEF2 family members are the foremost characterized (3). Overall, class IIa HDACs genomic activities require their assembly into multiprotein complexes where they operate as platforms coordinating the activity of TFs, as well as of other epigenetic regulators (1–3,8).

These deacetylases are subjected to multiple levels of regulation. The phosphorylation-dependent control of the nuclear/cytoplasmic shuttling has been the most commonly investigated (3,9). Curiously, although the lineage-dependent expression is a main feature of class IIa, signalling pathways and mechanisms controlling their transcription are largely unknown (3). An exception is the muscle tissue. Here HDAC9 transcription is under the direct control of MEF2D. In this manner, the MEF2D-HDAC9 axis sustains a negative-feedback loop in the transcriptional circuit of muscle differentiation to buffer MEF2D activities (10). Importantly, in specific cancer types, this circuit seems to be misused. In pre-B acute lymphoblastic leukaemia MEF2D oncogenic fusions dramatically up-regulate HDAC9 expression (11,12). Abrogation of the MEF2D-HDAC9 negative circuit was also observed in highly aggressive malignant rhabdoid tumor, non-small cell lung cancer, oral squamous cell carcinoma and leiomyosarcoma (13). Since the pro-oncogenic roles of class IIa HDAC have been proved by different studies, understanding the reasons and the importance of such abrogation is of primary interest in cancer research (14–18).

\*To whom correspondence should be addressed. Tel: +39 0432 494382; Fax: +39 0432 494301; Email: claudio.brancolini@uniud.it

In this manuscript, we have investigated the MEF2-HDAC axis in cellular models of leiomyosarcoma (LMS). LMS are rare highly malignant tumors of mesenchymal origin, with cells presenting features of the smooth muscle lineage (19). We have demonstrated that the MEF2D-HDAC9 axis plays a key role in the maintenance of the transformed phenotype and deciphered the genomic, epigenomic, and transcriptomic landscapes under the control of class IIa HDACs.

## MATERIALS AND METHODS

### Cell cultures and cytofluorimetric analysis

Leiomyosarcomas cells (LMS), SK-UT-1, SK-LMS-1, MES-SA and DMR were grown as previously described (15). HEK-293T and AMPHO cells were grown in Dulbecco's modified Eagle's medium (DMEM) supplemented with 10% FBS. For PI staining, cells were collected and resuspended in 0.1 ml of 10  $\mu$ g/ml propidium iodide (PI) (Sigma-Aldrich), in PBS and incubated for 10 min at RT. After washes, cells were fixed with 1% formaldehyde (Sigma-Aldrich) and treated with 10  $\mu$ g/ml RNase A. Fluorescence was determined with a FACScan™ (Beckman Dickinson).

### CRISPR/Cas9 technology

The generation of HDAC4 and HDAC9 null SK-UT-1 cells was previously described (6). SK-UT-1 cells mutated in the MEF2-binding sites within the HDAC9 promoter were obtained after co-transfection of the pSpCas9-2A Puro plasmid expressing the two sgRNA (GGTCGGCCTGAGCCAAAAT, CTGGACAGCTGGGTTTGCTG) and the ssODN repair templates (20) (AAAGATAGAGGCTGGACAGCTGGGTTTGCTCGCGTAGGATCCAATGCATTAATGCAGGCT, AATCACTCGGCCATGCTTGACCTAGGATCCGCTCAGGCCGACCATTGTTCTATTTCTGTG) (ratio 10:1). After selections, clones were screened by PCR and immunoblot. Sanger sequencing was applied for the final validation.

### Immunofluorescence, random cell motility and immunoblotting

Cells were fixed with 3% paraformaldehyde and permeabilized with 0.1% Triton X-100. The secondary antibodies were Alexa Fluor 488-, 546- or 633-conjugated anti-mouse and anti-rabbit secondary antibodies (Molecular Probes). Actin was labelled with phalloidin-AF546 (Molecular Probes). Cells were imaged with a Leica confocal scanner microscopy SP2. Nuclei were stained with Hoechst 33258 (Sigma-Aldrich). For S phase analysis, cells were grown for 3 h with 50  $\mu$ M bromodeoxyuridine (BrdU). After fixation, coverslips were treated with HCl and processed for immunofluorescence. For random cell motility measurements, cells were seeded in six-well plates coated with fibronectin and subjected to time-lapse analysis. Images were recorded every 15 min for 6 h with a Leica AF6000 station. Time-lapse experiments were analyzed with the Metamorph software (Molecular Devices).

Cell lysates after SDS-PAGE and immunoblotting on nitrocellulose (Whatman) were incubated with primary antibodies. HRP-conjugated secondary antibodies were obtained from Sigma-Aldrich and blots were developed with Super Signal West Dura (Pierce), as previously described (20).

### Antibodies and chemicals

The primary antibodies used were anti: MEF2D (BD Bioscience); MEF2A (C-21), Caspase-3 (E-8) and FAS (M-20) (Santa Cruz Biotechnology); RAN and Caspase 8 (D35G2) (Cell Signaling Technology); Actin, BrdU, and FLAG/M2 (Sigma-Aldrich); GFP, HDAC4 and Caspase-9 (15); HDAC5 (21); H3K27ac (ab4729) and H3K27me3 (ab6002) (Abcam); H3K4me3 (GTX128954, GeneTex). The anti-HDAC9 antibody was produced in rabbit by injecting a His-tagged fragment of HDAC9 (aa 275–600) expressed in *Escherichia coli*. The antiserum was affinity purified against the same fragment GST-tagged of HDAC9.

The following chemicals were used: Doxorubicin and Metformin (Alexis); Lapatinib and Imatinib (LC Laboratories); MKK2206 and SAHA (Cayman Chemicals); BrdU (Sigma-Aldrich); FasL (Peprotech).

### Plasmid construction, transfection, retroviral and lentiviral infection, silencing

pLENTI-CRISPR/V2 (Plasmid #52961) and pSpCas9(BB)-2A-GFP(PX458) (Plasmid #48138) were from Addgene. pWZL-HYGRO FLIPs FLAG was obtained by a restriction-based approach from pcDNA3-FLIPs. pWZL-HYGRO FLAG plasmid was used as acceptor plasmid and as control for infection. The knock-down of MEF2D and MEF2A was achieved by using pLKO.1 shRNAs (TRCN0000015897, TRCN00000274054, TRCN00000432718, TRCN000005133), as already described (6). For the Luc assay on HDAC9 promoter the 15897 and 432718 shRNAs were selected and used in consideration of their higher efficiency (6). HDAC9 promoter (6) (bp –1160/+23) activity was measured in transfected 293-T or SK-UT-1 cells according to the manufacturer (Dual-Glo Luciferase Assay System, Promega) and expressed as a ratio to the luciferase activity of pRenilla. Transfections, viral infections and siRNA delivery were done as previously described (20,21). The following Invitrogen Stealth RNAi siRNAs (148 pmol) were used:

HDAC4 (CCACCGGAAUCUGAACCACUGCAUU),  
HDAC9 1 (GAACAAACUGCUUUCGAAAUCUAU  
U),  
HDAC9 2 (UGGGCCAACUGGAAGUGUUACUGA  
A).

### Caspase and Resazurin reduction assays

The caspase activity was evaluated using the Apo-ONE caspase-3/7 homogeneous assay (Promega). Cells grown in 96-well plates were treated with the different insults and tested for caspase activity as recommended by the vendor. Resazurin assay was done as already described (22). Briefly,

cells were incubated for 150 min. at 37°C with resazurin solution (0.15 mg/ml) (Sigma-Aldrich). The product of reduction was quantified by using the PerkinElmer EnSpire 2300 Multilabel Reader.

### ChIP, library construction, ChIP-seq and NGS data analysis

ChIP was performed as previously described (18). Chromatin was immunoprecipitated with 2 µg of anti-H3K27ac, 2.5 µg of anti-MEF2D, 4 µg of anti-HDAC4 and anti-HDAC9 antibodies or control IgG. Three independent experiments were pulled and 5 ng of total DNA were used to prepare ChIP-seq libraries, according to TruSeq ChIP Sample Preparation guide (Illumina). Libraries were sequenced on the Illumina HiSeq 2000 sequencer. The quality of sequencing reads was evaluated using the ShortRead R/Bioconductor package (23). Sequencing reads from ChIP-seq experiments were aligned to the NCBI *GRCh38* human reference with Bowtie 2 (24). Peak calling was performed against input sequences using MACS2 (25). Gene annotation, Venn diagrams and bar plots representing the peak localization in genomic elements/distance from TSS were obtained using the ChIPseeker R/Bioconductor package (26). Peak heatmaps and genomic loci visualization were generated using the gplots, biomaRt and Gviz R/Bioconductor packages (27–30). H3K27ac signals were normalized using the MAnorm method for quantitative comparison of ChIP-seq data (31).

### RNA extraction and quantitative qRT-PCR

Cells were lysed using Tri-Reagent (Molecular Research Center). 1.0 µg of total RNA was retro-transcribed by using 100 units of M-MLV Reverse transcriptase (Life Technologies) in the presence of 1.6 µM oligo(dT) and 4 µM Random hexamers. qRT-PCRs were performed using SYBR green technology (KAPA Biosystems). Data were analyzed by comparative threshold cycle (delta delta Ct  $\Delta\Delta Ct$ ) using *HPRT* and *GAPDH* as normalizer. A list of the primers used for qRT-PCR and ChIP-qPCR is provided in Supplementary Table S1.

### RNA expression array and data analysis

Aliquots of RNAs, purified using RNeasy columns (Qiagen), were amplified according to the specifications of the Illumina TotalPrep RNA Amplification Kit (Ambion). Hybridization on Illumina whole-genome HumanHT-12 v 4.0 chip (Illumina), scanning and background subtraction were done according to the manufacturer's specification. Fold-change and *P*-values for each probe set were calculated as previously described (18). *P*-values data were then corrected for multiple hypotheses testing using the Benjamini–Hochberg methods. Differentially expressed genes (DEGs) were selected based on fold changes and adjusted *P*-values <0.05. Gene set enrichment analysis (GSEA) and the MSigDB database <http://software.broadinstitute.org/gsea/index.jsp> (32,33) were used to investigate statistically relevant biological associations.

Gene lists were analyzed separately using the GeneOntology (BiologicalProcess and ImmuneSystemProcess; Min GO Level = 3 and Max GO Level = 8),

KEGG, WikiPathways, CORUM-FunCat-MIPS, REACTOME\_Pathways and REACTOME\_Reactions databases as source of information. A right-sided hypergeometric test (corrected using the Benjamini–Hochberg) was applied to find enriched terms.

### Statistics

For experimental data Student t-test was employed. Mann–Whitney test was applied when normality could not be assumed. *P* < 0.05 was chosen as statistical limit of significance. For comparisons between samples >2, the Anova test was applied coupled to Kruskal–Wallis and Dunn's Multiple Comparison Test. We marked with \**P* < 0.05, \*\**P* < 0.01, \*\*\**P* < 0.001. Unless otherwise indicated, all the data in the figures were represented as arithmetic means ± the standard deviations from at least three independent experiments.

## RESULTS

### HDAC9 is a MEF2-target gene highly transcribed in leiomyosarcomas cells

Class IIa HDACs and particularly HDAC5 and HDAC9, are overexpressed in approximately 30% of leiomyosarcomas (LMS) (20,34). The mechanisms responsible for this up-regulation are not defined. The TCGA data analysis (Figure 1A) shows that in LMS patients the co-overexpression of one class IIa HDAC and one MEF2 TF is frequent. In fact, a significant co-occurrence of MEF2D and HDAC9 overexpression (*P*-value 0.035, log odds ratio 1427) and a trend of co-occurrence for MEF2A and HDAC5 mark these patients. ENCODE data evidence the presence of MEF2 binding sites, which are conserved through evolution, in the proximal promoter of HDAC9 (Figure 1B). We proved that MEF2D up-regulates the transcription from the HDAC9 promoter in different cell lines including LMS cells (Figure 1C). SK-UT-1 cells faithfully reflect LMS in terms of MEF2D and HDAC9 deregulation. Both proteins are highly up-regulated in these aggressive cells (6). When MEF2D was silenced, HDAC9 expression was down-regulated at the mRNA and protein levels (Figure 1D, F). By contrast, MEF2A silencing does not influence HDAC9 levels (Supplementary Figure S1A, B). Finally, in SK-UT-1 cells transcription from the HDAC9 promoter was strongly dependent on MEF2D (Figure 1E).

ChIP experiments demonstrated that MEF2D binds the promoter of HDAC9 (Figure 1G). MEF2D is required to sustain an open chromatin status, characterized by high levels of H3K4me3 and H3K27ac, on the HDAC9 promoter but not on the control TK promoter (Figure 1H and Supplementary Figure S1C). MEF2D down-regulation favors the appearance of H3K27me3 (Figure 1H and Supplementary Figure S1C). In summary, MEF2D is a key TF that boosts HDAC9 transcription in SK-UT-1 cells.

### HDAC4 and HDAC9 show different subcellular localizations in LMS cells

To study the role of class IIa HDACs in LMS, we generated SK-UT-1 cells knocked-out for *HDAC4* and *HDAC9*

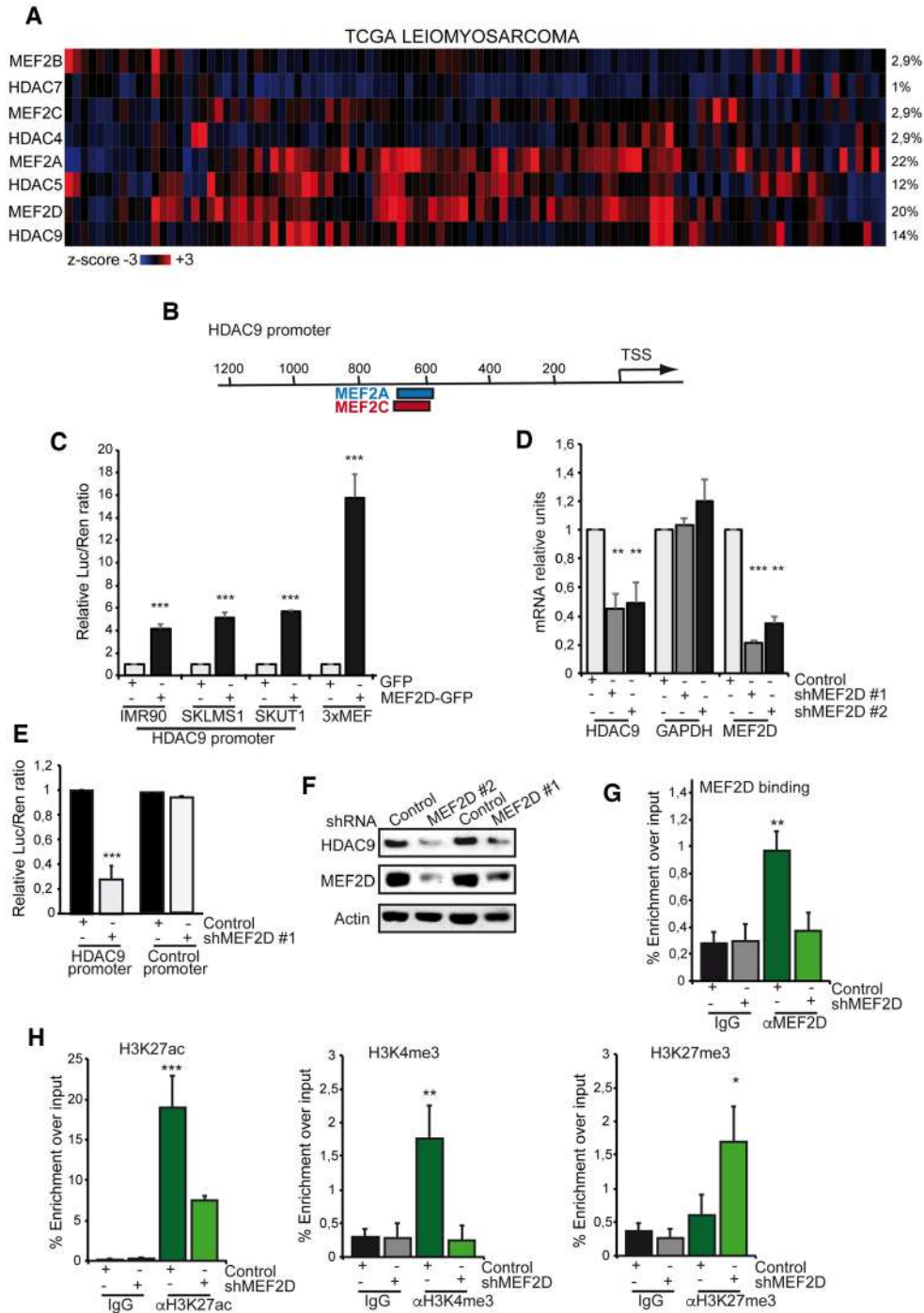


**Figure 1.** The MEF2D-HDAC9 circuit in leiomyosarcomas. (A) Oncoprint of mRNA expression variations for the indicated MEF2 and class IIa HDACs family members. Data were obtained from the TCGA database and include RNAseq data of 100 patients with LMS. The heatmap shows the expression levels (z-score normalized  $\log_2$  (FPKM) values) and was generated through cBioPortal (<http://www.cbioportal.org>). (B) The evolutionary conserved binding site, validated by ENCODE, for MEF2A (blue) and for MEF2C (red) in the proximal promoter of HDAC9 are shown. (C) Luciferase assay for HDAC9 promoter activity in HEK-293 cells transfected with MEF2D-GFP or GFP and the promoter regions (bp -1160/+23) amplified from IMR90, SK-LMS-1 and SK-UT-1 cells. 3xMEF construct, presenting three binding sites for MEF2, was used as positive control. Data were normalized by co-transfecting pRenilla and expressed as mean  $\pm$  S.D.,  $n = 3$ . (D) mRNA expression levels of the indicated genes, as measured by qRT-PCR, in MEF2D knock-down cells with respect to control. Two independent shRNA were used. Data are expressed as mean  $\pm$  S.D.,  $n = 3$ . (E) Luciferase assay for HDAC9 or control promoter activities in SK-UT-1 cells silenced for MEF2D expression. Data were normalized by co-transfecting pRenilla and expressed as mean  $\pm$  S.D.,  $n = 3$ . (F) Immunoblot analysis in SK-UT-1 MEF2D knock-down cells, using the indicated antibodies. Actin was used as loading control. (G) Chromatin was immunoprecipitated from SK-UT-1 cells WT or silenced for MEF2D, using the anti-MEF2D antibodies. Normal rabbit IgGs were used as control. The HDAC9 promoter region (-758:-528) containing the MEF2 binding sites was amplified. Data are presented as mean  $\pm$  S.D.,  $n = 4$ . (H) Chromatin was immunoprecipitated using the anti-H3K4me3, anti-H3K27ac and anti-H3K27me3 antibodies from SK-UT-1 cells and SK-UT-1 silenced for MEF2D. Data are presented as mean  $\pm$  S.D.,  $n = 3$ .

using the CRISPR/Cas9 technology (6). Two different clones, generated using two different guides, were selected for each KO. Immunoblot analysis shows that LMS cells express HDAC9 and high levels of its splicing variant MITR (Figure 2A). As predicted, in HDAC9 KO cells both isoforms are absent. Curiously, in *HDAC4*<sup>-/-</sup> cells a different pattern of HDAC9 can be appreciated. Levels of the full-length HDAC9 are reduced and a shorter isoform is increased. Similarly, also the levels of MITR are augmented. In *HDAC9*<sup>-/-</sup> cells, a fast migrating HDAC4 isoform is detectable, which shows a size similar to the caspase-cleaved fragment of this deacetylase (35) (see below). The levels of HDAC5 are augmented in the two KO cells, more strongly in *HDAC9*<sup>-/-</sup> cells, possibly as part of a compensatory mechanism. HDAC7 is expressed at extremely low/undetectable levels in SK-UT-1 cells. Similarly, MEF2A and MEF2D levels are augmented in the KO cells, with MEF2A showing a higher increase in *HDAC9*<sup>-/-</sup> cells. These increases correlate with elevated levels of the corresponding mRNAs (Supplementary Figure S3A).

Regulation of class IIa HDACs nuclear-cytoplasmic shuttling is a key aspect for the control of their repressive activities. Immunofluorescence analysis proved that HDAC9 is prevalently nuclear in these LMS cells (Figure 2B). As a consequence, its localization is not influenced by leptomycin B treatment (Figure 2B). By contrast, HDAC4 shows a pan/diffused localization, which can be converted into nuclear after the inhibition of the CRM1-dependent nuclear export (Figure 2B). Ran localization was used as counterstaining. The KO cells have proved the antibodies specificity. In summary, while HDAC9 is largely nuclear resident, HDAC4 is constantly subjected to nuclear/cytoplasmic shuttling.

### Transcriptomes under HDAC4 and HDAC9 regulation in LMS cells

To investigate the genetic repertoire under the control of HDAC4 and HDAC9 in LMS, the transcriptome of two *HDAC4*<sup>-/-</sup> clones (26 and 125) and two *HDAC9*<sup>-/-</sup> clones (167 and D43) generated with independent guide pairs were compared.

The vast majority of the up- and down-regulated genes ( $n = 566$  and  $n = 533$ , respectively), were shared between the two *HDAC4*<sup>-/-</sup> clones (Figure 3A). By contrast, *HDAC9*<sup>-/-</sup> clones have much less commonly regulated genes ( $n = 130$  up- and  $n = 71$  down-regulated) and a consistent number ( $n = 192$  up- and  $n = 159$  down-regulated) were clone-specific (Figure 3B, Supplementary Tables S2, S3 and Figure S2).

In order to define a common gene signature, we compared the lists of up- and down-regulated genes between *HDAC4*<sup>-/-</sup> and *HDAC9*<sup>-/-</sup> cells. Twenty nine induced and 21 repressed genes represent the common signature of the two class IIa HDACs (Figure 3C). This result suggests that the two HDACs play distinct roles in LMS cells.

Since class IIa HDACs are well-known repressors of transcription, we focused the attention on transcripts whose levels increased after the knock-outs. To further confirm the specific activities of the two HDACs, we compared the levels of genes up-regulated in *HDAC4*<sup>-/-</sup> cells with those in

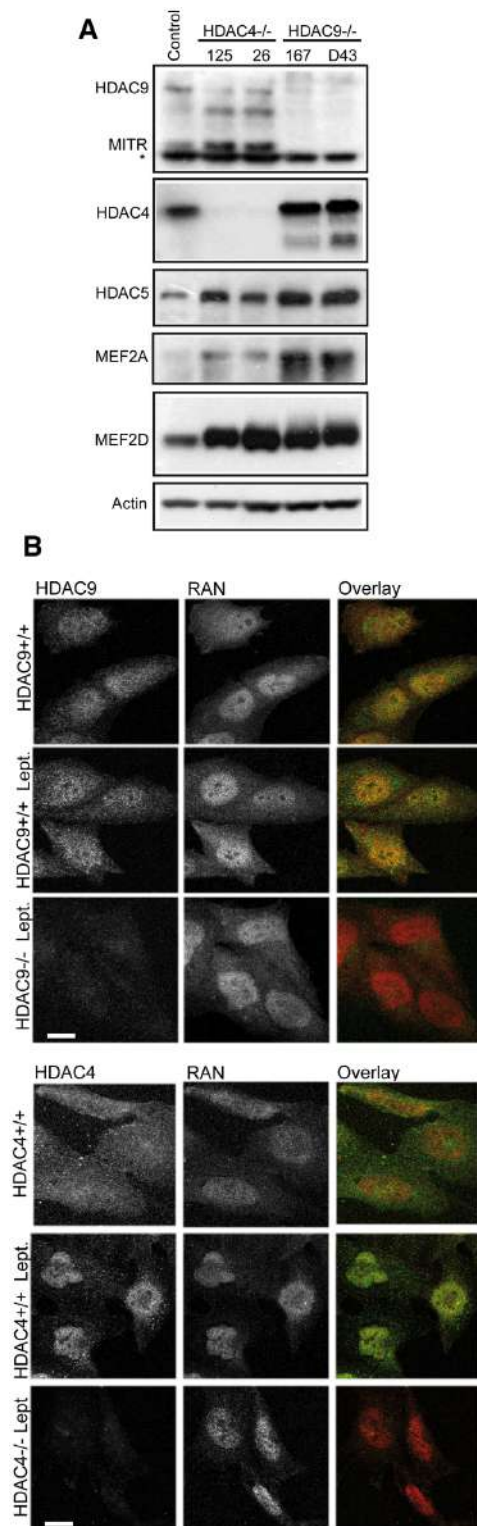


**Figure 2.** Characterization of SK-UT-1 cells knocked-out for HDAC4 and HDAC9. (A) Immunoblot analysis of HDAC9, MITR, HDAC4, HDAC5, MEF2A and MEF2D in SK-UT-1 cells WT and in two KO clones for HDAC4 (125 and 26) and HDAC9 (167 and D43). Asterisk points to a non-specific band. Actin was used as loading control. (B) Immunofluorescence analysis in SK-UT-1 WT, *HDAC4*<sup>-/-</sup>, *HDAC9*<sup>-/-</sup> cells stained with the indicated antibody. Where indicated, cells were treated for 2 h with Leptomycin B (Lept. 50 ng/ml) to inhibit the nuclear export. The anti-RAN antibody was used to stain nuclei. Bar: 50  $\mu$ m.

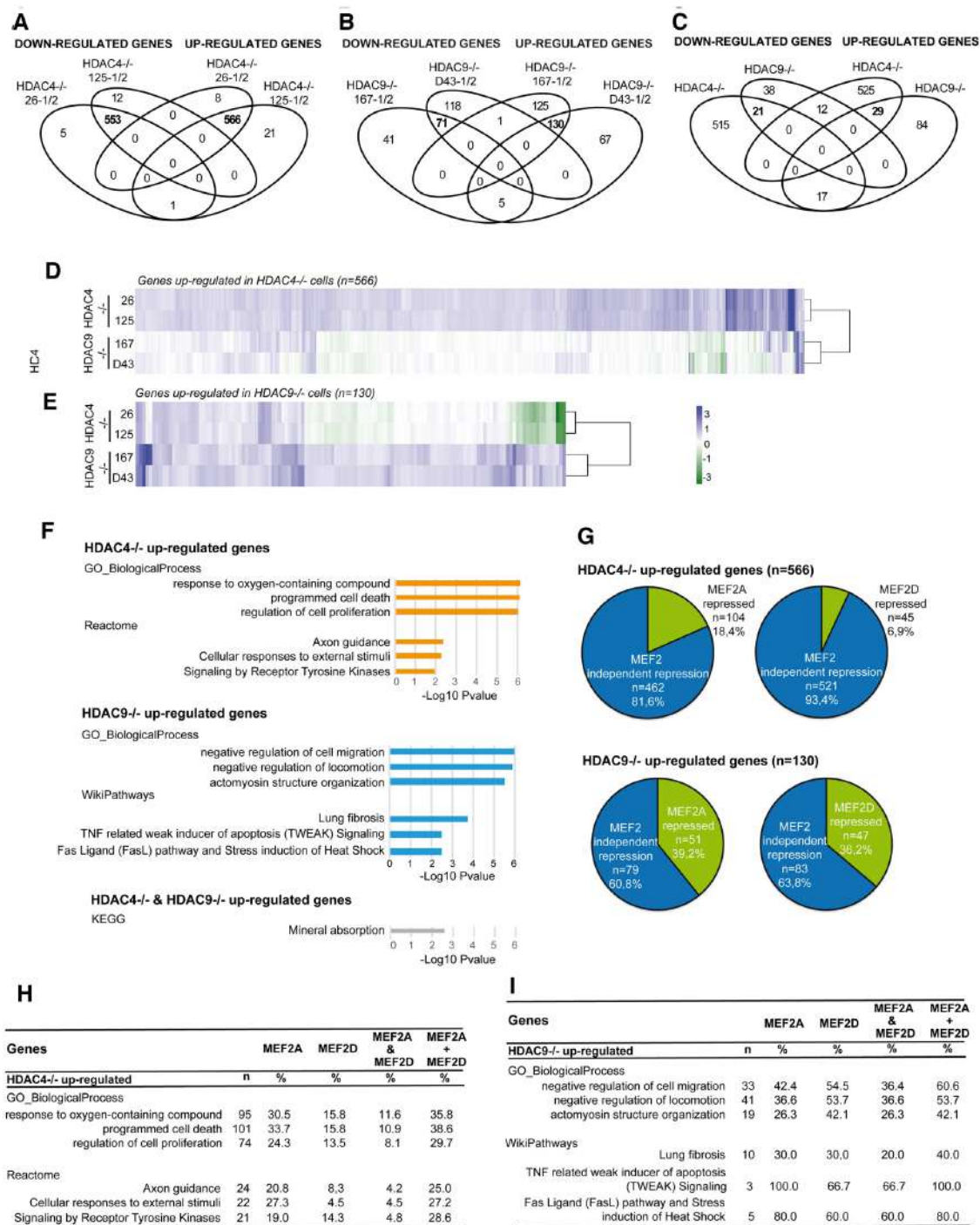


**Figure 3.** HDAC4 and HDAC9 regulate different patterns of genes, only partially overlapping. (A) Venn diagrams showing the number of transcripts commonly and differentially up-regulated or down-regulated between the two clones of *HDAC4*<sup>-/-</sup> cells. (B) Venn diagrams showing the number of transcripts commonly and differentially up-regulated or down-regulated between the two clones of *HDAC9*<sup>-/-</sup> cells. (C) Venn diagrams showing the number of transcripts commonly and differentially up-regulated or down-regulated among the different clones of *HDAC4*<sup>-/-</sup> and *HDAC9*<sup>-/-</sup> cells. (D) Heatmap of the 566 significantly up-regulated genes in *HDAC4*<sup>-/-</sup> cells and their expression levels in *HDAC9*<sup>-/-</sup> cells. In the heatmap genes up-regulated are shown in green and down-regulated in blue, as fold changes. (E) Heatmap of the 130 significantly up-regulated genes in *HDAC9*<sup>-/-</sup> cells and their behavior in *HDAC4*<sup>-/-</sup> cells. In the heatmap genes up-regulated are shown in green and down-regulated in blue, as fold changes. (F) Bar plots of the Cytoscape-ClueGO most significantly enriched functional terms according to the GO: Biological Process, Reactome or WikiPathways databases. Analysis was performed for the indicated groups of up-regulated genes, retaining the top 3 terms defined by the two most informative functional databases. (G) Pie charts illustrating the dependency on MEF2 of the genes up-regulated in *HDAC4*<sup>-/-</sup> and *HDAC9*<sup>-/-</sup> cells. The dependency on MEF2 was scored by looking at the genes affected by MEF2A/D knock-down (6). (H) Effect of MEF2A and MEF2D silencing on the gene lists associated with the most significantly enriched functional terms of the Cytoscape-ClueGO analysis as shown in (A) in SK-UT-1 *HDAC4*<sup>-/-</sup> cells. The dependency on MEF2 was expressed as percentage. (I) Effect of MEF2A and MEF2D silencing on the gene lists associated with the most significantly enriched functional terms of the Cytoscape-ClueGO analysis as shown in (A) in SK-UT-1 *HDAC9*<sup>-/-</sup> cells. The dependency on MEF2 was expressed as percentage.

*HDAC9*<sup>-/-</sup> cells and vice versa. Heatmaps show that although a group of genes was similarly up-regulated by the knock-out of the two HDACs, many genes were specific for each HDAC, as they were unperturbed in the other KO or, in some instances, repressed (Figure 3D and E). qRT/PCR analysis on a panel of these differentially regulated genes further validated these results (Supplementary Figure S3A).

### The genetic programs regulated by HDAC4 and HDAC9

We used the Cytoscape plugin ClueGO (36,37) to understand the functions of genes up-regulated in *HDAC4*<sup>-/-</sup> and *HDAC9*<sup>-/-</sup> cells, as well as of genes induced in both conditions. As expected, the most significantly enriched functional terms differ from HDAC4 and HDAC9 (Figure 3F). HDAC4-repressed genes are involved in the oxidative stress response, proliferation and programmed cell death. By contrast, HDAC9 repressed genes include negative regulators of cell migration/locomotion and regulators of actin cytoskeleton. Interestingly, death receptor signaling emerged as a pathway under HDAC9 influence. A common genetic program regards the mineral absorption.

In order to identify genes under the influence of the MEF2-HDAC axis, we compared the lists of genes up-regulated in *HDAC4*<sup>-/-</sup> and *HDAC9*<sup>-/-</sup> cells with genes that are repressed by MEF2A and MEF2D in the same cells (6). Figure 3G highlights such overlaps, indicating a similar and strong contribution of these TFs to HDAC9-mediated repression. Although the majority of the HDAC4-repressed genes are not under the influence of MEF2A or MEF2D, the absolute number of MEF2A/D target genes is similar to HDAC9. Furthermore, within the HDAC4-repressed genes, MEF2A influence is more pronounced compared to MEF2D. This observation was confirmed by GSEA (Genes Set Enrichment Analysis). Here significant enrichments were obtained only when the comparisons were performed between HDAC9 and MEF2A or MEF2D regulated genes (Supplementary Figure S3B).

Subsequently, we wondered to what extent MEF2-HDAC co-targets could recapitulate the previously identified biological functions associated with genes repressed by HDAC4 or HDAC9. Figures 3H/I summarizes the number (n) of genes associated with each enriched term, the percentage of genes that are also MEF2A or MEF2D targets, the percentage of those in common between MEF2A and MEF2D (MEF2A & MEF2D) and the percentage of those that are targets of at least one MEF2 (MEF2A + MEF2D).

Finally, we used a right-sided Fisher's exact test to determine the probability that each biological function was significantly enriched in one of the HDAC/MEF2 co-target subsets with respect to the corresponding list of up-regulated genes in *HDAC4*<sup>-/-</sup> or *HDAC9*<sup>-/-</sup> cells. Firstly, this allowed the identification of 'response to oxygen-containing compound' and 'programmed cell death' as terms enriched in both MEF2A (*P*-value = 7e-03 and *P*-value = 7e-04, respectively) and MEF2D targets common to HDAC4 (*P*-value = 7.5e-03 and *P*-value = 5.3e-03, respectively). We also defined 'negative regulation of locomotion' as specifically enriched (*P*-value = 4.6e-02) in the HDAC9/MEF2A targets subset, representing the only HDAC9-related bio-

logical process showing specificity for one of the two MEF2 regulators.

In summary our data demonstrate that different MEF2-HDAC complexes can regulate distinct gene-networks.

### Mapping the genomic regions bound by HDAC4, HDAC9 and MEF2D

ChIP-seq experiments were performed to investigate, at a genomic level, HDAC4 and HDAC9 binding in relation to MEF2D. As expected from the transcriptomic analysis, HDAC4 shows a higher genomic binding (*n* = 7732) compared to HDAC9 (*n* = 1257), while MEF2D peaks are 2214, in agreement with previous studies (38). 68% of MEF2D peaks contains at least a MEF2 binding sites (Supplementary Table S4). By comparing the binding locations, 45% of MEF2D peaks co-localize with HDAC4, HDAC9 or both (Figure 4A). In particular, 56% of these events are in common with HDAC4 and HDAC9, 43% are MEF2D/HDAC4 specific and only 1.2% are MEF2D/HDAC9 specific. HDAC4 displays a substantial MEF2D-independent activity as 82% of its peaks are bound neither by MEF2D nor by HDAC9. On the contrary, HDAC9 specific peaks are less frequent (20%). DNA motif analysis on the HDAC4-specific peaks showed an enrichment for SMAD3 and CENPB binding motifs. When the same analysis was performed on HDAC4-specific peaks localized in H3K27ac enriched regions, BACH2 and ZNF384 showed the highest enrichments (Supplementary Figure S4). The ChIP-seq data for MEF2D, HDAC4, HDAC9 and the variations in H3K27ac were confirmed by ChIP-qPCR for 11 distinct genomic regions (Supplementary Figure S5). Overall, the analysis of the genomic binding sites confirms the different activities of the two HDACs, as emerged from the transcriptomic analysis.

The majority of HDAC4 and HDAC9 peaks localize in intergenic regions, (68% and 76%, respectively), as previously observed for other class IIa HDACs (18,39,40). By contrast only 36% of MEF2D peaks map in intergenic regions while 27% are in promoter regions (Figure 4B). Interestingly, MEF2D peaks localization undergoes significant changes when associated with common binding of HDAC4/HDAC9. In these cases 64% occur in intergenic, 14% in introns and only 18% in promoter regions. This re-localization seems to only partially depend on the presence of HDAC4 alone, since MEF2D/HDAC4 common mapping is 47% intergenic, 29% intronic and 17% in promoter regions. To further evaluate the chromatin status around these peaks, we mapped the H3K27 acetylation either as a perfect overlap (min. 1 bp in common) or in a 2 kb interval from the peak summit (Figure 4C). Overall, the presence of HDAC4 frequently correlates with an open chromatin status, while HDAC9 peaks are commonly confined in regions marked by poor H3K27 acetylation. These correlations are MEF2-independent. In general, the co-presence of MEF2D increases H3K27 acetylation incidence (Figure 4C).

It is plausible that the genomic binding sites of the two class IIa HDACs and possibly of MEF2D, within the regulative elements of the genes up-regulated after the KO of HDAC4 and HDAC9, may influence their epigenetic status and subsequently the transcriptional output. Hence, we

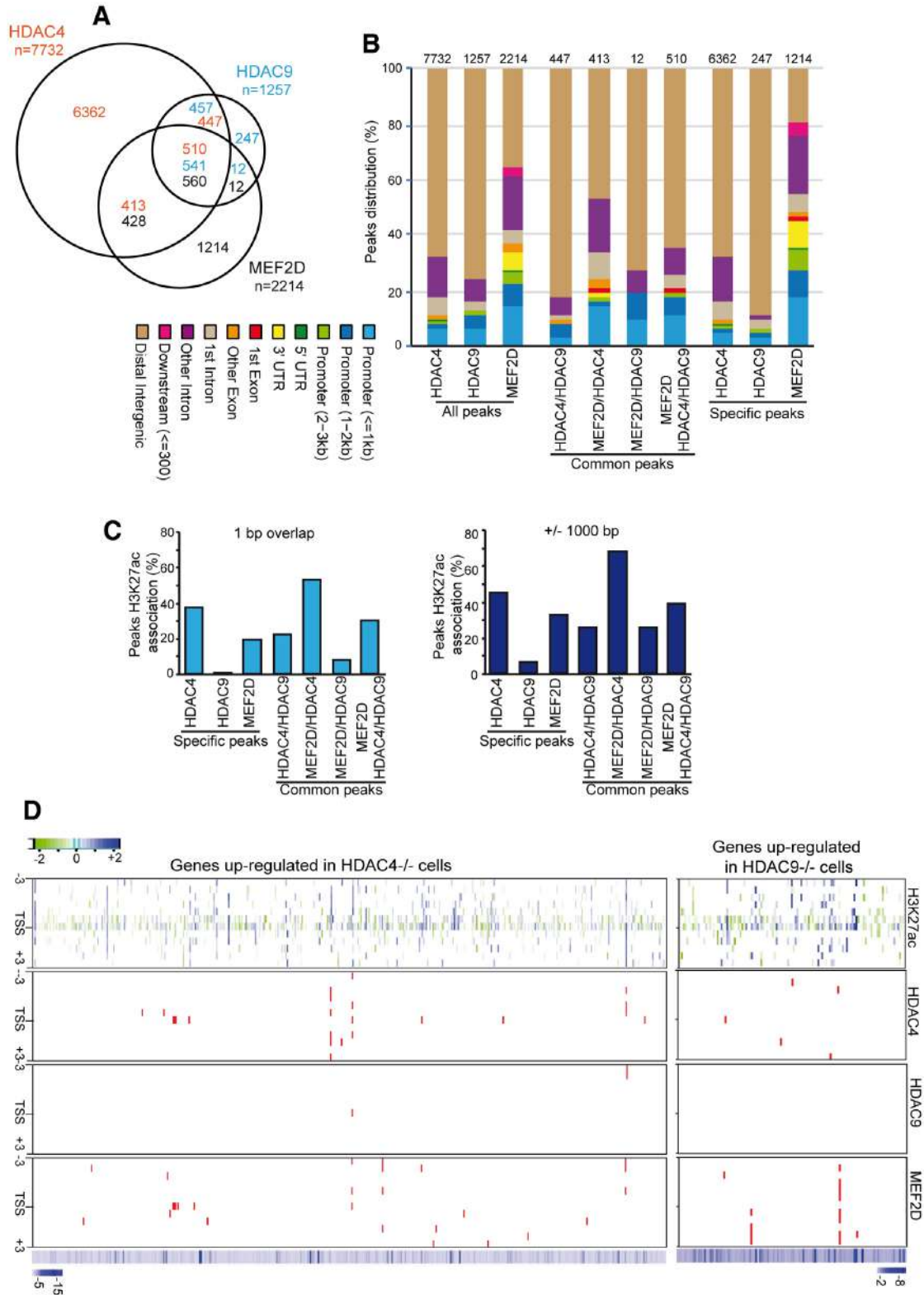


**Figure 4.** Defining the genomic binding sites and influences of MEF2D, HDAC4 and HDAC9 on H3K27ac. (A) Venn diagrams showing the overlaps between the MACS2-defined MEF2D, HDAC4 and HDAC9 ChIP-seq enriched peaks in SK-UT-1 cells. (B) Genomic distribution of the MACS2-defined MEF2D, HDAC4 and HDAC9 ChIP-seq enriched peaks in SK-UT-1 cells. (C) Proximity, expressed as percentage, of H3K27ac marks to the MEF2D, HDAC4 and HDAC9 ChIP-seq enriched peaks in SK-UT-1 cells. The minimum distance is 0bp (overlapping) and 1kbp, respectively, for the left and right panel. (D) Heatmaps showing the differences in H3K27ac distribution between *HDAC4*<sup>-/-</sup> and *HDAC4*<sup>+/+</sup> or *HDAC9*<sup>-/-</sup> and *HDAC9*<sup>+/+</sup> SK-UT-1 cells. The displayed regions are located  $\pm 3$ kb around the TSS of a subset of 475 microarray-defined HDAC4 repressed genes (left panel) and of 118 microarray-defined HDAC9 repressed genes (right panel). Binding peaks for MEF2D, HDAC4 and HDAC9 in the same regions are also provided. The differences in mRNAs levels are indicated by the heatmaps at the bottom.

evaluated variations of the H3K27ac status around the TSS (-/+3kb) of these genes. In the same regions, we also investigated the presence of MEF2D, HDAC4 and HDAC9 peaks. We excluded from the analysis transcripts with undefined functional annotations, thus resulting in 475 genes for *HDAC4*<sup>-/-</sup> and 118 genes for *HDAC9*<sup>-/-</sup> cells.

The levels of H3K27ac were augmented around the TSS of several genes up-regulated in *HDAC4*<sup>-/-</sup> and *HDAC9*<sup>-/-</sup> cells. This increase was evident also in regions more distal with respect to the TSS (Figure 4D). Frequently, acetylation spreading emerged as a consequence of *HDAC4* and *HDAC9* deletions.

Fourteen genes are characterized by HDAC4 binding within 3 kb from the TSS and six of them also show co-binding with MEF2D. Among these six genes, *ARMC4* and *MPP7* evidence multiple binding events for MEF2D and HDAC4 (Figure 4D). These two genes are marked by intense spreading of H3K27ac in the absence of HDAC4. Surprisingly, peaks for HDAC9 were not found around the TSS of genes up-regulated in knocked-out cells, even though for 4 genes (*CXCL1*, *ENCI*, *PLK2* and *SORT1*) MEF2D binding was observed.

Next, we expanded the analysis up to ±30 kb from the TSS to find evidence of distal regulative elements. The increase of H3K27ac and the spreading effects elicited by the absence of the two HDACs was confirmed (Figure 5A). *ARMC4*, *MKX*, *MPP7*, *NFIB*, *RORI*, *ZNRF3* are among the most evident examples of this behavior in the absence of HDAC4. *CXCL1*, *CXCL8/IL8* and *SMAD3* in the case of HDAC9 absence. Importantly, *CXCL1* and *IL8* are among the highest up-regulated genes in *HDAC9*<sup>-/-</sup> cells (Supplementary Table S2).

Twenty five genes show HDAC4 binding within 30kb from the TSS and frequently with multiple binding events. Peaks for HDAC9 were again rare, with only *RAB31* with a positive hit. MEF2D genomic binding was found in 28 genes up-regulated in *HDAC4*<sup>-/-</sup> cells, of which seven shared with HDAC4 and in eight genes up-regulated in *HDAC9*<sup>-/-</sup> cells (Figure 5A).

### HDAC4 and HDAC9 regulate H3K27ac levels in regulative regions distal from the TSS

The previous analysis has revealed that, although changes in H3K27ac are prominent in regions around the TSS of genes up-regulated after the KO of the two HDACs, only a fraction of these genes displays the binding of HDAC4 (5,3%) and rarely of HDAC9 (0.8%). Certainly, some of these genes could be indirect target of the deacetylases. However, since several HDAC4 and HDAC9 peaks were found in the intergenic regions, we hypothesized that HDAC4 and HDAC9 in particular, could preferentially influence gene expression from distal regulative elements such as enhancers.

To explore this possibility, we investigated the variations of H3K27ac status after the knock-out of the two HDACs, at the distal regions marked by the co-presence of MEF2D, HDAC4 and HDAC9 peaks (Figure 4A; *n* = 510). Through this strategy we should identify the functional/active distal regulative regions of MEF2D target genes.

Approximately 42% of these common peaks lie in H3K27 acetylated regions. 57% of these acetylated regions are found away from a TSS (>30 kb from the TSS).

Next, we investigated whether some of these distal regions showed HDAC4 or HDAC9 dependent regulation of H3K27ac levels. Three different groups of peaks can be identified (Figure 5B). A first group comprises common peaks that do not show strong variations in relative H3K27ac fold increases, after the knock-out of both deacetylases (gray dots). A second group of common peaks shows increases in relative H3K27ac, which are more marked in the absence of one of the two deacetylases, more frequently in *HDAC4*<sup>-/-</sup> cells. The third group comprises H3K27ac peaks that appeared exclusively enriched after the knock-out of either HDAC4 or of HDAC9.

Within these distal regions differentially modulated by the two class IIa HDACs, we could expect to find regulative elements that orchestrate the expression of genes differentially regulated by HDAC9 and responsible for the different impact on the proliferation of SK-UT-1 cells.

Chromosome conformation capture (3C) assay, combined with Next Generation Sequencing (Hi-C) can provide a global view of all chromosomal interactions across the genome and maps Topologically Associated Domains (TADs) (41,42). Within these domains distal regulative regions can be identified. A distal intergenic region, where H3K27ac was modulated by HDAC9, is located almost 100kb downstream from *ARHGEF28* locus. To understand whether it could act as a distal enhancer, we compared our ChIP-seq data to available Hi-C data obtained from the IMR90 cell line (43).

Figure 6 shows that a region, marked by multiple binding sites for MEF2D, HDAC4 and HDAC9 dramatically increases H3K27ac acetylation levels only after the knock-out of HDAC9. Hi-C data indicate that this region lies within a defined TAD and that, through chromatin looping, it could act distally to influence a region close to the TSS of *ENCI*. As a matter of fact, the ablation of HDAC9 augments H3K27ac levels in the proximity of *ENCI*.

Overall this analysis suggests that an intergenic region, where H3K27ac acetylation is modulated by HDAC9, could act as distal regulative region (enhancer) for the *ENCI* gene. The detection of eRNAs in the same region regulated by HDAC9, as defined by SlideBase – FANTOM5 Human Enhancers Selector, further supports this possibility (44). Importantly, the *ENCI* transcript is specifically up-regulated in *HDAC9*<sup>-/-</sup> cells (Supplementary Figures S3B and S5).

Another example of HDAC9-controlled, distal regulative region is represented by the intragenic locus of *INSYN2B*, which perfectly superimposes to a sub-TAD characterized by the presence of eRNAs (Supplementary Figure S6A). Finally, an example of a distal regulative region under the specific influence of HDAC4 is represented in Supplementary Figure S6B. This regulative intergenic region is located ~35 kb upstream from the *SLC8A1* locus. Within the TAD, binding of MEF2D, HDAC4 and HDAC9 can be found. In this case, however, it is the KO of HDAC4 that causes a diffuse spreading of H3K27ac throughout the sub-TAD (Supplementary Figure S6B).

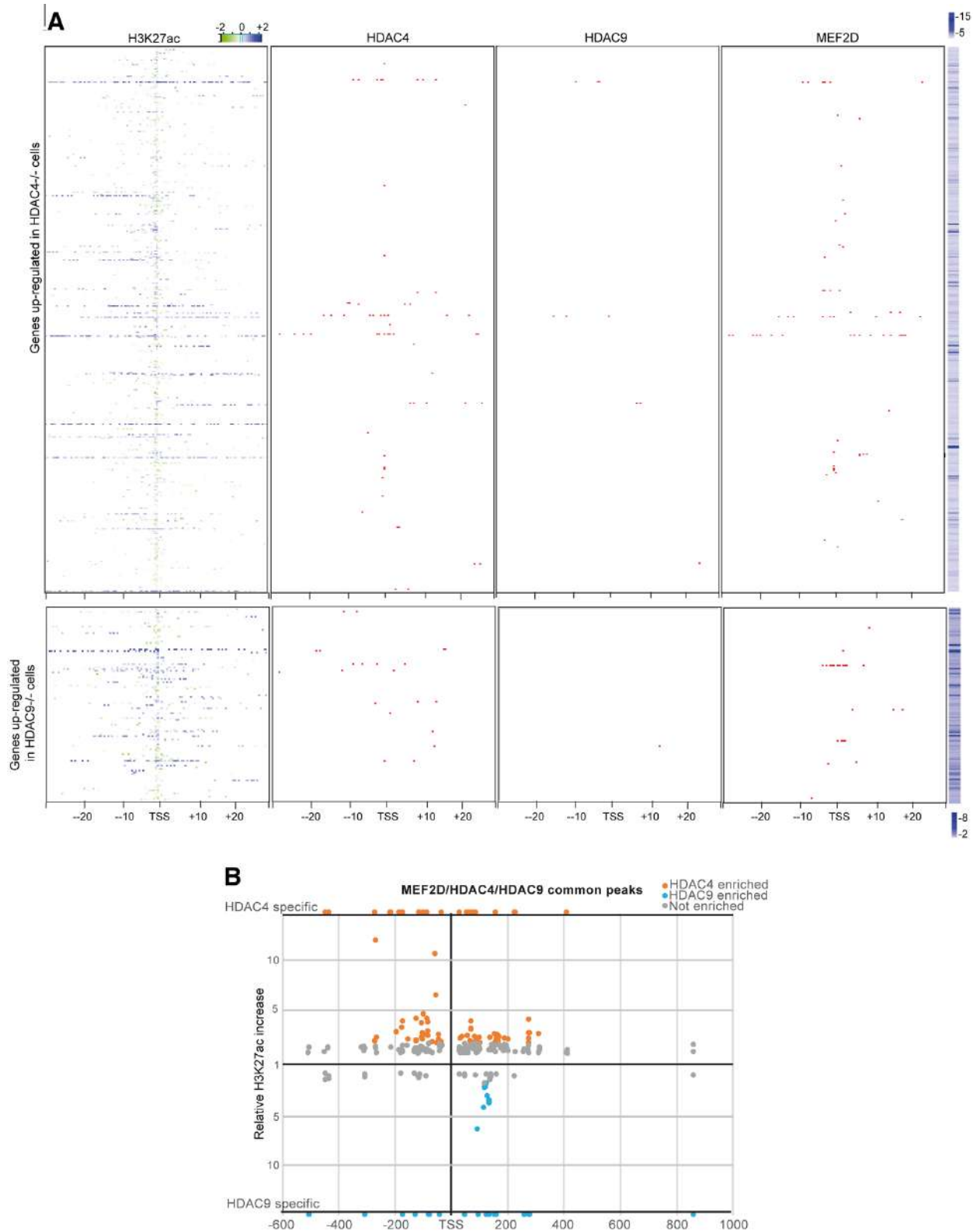


**Figure 5.** Impact of HDAC4 and HDAC9 on H3K27 acetylation at genomic regions distal from the TSS. **(A)** Heatmaps showing the differences in H3K27ac distribution between *HDAC4*<sup>-/-</sup> and *HDAC4*<sup>+/+</sup> or *HDAC9*<sup>-/-</sup> and *HDAC9*<sup>+/+</sup> SK-UT-1 cells. The displayed regions are located ±30kb around the TSS of a subset of 475 microarray-defined HDAC4 repressed genes (top panel) and of 118 microarray-defined HDAC9 repressed genes (mid panel). Binding peaks for MEF2D, HDAC4 and HDAC9 in the same regions are also provided. The differences in mRNAs levels are indicated by the heatmaps at the right side. **(B)** Acetylation status of MEF2D/HDAC4/HDAC9 co-localizing peaks. Distances from the TSS of the closest coding genes are shown. The increase of the relative H3K27ac signal after the knock-out of HDAC4 (orange) or HDAC9 (light blue) is indicated. H3K27ac peaks that are exclusively enriched only after the knock-out of either HDAC4 or of HDAC9 are shown at the edges of the charts as HDAC4 or HDAC9 specific.



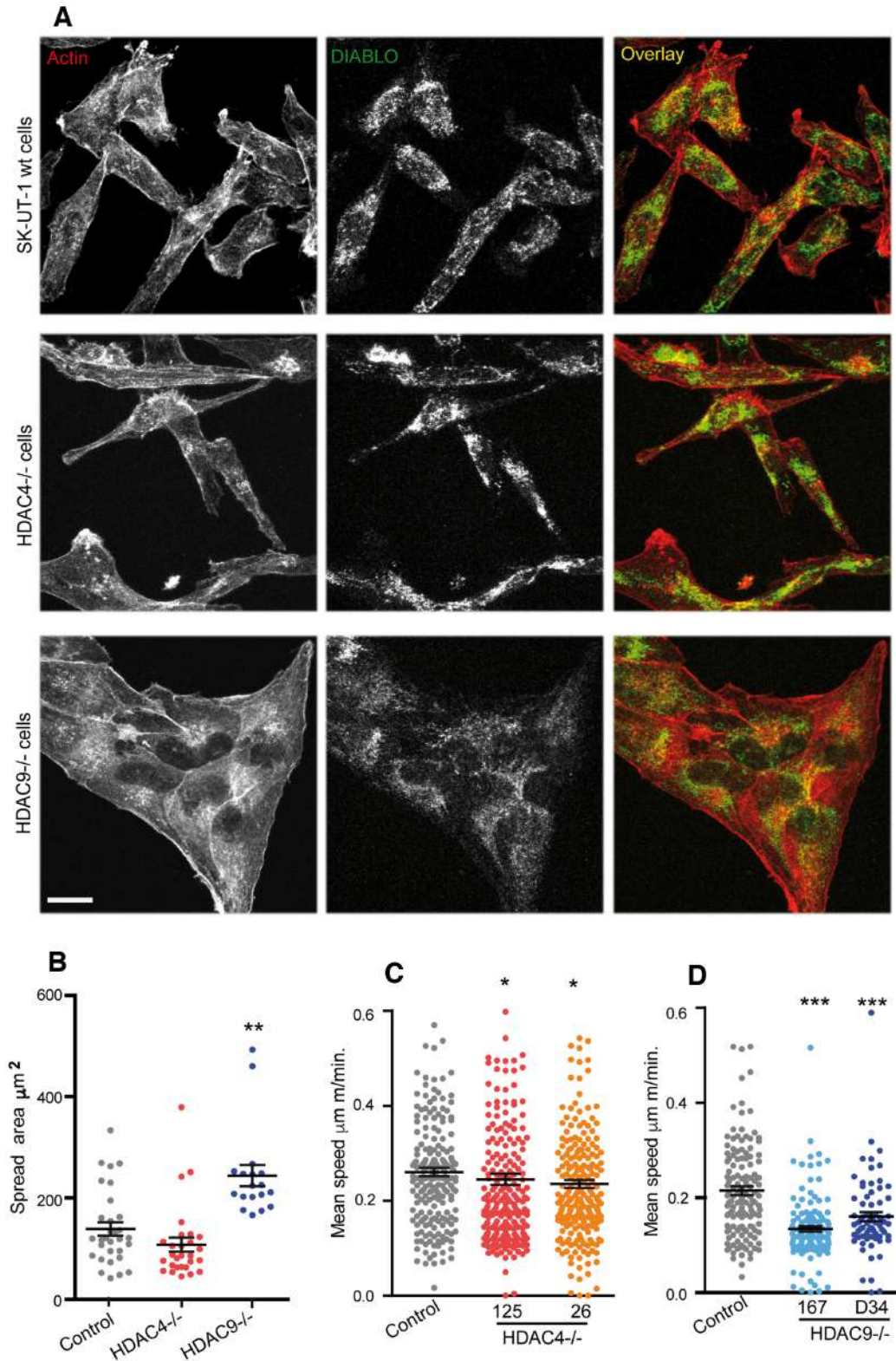


**Figure 7.** HDAC9 controls spreading and motility in LMS cells. (A) Confocal images of the indicated LMS cell lines stained for actin (red), using phalloidin and DIABLO (green), by immunofluorescence to visualize mitochondria. Bar 50  $\mu\text{m}$ . (B) Dot plot representing the spread area of the indicated SK-UT-1 cells. The median and the first and third quartiles are indicated;  $n > 25$ . (C) Dot plot representing the mean speed of the indicated SK-UT-1 cells. Time-lapse experiments were performed over a period of 6 h. The median and the first and third quartiles are indicated  $n > 134$ . (D) Dot plot representing the mean speed of the indicated SK-UT-1 cells. Time-lapse experiments were performed over a period of 6 hours. The median and the first and third quartiles are indicated;  $n > 89$ .

rescence studies, the spreading was markedly increased in *HDAC9*<sup>-/-</sup> cells (Figure 7B). We also performed time-lapse studies to compare the random cell motility of the different cell lines. *HDAC9*<sup>-/-</sup> but not *HDAC4*<sup>-/-</sup> cells are characterized by a dramatically reduced random cell motility (Figure 7C, D). Overall these studies demonstrate that HDAC9, by repressing the expression of cytoskeletal components, controls cell adhesion, morphology and motility.

### HDAC9 sustains cell survival by repressing FAS expression

The transcriptomic studies indicate that HDAC9 could repress apoptosis and particularly the activation of the extrinsic apoptotic pathway (Figure 3I). *FAS* emerged as a gene specifically up-regulated in *HDAC9*<sup>-/-</sup> cells. Analysis of Hi-C data shows that the *FAS* locus is embedded within a subTAD adjacent to the subTAD containing the *ACTA2* locus, which is transcribed in the opposite orientation. Interestingly, a specific *ACTA2* isoform share with *FAS* the promoter region (Figure 8A). The ChIP-seq did not identify peaks for MEF2D and HDAC9 within the *FAS* locus. Despite this, H3K27 acetylation is clearly augmented around the TSS and throughout the first intron of *FAS*, in the absence of HDAC9. Similarly a downstream intergenic region (approx. 40kb from the *FAS* TSS) is highly acetylated in *HDAC9*<sup>-/-</sup> cells. Interestingly, Hi-C data indicate that this intergenic region can make contact with the *FAS* promoter. H3K27 acetylation in *HDAC9*<sup>-/-</sup> cells was augmented also at the *ACTA2* locus (Figure 8A). We validated the contribution of HDAC9 in the control of *FAS* and *ACTA2* mRNA levels by qRT-PCR. As expected, *FAS* and *ACTA2* expression was up-regulated in *HDAC9*<sup>-/-</sup> cells (Figure 8B). Up-regulation of the *FAS* protein was also verified by immunoblot (Figure 8C).

Overall these data suggest that HDAC9 can sustain SK-UT-1 transformation by repressing the extrinsic apoptotic pathway. To prove this hypothesis, we analyzed the proliferative features of the different engineered SK-UT-1 cells. HDAC9 absence marginally reduced the percentage of cells in S phase. *HDAC4*<sup>-/-</sup> cells did not show overt defects (Supplementary Figure S7A). Time-course experiments showed that *HDAC4*<sup>-/-</sup> cells have a partial proliferative deficit, whereas proliferation of *HDAC9*<sup>-/-</sup> cells was dramatically impaired (Supplementary Figure S7B) and marked by an increased level of cell death. This low constitutive activation of the apoptotic machinery was confirmed by the Caspase-9 and Caspase-3 processing observed in the absence of apoptotic insults (Supplementary Figure S7C). When the different LMS cells were grown without serum, cell death was dramatically induced in the absence of HDAC9 (Supplementary Figure S7D). Finally, we compared the proliferation of the different SK-UT-1 cells when incubated with different pro-apoptotic drugs including: tyrosine-kinase, HDACs, isopeptidases (22) and Akt inhibitors or metmorfin. With the exclusion of the two TK inhibitors, only in *HDAC9*<sup>-/-</sup> cells all drugs showed a significant stronger anti-proliferative outcome (Supplementary Figure S7E). As expected, apoptosis elicited by *FAS* ligand (*FASL*) was clearly augmented in *HDAC9*<sup>-/-</sup> SK-UT-1 cells (Figure 8D). In vivo, analysis of TCGA data on leiomyosarcomas showed low levels of *FAS* mRNA and a

significant anti-correlation between the *FAS* and *HDAC9* mRNA levels (Figure 8E).

### The extrinsic apoptotic pathway is activated in the absence of HDAC9

To prove the involvement of the extrinsic pathway we expressed the inhibitor of DISC activation FLIPs, the short isoform of CFLAR/FLIP (45). *FAS*-induced caspase activation was strongly attenuated in the presence of FLIPs (Figure 8F). Importantly, also the increase of caspase activity observed in the KO cells in the absence of added apoptotic insults, was blunted by FLIPs (Figure 8F). Next, we evaluated the percentage of cell death in untreated cells. The increase of cell death observed in the *HDAC9*<sup>-/-</sup> cells was completely abrogated by the presence of FLIPs (Figure 8G).

To exclude that the HDAC9-dependent regulation of *FAS* levels was a peculiar aspect of SK-UT-1 cells, we analyzed a panel of LMS cells for HDAC9 expression. HDAC9 levels were abundant also in DMR cells but not in SK-LMS-1 and MES-SA uterine sarcoma cells (Supplementary Figure S8A). When HDAC9 was downregulated by two different siRNAs in DMR cells, *FAS*, *ACTA2* and *IL8* levels were all augmented (Supplementary Figure S8B). The up-regulation of these genes was not observed after HDAC4 silencing. In agreement with SK-UT-1 cells, apoptosis was increased after HDAC9 silencing also in DMR cells (Supplementary Figure S8C). We also investigated whether an anti-correlation between class IIa HDACs and *FAS* levels could be observed in leiomyosarcomas *in vivo*. Supplementary Figure S8D shows that a significant anti-correlation with *FAS* expression in LMS involves also *HDAC5*, in addition to *HDAC9*.

We also investigated whether HDAC9 absence increased the apoptotic susceptibility of SK-UT-1 cells to different apoptotic insults such as: DNA damage (doxorubicin), Akt inhibition (MKK2206) and the proteotoxic stressor G5 (Figure 8H). Only apoptosis triggered by doxorubicin and G5 was potentiated by *HDAC9* deletion. This increase was largely suppressed by the presence of FLIPs, thus suggesting an involvement of the extrinsic pathway. Analysis of caspase activation confirmed that the up-regulation of the extrinsic pathway characterizes the increased apoptotic susceptibility of *HDAC9*<sup>-/-</sup> cells in response to doxorubicin (Figure 8I).

### Deletion of the MEF2-binding sites in the HDAC9 promoter recapitulates the knock-out of HDAC9

Our manuscript opened with the demonstration that MEF2D is the critical TFs involved in the up-regulation of HDAC9. Subsequently, we proved that HDAC9 plays a critical role in *FAS* expression and in the regulation of SK-UT-1 survival. To conclude our study we needed to demonstrate that the abrogation of the vicious loop between MEF2D and HDAC9 suppresses cell proliferation, up-regulates *FAS* expression and triggers apoptosis.

To this purpose we used the CRISPR/Cas9 technology to mutagenize the MEF2 binding sites in the *HDAC9* promoter (Figure 9A). ChIP experiment demonstrated the absence of MEF2D binding in the *HDAC9* promoter of engi-

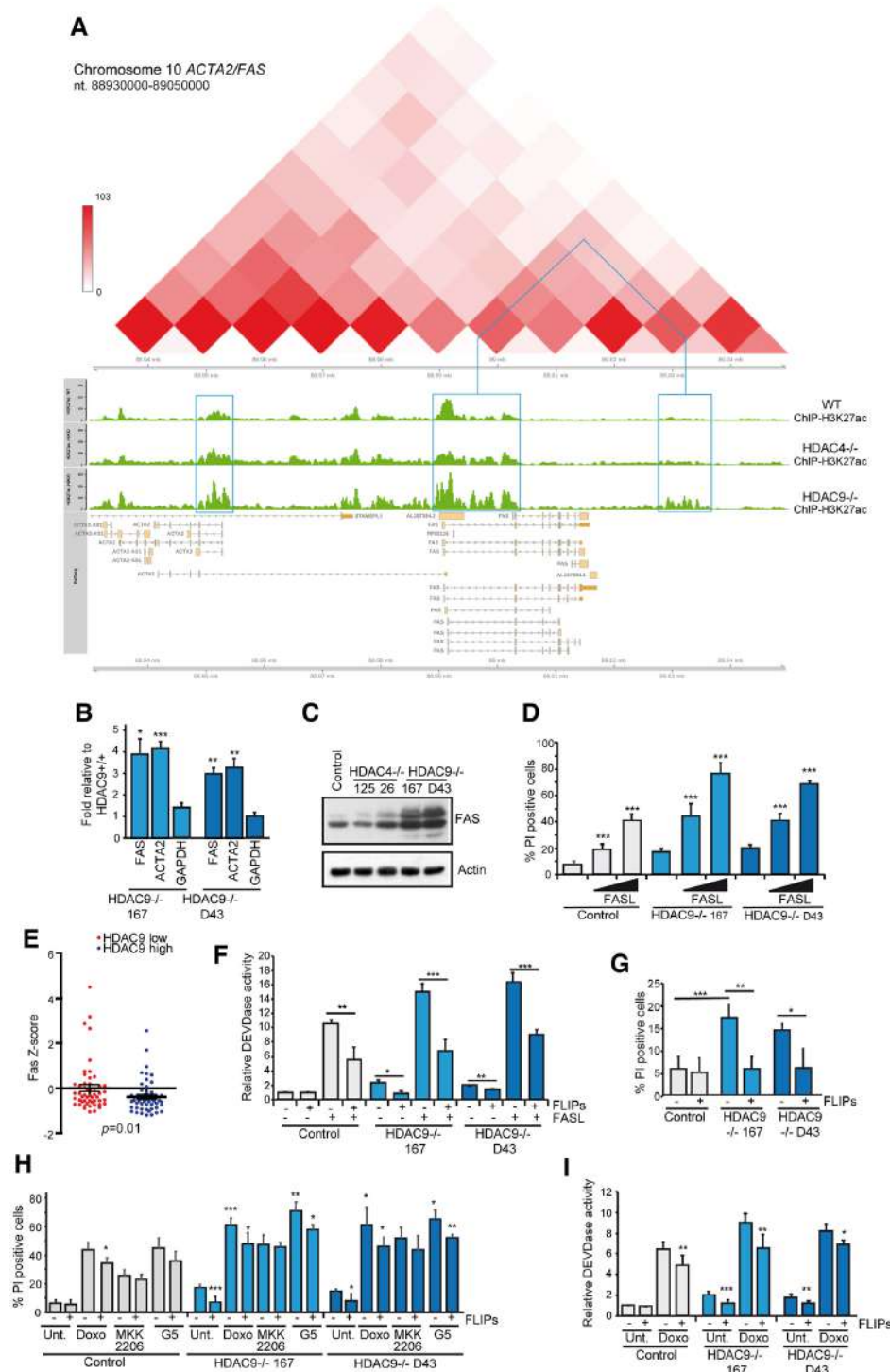


**Figure 8.** HDAC9 promotes cell survival by repressing FAS transcription. (A) Genomic view of the *ACTA2/FAS* locus on chromosome 1 (GRCh38). Detailed view of H3K27ac normalized tracks (green) for WT, *HDAC4*<sup>-/-</sup> and *HDAC9*<sup>-/-</sup> SK-UT-1 cells. The boxes (light blue) evidence the chromatin looping between a distal regulative element and the *FAS* promoter. Hi-C data were used to define the TADs within the *FAS* locus. (B) mRNA expression levels of *ACTA2*, *FAS* and *GAPDH*, as measured by qRT-PCR. Data are presented as mean  $\pm$  S.D relative to wild-type SK-UT-1 cells,  $n = 3$ . (C) Immunoblot analysis of FAS levels in the indicated SK-UT-1 clones. Actin was used as loading control. (D) Histogram representing the percentage of PI positivity in the indicated SK-UT-1 cells, treated with 25 and 50ng/ml of FASL. Data are presented as mean  $\pm$  S.D.  $n = 3$ . (E) Scatter dot plot representing the z-scores of FAS mRNA levels in individual TCGA tumors ( $n = 100$ ) divided in two classes accordingly to HDAC9 levels. (F) Histogram representing the percentage of PI positivity in the indicated SK-UT-1 cells, expressing or not FLIPs and treated for 24 hours with 25ng/ml FASL. Data are expressed as mean  $\pm$  S.D.  $n = 3$ . (G) Caspases activation (DEVDase activity) in the indicated SK-UT-1 cells, expressing or not FLIPs and treated for 24 hours with 25ng/ml of FASL. Data are expressed as mean  $\pm$  S.D.  $n = 3$ . (H) Histogram representing the percentage of PI positivity in the indicated SK-UT-1 cells, expressing or not FLIPs. Data are expressed as mean  $\pm$  S.D.  $n = 3$ . (I) Caspases activation (DEVDase activity) in the indicated SK-UT-1 cells, expressing or not FLIPs and treated for 24 hours with the indicated drugs. Data are expressed as mean  $\pm$  S.D.  $n = 3$ .

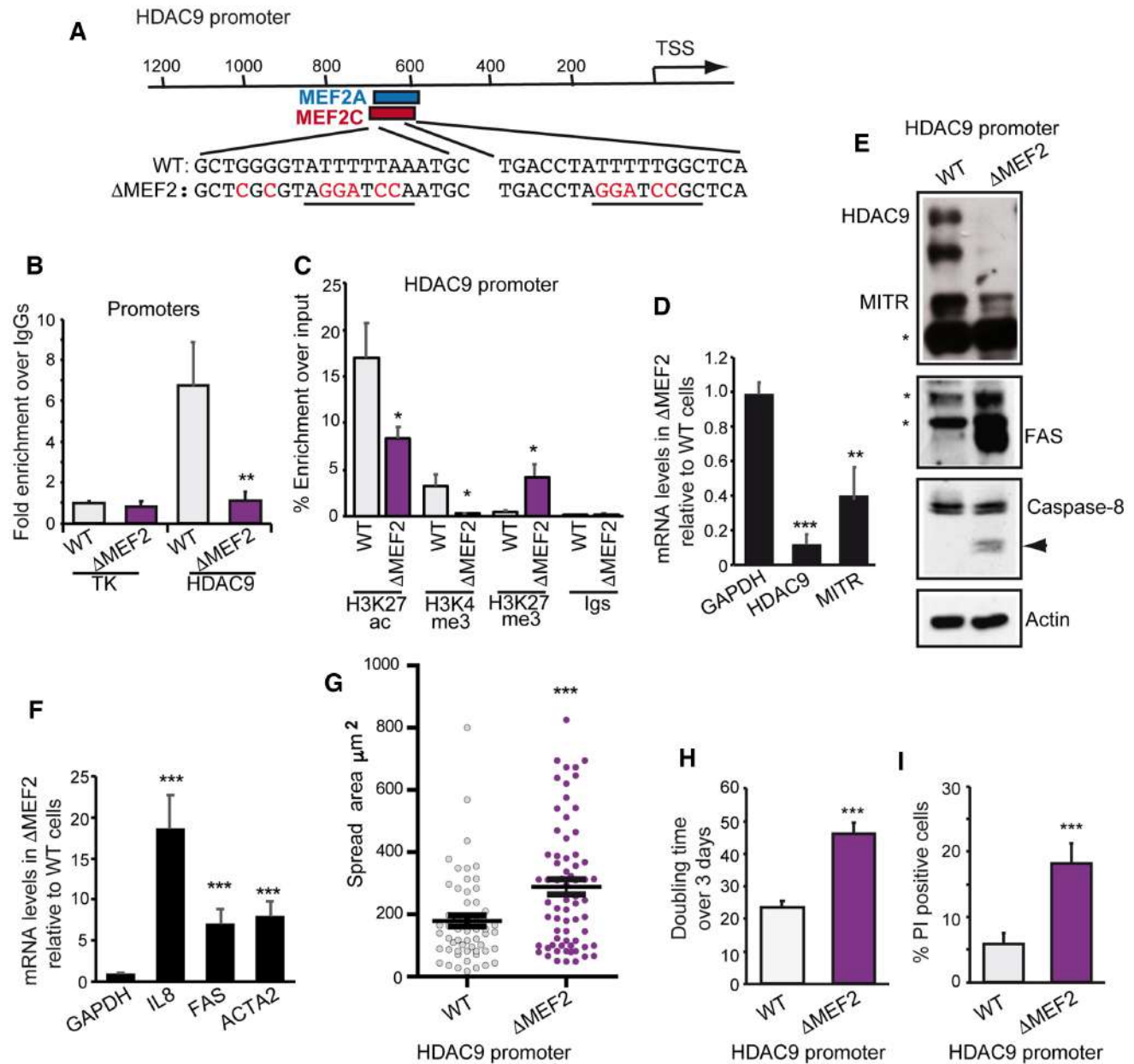


**Figure 9.** MEF2D regulative elements in the HDAC9 promoter are required for HDAC9 overexpression, FAS silencing and cell survival (A) Scheme of the CRISPR-mediated mutagenesis of the two MEF2-binding sites in the HDAC9 promoter (B) Chromatin was immunoprecipitated from SK-UT-1 cells WT or mutagenized in the 2 MEF2D binding sites, using anti-MEF2D antibody. Normal rabbit IgGs were used as control. The HDAC9 promoter region containing the MEF2 binding sites was amplified. Data are presented as mean  $\pm$  S.D.,  $n = 3$ . (C) Chromatin was immunoprecipitated using the anti-H3K4me3, anti-H3K27ac and anti-H3K27me3 antibodies from SK-UT-1 cells WT or mutagenized in the 2 MEF2D binding sites. Data are presented as mean and standard error.  $n = 3$ . (D) Relative mRNA expression levels of *GAPDH* and *HDAC9*, as measured by qRT-PCR in WT and SK-UT-1 cells with mutated MEF2 binding sites in the HDAC9 promoter ( $\Delta$ MEF2). Data are presented as mean  $\pm$  S.D.  $n = 3$ . (E) Immunoblot analysis of HDAC9, FAS, Caspase-8 and Actin in SK-UT-1 cells WT and with mutated MEF2 binding sites in the HDAC9 promoter ( $\Delta$ MEF2). Actin was used as loading control. Asterisks point to non-specific bands, arrowhead to the caspase-8 cleaved form. (F) Relative mRNA expression levels of *GAPDH*, *IL8*, *FAS* and *ACTA2*, as measured by qRT-PCR in WT and SK-UT-1 cells with mutated MEF2 binding sites in the HDAC9 promoter ( $\Delta$ MEF2). Data are presented as mean  $\pm$  S.D.  $n = 3$ . (G) Dot plot representing the spread area of the indicated SK-UT-1 cells. The median and the first and third quartiles are indicated.  $n > 70$ . (H) Histogram representing the doubling time of the indicated SK-UT-1 cells over a period of three days in culture. Data are presented as mean  $\pm$  S.D.  $n = 3$ . (I) Histogram representing the percentage of PI positivity in the indicated SK-UT-1 cells, growing in the absence of any added apoptotic insult. Data are presented as mean  $\pm$  S.D.  $n = 3$ .

neered SK-UT-1 cells ( $\Delta$ MEF2) (Figure 9B). As a consequence, epigenetic markers of open and active chromatin are reduced (H3K27ac and H3K4me3) while marker of closed/repressed chromatin (H3K27me3) appeared once MEF2 binding site were removed from the HDAC9 promoter. *HDAC9* mRNA levels were dramatically decreased (Figure 9C). Immunoblot analysis confirmed the strong downregulation of HDAC9 expression, the concomitant up-regulation of FAS and the activation of Caspase-8 (Figure 9D). Similarly to *FAS*, other HDAC9 target genes (*IL8* and *ACTA2*) were up-regulated at the mRNA level when the MEF2 binding sites in the *HDAC9* promoter were mutagenized (Figure 9E). Finally, cell spreading, growth arrest and cell death were all up-regulated in SK-UT-1 cells with mutated *HDAC9* promoter.

In summary, abrogation of MEF2 binding at the *HDAC9* promoter mirrors the effect of *HDAC9* deletion on SK-UT-1 cells survival.

## DISCUSSION

Dysregulations of class IIa HDACs expression have been reported in different tumors (1,3,6,13,46). How these alterations influence the epigenetic plasticity of cancer cells is still unknown. In this manuscript we have investigated the altered expression and dissected the functions of class IIa HDACs in LMS. These tumors are considered *genetically complex* soft tissue sarcomas, with a high mutational burden and a complex karyotype with several losses, gains and amplifications (19,47). Alterations in the PI3K/AKT/PTEN pathway, deletions of the tumor suppressors TP53 and RB1 and mutations in ATRX and MED12 (34,48,49) are frequent in LMS. Up-regulation of miR-143 and miR-145 and low expression of inflammatory response genes are also common in LMS (34). Approximately 30% of LMS express high levels of a class IIa HDACs, and of HDAC9 in particular (6).

We have demonstrated that the increased expression of HDAC9 stems from an alteration of the MEF2-HDAC feed-back loop. Silencing of MEF2D causes a parallel downregulation of HDAC9 levels and it is coupled to the appearance of a repressive epigenetic state at its promoter. Furthermore, the CRISPR-mediated deletion of the MEF2D binding sites in the HDAC9 promoter switches off HDAC9 transcription and perfectly recapitulates the proliferative defects of SK-UT-1 cells knocked out for HDAC9.

Our *in vitro* studies find substantiation *in vivo*. In LMS patients the high levels of HDAC9 are significantly correlated with high levels of MEF2D expression. A similar alteration in the MEF2-class IIa HDACs loop could be responsible for the overexpression of HDAC5. In this case MEF2A seems to be involved. Dysfunctions of the MEF2D-HDAC9 circuit might be common to other tumor types (50). For example in pre-B acute lymphoblastic leukemia, characterized by MEF2D translocations, HDAC9 is frequently up-regulated (11–13).

Three important questions still deserve specific answers: i) which is the mechanism that up-regulates MEF2D expression in LMS? ii) why does not the MEF2D-HDAC9 complex repress HDAC9 transcription, by binding the HDAC9 promoter? iii) why is the relationship between MEF2D and

HDAC9 so exclusive? Does HDAC9 play a different epigenetic role with respect to the other class IIa HDACs?

We do not have an answer to the first question. However, by defining the genomic binding sites for MEF2D, HDAC4 and HDAC9 we provide some cues to the others points.

Class IIa HDACs have been described as tissue specific deacetylases (1–3,46). Certain phenotypes, observed after members specific knock-outs in mice or ablation in human cells, have been explained as the consequence of their lineage-dependent expression (6,18,21,51–54). Our study demonstrates that further levels of complexity do exist. The first level concerns the genomic bindings. HDAC4 and HDAC9 share several genomic binding sites but HDAC4, in particular, binds many additional regions, which possibly escape a HDAC9-dependent regulation.

The second level of complexity concerns MEF2D. This important class IIa HDACs partner can assemble onto specific genomic regions both the HDAC4 and the HDAC9 repressive complexes, while in other regions only a specific repressive complex is recruited, most frequently containing HDAC4 rather than HDAC9. Through the selective recruitment of a specific HDAC or a combination of more HDACs, MEF2 can monitor different patterns of gene expression, as verified by the transcriptomic analysis and proved by the different genetic programs under the control of the two HDACs examined. Within this level of complexity also the MITR isoform can be included. In fact, although MITR has been described as a transcriptional repressor, it contains 16 aa of unknown function at the carboxy-terminus that differ from the HDAC9 canonical isoform (55). Perhaps this complex, when assembled on the HDAC9 promoter, could impair the manifestation of a full repressive state.

A third level of complexity is obtained by a locus-dependent influence of a specific class IIa HDAC. In fact, even though a region is characterized by the co-presence of MEF2D/HDAC4/HDAC9 complexes, frequently only a family member plays an active role in the epigenetic regulation. We define this phenomenon as the *dominant positional effect* of a specific class IIa HDAC. An example is the intergenic region distal from the *AHRGEF28* locus. This region shows features of an enhancer and through chromatin looping could regulate the expression of *ENC1*. Although both HDAC4 and HDAC9 bind this region, only the knock-out of HDAC9 increases H3K27ac levels at the enhancer and promoter sites thus augmenting *ENC1* expression.

In general, the paucity of promoter regions bound by HDAC9 suggests that this HDAC is recruited by MEF2D or by alternative TFs to repress gene expression principally from distal regulative elements showing features of enhancers.

Another important difference marks HDAC9 with respect to HDAC4. HDAC9 very rarely binds the genome in open chromatin regions, as defined by H3K27ac. This data indicates that HDAC9 typifies stably repressed chromatin domains while HDAC4 influences more dynamic genomic regions, or could suggest that HDAC4 acts as the priming pioneering repressive factor for HDAC9.

Finally, a further layer of regulation is represented by MEF2D complexes that are not recognized by both HDAC4 and HDAC9. Although a contribution of HDAC5

should be taken into account, the demonstration that MEF2A and MEF2D can still sustain transcription on specific loci discourages the HDAC5 hypothesis (6). On these loci, MEF2D acts positively by promoting the transcription of the associated genes. This evidence demonstrates that MEF2D has the capability to selectively escape the surveillance of class IIa HDACs on some well-defined genomic regions.

Despite the less numerous genomic binding sites and reduced number of genes under its influence, HDAC9 shows a strong impact on LMS cells proliferation. Cells deprived of HDAC9 show a higher apoptotic index that limits their prolonged maintenance in tissue culture. In this respect, we speculate that a certain degree of transcriptional heterogeneity, observed among the different *HDAC9*<sup>-/-</sup> clones, could reflect adaptive mechanisms that cells engage to survive the strong apoptotic pressure.

FAS up-regulation and the activation of the extrinsic pathway are responsible for the increased apoptotic pressure. Cytokines such as TNF- $\alpha$ , IL12 and IFN $\gamma$  can sustain FAS transcription through the engagement of NF- $\kappa$ B, SP1, STAT1 and IRF8 (56–60). Also TP53 family members are involved in FAS transcription (61,62).

We could not find HDAC9 and MEF2D binding sites at the promoter region of FAS. However H3K27ac was increased after the deletion of HDAC9, both at the promoter and at a distal site within the subTAD. This distal region can undergo looping with the FAS promoter.

How HDAC9 could influence H3K27 acetylation at the FAS/ACTA2 locus is mysterious. It could operate through a distal enhancers or indirectly by controlling the expression of specific TFs. In fact, approx. 10% of the genes repressed by HDAC9 encode for TFs or epigenetic regulators and among them SMAD3 has been demonstrated to up-regulate FAS transcription (63). Although FAS is a key element of the increased apoptotic response in HDAC9 deficient SK-UT-1 cells, MEF2 are pleiotropic TFs and in other contexts their pro-survival activities can be mediated by the regulation of different pro-survival or pro-death genes (64–66).

The impact of HDAC9 on LMS cells proliferation/survival is not limited to SK-UT-1 cells. DMR cells similarly overexpress HDAC9 and HDAC9 downregulation up-regulates FAS levels and triggers apoptosis in DMR cells too. We are confident that the repressive influence of HDAC9 on FAS transcription is a critical event for LMS survival/aggressiveness, as proved by the anti-correlation observed in tumors.

## CONCLUSIONS

LMS are aggressive cancers, local recurrence and metastasis develop in approximately 40% of cases, which drastically reduce survival (19,34,47–49). Under these conditions available therapies are largely ineffective and the identification of new therapeutic targets is mandatory. Our studies point to class IIa HDACs and HDAC9 in particular as interesting targets to revitalize the extrinsic apoptotic pathway. Furthermore, the simultaneous up-regulation of chemokines, cytokines and secreted factors, exemplified by CXCL1, IL8, THBS1 and CYR61, after HDAC9 depletion,

can sustain FAS-induced apoptosis and the action of the immune system for a better elimination of the neoplastic cells (67–69). This represent a strong incitement to evaluate HDAC9 inhibitors as possible onco-immunological drugs. Finally, we are confident that our deep investigation and description of the genomic preferences of MEF2D-HDAC4-HDAC9 complexes can fit to other models and help researchers in finding a genetic and epigenetic explanation to the pleiotropic actions of MEF2 TFs.

## DATA AVAILABILITY

The transcriptomic raw data are available as GEO accession GSE132569: [https://www.ncbi.nlm.nih.gov/geo/query/acc.cgi?acc = GSE132569](https://www.ncbi.nlm.nih.gov/geo/query/acc.cgi?acc=GSE132569).

Raw data corresponding to ChIP-seq experiments are uploaded with GEO accession GSE132622: [https://www.ncbi.nlm.nih.gov/geo/query/acc.cgi?acc = GSE132622](https://www.ncbi.nlm.nih.gov/geo/query/acc.cgi?acc=GSE132622).

The link to a UCSC genome browser session displaying the uploaded sequence tracks is [http://genome.ucsc.edu/s/DameBioinfo/DiGiorgio\\_et.al](http://genome.ucsc.edu/s/DameBioinfo/DiGiorgio_et.al).

## SUPPLEMENTARY DATA

Supplementary Data are available at NAR Online.

## ACKNOWLEDGEMENTS

We thank Michele Gentile for the help in some experiments and Dr Ed Seto for providing HDAC9 cDNA. We also thank ‘Studio Associato Molaro Pezzetta Romanelli Del Fabbro e associati’ for the donation of computing devices

## FUNDING

AIRC Associazione Italiana per la Ricerca sul Cancro [IG 15640]; POR-FESR regione Friuli-Venezia Giulia ATeNA and Sarcoma Foundation of America (to C.B.); EDG received an AIRC fellowship (Volontari Jesolo). Funding for open access charge: Sarcoma Foundation of America (SFA) Ricerca Libera Claudio Brancolini.

*Conflict of interest statement.* None declared.

## REFERENCES

- Parra, M. (2015) Class IIa HDACs - new insights into their functions in physiology and pathology. *FEBS J.* **282**, 736–744.
- Fitzsimons, H.L. (2015) The Class IIa histone deacetylase HDAC4 and neuronal function: Nuclear nuisance and cytoplasmic stalwart? *Neurobiol. Learn. Mem.*, **123**, 149–145.
- Di Giorgio, E. and Brancolini, C. (2016) Regulation of class IIa HDAC activities: it is not only matter of subcellular localization. *Epigenomics*, **8**, 251–269.
- Lahm, A., Paolini, C., Pallaoro, M., Nardi, M.C., Jones, P., Neddermann, P., Sambucini, S., Bottomley, M.J., Lo Surdo, P., Carfi, A. *et al.* (2007) Unraveling the hidden catalytic activity of vertebrate class IIa histone deacetylases. *Proc. Natl. Acad. Sci. U.S.A.*, **104**, 17335–17340.
- Park, S.-Y., Kim, G.S., Hwang, H.-J., Nam, T.-H., Park, H.-S., Song, J., Jang, T.-H., Lee, Y.C. and Kim, J.-S. (2018) Structural basis of the specific interaction of SMRT corepressor with histone deacetylase 4. *Nucleic Acids Res.*, **926**, 1–13.
- Di Giorgio, E., Franforte, E., Cefalù, S., Rossi, S., Dei Tos, A.P., Brenca, M., Polano, M., Maestro, R., Paluvai, H., Picco, R. *et al.* (2017) The co-existence of transcriptional activator and transcriptional

- repressor MEF2 complexes influences tumor aggressiveness. *PLoS Genet.*, **13**, 1–29.
7. Sparrow, D.B., Miska, E.A., Langley, E., Reynaud-Deonauth, S., Kotecha, S., Towers, N., Spohr, G., Kouzarides, T. and Mohun, T.J. (1999) MEF-2 function is modified by a novel co-repressor, MITR. *EMBO J.*, **18**, 5085–5098.
  8. Harris, L.G., Wang, S.H., Mani, S.K., Kasiganesan, H., Chou, C.J. and Menick, D.R. (2016) Evidence for a non-canonical role of HDAC5 in regulation of the cardiac *Ncx1* and *Bnp* genes. *Nucleic Acids Res.*, **44**, 3610–3617.
  9. Mathias, R.A., Guise, A.J. and Cristea, I.M. (2015) Post-translational modifications regulate class IIa histone deacetylase (HDAC) function in health and disease. *Mol. Cell Proteomics*, **14**, 456–470.
  10. Haberland, M., Arnold, M.A., McAnally, J., Phan, D., Kim, Y. and Olson, E.N. (2007) Regulation of HDAC9 gene expression by MEF2 establishes a negative-feedback loop in the transcriptional circuitry of muscle differentiation. *Mol. Cell Biol.*, **27**, 518–525.
  11. Gu, Z., Churchman, M., Roberts, K., Li, Y., Liu, Y., Harvey, R.C., McCastlain, K., Reshmi, S.C., Payne-Turner, D., Iacobucci, I. *et al.* (2016) Genomic analyses identify recurrent MEF2D fusions in acute lymphoblastic leukaemia. *Nat. Commun.*, **7**, 13331.
  12. Suzuki, K., Okuno, Y., Kawashima, N., Muramatsu, H., Okuno, T., Wang, X., Kataoka, S., Sekiya, Y., Hamada, M., Murakami, N. *et al.* (2016) MEF2D-BCL9 fusion gene is associated with high-risk acute B-cell precursor lymphoblastic leukemia in adolescents. *J. Clin. Oncol.*, **34**, 3451–3459.
  13. Di Giorgio, E., Hancock, W.W. and Brancolini, C. (2018) BBA - reviews on cancer MEF2 and the tumorigenic process, hic sunt leones. *BBA - Rev. Cancer*, **1870**, 261–273.
  14. Rad, R., Rad, L., Wang, W., Cadinanos, J., Vassiliou, G., Rice, S., Campos, L.S., Yusa, K., Banerjee, R., Li, M.A. *et al.* (2010) PiggyBac transposon mutagenesis: A tool for cancer gene discovery in mice. *Science*, **330**, 1104–1107.
  15. Di Giorgio, E., Clocchiatti, A., Piccinin, S., Sgorbissa, A., Viviani, G., Peruzzo, P., Romeo, S., Rossi, S., Dei Tos, A.P., Maestro, R. *et al.* (2013) MEF2 is a converging hub for HDAC4 and PI3K/Akt-induced transformation. *Mol. Cell Biol.*, **22**, 4473–4491.
  16. Lei, Y., Liu, L., Zhang, S., Guo, S., Li, X., Wang, J., Su, B., Fang, Y., Chen, X., Ke, H. *et al.* (2017) Hdac7 promotes lung tumorigenesis by inhibiting Stat3 activation. *Mol. Cancer*, **16**, 1–13.
  17. Paluvai, H., Giorgio, E. Di. and Brancolini, C. (2018) Unscheduled HDAC4 repressive activity in human fibroblasts triggers TP53-dependent senescence and favors cell transformation. *Mol. Oncol.*, **10**, 1–17.
  18. Cutano, V., Di Giorgio, E., Minisini, M., Picco, R., Dalla, E. and Brancolini, C. (2019) HDAC7-mediated control of tumor microenvironment maintains proliferative and stemness competence of human mammary epithelial cells. *Mol. Oncol.*, **13**, 1651–1668.
  19. Duffaud, F., Ray-Coquard, I., Salas, S. and Pautier, P. (2015) Recent advances in understanding and managing leiomyosarcomas. *F1000Prime Rep.*, **7**, 55.
  20. Ran, F.A., Hsu, P.D., Wright, J., Agarwala, V., Scott, D.A. and Zhang, F. (2013) Genome engineering using the CRISPR-Cas9 system. *Nat. Protoc.*, **8**, 2281–2308.
  21. Clocchiatti, A., Di Giorgio, E., Ingrao, S., Meyer-Almes, F.J., Tripodo, C. and Brancolini, C. (2013) Class IIa HDACs repressive activities on MEF2-dependent transcription are associated with poor prognosis of ER<sup>+</sup> breast tumors. *FASEB J.*, **27**, 942–954.
  22. Cersosimo, U., Sgorbissa, A., Foti, C., Drioli, S., Angelica, R., Tomasella, A., Picco, R., Semrau, M.S., Storici, P., Benedetti, F. *et al.* (2015) Synthesis, characterization, and optimization for in vivo delivery of a nonselective isopeptidase inhibitor as new antineoplastic agent. *J. Med. Chem.*, **58**, 1691–1704.
  23. Morgan, M., Anders, S., Lawrence, M., Aboyoun, P., Pagès, H. and Gentleman, R. (2009) ShortRead: a bioconductor package for input, quality assessment and exploration of high-throughput sequence data. *Bioinformatics*, **25**, 2607–2608.
  24. Langmead, B. and Salzberg, S.L. (2012) Fast gapped-read alignment with Bowtie 2. *Nat. Methods*, **9**, 357–360.
  25. Zhang, Y., Liu, T., Meyer, C.A., Eeckhoute, J., Johnson, D.S., Bernstein, B.E., Nusbaum, C., Myers, R.M., Brown, M., Li, W. *et al.* (2008) Model-based analysis of ChIP-Seq (MACS). *Genome Biol.*, **9**, R137.
  26. Yu, G., Wang, L. and He, Q. (2015) Genome analysis ChIPseeker: an R / Bioconductor package for ChIP peak annotation, comparison and visualization. *Bioinformatics*, **31**, 2382–2383.
  27. Durinck, S., Moreau, Y., Kasprzyk, A., Davis, S., De Moor, B., Brazma, A. and Huber, W. (2005) BioMart and Bioconductor: a powerful link between biological databases and microarray data analysis. *Bioinformatics*, **21**, 3439–3440.
  28. Durinck, S., Spellman, P.T., Birney, E. and Huber, W. (2009). Mapping identifiers for the integration of genomic datasets with the R/Bioconductor package biomaRt. *Nat. Protoc.*, **4**, 1184–1191.
  29. Hahne, F. and Ivanek, R. (2016). Visualizing genomic data using Gviz and bioconductor. *Methods Mol. Biol.*, **1418**, 335–351.
  30. Warnes, G.R., Bolker, B., Bonebakker, L., Gentleman, R., Huber, W., Liaw, A., Lumley, T., Maechler, M., Magnusson, A., Moeller, S. *et al.* (2019) gplots: Various R Programming Tools for Plotting Data. R package version 3.0.1.1.
  31. Shao, Z., Zhang, Y., Yuan, G.C., Orkin, S.H. and Waxman, D.J. (2012) Anorm: a robust model for quantitative comparison of ChIP-Seq data sets. *Genome Biol.*, **13**, R16.
  32. Subramanian, A., Tamayo, P., Mootha, V.K., Mukherjee, S., Ebert, B.L., Gillette, M.A., Paulovich, A., Pomeroy, S.L., Golub, T.R., Lander, E.S. *et al.* (2005) Gene set enrichment analysis: a knowledge-based approach for interpreting genome-wide expression profiles. *Proc. Natl. Acad. Sci. U.S.A.*, **102**, 15545–15550.
  33. Liberzon, A., Birger, C., Thorvaldsdóttir, H., Ghandi, M., Mesirov, J.P. and Tamayo, P. (2015) The molecular signatures database hallmark gene set collection. *Cell Syst.*, **6**, 417–425.
  34. Cancer Genome Atlas Research Network. (2017) Comprehensive and integrated genomic characterization of adult soft tissue sarcomas. *Cell*, **171**, 950–965.
  35. Paroni, G., Mizzau, M., Henderson, C., Del Sal, G., Schneider, C. and Brancolini, C. (2004) Caspase-dependent regulation of histone deacetylase 4 nuclear-cytoplasmic shuttling promotes apoptosis. *Mol. Biol. Cell*, **15**, 2804–2818.
  36. Shannon, P., Markiel, A., Ozier, O., Baliga, N.S., Wang, J.T., Ramage, D., Amin, N., Schwikowski, B. and Ideker, T. (2003) Cytoscape: a software environment for integrated models of biomolecular interaction networks. *Genome Res.*, **13**, 2498–2504.
  37. Bindea, G., Mlecnik, B., Hackl, H., Charoentong, P., Tosolini, M., Kirilovsky, A., Fridman, W.H., Pagès, F., Trajanoski, Z. and Galon, J. (2009) ClueGO: a Cytoscape plug-in to decipher functionally grouped gene ontology and pathway annotation networks. *Bioinformatics*, **25**, 1091–1093.
  38. Wales, S., Hashemi, S., Blais, A. and McDermott, J.C. (2014) Global MEF2 target gene analysis in cardiac and skeletal muscle reveals novel regulation of DUSP6 by p38MAPK-MEF2 signaling. *Nucleic Acids Res.*, **42**, 11349–11362.
  39. Taniguchi, M., Carreira, M.B., Cooper, Y.A., Bobadilla, A.C., Heinsbroek, J.A., Koike, N., Larson, E.B., Balmuth, E.A., Hughes, B.W., Penrod, R.D. *et al.* (2017) HDAC5 and its target gene, *Npas4*, function in the nucleus accumbens to regulate cocaine-conditioned behaviors. *Neuron*, **96**, 130–144.
  40. Azagra, A., Román-González, L., Collazo, O., Rodríguez-Ubreva, J., de Yébenes, V.G., Barneda-Zahonero, B., Rodríguez, J., Castro de Moura, M., Grego-Bessa, J., Fernández-Duran, I. *et al.* (2016) In vivo conditional deletion of HDAC7 reveals its requirement to establish proper B lymphocyte identity and development. *J. Exp. Med.*, **213**, 2591–2601.
  41. Rao, S.S.P., Huntley, M.H., Durand, N.C., Stamenova, E.K., Bochkov, I.D., Robinson, J.T., Sanborn, A.L., Machol, I., Omer, A.D., Lander, E.S. *et al.* (2014) A 3D map of the human genome at kilobase resolution reveals principles of chromatin looping. *Cell*, **159**, 1665–1680.
  42. Roy, S.S., Mukherjee, A.K. and Chowdhury, S. (2018) Insights about genome function from spatial organization of the genome. *Hum. Genomics*, **12**, 8.
  43. Wang, Y., Song, F., Zhang, B., Zhang, L., Xu, J., Kuang, D., Li, D., Choudhary, M.N.K., Li, Y., Hu, M. *et al.* (2018) The 3D Genome Browser: a web-based browser for visualizing 3D genome organization and long-range chromatin interactions. *Genome Biol.*, **19**, 151.
  44. Ienasescu, H., Li, K., Andersson, R., Vitezic, M., Rennie, S., Chen, Y., Vitting-Seerup, K., Lagoni, E., Boyd, M., Bornholdt, J., de Hoon, M.J. *et al.* (2016) On-the-fly selection of cell-specific enhancers, genes,

- miRNAs and proteins across the human body using SlideBase. *Database*, **26**, 2016.
45. Thome, M., Schneider, P., Hofmann, K., Fickenscher, H., Meinl, E., Neipel, F., Mattmann, C., Burns, K., Bodmer, J.L., Schröter, M. *et al.* (1997) Viral FLICE-inhibitory proteins (FLIPs) prevent apoptosis induced by death receptors. *Nature*, **386**, 517–521.
  46. Clocchiatti, A., Florean, C. and Brancolini, C. (2011) Class IIa HDACs: From important roles in differentiation to possible implications in tumorigenesis. *J. Cell Mol. Med.*, **15**, 1833–1846.
  47. Miettinen, M. (2014) Smooth muscle tumors of soft tissue and non-uterine viscera: biology and prognosis. *Mod Pathol.*, **27**(Suppl. 1), S17–S29.
  48. Hoang, N.T., Acevedo, L.A., Mann, M.J. and Tolani, B. (2018) A review of soft-tissue sarcomas: translation of biological advances into treatment measures. *Cancer Manag. Res.*, **10**, 1089–1114.
  49. Mäkinen, N., Aavikko, M., Heikkinen, T., Taipale, M., Taipale, J., Koivisto-Korander, R., Bützow, R. and Vahteristo, P. (2016) Exome sequencing of uterine leiomyosarcomas identifies frequent mutations in TP53, ATRX, and MED12. *PLoS Genet.*, **12**, e1005850.
  50. Gil, V.S., Bhagat, G., Howell, L., Zhang, J., Kim, C.H., Stengel, S., Vega, F., Zelent, A. and Petrie, K. (2016) Dereglated expression of HDAC9 in B cells promotes development of lymphoproliferative disease and lymphoma in mice. *Dis. Model Mech.*, **9**, 1483–1495.
  51. Chang, S., Young, B.D., Li, S., Qi, X., Richardson, J.A. and Olson, E.N. (2006) Histone deacetylase 7 maintains vascular integrity by repressing matrix metalloproteinase 10. *Cell*, **126**, 321–334.
  52. Pigna, E., Simonazzi, E., Sanna, K., Bernadzki, K.M., Proszynski, T., Heil, C., Palacios, D., Adamo, S. and Moresi, V. (2019) Histone deacetylase 4 protects from denervation and skeletal muscle atrophy in a murine model of amyotrophic lateral sclerosis. *EBioMedicine*, **40**, 717–732.
  53. Vega, R.B., Matsuda, K., Oh, J., Barbosa, A.C., Yang, X., Meadows, E., McAnally, J., Pomajzl, C., Shelton, J.M., Richardson, J.A. *et al.* (2004) Histone deacetylase 4 controls chondrocyte hypertrophy during skeletogenesis. *Cell*, **119**, 555–566.
  54. Chang, S., McKinsey, T.A., Zhang, C.L., Richardson, J.A., Hill, J.A. and Olson, E.N. (2004) Histone deacetylases 5 and 9 govern responsiveness of the heart to a subset of stress signals and play redundant roles in heart development. *Mol. Cell Biol.*, **24**, 8467–8476.
  55. Petrie, K., Guidez, F., Howell, L., Healy, L., Waxman, S., Greaves, M. and Zelent, A. (2003) The histone deacetylase 9 gene encodes multiple protein isoforms. *J. Biol. Chem.*, **278**, 16059–16072.
  56. Chan, H., Bartos, D.P. and Owen-Schaub, L.B. (1999) Activation-dependent transcriptional regulation of the human Fas promoter requires NF-kappaB p50-p65 recruitment. *Mol. Cell Biol.*, **19**, 2098–2108.
  57. Kühnel, F., Zender, L., Paul, Y., Tietze, M.K., Trautwein, C., Manns, M. and Kubicka, S. (2000) NFkappaB mediates apoptosis through transcriptional activation of Fas (CD95) in adenoviral hepatitis. *J. Biol. Chem.*, **275**, 6421–6427.
  58. Li-Weber, M., Laur, O., Dern, K. and Krammer, P.H. (2000). T cell activation-induced and HIV tat enhanced CD95(APO-1/Fas) ligand transcription involves NF-kappaB. *Eur. J. Immunol.*, **30**, 661–670.
  59. Zhou, Z., Lafleur, E.A., Koshkina, N.V., Worth, L.L., Lester, M.S. and Kleinerman, E.S. (2005). Interleukin-12 up-regulates Fas expression in human osteosarcoma and Ewing's sarcoma cells by enhancing its promoter activity. *Mol. Cancer Res.*, **3**, 685–691.
  60. Yang, D., Thangaraju, M., Browning, D.D., Dong, Z., Korchin, B., Lev, D.C., Ganapathy, V. and Liu, K. (2007) IFN regulatory factor 8 mediates apoptosis in nonhemopoietic tumor cells via regulation of Fas expression. *J. Immunol.*, **179**, 4775–4782.
  61. Gressner, O., Schilling, T., Lorenz, K., Schulze Schleithoff, E., Koch, A., Schulze-Bergkamen, H., Lena, A.M., Candi, E., Terrinoni, A., Catani, M.V. *et al.* (2005) TAp63alpha induces apoptosis by activating signaling via death receptors and mitochondria. *EMBO J.*, **24**, 2458–2471.
  62. Schilling, T., Schleithoff, E.S., Kairat, A., Melino, G., Stremmel, W., Oren, M., Krammer, P.H. and Müller, M. (2009) Active transcription of the human FAS/CD95/TNFRSF6 gene involves the p53 family. *Biochem. Biophys. Res. Commun.*, **387**, 399–404.
  63. Kim, S.G., Jong, H.S., Kim, T.Y., Lee, J.W., Kim, N.K., Hong, S.H. and Bang, Y.J. (2004) Transforming growth factor-beta 1 induces apoptosis through Fas ligand-independent activation of the Fas death pathway in human gastric SNU-620 carcinoma cells. *Mol. Biol. Cell*, **15**, 420–434.
  64. Estrella, N.L., Clark, A.L., Desjardins, C.A., Nocco, S.E. and Naya, F.J. (2015) MEF2D deficiency in neonatal cardiomyocytes triggers cell cycle re-entry and programmed cell death in vitro. *J. Biol. Chem.*, **290**, 24367–24380.
  65. Tobin, S.W., Hashemi, S., Dadson, K., Turdi, S., Ebrahimian, K., Zhao, J., Sweeney, G., Griggall, J. and McDermott, J.C. (2017) Heart Failure and MEF2 Transcriptome Dynamics in Response to  $\beta$ -Blockers. *Sci. Rep.*, **7**, 4476.
  66. Brown, F.C., Still, E., Koche, R.P., Yim, C.Y., Takao, S., Cifani, P., Reed, C., Gunasekera, S., Ficarro, S.B., Romanienko, P. *et al.* (2018) MEF2C Phosphorylation Is Required for Chemotherapy Resistance in Acute Myeloid Leukemia. *Cancer Discov.*, **8**, 478–497.
  67. Volpert, O.V., Zaichuk, T., Zhou, W., Reiher, F., Ferguson, T.A., Stuart, P.M., Amin, M. and Bouck, N.P. (2002) Inducer-stimulated Fas targets activated endothelium for destruction by anti-angiogenic thrombospondin-1 and pigment epithelium-derived factor. *Nat. Med.*, **8**, 349–357.
  68. Juric, V., Chen, C.C. and Lau, L.F. (2009) Fas-mediated apoptosis is regulated by the extracellular matrix protein CCN1 (CYR61) in vitro and in vivo. *Mol. Cell Biol.*, **29**, 3266–3279.
  69. Cullen, S.P., Henry, C.M., Kearney, C.J., Logue, S.E., Feoktistova, M., Tynan, G.A., Lavelle, E.C., Leverkus, M. and Martin, S.J. (2013) Fas/CD95-induced chemokines can serve as “find-me” signals for apoptotic cells. *Mol. Cell*, **49**, 1034–1048.

RESEARCH ARTICLE

# The co-existence of transcriptional activator and transcriptional repressor MEF2 complexes influences tumor aggressiveness

Eros Di Giorgio<sup>1</sup>, Elisa Franforte<sup>1</sup>, Sebastiano Cefalù<sup>1</sup>, Sabrina Rossi<sup>2</sup>, Angelo Paolo Dei Tos<sup>2,3</sup>, Monica Brenca<sup>4</sup>, Maurizio Polano<sup>4</sup>, Roberta Maestro<sup>4</sup>, Harikrishnareddy Paluvai<sup>1</sup>, Raffaella Picco<sup>1</sup>, Claudio Brancolini<sup>1\*</sup>

**1** Department of Medical and Biological Sciences, Università degli Studi di Udine, P.le Kolbe 4—Udine Italy, **2** Department of Anatomical Pathology, Treviso General Hospital, Treviso, Italy, **3** Department of Medicine, University of Padua, Padua, Italy, **4** Experimental Oncology 1, CRO National Cancer Institute, Aviano, Italy

\* [claudio.brancolini@uniud.it](mailto:claudio.brancolini@uniud.it)



**OPEN ACCESS**

**Citation:** Di Giorgio E, Franforte E, Cefalù S, Rossi S, Dei Tos AP, Brenca M, et al. (2017) The co-existence of transcriptional activator and transcriptional repressor MEF2 complexes influences tumor aggressiveness. *PLoS Genet* 13 (4): e1006752. <https://doi.org/10.1371/journal.pgen.1006752>

**Editor:** John C. McDermott, York University, Toronto, UNITED STATES

**Received:** January 17, 2017

**Accepted:** April 10, 2017

**Published:** April 18, 2017

**Copyright:** © 2017 Di Giorgio et al. This is an open access article distributed under the terms of the [Creative Commons Attribution License](https://creativecommons.org/licenses/by/4.0/), which permits unrestricted use, distribution, and reproduction in any medium, provided the original author and source are credited.

**Data Availability Statement:** All relevant data are within the paper and its Supporting Information files. Microarray data have been deposited in NCBI Gene Expression Omnibus (GEO) with GEO accession GSE94416.

**Funding:** This work was supported by AIRC (Associazione Italiana per la Ricerca sul Cancro) IG 15640 to CB and by Ministero della Salute (Ricerca Finalizzata) to RM and APDT. EDG. received the Alberta Baruchello e Maurizio Scalabrin fellowship

## Abstract

The contribution of MEF2 TFs to the tumorigenic process is still mysterious. Here we clarify that MEF2 can support both pro-oncogenic or tumor suppressive activities depending on the interaction with co-activators or co-repressors partners. Through these interactions MEF2 supervise histone modifications associated with gene activation/repression, such as H3K4 methylation and H3K27 acetylation. Critical switches for the generation of a MEF2 repressive environment are class IIa HDACs. In leiomyosarcomas (LMS), this two-faced trait of MEF2 is relevant for tumor aggressiveness. Class IIa HDACs are overexpressed in 22% of LMS, where high levels of MEF2, HDAC4 and HDAC9 inversely correlate with overall survival. The knock out of HDAC9 suppresses the transformed phenotype of LMS cells, by restoring the transcriptional proficiency of some MEF2-target loci. HDAC9 coordinates also the demethylation of H3K4me3 at the promoters of MEF2-target genes. Moreover, we show that class IIa HDACs do not bind all the regulative elements bound by MEF2. Hence, in a cell MEF2-target genes actively transcribed and strongly repressed can coexist. However, these repressed MEF2-targets are poised in terms of chromatin signature. Overall our results candidate class IIa HDACs and HDAC9 in particular, as druggable targets for a therapeutic intervention in LMS.

## Author summary

The tumorigenic process is characterized by profound alterations of the transcriptional landscape, aimed to sustain uncontrolled cell growth, resistance to apoptosis and metastasis. The contribution of MEF2, a pleiotropic family of transcription factors, to these changes is controversial, since both pro-oncogenic and tumor-suppressive activities have been reported. To clarify this paradox, we studied the role of MEF2 in an aggressive type of soft-tissue sarcomas, the leiomyosarcomas (LMS). We found that in LMS cells MEF2 become oncogenes when in complex with class IIa HDACs. We have identified different

from AIRC. MB was a FIRC fellow. The funders had no role in study design, data collection and analysis, decision to publish, or preparation of the manuscript.

**Competing interests:** The authors have declared that no competing interests exist.

sub-classes of MEF2-target genes and observed that HDAC9 converts MEF2 into transcriptional repressors on some, but not all, MEF2-regulated loci. This conversion correlates with the acquisition by MEF2 of oncogenic properties. We have also elucidated some epigenetic re-arrangements supervised by MEF2. In summary, our studies suggest that the paradoxical actions of MEF2 in cancer can be explained by their dual role as activators/repressors of transcription and open new possibilities for therapeutic interventions.

## Introduction

MEF2 is a family of transcriptional regulators involved in the control of pleiotropic responses during development and adult life. In vertebrates four members, MEF2A/B/C/D, compose the family. MEF2 are characterized by the presence of a highly conserved N-terminal MADS/MEF2 domain involved in dimerization and DNA-binding, followed by the less conserved C-terminal transactivation region [1]. Although some actions of MEF2 are redundant, functional studies have also credited specific activities to each member of the family [2–6].

The transcriptional programs under MEF2 supervision diverge in different cell types. MEF2-targets include genes involved in various differentiation activities [7–9]. Some of these targets must be switched off, if they are not part of the ongoing differentiation program, even though a transcriptionally active MEF2 is present in the same cell. Dominant epigenetic regulations and/or the existence of multiple MEF2 transcriptional partners contribute to orchestrate the context-dependent MEF2 transcriptional landscape [3,4,8]. The four family members and their splicing variants can provide further layers of complexity to the MEF2 transcriptome [10–13]. Furthermore, MEF2 can be converted into transcriptional repressors after the binding to Cabin1, G9a or class IIa HDACs [14–16]. Among these transcriptional co-repressors, class IIa HDACs (HDAC4/5/7/9) play a pivotal role and their activity is subjected to tight cellular and environmental controls [17].

Dysfunctions in MEF2 characterize several pathological conditions, including cognitive disorders, cardiac hypertrophy and cancer [18–21]. Specifically, pro-oncogenic roles of MEF2 have been reported for certain hematological malignancies and hepatocarcinomas, which are linked to the increased expression, mutations or genetic rearrangements of these TFs [22–27]. By contrast, actions as tumor suppressors have been described in the case of soft-tissue sarcomas or in the case of mutations, mostly of MEF2B, in non-Hodgking lymphomas [11, 28–30].

The antagonistic roles of MEF2 in oncogenesis, suggested by these studies, cannot be completely explained by the context-dependent regulation of their target genes [24, 30–32]. In this scenario, the ability of MEF2 to act either as transcriptional activators or as repressors on varying the environmental and genetic backgrounds has been so far underestimated. Hence, we decided to address this point by dissecting the contribution of MEF2 to the tumorigenic process using the leiomyosarcomas (LMS) as a model. LMS are rare soft tissue sarcomas showing certain degrees of smooth muscle differentiation [33, 34]. In this manuscript we have explored the transcriptional landscape and the epigenetic modifications under the control of these TFs in relation to the tumorigenic process.

## Results

### The MEF2-HDAC axis in leiomyosarcomas

We have previously observed that among STS, LMS evidenced the highest repression of a MEF2 signature, identified in HDAC4-transformed mouse fibroblasts and described in S1

[Table \[28\]](#). Hence, we used the LMS as a model to better explore the role of MEF2 on tumor aggressiveness. [Fig 1A](#) confirms that the MEF2-signature was significantly repressed in uterine LMS compared to benign leiomyomas and normal tissues. This repression could be mediated by the activation of the PI3K/AKT/SKP2 pathway, which triggers the degradation of MEF2 proteins [35]. Alternatively, it might depend on the engagement of MEF2 transcriptional repressors. In LMS, among the different MEF2-repressors, only HDAC4 and HDAC9 mRNA levels negatively correlate with the expression of MEF2-targets ([Fig 1B and 1C](#)). We validated these data by IHC analysis, scoring HDAC4, MEF2C and SKP2 levels in a Tissue-MicroArray (TMA) of 57 LMS. HDAC4 levels were increased in tumors featuring higher proliferative activity (Ki67 positivity and high mitotic index M.I.) ([Fig 1D and 1E](#) and [S2 Table](#)). Moreover, a negative correlation between SKP2 and MEF2C was significant only in samples characterized by low (<20) M.I. ([Fig 1F and 1G](#) and [S2 Table](#)). This observation suggests that SKP2-dependent degradation of MEF2C occurs preferentially in low proliferating tumors. Interestingly, in LMS showing the highest expression of MEF2, the Kaplan-Meier analysis indicates that high levels of class IIa HDACs are associated with reduced patients' survival ([Fig 1H](#)).

To prove the role of the MEF2-HDACs axis in LMS, we used well-established LMS cell lines. As a first step, we investigated if the repression of MEF2-target genes observed in LMS could be recapitulated in a cellular model. Two LMS cell lines, SK-LMS-1 and SK-UT-1, originally isolated from tumors with different grading (G2 and G3 respectively) [36], evidenced a robust decrease of MEF2 transcriptional activities, when compared to normal smooth muscle cells (SMC) ([Fig 1I](#)). Therefore, they could be used for our purpose.

### Differential regulation of MEF2 proteins in leiomyosarcoma cells

SK-LMS-1 and SK-UT-1 cells were characterized for the expression of MEF2D, MEF2C and HDAC4. The levels of HDAC4 were slightly increased in SK-UT-1 cells, whereas MEF2C and MEF2D levels were dramatically augmented ([Fig 2A](#)). Importantly, proteasome inhibition increased MEF2 levels only in SK-LMS-1. The UPS-independence and the high-levels of MEF2C and MEF2D in SK-UT-1 cells can be explained by the presence of a cytoplasmic retained, splicing variant of SKP2, the E3 ligase responsible for MEF2 poly-ubiquitylation [35, 37].

We also evaluated the expression of the ubiquitously expressed MEF2D $\alpha$ 1 isoform and of the muscle-specific splicing variant MEF2D $\alpha$ 2 [10]. MEF2D $\alpha$ 2 was expressed only in SK-LMS-1 cells ([Fig 2A](#)), in agreement with the less aggressive G2 phenotype. MG132 treatment did not influence MEF2D $\alpha$ 2 levels. This result indicates that the exon-switch allows escaping from inhibitory controls, probably because the  $\alpha$ 2 isoform is defective in SKP2-binding [35]. Similarly to MG132 treatment, the introduction of a dominant negative version of SKP2 (SKP2DN) augmented MEF2D $\alpha$ 1, but not MEF2D $\alpha$ 2 levels and only in SK-LMS-1 cells ([Fig 2B](#)). By contrast, introduction of an inducible version of SKP2 (SKP2-ER) diminished MEF2D levels in both cell lines ([Fig 2C](#)). Finally, poly-ubiquitylation of MEF2D $\alpha$ 1 can be abrogated in SK-LMS-1 cells in the presence of SKP2DN ([Fig 2D](#)), whereas this poly-ubiquitylation was almost undetectable in SK-UT-1 cells ([Fig 2E](#)). In summary, these data demonstrate that in the two LMS cells the MEF2-HDAC axis is subjected to different regulations.

### Context dependent pro-oncogenic and tumor-suppressive roles of MEF2D

To clarify the contribution of MEF2 to the tumorigenic process, we knocked down (KD) MEF2D expression in SK-LMS-1 using two different shRNAs ([Fig 3A](#)). MEF2D silencing was accompanied by the down-regulation of CDKN1A. mRNA quantities of a set of MEF2-target

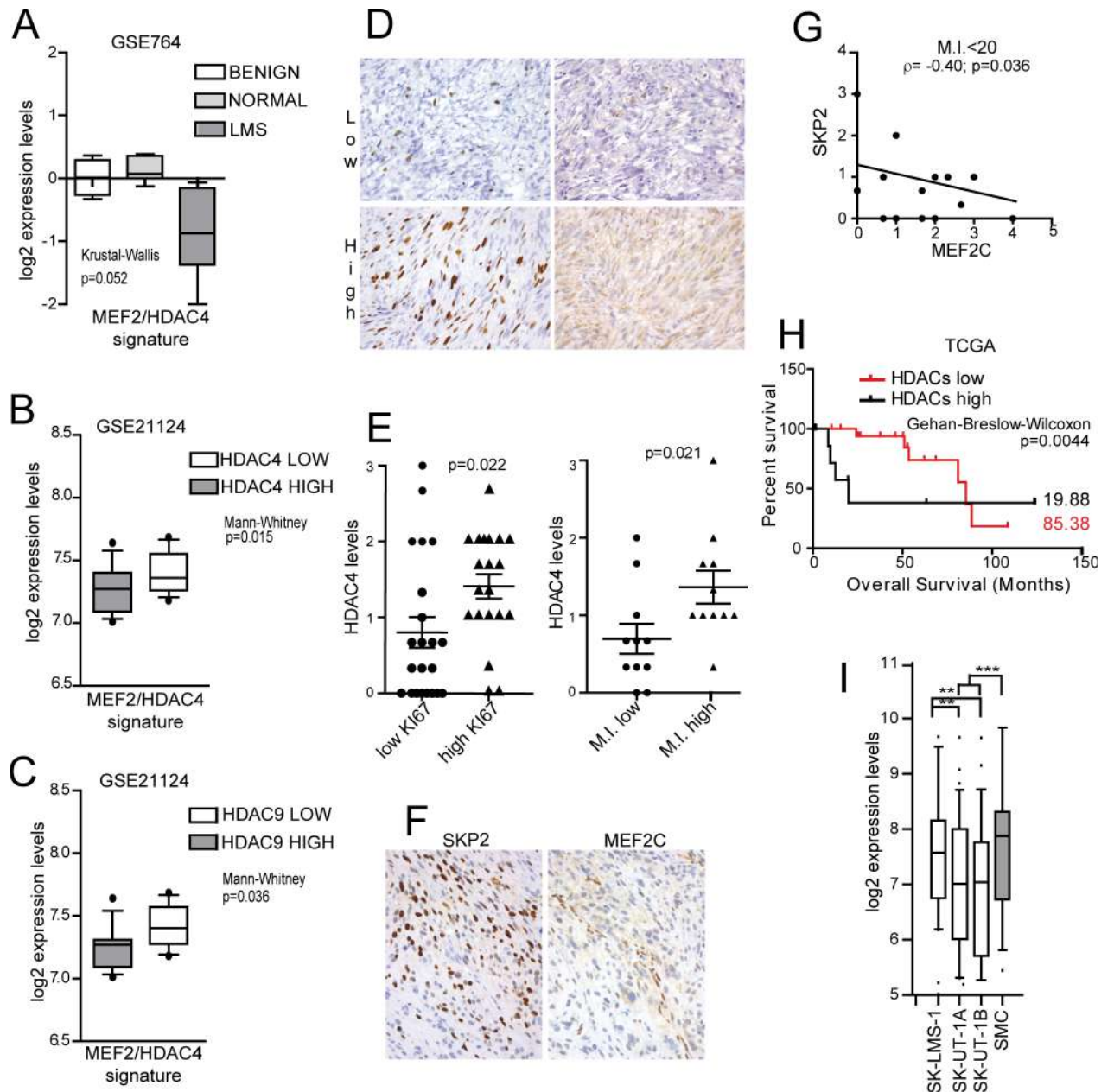


**Fig 1. Analysis of MEF2 signature, HDAC4, SKP2 and MEF2C expression levels in leiomyosarcomas.** A) Turkey box-plots illustrating the mRNA expression levels (GSE764) of MEF2-target genes in normal uterus, benign leiomyomas and malignant leiomyosarcomas. The latter are characterized by a significant (Kruskal-Wallis  $p < 0.1$ ) repression of MEF2 targets. B-C) The mRNA expression levels of the MEF2 targets in malignant leiomyosarcoma (GSE21124) were clustered in two sub-groups according to the expression levels of well-known MEF2 repressors (*HDAC4*, *HDAC5*, *HDAC7*, *HDAC9*, *CABIN1*). Only in the case of HDAC4 and HDAC9 a higher expression is significantly correlated to a decrease in the expression of MEF2 targets, as depicted in the Turkey box-plots. Mann-Whitney  $p < 0.05$ . D) Top pictures representing a case of uterine LMS with low Ki67 and weak and focal HDAC4 cytoplasmic expression; bottom pictures representing a case of uterine LMS with high Ki67 and diffuse cytoplasmic expression of HDAC4. E) IHC analysis of HDAC4 protein levels in LMS samples, clustered into two groups according to Ki67 positivity (1<sup>st</sup> quartile = low; 3<sup>rd</sup> quartile = high) (left) and M.I. (1<sup>st</sup> quartile = low; 3<sup>rd</sup> quartile = high) (right). Mann-Whitney  $p < 0.05$ .  $n = 22$ . F) A case of uterine LMS with nuclear expression of SKP2 in the majority of the cells and weak and focal cytoplasmic expression of MEF2C. Nuclear expression of MEF2C is present in non-neoplastic endothelial cells. Quantitative data are presented in S2 Table. G) Correlations between SKP2 and MEF2C protein levels in LMS samples, characterized by a M.I.  $< 20$ .  $n = 20$ .  $R^2 = 0.3$ . H) Kaplan-Meier survival analysis related to the expression levels of class IIa HDACs in TCGA LMS samples. From all cases ( $n = 106$ ), the ones characterized by high levels of MEF2s (above the third quartile,  $n = 26$ ) were analysed and clustered into two groups according to class IIa HDAC expression levels (high levels = above the third quartile,  $n = 8$ ); Wilcoxon  $p < 0.05$ . I) Turkey box-plots illustrating the mRNA expression levels (GSE39262) of MEF2 target genes in LMS cell lines (filled in white) compared to the normal smooth muscle cells (filled in gray). Anova  $p < 0.05$ , Turkey  $p < 0.05$ . \*  $p < 0.05$ , \*\*  $p < 0.01$ , \*\*\*  $p < 0.001$

<https://doi.org/10.1371/journal.pgen.1006752.g001>

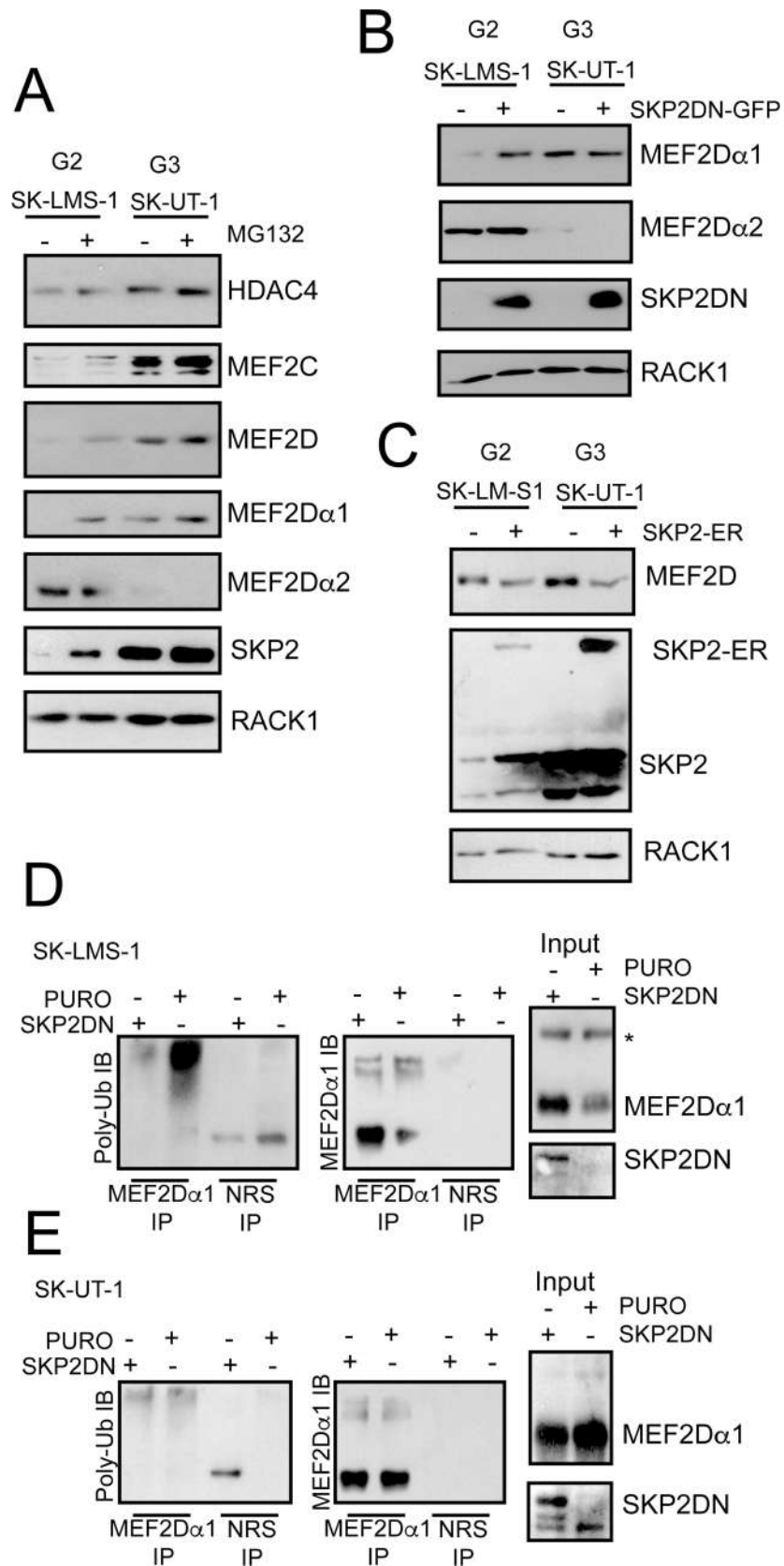


**Fig 2. Defect in UPS-mediated MEF2-degradation in the most aggressive LMS cell line.** A) Immunoblot analysis of HDAC4, SKP2 and MEF2 family members in LMS cells. Cells were treated for 8 hours with 2.5 $\mu$ M of the UPS inhibitor MG132. RACK1 was used as loading control. B) Immunoblot analysis of MEF2D isoforms in LMS cells engineered to express the dominant negative version of SKP2 (DN). RACK1 was used as loading control. C) Immunoblot analysis of MEF2D in LMS cells engineered to express an inducible version of SKP2 fused to ER as indicated. SKP2 was induced for 30 hours with 0.5 $\mu$ M 4-OHT. RACK1 was used as loading control and the nuclear relocalization of SKP2 after 4-OHT treatment was scored by immunofluorescence. D) Cellular lysates obtained in SK-LMS-1 cells expressing the DN mutant of SKP2 were immunoprecipitated using anti-MEF2D $\alpha$ 1 antibody and immunoblotted with the indicated antibodies. Immunoblots with total lysates (input) are also included. E) Cellular lysates obtained in SK-UT-1 cells expressing the DN mutant of SKP2 were immunoprecipitated using anti-MEF2D $\alpha$ 1 isoform and immunoblotted with the indicated antibodies. Immunoblots with total lysates (input) using the indicated antibodies are also included.

<https://doi.org/10.1371/journal.pgen.1006752.g002>

genes (*CDKN1A*, *KLF2*, *RHOB*, *CDKN1A*, *JUN*, *CNN1*, *IRS1*) were reduced in MEF2D silenced cells (Fig 3B). In SK-LMS-1 cells, MEF2D KD increases the number of cells in S phase (Fig 3C), the random cell motility (Fig 3D) and invasiveness, as scored by *in vitro* Matrigel invasion assay (Fig 3E and S1 Fig). Finally, to complete the analysis of the tumorigenic properties, we investigated the ability to grow in soft agar. SK-LMS-1 cells with KD MEF2D develop a higher number of colonies, when grown in soft agar (Fig 3F).

When MEF2D expression was down-regulated in SK-UT-1 cells (Fig 3G) the scenario was the opposite. *CDKN1A* was not affected, and other MEF2-targets showed a heterogeneous behavior (Fig 3H). *RHOB* and *CNN1* expression was down-regulated, whereas *KLF2*, *JUN* and *IRS1* were up-regulated. DNA replication was not augmented, instead a trend toward a slight reduction was observed (Fig 3I). The random cell motility, the invasiveness properties and the growth in soft agar were all impaired in SK-TU-1 cells KD for MEF2D (Fig 3J, 3K and 3L and S1 Fig).

To exclude that the opposite tumorigenic functions of MEF2D were due to the presence of the muscle-specific MEF2D $\alpha$ 2 splicing variant only in SK-LMS-1 cells, we specifically silenced the MEF2D $\alpha$ 1 isoform. We then compared the phenotype with the KD of both  $\alpha$ 1 and  $\alpha$ 2 isoforms (S2A and S2B Fig). Expression of MEF2-target genes was similarly repressed in cells silenced for both isoforms or for only the  $\alpha$ 1 (S2C Fig). In addition, the impact on the growth in soft agar was undistinguishable between cells KD for both isoforms or only for the MEF2D $\alpha$ 1 splicing variant (S2D Fig).

After MEF2D, MEF2A is the MEF2 paralogue more expressed in LMS. We then asked whether also MEF2A plays a similar bi-faced role. MEF2A silencing in SK-LM-1 cells photo-copied the MEF2D KD in terms of MEF2-target genes expression (S3A and S3B Fig), proliferation, cell motility, invasiveness and growth in soft agar (S3C, S3D, S3E and S3F Fig). Also in SK-UT-1 cells MEF2A silencing replicated MEF2D KD. Certain MEF2-targets were up-regulated (*KLF2*, *JUN*, *IRS1*) (S3G and S3H Fig), random cell motility, invasiveness and growth in soft agar were all impaired in MEF2A silenced cells (S3J, S3K and S3L Fig). In summary these data demonstrate that MEF2 exert opposite transforming activities in the two LMS cells.

## HDAC4 binding to promoters of MEF2-target genes is increased in SK-UT-1 cells

Our data indicate that only in SK-UT-1 cells MEF2 can exert a dominant repressive influence on certain targets. Well-known repressive partners of these TFs are the class IIa HDACs [17]. Hence, we compared the status of HDAC4 among the two cell lines. HDAC4 levels were increased in SK-UT-1 cells (Fig 2A) and also its nuclear/pan fraction (Fig 4A). In both LMS cells, HDAC4 underwent nuclear/cytoplasmic shuttling, as proved by the nuclear accumulation in response to leptomycin treatment.

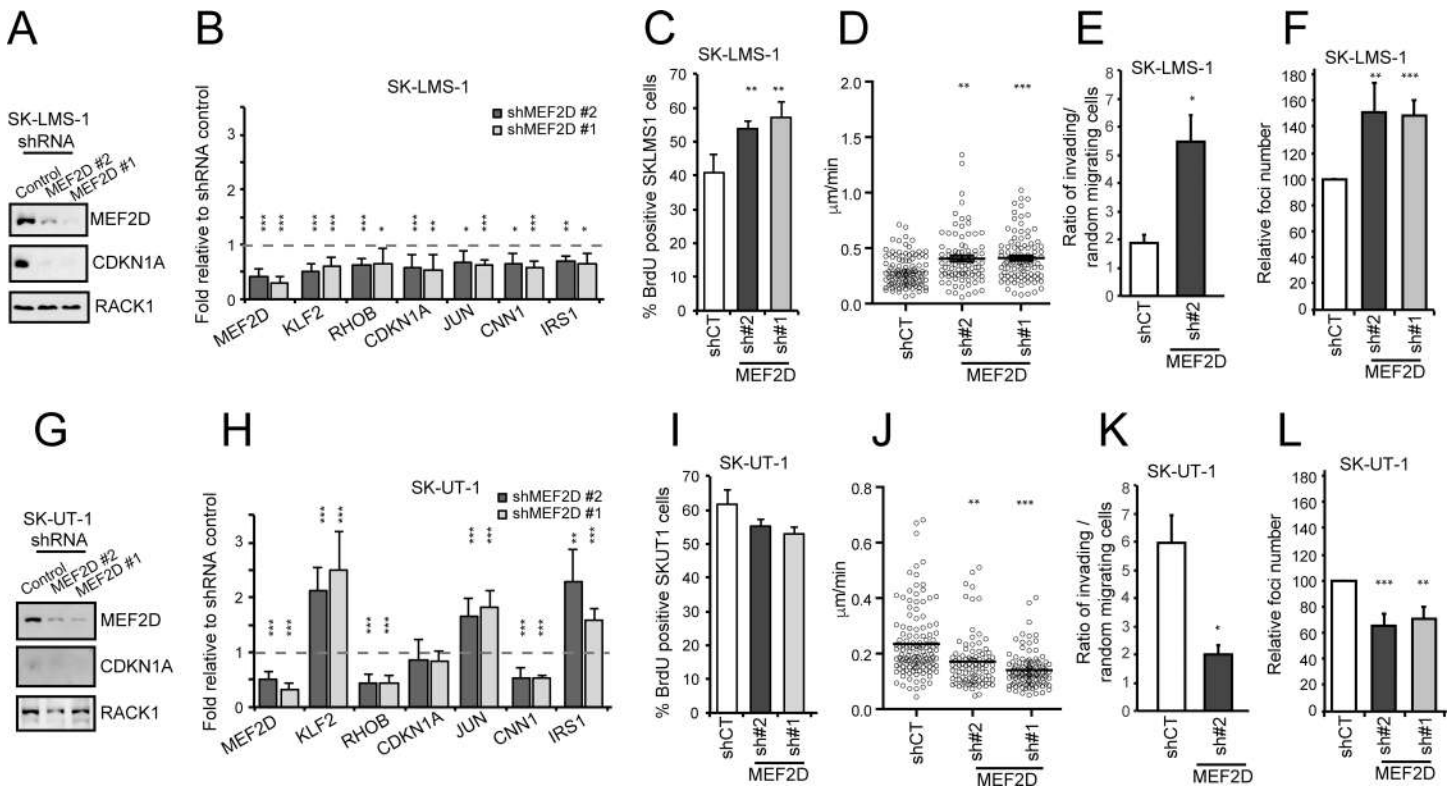


**Fig 3. MEF2 silencing causes opposite effect in SK-LMS-1 and SK-UT-1 cells.** A) MEF2D expression was silenced by lentiviral infection using two different shRNAs. Immunoblot analysis of MEF2D and CDKN1A levels in SK-LMS-1 cells expressing the control shRNA or two different shRNAs against MEF2D. RACK1 was used as loading control. B) qRT-PCR analysis of mRNA expression levels of MEF2D and of some MEF2-target genes (*KLF2*, *RHOB*, *CDKN1A*, *JUN*, *CNN1*, *IRS1*) in SK-LMS-1 cells expressing the different shRNAs. mRNA levels are relative to control shRNA. Data are presented as mean  $\pm$  SD; n = 4. C) Analysis of the cells synthesizing DNA as scored after BrdU staining. Mean  $\pm$  SD; n = 3. D) SK-LMS-1 cells expressing the indicated shRNAs were seeded at  $2 \times 10^4$ /ml in plates coated with 10  $\mu$ g/ml fibronectin, or BSA; after 16h they were subjected to time-lapse analysis for 6 hours. Results represent the individual migration rate and the average (bar) from at least 140 cells from three independent experiments. Mean and SEM are indicated. E) Invasion properties of the SK-LMS-1 cells expressing the shRNA2 against MEF2D or the control. Data are presented as mean  $\pm$  SD; n = 4. Invasion of the Matrigel was scored after 16 hours and was expressed as ratio between cells invading the matrix in presence (oriented motility) and absence (random invasion) of the chemoattractant. Cells were evidenced with Hoechst 33342 staining. At least 5 fields for each condition were acquired and the invading cells were counted by using ImageJ. F) Growth in soft agar of SK-LMS-1 cells expressing the indicated shRNAs, foci were stained with MTT and counted. Data are presented as mean  $\pm$  SD; n = 4. G) MEF2D expression was silenced by lentiviral infection using two different shRNAs. Immunoblot analysis of MEF2D and CDKN1A levels in SK-UT-1 cells expressing the control shRNA or two different shRNAs against MEF2D. RACK1 was used as loading control. H) qRT-PCR analysis of mRNA expression levels of MEF2D and of some MEF2-target genes (*KLF2*, *RHOB*, *CDKN1A*, *JUN*, *CNN1*, *IRS1*) in SK-UT-1 cells expressing the different shRNAs. mRNA levels are relative to control shRNA. Data are presented as mean  $\pm$  SD; n = 4. I) Analysis of the cells synthesizing DNA as scored after BrdU staining. Mean  $\pm$  SD; n = 3. J) SK-UT-1 cells expressing the indicated shRNAs were subjected to time-lapse analysis for 6 hours as in Fig 3D. Results represent the individual migration rate and the average (bar) from at least 140 cells from three independent experiments. Mean and SEM are indicated. K) Invasion properties of the SK-UT-1 cells expressing the shRNA2 against MEF2D or the control. Data are presented as mean  $\pm$  SD; n = 4. Invasion of the Matrigel was scored after 16 hours and was expressed as ratio between cells invading the matrix in presence (oriented motility) and absence (random invasion) of the chemoattractant. Cells were evidenced with Hoechst 33342 staining. At least 5 fields for each condition were acquired and the invading cells were counted by using ImageJ. L) Growth in soft agar of SK-UT-1 cells expressing the indicated shRNAs, foci were stained with MTT and counted. Data are presented as mean  $\pm$  SD; n = 4. \* p < 0.05, \*\* p < 0.01, \*\*\* p < 0.001

<https://doi.org/10.1371/journal.pgen.1006752.g003>

Also the pool of MEF2D in complex with HDAC4 was greater in SK-UT-1 cells (Fig 4B). Finally, the binding of MEF2D and HDAC4 to the promoters of a set of well-known MEF2--target genes (*IRS1*, *JUN*, *CDKN1A*, *KLF2*, *RHOB*) between the two LSM cell lines was assessed and compared (Fig 4C). Except for *IRS1* and *CDKN1A*, the binding of MEF2D to the different promoters was similar between the two LMS cells. By contrast, the binding of HDAC4 to *JUN* and *KLF2* promoters was more pronounced in SK-UT-1 cells. Importantly, the expression of these genes was augmented in these cells after MEF2 silencing. Accordingly, binding of

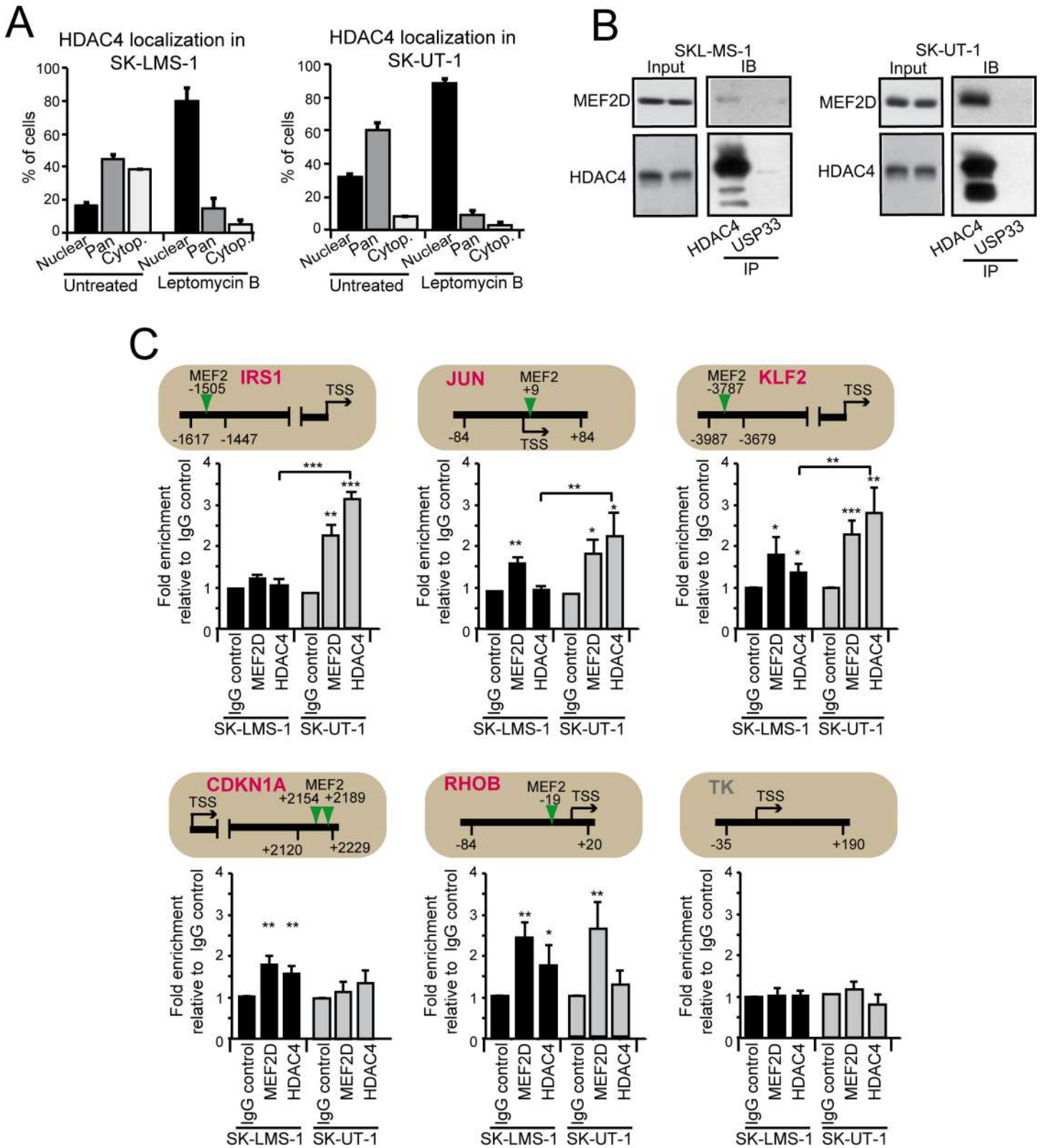


**Fig 4. Analysis of MEF2D-HDAC4 repressive complexes in LMS cells.** A) Quantitative analysis of the immunofluorescence studies. LMS cells were treated or not for 2 hours with 5ng/ml leptomycin B (LC Laboratories). After fixation of the cells, immunofluorescence analysis was performed to visualize HDAC4. Nuclei were stained with Hoechst 33342. Data are presented as mean  $\pm$  SD (n = 3). B) MEF2D-HDAC4 complexes were immunoprecipitated using 1 $\mu$ g of anti-

HDAC4, or anti-USP33, as a control, antibodies. Immunoblotting using an anti-MEF2D antibody was next used for the detection. The same amounts of cellular lysates were immunoprecipitated and the immunoblot were developed under the same circumstances. C) Chromatin was immunoprecipitated from SK-LMS-1 or SK-UT-1 cells using the anti-MEF2D and the anti-HDAC4 antibodies. Anti-FLAG antibody was used as control. *TK* promoter was used as negative control. The MEF2 binding site, the amplified region and the TSS are indicated for each tested gene, respectively with a vertical arrow, two arrowheads and a horizontal arrow. The *TK* promoter was used as negative control.

<https://doi.org/10.1371/journal.pgen.1006752.g004>

HDAC4 to *RHOB* promoter, whose expression was reduced in both LMS cell lines after MEF2 silencing, was undetectable in SK-UT-1 cells. Finally, ChIP-reChIP experiments confirmed the co-occupancy by MEF2D and HDAC4 of *KLF2* but not of *RHOB* promoter (S4 Fig).

### HDAC9 expression is highly induced in SK-UT-1 cells and in a relevant proportion of LMS *in vivo*

By scrutinizing a public available database (<http://www.cbioportal.org/>), we noticed that also the expression of HDAC5 and HDAC9, but not of HDAC7, was augmented in certain LMS patients (Fig 5A). Collectively, approximately 22% of patients present increased expression of a class IIa HDAC member. This feature is mirrored in the SK-UT-1 cells, which are characterized by high levels of HDAC9 and by a reduction in HDAC7 expression (Fig 5B). Only in SK-UT-1 cells, proteasome inhibition increased the amount of HDAC9. Conversely, MG132 treatment stabilized MEF2A in SK-LMS-1 cells but not in SK-UT-1 cells, as above described for MEF2C and MEF2D. The high levels of HDAC9 in SK-UT-1 cells correlate with the augmented levels of the corresponding mRNA (Fig 5C). Luciferase assay using the HDAC9 promoter demonstrated that the high levels of HDAC9 in SK-UT-1 cells arise from an increased transcriptional activity (Fig 5D). ChIP on this promoter demonstrated a dramatic enrichment of an epigenetic signature (H3K27ac and H3K4me3), typical of open chromatin/active transcription only in SK-UT-1 cells (Fig 5E). Finally, ChIP experiments demonstrated a selective binding of HDAC9 to the promoters of certain MEF2-target genes (*KLF2* and *IRS1*) only in SK-UT-1 cells. By contrast, MEF2A binding to the same promoters occurs in both LMS cells (Fig 5F). In summary these data demonstrate that class IIa HDACs are overexpressed in 22% of LMS and that SK-UT-1 cells recapitulate this alteration.

### MEF2A and MEF2D-dependent transcriptional landscapes in LMS cells: definition of *classical* and *atypical* target genes

To comprehend the molecular basis responsible for the antagonistic effects of MEF2 on cancer aggressiveness, we compared the transcriptomes of the different MEF2 KD LMS cells. Several genes resulted modulated in a MEF2-dependent manner (Fig 6A). In addition to a pool of genes commonly regulated by MEF2D and MEF2A, we observed that in both cell lines some genes are under the specific regulation of one of the two paralogues (Fig 6A). For the purposes of this work we focused our attention only on genes commonly regulated by MEF2D and MEF2A. Gene-Ontology analysis revealed that in SK-LMS-1 cells, the KD of MEF2 elicits the down-modulation of genes involved in the epithelial/mesenchymal transition and in inflammation, while genes involved in proliferation and cell-cycle progression were up-regulated (Fig 6B upper part). Interestingly, both MEF2 KDs show opposite effects in SK-UT-1 cells, since genes involved in inflammation and epithelial/mesenchymal transition were instead up-regulated, while the E2F targets were repressed (Fig 6B).

Several genes down-regulated after MEF2D and MEF2A KDs in SK-LMS-1 cells were, on the opposite, up-regulated in SK-UT-1 cells after the same KDs (Fig 6C). This evidence suggests that MEF2 can preferentially behave as transcriptional activators in SK-LMS-1 cells and as transcriptional repressors in SK-UT-1 cells. To better clarify this occurrence, we focused

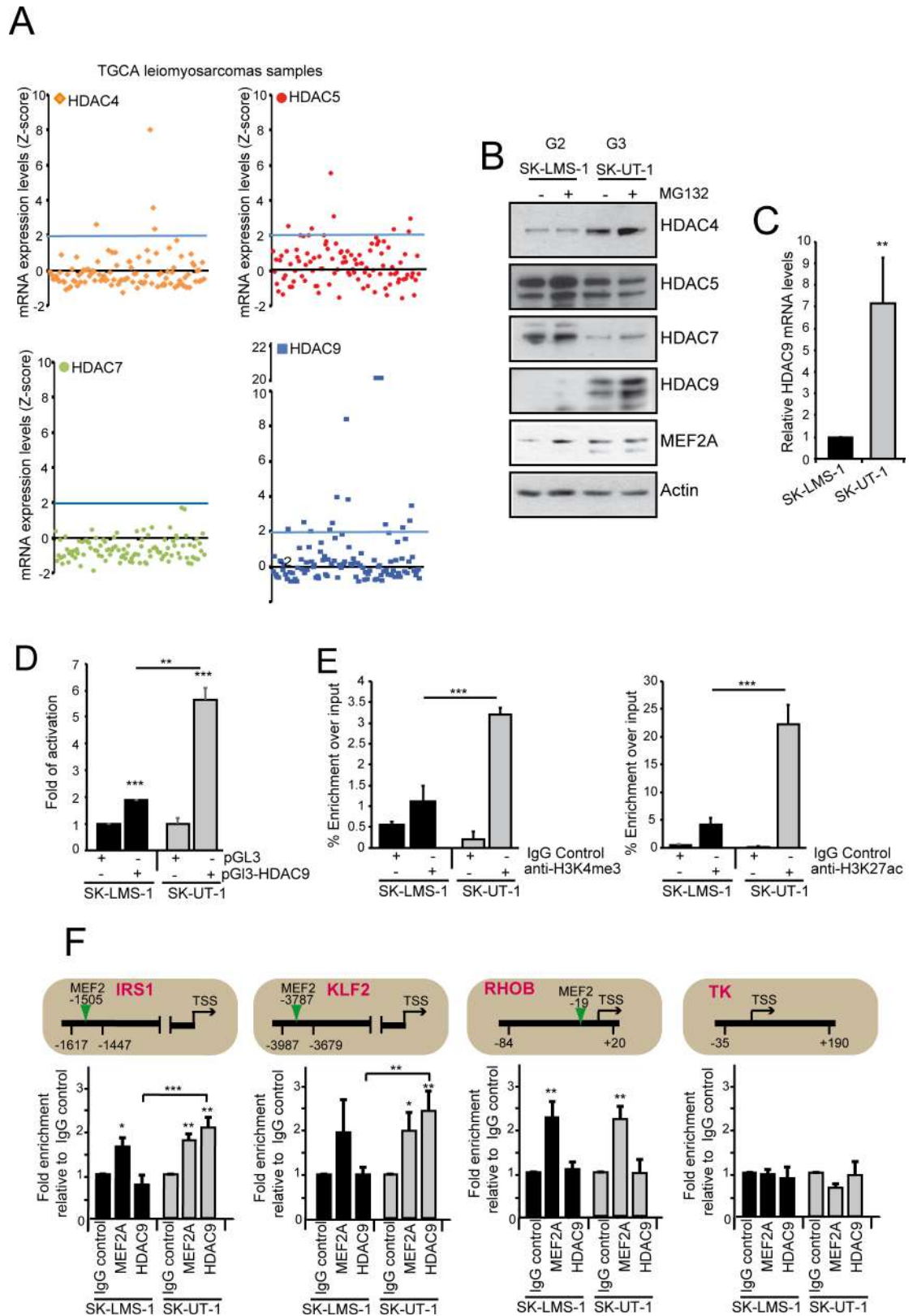


**Fig 5. Class IIa HDACs expression in LMS.** A) TCGA samples of leiomyosarcomas were analysed for the mRNA expression levels of the different class IIa HDACs. Individual tumors ( $n = 106$ ) were aligned along the x axis. Data were

extracted from CBio Portal (<http://www.cbioportal.org/>). B) Immunoblot analysis of class IIa HDACs family members and MEF2A in LMS cells. Cells were treated for 12 hours with 1  $\mu$ M of MG132. Actin was used as loading control. C) *HDAC9* mRNA expression levels in the two LMS cell lines. Data are presented as mean  $\pm$  SD; n = 3. D) Luciferase activity after transfection in LMS cells of the empty plasmid pGL3 or the same plasmid with cloned the *HDAC9* promoter isolated from SK-LMS-1 cells (bp -1160/+23). The Renilla luciferase plasmid was used as an internal control. Data are presented as mean  $\pm$  SD; n = 3. E) ChIP analysis of the chromatin status in the *HDAC9* promoter. Chromatin was immunoprecipitated from SK-LMS-1 or SK-UT-1 cells using the anti-H3K4me3 and anti-H3K27ac antibodies. Normal rabbit IgGs were used as control. Data are presented as mean  $\pm$  SD; n = 3. F) Chromatin was immunoprecipitated from SK-LMS-1 or SK-UT-1 cells using the anti-MEF2A and the anti-*HDAC9* antibodies. Normal rabbit IgGs were used as control. *TK* promoter was used as negative control. The MEF2 binding site, the amplified region and the TSS are indicated for each tested gene, respectively with a vertical arrow, two arrowheads and a horizontal arrow. \* p < 0.05, \*\* p < 0.01, \*\*\* p < 0.001

<https://doi.org/10.1371/journal.pgen.1006752.g005>

our analysis on 85 genes, which, in SK-LMS-1 cells, were repressed after MEF2D as well as after MEF2A silencing and that were also significantly modulated in SK-UT-1 cells ( $|FC| > 1.5$ ,  $p < 0.05$ ; [S3 Table](#)).

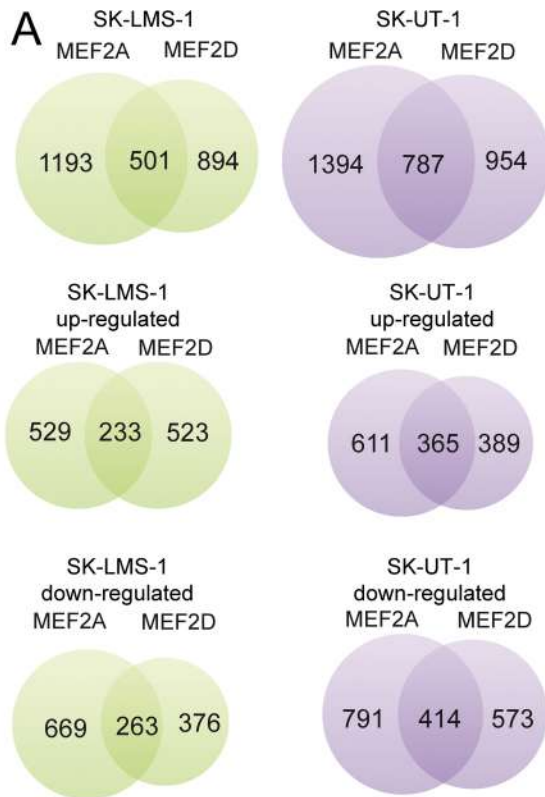
Many (n = 58) of these 85 MEF2-target genes were up-regulated in SK-UT-1 cells after MEF2 KD ([Fig 6D and 6E](#)). We defined as “atypical loci” genes that were up-regulated after MEF2 silencing in SK-UT-1 cells, and as “classical loci” genes repressed by the KD of MEF2 in both cell lines. By contrast, the majority of genes up-regulated by MEF2 KD in SK-LMS-1 cells (n = 52) were also up-regulated (n = 45) by MEF2 KD in SK-UT-1 cells ([Fig 6F](#)). Hence, the “atypical” behavior specifically originates in SK-UT-1 cells, because of a shift towards a repressive environment under MEF2 supervision. These common MEF2-target genes, with divergent behavior, could be responsible for the antagonistic effects of MEF2 on cancer aggressiveness in the two LMS cells.

We also compared the absolute levels of expression of the classical and atypical genes between the two LMS cells. Only the atypical genes were significantly less expressed in SK-UT-1 compared to SK-LMS-1 cells, both in our microarray experiments and in another dataset ([Fig 6G](#)).

To validate the microarray studies, we performed qRT-PCR analysis on sets of classical (*ALDH2*, *ALDH6A1*, *MDX4*, *FUCA1*) and atypical (*ALPK2*, *COL1A2*, *IL8*, *SMOX*, *LEPREL1*) MEF2-targets. The expression of all classical genes was reduced in both LMS cells when MEF2A or MEF2D were silenced ([S5A](#), [S5B](#), [S5C](#) and [S5D Fig](#)). By contrast, only in SK-UT-1 cells the expression of the atypical MEF2-targets was up-regulated after MEF2A or MEF2D KD ([S5B](#) and [S5D Fig](#)). We also compared the binding of MEF2 to the promoters of the newly identified genes in both LMS cells. The positions of the MEF2 binding sites in the regulatory elements of these genes are shown in [S4 Table](#). All tested MEF2-targets contain the consensus-binding site for MEF2, although at different distances from the TSS ([S5E Fig](#)). MEF2D equally binds the promoters of classical and atypical genes and this binding was dramatically reduced in MEF2D silenced cells ([S5E Fig](#)). In summary these data demonstrate that MEF2 can exert opposite transcriptional influences in different contexts.

## MEF2 differentially supervise epigenetic changes at the promoters of classical and atypical genes

We hypothesized that the differential transcriptional impact of MEF2 KD in the two LMS cells might reflect a specific epigenetic reprogramming. Since MEF2 can recruit HATs and HDACs onto promoter/enhancer of target genes [[35](#), [38](#)], levels of H3K27 acetylation were measured for a selected set of atypical genes (*ALPK2*, *COL1A2*, *IL8*, *KLF2*, *SMOX*) and of classical genes (*ALDH6A1*, *FUCA1*, *MDX4*, *RHOB*). We also evaluated the status of H3K4me3 at the TSSs, since this modification is associated to transcriptionally active open chromatin. Data are



**B**

*MEF2-regulated genes in SK-LMS-1*

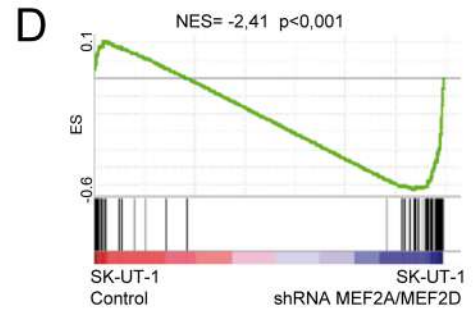
Rank	Gene set	NES	p-value	FDR q-value
1	Epithelial Mesenchymal Transition	2.877	0.000	0.000
2	TNF $\alpha$ Signaling	2.396	0.000	0.000
3	Interferon- $\gamma$ response	2.191	0.000	0.000
1	E2F Targets	-2.885	0.000	0.000
2	G2M Checkpoint	-2.712	0.000	0.000
3	MYC Targets	-2.217	0.000	0.000

*MEF2-regulated genes in SK-UT-1*

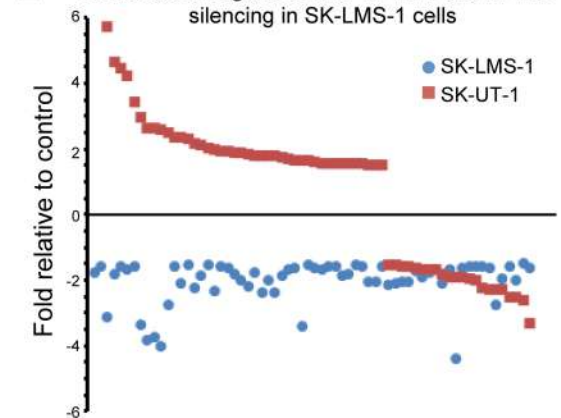
Rank	Gene set	NES	p-value	FDR q-value
1	E2F Targets	1.403	0,049	0,501
1	TNF $\alpha$ Signaling	-3.082	0.000	0.000
3	Interferon- $\gamma$ response	-2.699	0.000	0.000
4	Epithelial Mesenchymal Transition	-2.544	0.000	0.000

**C**

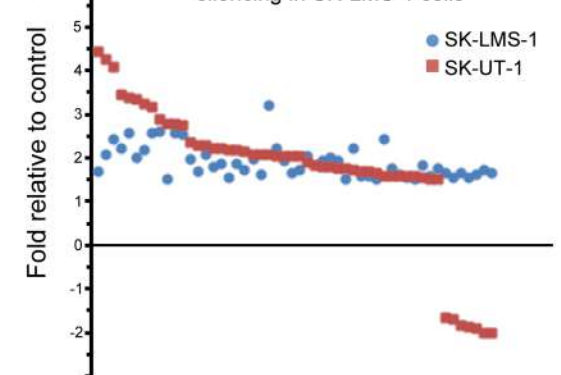
GENES	NES in SK-UT-1 (shCont versus shMEF2)
Genes repressed by shMEF2A in SK-LMS-1	NES = -1.56; p<0,001
Genes repressed by shMEF2D in SK-LMS-1	NES = -1.94; p<0,001
Genes induced by shMEF2A in SK-LMS-1	NES = -1.26; p<0,001
Genes induced by shMEF2D in SK-LMS-1	NES = -1.44; p<0,001



**E** Genes down-regulated after MEF2A and MEF2D silencing in SK-LMS-1 cells



**F** Genes up-regulated after MEF2A and MEF2D silencing in SK-LMS-1 cells



**G**

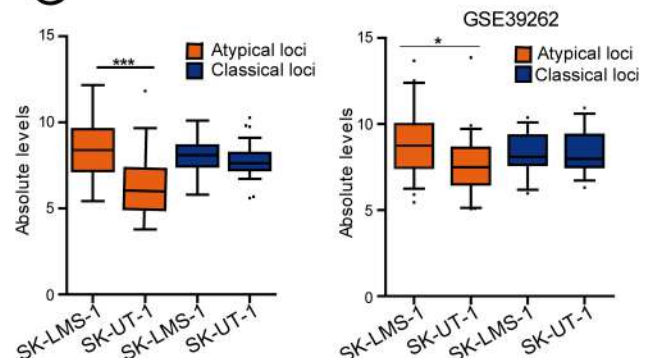


**Fig 6. The MEF2 transcriptome.** A) Venn diagrams showing the number of transcripts differing significantly in response to MEF2A and MEF2D silencing in SK-LMS-1 cells (green) or in SK-UT-1 cells (violet). Differentially expressed genes (DEGs) were selected based on fold change  $>1.5$  and  $<-1.5$  fold and p values  $<0.05$ . B) Gene ontology (GO) analysis was performed to interpret the principal biological processes under the regulation of MEF2 in SK-LMS-1 and SK-UT-1 cells. The NES (normalized enrichment score), the FDR (false discovery rate) and the p-value are provided. C) GSEA was performed by using SK-UT-1 DNA microarray data and genes repressed or induced by MEF2D/A KD in SK-LMS-1 cells, as indicated. Two groups were created in SK-UT-1 samples: A = shControl; B = shMEF2D/A. D) GSEA was performed by using SK-UT-1 DNA microarray data and genes repressed both by MEF2D/A KD in SK-LMS-1 and significantly modulated also in SK-UT-1 cells. Two groups were created in SK-UT-1 samples: A = shControl; B = shMEF2D/A. E) Scatter plot representing genes commonly down-regulated after MEF2A and MEF2D silencing in SK-LMS-1 cells (blue dots) and significantly modulated, after the same silencing, also in SK-UT-1 cells (red squares). F) Scatter plot representing genes commonly up-regulated after MEF2A and MEF2D silencing in SK-LMS-1 cells (blue dots) and significantly modulated, after the same silencing, also in SK-UT-1 cells (red squares). G) Turkey box-plots illustrating the mRNA expression levels of classical and atypical MEF2-target genes in SK-LMS-1 and SK-UT-1 cells in our DNA microarray and in another public available DNA microarray study (GSE39262). \*  $p < 0.05$ , \*\*  $p < 0.01$ , \*\*\*  $p < 0.001$

<https://doi.org/10.1371/journal.pgen.1006752.g006>

illustrated as ratio between the two LMS cell lines and correlated to the levels of the respective mRNAs (Fig 7A). The extended data are shown in S6 and S7 Figs.

The repression of the atypical genes in SK-UT-1 cells correlated with a dramatic reduction of H3K4me3 at the respective promoters. By contrast, the levels of H3K27ac were subjected to minor fluctuations, except for *SMOX*, which promoter is much more acetylated in SK-LMS-1 cells. For all the classical genes, only minor differences were observed between the two cell lines in the case of the three investigated parameters.

After MEF2D silencing in SK-LMS-1 cells the abundance of the mRNAs, as well as H3K27ac and H3K4me3 levels, at the respective regulative regions and TSSs for all tested genes, were reduced (Fig 7B). When the contribution of MEF2D was evaluated in SK-UT-1 cells the scenario was different. mRNA levels of atypical genes were augmented, as well as H3K4me3 (Fig 7C). H3K27ac was significantly increased only for *KLF2* and *COL1A2* (modestly) and reduced for *SMOX*. In the case of the classical genes, their expression and the two histone-modifications linked to open chromatin were all reduced after MEF2D silencing, similarly to SK-UT-1 cells (Fig 7C).

Overall this analysis suggests that MEF2 can concurrently supervise H3K27 acetylation/deacetylation and H3K4 methylation/demethylation on different promoters in the same cell population.

## HDAC9 is the critical player for switching MEF2 towards a repressive influence and it is required for the transformed phenotype of LMS cells

The dominant repressive influence exerted by MEF2 on some promoters in SK-UT-1 cells could stem from their assembly into a repressive complex. Likely candidates for this role are HDAC4 and HDAC9. To prove this hypothesis, we used the CRISPR/Cas9 technology [39] to generate SK-UT-1 cells knock-out (KO) for *HDAC4* or *HDAC9* (S8 Fig). We analyzed in parallel two different LMS clones for each KO (Fig 8A and 8D). In SK-UT-1 *HDAC9*<sup>-/-</sup> cells the expression of the atypical genes was augmented, except for *SMOX*, which was weakly up-regulated only in the clone 2. The expression of the classical genes was not influenced by the absence of HDAC9, with the exclusion of *RHOB*, which expression was slightly augmented. Fig 8C extended this analysis to 8 atypical and 6 classical genes and confirmed the specific effect of *HDAC9* deletion on the atypical genes. Moreover, as expected, no residual binding between HDAC9 and MEF2D could be observed in SK-UT-1 *HDAC9*<sup>-/-</sup> cells (S9 Fig).

Among the atypical genes, ablation of HDAC4 provoked the modest up-regulation of only *KLF2* mRNA (Fig 8E). This is an expected result considering the capability of HDAC4 to bind its promoter (Fig 4C). Surprisingly, the KO of HDAC4 caused the down-regulation of *ALPK2* and *IL8* mRNAs (Fig 8E). These data prove that class IIa HDACs exert non-redundant

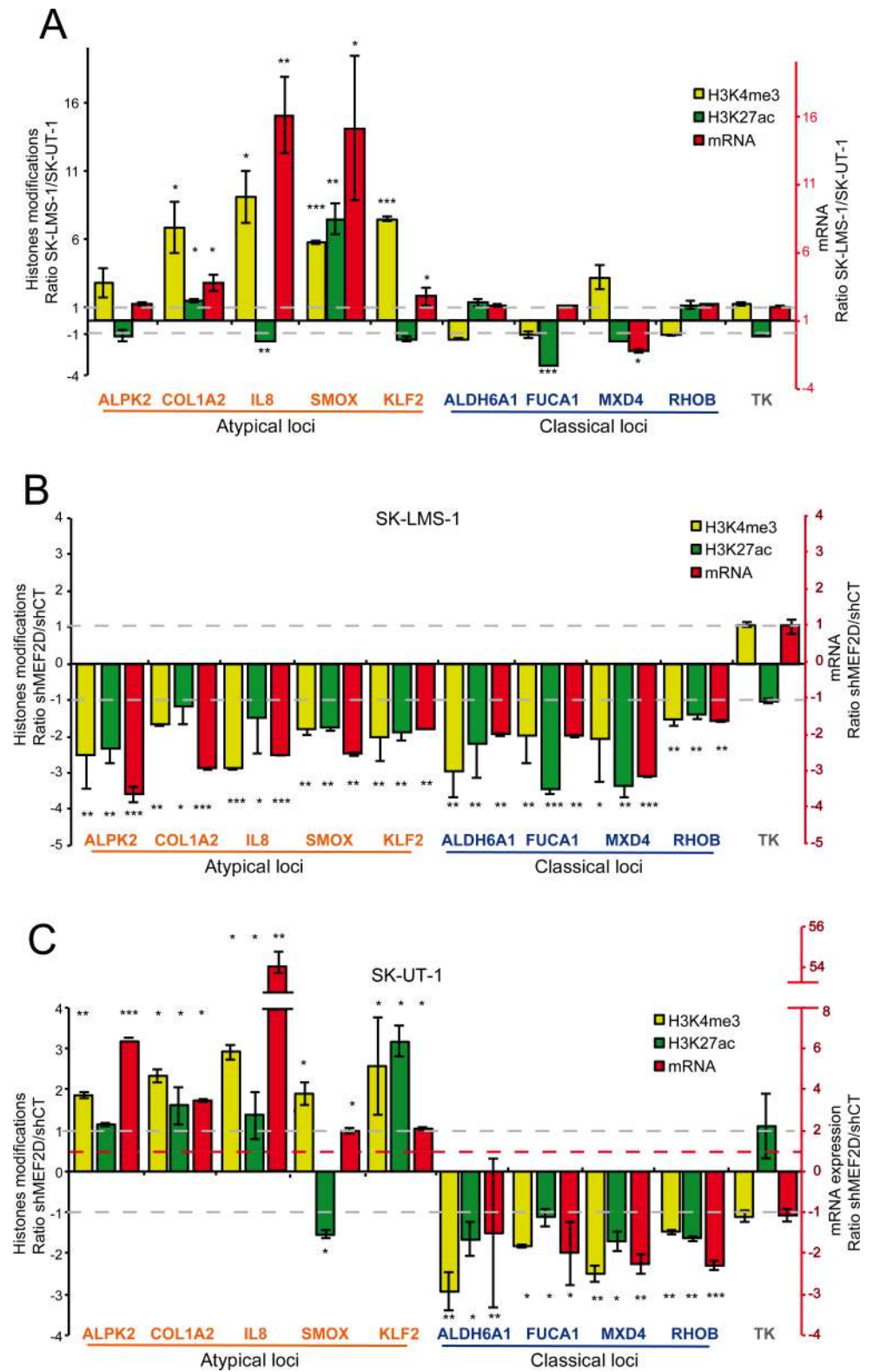


**Fig 7. MEF2D supervised epigenetic changes on atypical and classical genes.** A) Ratio between SK-LMS-1 and SK-UT-1 cells of H3K27ac, H3K4me3 and mRNA levels for a set of atypical and classical genes. *TK* was used as control. B) Ratio between SK-LMS-1 cells, WT and KD for MEF2D expression, of H3K27ac, H3K4me3 and mRNA levels for a set of atypical and classical genes. *TK* was used as control. C)

Ratio between SK-UT-1 cells, WT and KD for MEF2D expression, of H3K27ac, H3K4me3 and mRNA levels for a set of atypical and classical genes. *TK* was used as control. Data are presented as mean ± SD; n ≥ 3. The binding of MEF2 was validated by ChIP (S5 Fig) and the position of binding was expressed as relative to the major TSS, according to the hg38 assembly of the human genome. \* p < 0.05, \*\* p < 0.01, \*\*\* p < 0.001

<https://doi.org/10.1371/journal.pgen.1006752.g007>

functions and encourages further studies to clarify this de-regulation. The expression of classical genes was largely unperturbed in HDAC4-/- cells (Fig 8E). Box plot analysis on 8 atypical

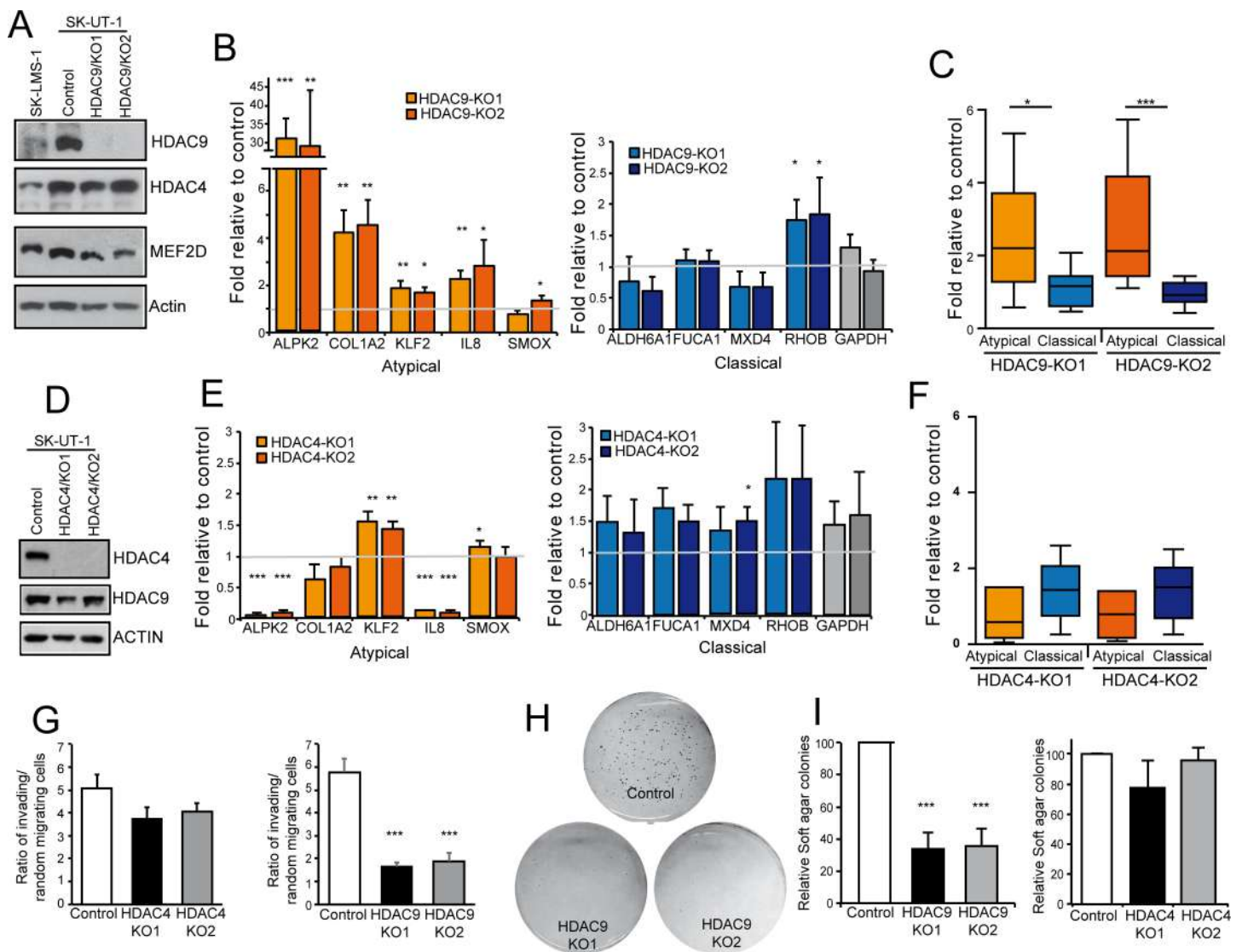


**Fig 8. HDAC4 and HDAC9 KO in SK-UT-1 cells.** A) Immunoblot analysis of HDAC4, HDAC9 and MEF2D in the indicated SK-UT-1 clones. Two different HDAC9 KO clones were selected. Actin was used as loading control. B) mRNA expression levels of the indicated atypical and classical MEF2-target genes in SK-UT-1 cells WT or KO for HDAC9. Data are presented as mean ± SD; n = 3. C) Turkey box-plots illustrating the mRNA expression levels of classical and atypical MEF2-target genes in SK-UT-1 cells WT or KO for HDAC9. Dunn's Multiple Comparison Test was applied to test the significance. D) Immunoblot analysis of HDAC4 and HDAC9 in the indicated SK-UT-1 clones. Two different HDAC4 KO clones generated by different sgRNAs were selected. Actin was used as loading control. E) mRNA expression levels of the indicated atypical and classical MEF2-target genes in SK-UT-1 cells WT or KO for HDAC4. Data are presented as mean ± SD; n = 3. F) Turkey box-plots illustrating the mRNA expression levels of classical and atypical MEF2-target genes in SK-UT-1 cells WT or KO for HDAC4. Dunn's Multiple Comparison Test was applied to test the significance. G) Invasion properties of the SK-UT-1 cells WT, KO for HDAC4 or KO for HDAC9, as indicated. Data are presented as mean ± SD; n = 4. H) Example of growth in soft agar of SK-UT-1 cells WT or KO for HDAC9. Foci were stained with MTT. I) Quantitative results of colony formation assay for SK-UT-1 cells WT, KO for HDAC4 or KO for HDAC9, as indicated. Data are presented as mean ± SD; n ≥ 3. \* p < 0.05, \*\* p < 0.01, \*\*\* p < 0.001

<https://doi.org/10.1371/journal.pgen.1006752.g008>

and 6 classical genes confirmed the limited impact of HDAC4 on the MEF2-dependent repressive action in SK-UT-1 cells (Fig 8F).

Finally, the tumorigenic potential of SK-UT-1 cells, as assessed in terms of invasiveness (Fig 8G) or by grow in soft agar (Fig 8H and 8I), was strongly dependent on HDAC9 and largely independent from HDAC4.

### The binding of HDAC9 to the promoter of MEF2-target genes correlates with the classical or atypical behavior

In SK-UT-1 cells, the differential impact of MEF2 on transcription could depend on the selective recruitment of HDAC9-repressive complexes onto the promoters of atypical and classical MEF2-target genes. ChIP experiments proved that HDAC9 can be isolated, as a complex, from promoters of the atypical but not from promoters of classical genes (Fig 9A). Next, we evaluated whether HDAC9 was required to supervise H3 modifications linked to active transcription. KO of HDAC9 increased H3K4me3 content at the TSSs of the atypical genes, with again the exclusion of *SMOX*. H3K27 acetylation was increased at the promoters of *COL1A2*, *IL8* and *KLF2* (Fig 9B). When the analysis was performed on the promoters and TSSs of the classical genes, no significant changes were observed in the *HDAC9*<sup>-/-</sup> cells.

To further confirm the contribution of HDAC9 to LMS development, 26 cases of LMS were transcriptionally profiled by RNAseq and scrutinized for class IIa HDACs expression levels. Similarly to the TCGA dataset (Fig 5A), also in our LMS series HDAC9 turned out to be the most expressed class IIa HDAC (Fig 9C). Moreover, isoform quantification analyses revealed that MITR [40], the truncated HDAC9 isoform, was the more abundantly expressed (24 out of 26 samples) splicing variant in LMS (Fig 9D). Finally, the Kaplan-Meier analysis, as performed in Fig 1H but restricted to HDAC9, evidences the association of high MEF2 and HDAC9 levels with reduced patients' survival in LMS (Fig 9E). In summary these data demonstrate that HDAC9 is an important driver of MEF2-repressive influences in SK-UT-1 cells and a key factor for the maintenance of the transformed phenotype.

## Discussion

The involvement of MEF2 in the tumorigenic process is still enigmatic [21–30, 41]. In this manuscript we provide evidences that could help to solve this controversial issue. We took advantage from the leiomyosarcoma model to unveil the two-faced of MEF2, but we are confident that these results can be confirmed also in other cancer types.

Our studies suggest that LMS can be clustered in two groups, in terms of MEF2 dysfunctions. The first group exhibited low proliferation and low levels of MEF2 proteins, possibly because of the SKP2-mediated degradation [35, 42]. The second group comprised tumors with high expression of MEF2 and of class IIa HDACs. Under these conditions MEF2 are converted into transcriptional repressors. The combination of high MEF2 and class IIa HDACs levels is detrimental for patients' survival. Although the UPS-mediated degradation can remove MEF2 from promoters and enhancers, their conversion into repressors can provide a strongest silencing, which is translated in a worse prognosis. HDAC4, HDAC5 and HDAC9 or its splicing variant MITR are the class IIa HDACs more frequently overexpressed in LMS. A condition not limited to this tumor type, as testified by recent studies [43–47].

These observations can be recapitulated in two LMS cell lines. In SK-LMS-1 cells MEF2 are under UPS control. MEF2 ablation reduces the expression of MEF2-target genes and enhances the transformed phenotype. By contrast in SK-UT-1 cells, where HDAC9 is highly expressed, MEF2 are required for tumorigenesis and to repress the transcription of some MEF2-target genes. This conversion stems from MEF2 assembly into multi-protein repressive complexes,

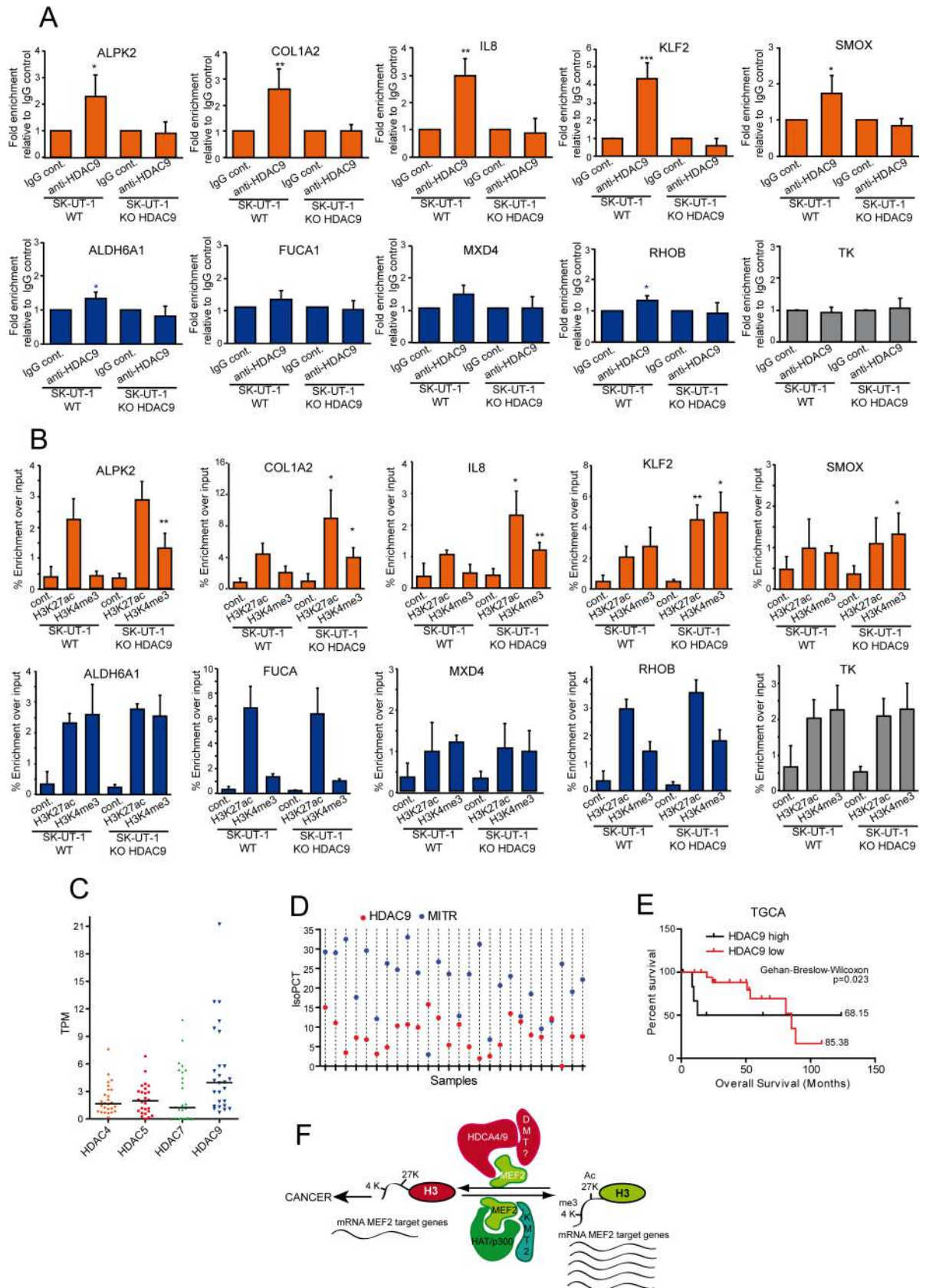


**Fig 9. Epigenetic changes monitored by HDAC9.** A) ChIP in SK-UT-1 cells WT or KO for HDAC9. Chromatin was immunoprecipitated using the anti-HDAC9 antibody. Normal rabbit IgGs were used as control. *TK* promoter was used as negative control. Atypical MEF2-targets are indicated in orange and the classical ones in blue. The genomic regions amplified by qPCR are the same as reported in [S5E Fig](#). Data are presented as mean  $\pm$  SD;  $n = 4$ . B) ChIP in SK-UT-1 cells WT or KO for HDAC9. Chromatin was immunoprecipitated using the anti-H3K27ac and the H3K4me3 antibodies as indicated. Normal rabbit IgGs were used as control. *TK* promoter was used as negative control. Atypical MEF2-targets are indicated in orange and the classical ones in blue. The genomic regions amplified by qPCR are the same as reported in [S6A and S6B Fig](#) (for H3H27ac) and in [S6A and S6B Fig](#) (for H3K4me3). Data are presented as mean  $\pm$  SD;  $n \geq 4$ . C) Scatter dot plot representing the coding mRNA TPM levels of the four class IIa HDACs in a cohort of 26 LMS samples. The horizontal lines indicate the median. Dunn's Multiple Comparison Test was applied to test the significance of HDAC9 up-regulation. D) Scatter dot plot representing the IsoPCT of the two main isoforms of HDAC9: HDAC9 WT (red) and MITR (blue). Individual tumors ( $n = 26$ ) were aligned along the x axis. E) Kaplan-Meier survival analysis related to the expression levels of HDAC9, performed on the same samples and according to the same criteria as in [Fig 1H](#). F) Summary of the shift in MEF2 transcriptional activities in relation to tumor progression in LMS. Possible co-activators and co-repressor are illustrated. The scheme describes the condition for the atypical MEF2-targets only. \*  $p < 0.05$ , \*\*  $p < 0.01$ , \*\*\*  $p < 0.001$ .

<https://doi.org/10.1371/journal.pgen.1006752.g009>

which erase histone marks of open chromatin configuration, such as H3K4me3 and H3K27ac, and thus repress the transcription of some MEF2-target genes ([Fig 9F](#)).

Our genes expression profile studies confirmed the complexity of the MEF2-transcriptome [[2](#), [8](#), [48](#), [49](#)]. Common as well as cell type and isoform specific MEF2-regulated genes exist. This multifaceted scenario could result from: i) a certain degree in DNA binding preferences of the different MEF2 [[50](#)]; ii) the presence of specific PTMs [[1](#)] and iii) the ability of forming complexes with other TFs, which hijack MEF2 away from canonical targets [[4](#), [8](#)].

Beside this complexity, we identified a common MEF2 signature, which can explain the opposite impact of MEF2 in the two LMS cells. Regulators of EMT, of the cell cycle and of inflammation are significantly enriched in this signature. Several genes of this signature are repressed by MEF2 in SK-UT-1 cells.

HDAC9 is the key factor for switching MEF2 into a repressor. However, HDAC9 is not recruited onto all promoters bound by MEF2. Hence, some MEF2-target genes are not repressed, even though SK-UT-1 cells express high levels of HDAC9. It is possible that these MEF2-targets govern some crucial activities of cancer cells.

The coexistence in the same cell population of TFs with both suppressive and activating activities on different loci, although surprising, was previously observed [[48](#), [51](#), [52](#)]. Different hypothesis have been formulated to explain this paradox but without a conclusive demonstration. We can exclude that the distance of the MEF2 binding site from the TSS could play a role, as previously hypothesized [[48](#)]. Since the repressive switch is cell lineage-dependent rather than gene-dependent, we could also exclude contributions of differences in the consensus of binding between promoters, as observed for p53 [[52](#)]. A fascinating hypothesis concerns contributions of the local nuclear organization, which might generate microenvironments proficient or exploitive for HDAC9 binding to MEF2.

MEF2 are required for H3K27 acetylation and H3K4 methylation. These activities can be explained by their ability to interact with Ash2L, a core subunit of KMT2 methyltransferase [[53](#)] and with the acetyl-transferase p300/CBP [[54](#)]. MEF2, once in complex with HDAC9, govern H3K27 deacetylation and H3K4 demethylation. Class IIa HDACs can bind the complex HDAC3/NuRD/SMRT, which delivers the deacetylase activity. Currently, we do not know whether a H3K4 demethylase is part of the same repressive complex with HDAC9. In principle, HDAC9 could act as a scaffold for a DMTase, as previously reported for HDAC4 and HDAC5 [[55–57](#)].

Interestingly, in SK-UT-1 cells genes repressed by MEF2-HDAC9 conserve H3K27 acetylation levels comparable to SK-LMS-1. These genes are in equilibrium between a closed and open chromatin conformation, similarly to the poised developmental regulatory genes in stem

cells [58]. This condition would make possible to revert the transcriptional output of these genes by simply inhibiting the demethylase involved.

Therapeutic intervention in advanced leiomyosarcomas represents a challenge. Important obstacles are the extreme genetic heterogeneity and the relatively low incidence of these malignancies [33, 34, 59]. Here we have found that over 20% of leiomyosarcomas present increased expression of a class IIa HDAC member. *In vitro* experiments indicate that the manipulation of the MEF2-HDAC axis impinges on the transformed phenotype. In conclusion, our discoveries suggest that small molecules targeting class IIa HDACs or the interaction between the deacetylase and MEF2 could afford success for the treatment of certain LMS.

## Materials and methods

### Ethics statement

The study was conducted according to the principles expressed in the declaration of Helsinki. Written informed consent was obtained for all patients. Tissue samples were provided by the Hospital of Treviso and no additional ethics approval was needed

### Cell culture and reagents

LMS cells were grown as previously described [28]. Primary antibodies used and reagents were: anti-SKP2 8D9 (Life Technologies); anti-MEF2C [35] anti-MEF2D  $\alpha 1/\alpha 2$  [10]; anti-GFP, anti-HDAC4 [60] and anti-HDAC5 [38]; anti-HDAC7 (sc-74563), anti-MEF2A (C-21 sc-313) and anti-RACK1 (sc-17754, Santa Cruz Biotechnology); anti-MEF2D (BD Transduction Laboratories); anti-Actin, p21 CP74 and FLAG M2 (Sigma-Aldrich); anti-ubiquitin (Covance); anti-HDAC9 (ab109446), anti-H3K27ac (ab4729) and anti-H3K27me3 (ab6002) (Abcam); anti-H3K4me3 (GTX128954, GeneTex); anti-KI67 (556003, BD Pharmingen).

### RNA extraction and quantitative qRT-PCR

Cells were lysed using TRI-REAGENT (Sigma-Aldrich). 1.0 $\mu$ g of total RNA was retro-transcribed by using 100 units of M-MLV Reverse transcriptase (Life Technologies). qRT-PCRs were performed using the Bio-Rad CFX96 and SYBR green (KAPA Biosystems) technology. Data were analysed by comparative threshold cycle using HPRT and  $\beta$ -actin as normalizer genes. All reactions were done in triplicate.

### Immunofluorescence and immunoblotting

Cells were fixed with 3% paraformaldehyde and permeabilized with 0.1% Triton X-100. Secondary antibodies were Alexa Fluor 488 anti-rabbit secondary antibodies (Molecular Probes). Actin was labeled with Phalloidin-AF546 (Molecular Probes). Cells were imaged with a Leica confocal scanner SP equipped with a 488  $\lambda$  Ar laser and a 543 to 633  $\lambda$  HeNe laser. Cell lysates after SDS/PAGE and immunoblotting were incubated with primary antibodies. Secondary antibodies were from Sigma-Aldrich and blots were developed with Super Signal West Dura (Pierce Waltham). For antibodies stripping, blots were incubated for 30min. at 60°C in stripping solution containing 100mM  $\beta$ -mercaptoethanol (Sigma-Aldrich).

### Immunoprecipitation

Co-immunoprecipitations were performed as previously described [35]. Briefly, cells were collected directly from culture dishes into RIPA buffer (50mM Tris-HCl pH8, 150mM NaCl, 0.2%SDS, 1%NP-40, 0.5% sodium deoxycholate), supplemented with protease inhibitors. Lysates were incubated for 5 h with the primary antibodies. After 1 hour of incubation with

protein A beads (GE) several washes were performed. Samples were resolved by SDS-PAGE and analysed by immunoblot.

### Chromatin immunoprecipitation

ChIP experiments were performed as previously described [35]. Briefly, for each ChIP,  $3 \times 10^6$  cells were employed. DNA-protein complexes were cross-linked with 1% formaldehyde (Sigma-Aldrich) in PBS for 15 minutes at RT. After quenching and two washes in PBS, cells were collected and then lysed for 10 minutes with Lysis buffer (5 mM Pipes, 85 mM KCl, 0.5% NP40) containing protease inhibitor cocktail. Pellets were re-suspended in RIPA-100 and sonicated using Bioruptor UCD-200 (Diagenode) with pulses of 30 seconds for 15 minutes, resulting in an average size of ~500 bp for genomic DNA fragments. Samples were precleared and immunoprecipitated O/N with: 1.5  $\mu$ g of anti-MEF2D and anti-MEF2A, 2  $\mu$ g of anti-HDAC4, 4  $\mu$ g of anti-HDAC9, 1  $\mu$ g of anti-H3K27ac, 2.5 of anti-H3K4me3 and H3K27me3 antibodies or the same amount of control antibodies (FLAG M2 and USP33 serum), followed by incubation with protein A blocked with BSA and SS DNA (1  $\mu$ g/ $\mu$ l) at 4°C for 90'. Beads and inputs were treated with proteinase K at 56°C for 3h to degrade proteins and the cross-linking was reversed O/N at 68°C. Genomic DNA was finally purified with Qiagen Qiaquick PCR purification kit and eluted in 100  $\mu$ l water.

### Plasmid construction, transfection, retroviral infection and silencing

pBABE-Puro plasmids expressing SKP2, SKP2DN-GFP were described previously [35]. pWZL-Hygro-SKP2 ER plasmid was obtained by subcloning with a PCR method SKP2 into pWZL-Hygro-MEF2-VP16 ER [28] and the nuclear relocalization of SKP2 after 4-OHT treatment was scored by immunofluorescence. Retroviral infections were performed as previously described [28]. pLKO-PURO plasmids expressing short hairpin RNAs (shRNAs) directed against MEF2D (15897 and 274054, referred to here as 1 and 2), MEF2D $\alpha$ 1 (15896, referred to here as 3) and MEF2A (432718 and 5133, referred to here as 4 and 5) were obtained from Sigma-Aldrich. pLKO-Hygro plasmid expressing the same shRNAs were obtained by oligo cloning, checked by restriction and sequencing. For lentivirus-based knock-down, HEK-293T cells were transfected with 1.8  $\mu$ g of VSV-G, 5  $\mu$ g of  $\Delta$ 8.9, and 8  $\mu$ g of pLKO plasmids. After 36h at 37°C, virions were collected and opportunely diluted in fresh medium.

### Random motility measurements, invasion and soft agar assays

Random motility was assayed by time-lapse video microscopy as previously described [61]. For soft agar growth,  $0.5 \times 10^5$  sarcoma cells were seeded in 0.3% top agar and incubated at 37°C. Foci were evidenced with MTT staining and counted by using ImageJ, as previously described [62]. For invasion assay, each well of the invasion chamber (CLS3428, Corning) was coated with 200  $\mu$ l of Matrigel matrix coating solution (Cultrex, Trevigen). Next, a cell suspension of  $0.5 \times 10^5$  LMS cells in 0.1%FBS-DMEM was added. As chemoattractant, 20%FBS-DMEM was added in each lower chamber. As a control 0.1%FBS-DMEM was used to evaluate random invasion.

### RNA expression array and data analysis

Total RNA was extracted using RNeasy columns (Qiagen). Aliquots of RNAs were amplified according to the specifications of the Illumina TotalPrep RNA Amplification Kit (Ambion). Hybridization on Illumina whole-genome HumanHT-12 v 4.0 chip (Illumina), scanning and background subtraction were done according to the manufacturer's specification. Fold-change

and p-values for each probe set were calculated using a moderated t-statistic in the limma package [63], with the variance estimate being adjusted by incorporating global variation measures for the complete set of probes on the array. The p-value data were then corrected for multiple hypotheses testing using the Benjamini and Hochberg.

Datasets were retrieved from GEO Dataset (GSE764, GSE21124, GSE21050, GSE39262) and analyzed as previously described [28]. For the expression levels and Kaplan–Meier analysis of TCGA sarcoma samples (265 sarcomas, 106 LMS), data were retrieved from CBio Portal [64] and expressed as z-score. Z-scores  $> |2|$  were selected as cut-off. Kaplan–Meier analysis was based on the expression levels of the four MEF2 and the four class IIa HDACs. GSEA and Gene Ontology-terms enrichment analysis were performed as described previously [28, 65].

## Tissue array construction and immunohistochemistry

Paraffin-embedded samples from leiomyosarcomas were available from 57 patients. All cases were histologically and immunohistochemically validated. Immunohistochemistry for HDAC4 (1:100), MEF2C and SKP2 was performed by an automated immunostainer (Dako Autostainer). Antigen retrieval was performed with citrate buffer at pH 6 for HDAC4 and at pH 9 with EnVision FLEX Target Retrieval Solution (Dako) for MEF2C and SKP2. All tumors were scored for the intensity of signal (range from 0 = no expression, to 4 = strong expression). Mean of intensity and percentage of duplicate cores were used for the final analysis.

## Generation of KO SK-UT-1 cells

CRISPR/Cas9 technology was applied to obtain HDAC4 and HDAC9 clones. The KO clones were screened by PCR, immunoblot and validated by Sanger sequencing. SpCas9 and D10A mutant of spCas9 [39] were used to obtain respectively HDAC4 and HDAC9 KO clones.

## Paired-end RNA-sequencing and isoform abundancy quantification

Total RNA was extracted from FFPE sections of 26 LMS samples using the Ambion RecoverAll Total Nucleic Acid Isolation Kit (Life Technology).

RNA-sequencing libraries were prepared as previously described [66] and sequenced on a Illumina HiSeq 1000 apparatus (Illumina) to a depth of 50–80 million paired-end reads per sample. The QoRts package was used to evaluate data quality and STAR2.5.2a for reads mapping to the GRCh37.74 genome assembly. RSEM was used for quantifying gene and isoform abundances [67]. Here we provide the list of class IIa HDACs isoforms analyzed: HDAC4 (ENST00000345617, ENST00000430200, ENST00000543185), HDAC5 (ENST00000225983, ENST00000336057, ENST00000393622, ENST00000586802), HDAC7 (ENST0000080059, ENST00000380610, ENST00000427332, ENST00000552960, ENST00000354334), HDAC9 (ENST00000401921, ENST00000406451, ENST00000432645, ENST00000441542), MITR (ENST00000405010, ENST00000406072, ENST00000417496, ENST00000428307, ENST00000456174, ENST00000524023).

## Statistic

For experimental data Student t-test was employed. Mann-Whitney test was applied when normality could not be assumed.  $p < 0.05$  was chosen as statistical limit of significance. For comparisons between samples  $> 2$  Anova test was applied, coupled to Krustal-Wallis and Dunn's Multiple Comparison Test. We mark with \*  $p < 0.05$ , \*\*  $p < 0.01$ , \*\*\*  $p < 0.001$ . Unless otherwise indicated, all the data in the figures were represented as arithmetic mean + SD of at least three independent experiments.

## Supporting information

### S1 Table. Genes comprised in the MEF2 signature.

(XLSX)

### S2 Table. Immunohistochemistry analysis.

(XLSX)

**S3 Table. The 85 common MEF2-target genes.** The list of the genes significantly regulated by MEF2A e MEF2D silencing in both SK-LMS-1 and SK-UT-1 cells. Values are indicated as mean fold change relative to the control. A prediction of the binding of MEF2 TFs on chromatin was done by scrutinizing all published BED files of ChIP-seq data: ENCF148PLM, ENCF001TXJ, GSE1499534, ENCF139PSX, GSE1499535, ENCF001UPO, ENCF001TXL, GSE73453, GSE61391, GSE43223. Pavis software was used for the annotation of the peaks [Huang W, Loganantharaj R, Schroeder B, Fargo D, Li L. PAVIS: A tool for Peak Annotation and Visualization. *Bioinformatics*. 2013;29: 3097–3099. doi:[10.1093/bioinformatics/btt520](https://doi.org/10.1093/bioinformatics/btt520)].

(XLSX)

### S4 Table. Characteristics of the selected atypical and classical MEF2-target genes.

(XLSX)

**S1 Fig. Roles of MEF2A and of MEF2D in tumor cells invasion.** Fluorescence analysis of Matrigel invading SK-LMS-1 and SK-UT-1 cells expressing the indicated shRNAs and stained with Hoechst 33342. Bar = 100µM.

(TIF)

**S2 Fig. Silencing of MEF2D isoforms in SK-LMS-1.** A) qRT-PCR analysis of the mRNAs expression levels of two alternative isoforms of MEF2D ( $\alpha 1$  and  $\alpha 2$ ) in SK-LMS-1 cells expressing the indicated isoform-specific shRNAs. mRNA levels are relative to control shRNA. Data are presented as mean  $\pm$  SD; n = 3.

B) Immunoblot analysis of the MEF2D isoforms levels in SK-LMS-1 cells expressing the indicated shRNAs. Actin was used as loading control.

C) qRT-PCR analysis of the mRNAs expression levels of some MEF2-target genes (*KLF2*, *RHOB*, *IRS1*) in SK-LMS-1 cells expressing the indicated isoform specific shRNAs. mRNA levels are relative to control shRNA. Data are presented as mean  $\pm$  SD; n = 3.

D) Growth in soft agar of SK-LMS-1 cells expressing the indicated shRNAs. Foci were stained with MTT and counted. Data are presented as mean  $\pm$  SD; n = 4.

(TIF)

**S3 Fig. MEF2A silencing causes opposite effects in SK-LMS-1 and SK-UT-1 cells.** A) MEF2A expression was silenced by lentiviral infection using two different shRNA (#4 and #5). Immunoblot analysis of MEF2D and CDKN1A levels in SK-LMS-1 cells expressing the control shRNA or two different shRNAs against MEF2A. Actin was used as loading control.

B) qRT-PCR analysis of the mRNA expression levels of MEF2A and of MEF2-target genes (*KLF2*, *RHOB*, *CDKN1A*, *JUN*, *CNN1*, *IRS1*) in SK-LMS-1 cells expressing the different shRNAs. mRNA levels are relative to control shRNA. Data are presented as mean  $\pm$  SD; n = 4.

C) Analysis of the cells synthesizing DNA as scored after BrdU staining. Data are presented as mean  $\pm$  SD; n = 3.

D) SK-LMS-1 cells expressing the indicated shRNAs were subjected to time-lapse analysis for 6 hours. Results represent the individual migration rate and the average (bar) from at least 140 cells from three independent experiments. Cell movements were quantified using MetaMorph software (Molecular Devices, Sunnyvale, CA).

- E) Invasion properties of the SK-LMS-1 cells expressing the shRNA4 against MEF2A or the control. Data are presented as mean  $\pm$  SD; n = 4.
- F) Growth in soft agar of SK-LMS-1 cells expressing the indicated shRNAs, foci were stained with MTT and counted. Data are presented as mean  $\pm$  SD; n = 4.
- G) MEF2A expression was silenced by lentiviral infection using two different shRNA (#4 and #5). Immunoblot analysis of MEF2D and CDKN1A levels in SK-UT-1 cells expressing the control shRNA or two different shRNAs against MEF2A. Actin was used as loading control.
- H) qRT-PCR analysis of the mRNA expression levels of MEF2A and of MEF2-target genes (*KLF2*, *RHOB*, *CDKN1A*, *JUN*, *CNN1*, *IRS1*) in SK-UT-1 cells expressing the different shRNAs. mRNA levels are relative to control shRNA. Data are presented as mean  $\pm$  SD; n = 4.
- I) Analysis of the cells synthesizing DNA as scored after BrdU staining. Data are presented as mean  $\pm$  SD; n = 3.
- J) SK-UT-1 cells expressing the indicated shRNAs were subjected to time-lapse analysis for 6 hours. Results represent the individual migration rate and the average (bar) from at least 140 cells from three independent experiments. Cell movements were quantified using MetaMorph software (Molecular Devices, Sunnyvale, CA).
- K) Invasion properties of the SK-UT-1 cells expressing the shRNA4 against MEF2A or the control. Data are presented as mean  $\pm$  SD; n = 4.
- L) Growth in soft agar of SK-UT-1 cells expressing the indicated shRNAs, foci were stained with MTT and counted. Data are presented as mean  $\pm$  SD; n = 4.
- (TIF)

**S4 Fig. MEF2D and HDAC4 co-occupancy.**  $6 \times 10^6$  cells were employed. First immunoprecipitations were conducted ON with 2 $\mu$ g of anti-MEF2D or anti-FLAG antibodies. Protein-DNA complexes were collected with 8 $\mu$ l of protein A magnetic beads (ZymoMag, Zymo research) and washed twice with RIPA and TE. Beads were incubated for 30' at 37°C in Re-Chip elution buffer (1 $\times$ TE, 2%SDS, 15mM DTT), diluted 15 times into RIPA buffer and subjected to the second immunoprecipitation using 3 $\mu$ g of anti-HDAC4 or USP33 IgG as control. *TK* promoter was used as negative control. Data are presented as mean fold enrichment relatively to the first input

(TIF)

- S5 Fig. Characterization of the new MEF2-target genes.** A) qRT-PCR analysis of the mRNA expression levels of the identified atypical and classical MEF2-target genes in SK-LMS-1 cells expressing the shRNAs against MEF2D. mRNA levels are relative to control shRNA. *GAPDH* was used as control. Data are presented as mean  $\pm$  SD; n = 3.
- B) qRT-PCR analysis of the mRNA expression levels of the identified atypical and classical MEF2-target genes in SK-UT-1 cells expressing the shRNAs against MEF2D. mRNA levels are relative to control shRNA. *GAPDH* was used as control. Data are presented as mean  $\pm$  SD; n = 3.
- C) qRT-PCR analysis of the mRNA expression levels of the identified atypical and classical MEF2-target genes in SK-LMS-1 cells expressing the shRNAs against MEF2A. mRNA levels are relative to control shRNA. *GAPDH* was used as control. Data are presented as mean  $\pm$  SD; n = 3.
- D) qRT-PCR analysis of the mRNA expression levels of the identified atypical and classical MEF2-target genes in SK-UT-1 cells expressing the shRNAs against MEF2A. mRNA levels are relative to control shRNA. *GAPDH* was used as control. Data are presented as mean  $\pm$  SD; n = 3.
- E) Chromatin was immunoprecipitated from SK-LMS-1 or SK-UT-1 cells using the anti-MEF2D antibody. Anti-FLAG antibody was used as control. Cells KD for MEF2D are indicated.

*TK* promoter was used as negative control. The MEF2 binding site (arrowheads), the amplified region and the TSS (arrows) are indicated for each tested gene.

Atypical MEF2-target genes are in orange whereas classical ones are in blue. Data are presented as mean  $\pm$  SD; n = 3.

(TIF)

**S6 Fig. Role of MEF2 in controlling histone H3K27 acetylation.** A) Chromatin was immunoprecipitated from SK-LMS-1 or SK-UT-1 cells WT or KD for MEF2D, using the anti-H3K27ac antibody. Normal rabbit IgGs were used as control. The MEF2 binding site (arrowheads), the amplified region and the TSS (arrows) are indicated for each tested atypical gene. Data are presented as mean  $\pm$  SD; n = 3.

B) Chromatin was immunoprecipitated from SK-LMS-1 or SK-UT-1 cells WT or KD for MEF2D, using the anti-H3K27ac antibody. Normal rabbit IgGs were used as control. *TK* promoter was used as negative control. The MEF2 binding site (arrowheads), the amplified region and the TSS (arrows) are indicated for each tested classical gene. Data are presented as mean  $\pm$  SD; n = 3. Atypical MEF2-target genes are in orange whereas classical ones are in blue.

(TIF)

**S7 Fig. Role of MEF2 in controlling histone H3K4 methylation.** A) Chromatin was immunoprecipitated from SK-LMS-1 or SK-UT-1 cells WT or KD for MEF2D, using the anti-H3K4me3 antibody. Normal rabbit IgGs were used as control. The MEF2 binding site (arrowheads), the amplified region and the TSS (arrows) are indicated for each tested atypical gene. Data are presented as mean  $\pm$  SD; n = 3.

B) Chromatin was immunoprecipitated from SK-LMS-1 or SK-UT-1 cells WT or KD for MEF2D, using the anti-H3K4me3 antibody. Normal rabbit IgGs were used as control. *TK* promoter was used as negative control. The MEF2 binding site (arrowheads), the amplified region and the TSS (arrows) are indicated for each tested classical gene. Data are presented as mean  $\pm$  SD; n = 3. Atypical MEF2-target genes are in orange whereas classical ones are in blue.

(TIF)

**S8 Fig. CRISPR/Cas9 mediated KO of HDAC4 and HDAC9.** A) Schematic representation of *HDAC9* genomic organization with indicated: the exons (vertical bars), the introns (junctions between the bars) and the PAM sequences utilized for the CRISPR approach.

B) Genomic sequences of the *HDAC9*<sup>-/-</sup> SK-UT-1 cells used in this study. The sequence of *HDAC9* genomic region targeted by the CRISPR/Cas9D10A is included. The PAMs and the two gRNAs are underlined. SKUT-1 *HDAC9* KO clones were obtained through the delivery of the D10A mutant of SpCas9. Two sgRNAs designed on the second coding exon of *HDAC9* were co-delivered to obtain two close cleavages on the genome to simulate a DSB (sgRNA1: CTGCTATCAGAAGCTGCTTC; sgRNA2: GAACCTTGACACGGCAGCACC). Five clones were selected for the presence of deletions or insertion and among them the indicated two were selected for the analysis.

C) Schematic representation of *HDAC4* genomic organization with indicated: the exons (vertical bars), the introns (junctions between the bars) and the PAM sequences utilized for the CRISPR approach.

D) Genomic sequences of the *HDAC4*<sup>-/-</sup> SK-UT-1 cells used in this study. The sequence of *HDAC4* genomic region targeted by the CRISPR/Cas9 is included. The PAMs and the two gRNAs are underlined. SKUT-1 *HDAC4* KO clones were obtained through the delivery of wild-type spCas9 (pLENTI-CRISPRv2). Two sgRNAs designed on the second coding exon were used (sgRNA1: GCAGGATTCAGCAGCTCCAC; sgRNA2: CGTGAACCACATGCC-CAGCA). One and three KO clones were obtained respectively with sgRNA1 and 2. The two

representative clones indicated here were selected for the analysis.  
(TIF)

**S9 Fig. MEF2D-HDAC9 complex.** The MEF2D-HDAC9 complexes were immunoprecipitated from the different cell lines using 1µg of anti-MEF2D, or anti-FLAG antibodies, as a control. Immunocomplexes were subjected to immunoblotting using the anti-MEF2D and HDAC9 antibodies.  
(TIF)

## Acknowledgments

We thank Valentina Cutano for the helpful discussions, Silvia Tonon and Elena Betto for help with sequencing. We also thank Soji Sebastian and Jeffrey Dilworth for isoforms specific MEF2D antibodies.

## Author Contributions

**Conceptualization:** EDG CB.

**Data curation:** EDG RP MP MB.

**Formal analysis:** EDG RP MP.

**Funding acquisition:** CB.

**Investigation:** EDG EF SC MB HP.

**Methodology:** EDG CB.

**Project administration:** CB.

**Resources:** RM SR APDT.

**Supervision:** CB.

**Validation:** MP EDG.

**Visualization:** CB EDG.

**Writing – original draft:** CB EDG.

**Writing – review & editing:** CB EDG.

## References

1. Potthoff MJ, Olson EN. MEF2: a central regulator of diverse developmental programs. *Development*. 2007; 134: 4131–4140. <https://doi.org/10.1242/dev.008367> PMID: 17959722
2. Estrella NL, Desjardins C a., Nocco SE, Clark AL, Maksimenko Y, Naya FJ. MEF2 Transcription Factors Regulate Distinct Gene Programs in Mammalian Skeletal Muscle Differentiation. *J Biol Chem*. 2015; 290: 1256–68. <https://doi.org/10.1074/jbc.M114.589838> PMID: 25416778
3. Kong NR, Davis M, Chai L, Winoto A, Tjian R. MEF2C and EBF1 Co-regulate B Cell-Specific Transcription. *PLoS Genet*. 2016; 12: e1005845. <https://doi.org/10.1371/journal.pgen.1005845> PMID: 26900922
4. Andzelm MM, Cherry TJ, Harmin DA, Boeke AC, Lee C, Hemberg M, et al. MEF2D drives photoreceptor development through a genome-wide competition for tissue-specific enhancers. *Neuron*. 2015; 86: 247–263. <https://doi.org/10.1016/j.neuron.2015.02.038> PMID: 25801704
5. Potthoff MJ, Arnold M a, McAnally J, Richardson J a, Bassel-Duby R, Olson EN Regulation of skeletal muscle sarcomere integrity and postnatal muscle function by Mef2c. *Mol Cell Biol*. 2007; 27: 8143–8151. <https://doi.org/10.1128/MCB.01187-07> PMID: 17875930

6. Liu N, Nelson BR, Bezprozvannaya S, Shelton JM, Richardson JA, Bassel-Duby R, et al. Requirement of MEF2A, C, and D for skeletal muscle regeneration. *Proc Natl Acad Sci U S A*. 2014; 111: 4109–14. <https://doi.org/10.1073/pnas.1401732111> PMID: 24591619
7. Flavell SW, Cowan CW, Kim T-K, Greer PL, Lin Y, Paradis S, et al. Activity-dependent regulation of MEF2 transcription factors suppresses excitatory synapse number. *Sci (New York, NY)*. 2006; 311: 1008–1012. <https://doi.org/10.1126/science.1122511> PMID: 16484497
8. Herglotz J, Unrau L, Hauschildt F, Fischer M, Kriebitzsch N, Alawi M, et al. Essential control of early B-cell development by Mef2 transcription factors. *Blood*. 2016; 127: 572–581. <https://doi.org/10.1182/blood-2015-04-643270> PMID: 26660426
9. Harrington AJ, Raissi A, Rajkovich K, Berto S, Kumar J, Molinaro G, Raduazzo J, Guo Y, Loerwald K, Konopka G, Huber KM, Cowan C. MEF2C regulates cortical inhibitory and excitatory synapses and behaviors relevant to neurodevelopmental disorders. *Elife*. 2016; 5: e20059. <https://doi.org/10.7554/eLife.20059> PMID: 27779093
10. Sebastian S, Faralli H, Yao Z, Rakopoulos P, Pali C, Cao Y, et al. Tissue-specific splicing of a ubiquitously expressed transcription factor is essential for muscle differentiation. *Genes Dev*. 2013; 27: 1247–1259. <https://doi.org/10.1101/gad.215400.113> PMID: 23723416
11. Zhang M, Zhu B, Davie J. Alternative splicing of MEF2C pre-mRNA controls its activity in normal myogenesis and promotes tumorigenicity in rhabdomyosarcoma cells. *J Biol Chem*. 2015; 290: 310–324. <https://doi.org/10.1074/jbc.M114.606277> PMID: 25404735
12. Gao C, Ren S, Lee J, Qiu J, Chapski DJ, Rau CD, et al. RBFox1-mediated RNA splicing regulates cardiac hypertrophy and heart failure. *J Clin Invest*. 2015; 126: 195–206. <https://doi.org/10.1172/JCI84015> PMID: 26619120
13. Baruffaldi F, Montarras D, Basile V, De Feo L, Badodi S, Ganassi M, et al. Phosphorylation of the Myocyte Enhancer Factor 2Cα1 Splice Variant Promotes Skeletal Muscle Regeneration and Hypertrophy. *Stem Cells*. 2017; 35: 725–738 <https://doi.org/10.1002/stem.2495> PMID: 27612437
14. Han A, Pan F, Stroud JC, Youn H-D, Liu JO, Chen L. Sequence-specific recruitment of transcriptional co-repressor Cabin1 by myocyte enhancer factor-2. *Nature*. 2003; 422: 730–734. <https://doi.org/10.1038/nature01555> PMID: 12700764
15. Choi J, Jang H, Kim H, Lee J-H, Kim S-T, Cho E-J, et al. Modulation of lysine methylation in myocyte enhancer factor 2 during skeletal muscle cell differentiation. *Nucleic Acids Res*. 2014; 42: 224–34. <https://doi.org/10.1093/nar/gkt873> PMID: 24078251
16. Miska EA, Karlsson C, Langley E, Nielsen SJ, Pines J, Kouzarides T. HDAC4 deacetylase associates with and represses the MEF2 transcription factor. *EMBO J*. 1999; 18: 5099–5107. <https://doi.org/10.1093/emboj/18.18.5099> PMID: 10487761
17. Di Giorgio E, Brancolini C. Regulation of class IIa HDAC activities: it is not only matter of subcellular localization. *Epigenomics*. 2016; 8: 251–269. <https://doi.org/10.2217/epi.15.106> PMID: 26791815
18. Cole CJ, Mercaldo V, Restivo L, Yiu AP, Sekeres MJ, Han J-H, et al. MEF2 negatively regulates learning-induced structural plasticity and memory formation. *Nat Neurosci*. 2012; 15: 1255–1264. <https://doi.org/10.1038/nn.3189> PMID: 22885849
19. Zhang Z, Cao M, Chang C, Wang C, Shi X, Zhan X, et al. Autism-Associated Chromatin Regulator Brg1/SmarcA4 Is Required for Synapse Development and Myocyte Enhancer Factor 2-Mediated Synapse Remodeling. *Mol Cell Biol*. 2015; 36: 70–83. <https://doi.org/10.1128/MCB.00534-15> PMID: 26459759
20. Kolodziejczyk SM, Wang L, Balazsi K, Derepentigny Y, Kothary R, Megeney LA. MEF2 is upregulated during cardiac hypertrophy and is required for normal post-natal growth of the myocardium. *Curr Biol*. 1999; 9: 1203–1206. [https://doi.org/10.1016/S0960-9822\(00\)80027-5](https://doi.org/10.1016/S0960-9822(00)80027-5) PMID: 10531040
21. Pon JR, Marra MA. MEF2 transcription factors: developmental regulators and emerging cancer genes. *Oncotarget*. 2015; 7: 2297–312. <https://doi.org/10.18632/oncotarget.6223> PMID: 26506234
22. Schwieger M, Schüler A, Forster M, Engelmann A, Arnold MA, Delwel R, et al. Homing and invasiveness of MLL/ENL leukemic cells is regulated by MEF2C. *Blood*. 2009; 114: 2476–2488. <https://doi.org/10.1182/blood-2008-05-158196> PMID: 19584403
23. Homminga I, Pieters R, Langerak AW, de Rooi JJ, Stubbs A, Verstegen M, et al. Integrated Transcript and Genome Analyses Reveal NKX2-1 and MEF2C as Potential Oncogenes in T Cell Acute Lymphoblastic Leukemia. *Cancer Cell*. 2011; 19: 484–497. <https://doi.org/10.1016/j.ccr.2011.02.008> PMID: 21481790
24. Ma L, Liu J, Liu L, Duan G, Wang Q, Xu Y, et al. Overexpression of the transcription factor MEF2D in hepatocellular carcinoma sustains malignant character by suppressing G2-M transition genes. *Cancer Res*. 2014; 74: 1452–1462. <https://doi.org/10.1158/0008-5472.CAN-13-2171> PMID: 24390737

25. Bai X, Wu L, Liang T, Liu Z, Li J, Li D, et al. Overexpression of myocyte enhancer actor 2 and histone hyperacetylation in hepatocellular carcinoma. *J Cancer Res Clin Oncol*. 2008; 134: 83–91. <https://doi.org/10.1007/s00432-007-0252-7> PMID: 17611778
26. Suzuki K, Okuno Y, Kawashima N, Muramatsu H, Okuno T, Wang X, et al. MEF2D-BCL9 Fusion Gene Is Associated With High-Risk Acute B-Cell Precursor Lymphoblastic Leukemia in Adolescents. *J Clin Oncol*. 2016; 34:3451–9. <https://doi.org/10.1200/JCO.2016.66.5547> PMID: 27507882
27. Prima V, Hunger SP. Cooperative transformation by MEF2D/DAZAP1 and DAZAP1/MEF2D fusion proteins generated by the variant t(1;19) in acute lymphoblastic leukemia. *Leukemia*. 2007; 21: 2470–5. <https://doi.org/10.1038/sj.leu.2404962> PMID: 17898785
28. Di Giorgio E, Clocchiatti A, Piccinin S, Sgorbissa A, Viviani G, Peruzzo P, et al. MEF2 is a converging hub for histone deacetylase 4 and phosphatidylinositol 3-kinase/Akt-induced transformation. *Mol Cell Biol*. 2013; 33: 4473–91. <https://doi.org/10.1128/MCB.01050-13> PMID: 24043307
29. Zhang M, Truscott J, Davie J. Loss of MEF2D expression inhibits differentiation and contributes to oncogenesis in rhabdomyosarcoma cells. *Mol Cancer*. 2013; 12: 150. <https://doi.org/10.1186/1476-4598-12-150> PMID: 24279793
30. Pon JR, Wong J, Saberi S, Alder O, Moksa M, Grace Cheng S-W-W, et al. MEF2B mutations in non-Hodgkin lymphoma dysregulate cell migration by decreasing MEF2B target gene activation. *Nat Commun*. 2015; 6: 7953. <https://doi.org/10.1038/ncomms8953> PMID: 26245647
31. Bai XL, Zhang Q, Ye LY, Liang F, Sun X, Chen Y, et al. Myocyte enhancer factor 2C regulation of hepatocellular carcinoma via vascular endothelial growth factor and Wnt/ $\beta$ -catenin signaling. *Oncogene*. 2015; 34: 4089–97. <https://doi.org/10.1038/nc.2014.337> PMID: 25328135
32. Ying CY, Dominguez-Sola D, Fabi M, Lorenz IC, Hussein S, Bansal M, et al. MEF2B mutations lead to deregulated expression of the oncogene BCL6 in diffuse large B cell lymphoma. *Nat Immunol*. 2013; 14: 1084–92. <https://doi.org/10.1038/ni.2688> PMID: 23974956
33. Guillou L, Aurias A. Soft tissue sarcomas with complex genomic profiles. *Virchows Archiv*. 2010. pp. 201–217. <https://doi.org/10.1007/s00428-009-0853-4> PMID: 20217954
34. Mäkinen N, Aavikko M, Heikkinen T, Taipale M, Taipale J, Koivisto-Korander R, et al. Exome Sequencing of Uterine Leiomyosarcomas Identifies Frequent Mutations in TP53, ATRX, and MED12. *PLoS Genet*. 2016 Feb 18; 12(2):e1005850. <https://doi.org/10.1371/journal.pgen.1005850> PMID: 26891131
35. Di Giorgio E, Gagliostro E, Clocchiatti A, Brancolini C. The control operated by the cell cycle machinery on MEF2 stability contributes to the downregulation of CDKN1A and entry into S phase. *Mol Cell Biol*. 2015; 35: 1633–47. <https://doi.org/10.1128/MCB.01461-14> PMID: 25733682
36. Celis JE. *Cell Biology, A Laboratory Handbook*. 3rd Editio. Elsevier; 2006.
37. Ganiatsas S, Dow R, Thompson A, Schulman B, Germain D. A splice variant of Skp2 is retained in the cytoplasm and fails to direct cyclin D1 ubiquitination in the uterine cancer cell line SK-UT. *Oncogene*. 2001; 20: 3641–3650. <https://doi.org/10.1038/sj.onc.1204501> PMID: 11439327
38. Clocchiatti A, Di Giorgio E, Viviani G, Streuli C, Sgorbissa A, Picco R, et al. The MEF2-HDAC axis controls proliferation of mammary epithelial cells and acini formation in vitro. *J Cell Sci*. 2015; 128: 3961–76. <https://doi.org/10.1242/jcs.170357> PMID: 26403201
39. Ran FA, Hsu PD, Lin CY, Gootenberg JS, Konermann S, Trevino AE, et al. Double nicking by RNA-guided CRISPR cas9 for enhanced genome editing specificity. *Cell*. 2013; 154: 1380–1389. <https://doi.org/10.1016/j.cell.2013.08.021> PMID: 23992846
40. Sparrow DB, Miska EA, Langley E, Reynaud-Deonauth S, Kotecha S, Towers N, et al. MEF-2 function is modified by a novel co-repressor, MITR. *EMBO J*. 1999; 18: 5085–5098. <https://doi.org/10.1093/emboj/18.18.5085> PMID: 10487760
41. Su L, Luo Y, Yang Z, Yang J, Yao C, Cheng F, et al. MEF2D Transduces Microenvironment Stimuli to ZEB1 to Promote Epithelial-Mesenchymal Transition and Metastasis in Colorectal Cancer. *Cancer Res*. 2016; 76: 5054–67. <https://doi.org/10.1158/0008-5472.CAN-16-0246> PMID: 27364559
42. Badodi S, Baruffaldi F, Ganassi M, Battini R, Molinari S. Phosphorylation-dependent degradation of MEF2C contributes to regulate G2/M transition. *Cell Cycle*. 2015; 14: 1517–1528. <https://doi.org/10.1080/15384101.2015.1026519> PMID: 25789873
43. Li X, Zhang Q, Ding Y, Liu Y, Zhao D, Zhao K, et al. Methyltransferase Dnmt3a upregulates HDAC9 to deacetylate the kinase TBK1 for activation of antiviral innate immunity. *Nat Immunol*. 2016; 17: 806–815. <https://doi.org/10.1038/ni.3464> PMID: 27240213
44. Lapierre M, Linares A, Dalvai M, Duraffourd C, Bonnet S, Boulahtouf A, et al. Histone deacetylase 9 regulates breast cancer cell proliferation and the response to histone deacetylase inhibitors. *Oncotarget*. 2016; 7: 19693–19708. <https://doi.org/10.18632/oncotarget.7564> PMID: 26930713

45. Kahali B, Gramling SJ, Marquez SB, Thompson K, Lu L, Reisman D. Identifying targets for the restoration and reactivation of BRM. *Oncogene*. 2014; 33: 653–64. <https://doi.org/10.1038/onc.2012.613> PMID: 23524580
46. Rastogi B, Raut SK, Panda NK, Rattan V, Radotra BD, Khullar M. Overexpression of HDAC9 promotes oral squamous cell carcinoma growth, regulates cell cycle progression, and inhibits apoptosis. *Mol Cell Biochem*. 2016; 415: 183–96. <https://doi.org/10.1007/s11010-016-2690-5> PMID: 26992905
47. Gil VS, Bhagat G, Howell L, Zhang J, Kim CH, Stengel S, et al. Deregulated expression of HDAC9 in B cells promotes development of lymphoproliferative disease and lymphoma in mice. *Dis Model Mech*. 2016; 9: 1483–1495. <https://doi.org/10.1242/dmm.023366> PMID: 27799148
48. Wales S, Hashemi S, Blais A, McDermott JC. Global MEF2 target gene analysis in cardiac and skeletal muscle reveals novel regulation of DUSP6 by p38MAPK-MEF2 signaling. *Nucleic Acids Res*. 2014; 42: 11349–11362. <https://doi.org/10.1093/nar/gku813> PMID: 25217591
49. Bernstein BE, Birney E, Dunham I, Green ED, Gunter C, Snyder M. An integrated encyclopedia of DNA elements in the human genome. *Nature*. 2012; 489: 57–74. <https://doi.org/10.1038/nature11247> PMID: 22955616
50. Andres V, Cervera M, Mahdavi V. Determination of the consensus binding site for MEF2 expressed in muscle and brain reveals tissue-specific sequence constraints. *J Biol Chem*. 1995; 270: 23246–23249. <https://doi.org/10.1074/jbc.270.40.23246> PMID: 7559475
51. Wu Q, Zhang L, Su P, Lei X, Liu X, Wang H, et al. MSX2 mediates entry of human pluripotent stem cells into mesendoderm by simultaneously suppressing SOX2 and activating NODAL signaling. *Cell Res*. 2015; 25: 1–19. <https://doi.org/10.1038/cr.2015.118> PMID: 26427715
52. Rinn JL, Huarte M. To repress or not to repress: This is the guardian's question. *Trends in Cell Biology*. 2011. pp. 344–353. <https://doi.org/10.1016/j.tcb.2011.04.002> PMID: 21601459
53. Rampalli S, Li L, Mak E, Ge K, Brand M, Tapscott SJ, et al. p38 MAPK signaling regulates recruitment of Ash2L-containing methyltransferase complexes to specific genes during differentiation. *Nat Struct Mol Biol*. 2007; 14: 1150–6. <https://doi.org/10.1038/nsmb1316> PMID: 18026121
54. He J, Ye J, Cai Y, Riquelme C, Liu JO, Liu X, et al. Structure of p300 bound to MEF2 on DNA reveals a mechanism of enhanceosome assembly. *Nucleic Acids Res*. 2011; 39: 4464–4474. <https://doi.org/10.1093/nar/gkr030> PMID: 21278418
55. Cao C, Vasilatos SN, Bhargava R, Fine JL, Oesterreich S, Davidson NE, et al. Functional interaction of histone deacetylase 5 (HDAC5) and lysine-specific demethylase 1 (LSD1) promotes breast cancer progression. *Oncogene*. 2017; 36: 133–145. <https://doi.org/10.1038/onc.2016.186> PMID: 27212032
56. Barrett A, Santangelo S, Tan K, Catchpole S, Roberts K, Spencer-Dene B, et al. Breast cancer associated transcriptional repressor PLU-1/JARID1B interacts directly with histone deacetylases. *Int J Cancer*. 2007; 121: 265–275. <https://doi.org/10.1002/ijc.22673> PMID: 17373667
57. Liu X, Greer C, Secombe J. KDM5 interacts with Foxo to modulate cellular levels of oxidative stress. *PLoS Genet*. 2014; 10:e1004676. <https://doi.org/10.1371/journal.pgen.1004676> PMID: 25329053
58. Lesch BJ, Page DC. Poised chromatin in the mammalian germ line. *Development*. 2014; 141: 3619–26. <https://doi.org/10.1242/dev.113027> PMID: 25249456
59. Demicco EG, Maki RG, Lev DC, Lazar AJ. New Therapeutic Targets in Soft Tissue Sarcoma. *Adv Anat Pathol*. 2012; 19: 170–180. <https://doi.org/10.1097/PAP.0b013e318253462f> PMID: 22498582
60. Paroni G, Mizzau M, Henderson C, Del Sal G, Schneider C, Brancolini C. Caspase-dependent regulation of histone deacetylase 4 nuclear-cytoplasmic shuttling promotes apoptosis. *Mol Biol Cell*. 2004; 15: 2804–2818. <https://doi.org/10.1091/mbc.E03-08-0624> PMID: 15075374
61. Cernotta N, Clocchiatti A, Florean C, Brancolini C. Ubiquitin-dependent degradation of HDAC4, a new regulator of random cell motility. *Mol Biol Cell*. 2011; 22: 278–89. <https://doi.org/10.1091/mbc.E10-07-0616> PMID: 21118993
62. Peruzzo P, Comelli M, Di Giorgio E, Franforte E, Mavelli I, Brancolini C. Transformation by different oncogenes relies on specific metabolic adaptations. *Cell Cycle*. 2016; 15: 2656–2668. <https://doi.org/10.1080/15384101.2016.1215387> PMID: 27485932
63. Ritchie ME, Phipson B, Wu D, Hu Y, Law CW, Shi W, et al. limma powers differential expression analyses for RNA-sequencing and microarray studies. *Nucleic Acids Res*. 2015; 43: e47. <https://doi.org/10.1093/nar/gkv007> PMID: 25605792
64. Cerami E, Gao J, Dogrusoz U, Gross BE, Sumer SO, Aksoy BA, et al. The cBio Cancer Genomics Portal: An open platform for exploring multidimensional cancer genomics data. *Cancer Discov*. 2012; 2: 401–404. <https://doi.org/10.1158/2159-8290.CD-12-0095> PMID: 22588877
65. Picco R, Tomasella A, Fogolari F, Brancolini C. Transcriptomic analysis unveils correlations between regulative apoptotic caspases and genes of cholesterol homeostasis in human brain. *PLoS One*. 2014; 9. <https://doi.org/10.1371/journal.pone.0110610> PMID: 25330190

66. Brenca M, Rossi S, Polano M, Gasparotto D, Zanatta L, Racanelli D, et al. Transcriptome sequencing identifies ETV6-NTRK3 as a gene fusion involved in GIST. *J Pathol*. 2016; 238: 543–549. <https://doi.org/10.1002/path.4677> PMID: [26606880](https://pubmed.ncbi.nlm.nih.gov/26606880/)
67. Li B, Dewey CN. RSEM: accurate transcript quantification from RNA-Seq data with or without a reference genome. *BMC Bioinformatics*. 2011; 12: 323. <https://doi.org/10.1186/1471-2105-12-323> PMID: [21816040](https://pubmed.ncbi.nlm.nih.gov/21816040/)